

University of Alberta

The *Drosophila* PVR Pathway Regulates Innate Immunity and
Intestinal Homeostasis

by

David James Edward Bond

A thesis submitted to the Faculty of Graduate Studies and Research
in partial fulfillment of the requirements for the degree of

Doctor of Philosophy

in

Immunology

Medical Microbiology and Immunology

©David James Edward Bond

Spring 2013

Edmonton, Alberta

Permission is hereby granted to the University of Alberta Libraries to reproduce single copies of this thesis and to lend or sell such copies for private, scholarly or scientific research purposes only.

Where the thesis is converted to, or otherwise made available in digital form, the University of Alberta will advise potential users of the thesis of these terms.

The author reserves all other publication and other rights in association with the copyright in the thesis and, except as herein before provided, neither the thesis nor any substantial portion thereof may be printed or otherwise reproduced in any material form whatsoever without the author's prior written permission.

To my loving wife Claire and my two beautiful children Ava and Matthew.

Abstract

The innate immune system is an evolutionarily conserved first line of defense against invasive microbes. Studies in the fruit fly, *Drosophila melanogaster*, revolutionized the field of immunology and cemented *Drosophila* as a premier model of innate immune defenses. The *Drosophila* immune deficiency (IMD) pathway detects bacterial DAP-type peptidoglycan and drives protective immune responses. The IMD pathway shares remarkable conservation of downstream signaling components with the human Tumor Necrosis Factor (TNF) pathway, including engagement of caspase, NF- κ B and Jun-N-terminal kinase (JNK) modules. Given conserved and pleiotropic roles of JNK in eukaryote biology, I performed the first quantitative high-throughput RNAi screen to identify novel regulators of *Drosophila* JNK (dJNK) activity in the IMD pathway. I identified numerous novel negative and positive regulators of dJNK signaling including the receptor tyrosine kinase PDGF- and VEGF- receptor related (PVR) pathway. Follow-up studies uncovered a previously unknown negative-feed back loop, whereby IMD pathway activation of dJNK results in the production of Pvr-ligands, *pvf2* and *pvf3*, and engagement of the PVR pathway, which in turn suppresses IMD immune responses. I extended these findings to the *Drosophila* posterior midgut (mammalian small intestine equivalent), a well-established *in vivo* model to study the genetic interplay between protective innate immune responses and potentially damaging environmental insults. The *Drosophila* intestine serves as a critical immunological barrier at the interface between a delicate internal milieu and a hostile microbial environment. The posterior midgut contains a dynamic pool of intestinal stem cells (ISC) that rapidly proliferate and differentiate into mature epithelial cells to maintain epithelial integrity in response to environmental toxins. My findings establish that Pvf/Pvr autocrine signals are essential for ISC

homeostatic proliferation and differentiation, and that loss of Pvr signals leads to midgut hypoplasia. I determined that extrinsic stress signals generated by enteropathogenic infection are epistatic to the hypoplasia generated in *pvr* mutants, making the PVR pathway unique among all previously studied intrinsic pathways. Together, these studies revealed the PVR pathway as a critical regulator of *Drosophila* innate immune defenses and intestinal homeostasis.

Acknowledgments

Throughout the course of my PhD studies I have had the privilege of working with many amazing people who have helped me immeasurably, and to whom I owe great thanks. I would like to thank the administrative professionals in the department of Medical Microbiology and Immunology for making everything run smoothly. In particular, I would like to thank Anne Giles for her guidance and reassurance, and Debbie Doudiet for always keeping the candy dish full.

Prior to starting my PhD studies I worked as a research technician in a number of research labs at the Universities of Alberta and Victoria. These experiences would seed my love of science, and direct me towards a PhD. Therefore, I thank Dr. Juan Ausio, Dr. Michele Barry and Dr. Norman Kneteman for expanding my horizons, and for helping me fill my scientific toolbox. In these labs I had the opportunity to learn from great scientists. In particular, I thank Shawn Wasilenko for his encouragement to pursue further scientific studies.

During my PhD studies I had the privilege of working alongside past and present members of the Foley lab. I would like to thank Anja Schindler, David Primrose, Silvia Guntermann, Brendon Parsons and Chelsea Davidson for their support and friendship over the past six years. I have thoroughly enjoyed my time with them, and their camaraderie will be sorely missed.

My success as a graduate student is a reflection of the exceptional mentorship I have received from my PhD supervisor Dr. Edan Foley. I thank Edan for teaching me how to think and write as a scientist, and for providing an excellent role model of how to balance work and family life. As well, I would like to thank my committee members Dr. Deborah Burshtyn and Dr. James Smiley for their continual guidance with my research projects.

I would like to thank my family for their loving support, and their belief in my abilities. As a child I was fascinated with how things worked, and I thank my Dad for letting me mess-up his workbench in the deconstruction of various mechanical devices. To my Mum, I am forever grateful for the countless hours of additional tutelage that helped me overcome my dyslexia, and more importantly taught me how to learn.

Lastly, I would like to thank my wife Claire for her immeasurable support. Over the period of my PhD studies, we have shared the births of our two children Ava and Matthew, who have greatly enriched my life. In short, I could not have done this without you.

Table of Contents

	Page
<u>CHAPTER 1. Introduction.</u>	1
<u>1.1. Innate Immunity.</u>	2
<u>1.2. <i>Drosophila</i> host defenses.</u>	4
<i>1.2.1. Barrier immunity.</i>	4
<i>1.2.2. Cellular immunity.</i>	6
<i>1.2.3. RNAi-mediated antiviral responses.</i>	7
<i>1.2.4. Drosophila humoral immunity.</i>	7
<i>1.2.4.1. Drosophila AMPs</i>	8
<u>1.3. Toll/TLR: <i>Drosophila</i> models of innate immunity.</u>	9
<u>1.4. TNF and IMD pathways.</u>	12
<i>1.4.1 TNF pathway.</i>	12
<i>1.4.2 IMD pathway.</i>	16
<i>1.4.2.1. Activation of the IMD pathway.</i>	17
<u>1.5. Rel (NF-κB) signaling module.</u>	19
<u>1.6. <i>Drosophila</i> JNK</u>	21
<i>1.6.1. MAPKs.</i>	21
<i>1.6.2. Conservation of dJNK.</i>	22
<i>1.6.3. Pleotropic roles of JNK.</i>	24
<i>1.6.4. JNK in the IMD Pathway.</i>	25
<u>1.7. Negative regulation of the IMD pathway.</u>	25
<u>1.8. RNA interference.</u>	29
<i>1.8.1. RNAi: a mechanism of gene suppression.</i>	29
<i>1.8.2. RNAi in <i>Drosophila</i> cell culture.</i>	31
<i>1.8.3. Genome-wide RNAi screens in <i>Drosophila</i>.</i>	32

1.8.4. RNAi screens of the IMD pathway.	33
1.8.4.1. <i>In vivo</i> RNAi screens.	34
<u>1.9. Intestinal immunity.</u>	35
1.9.1. <i>Drosophila</i> intestinal immunity.	37
1.9.2. Physiology of the <i>Drosophila</i> Gut.	38
1.9.2.1. Cellular architecture of the posterior midgut.	39
1.9.3. Stem cells.	39
1.9.3.1. Posterior midgut ISCs.	41
1.9.4. <i>Drosophila</i> posterior midgut homeostasis.	41
1.9.4.1. Posterior midgut equilibrium.	42
1.9.4.2. Midgut response to damage/infection	44
1.9.5. Conservation of <i>Drosophila</i> and human homeostatic controls.	44
<u>1.10. Pvr.</u>	46
1.10.1. <i>Drosophila</i> Pvfs	47
1.10.2. Human PDGF- and VEGF-pathway etiology.	49
1.10.3. Pvr biology	50
1.10.4. PVR pathway signals.	51
1.10.4.1. Initiation of RTK signals.	52
1.10.4.2. PVR pathway signal transduction.	53
1.10.4.3. Pvr-engagement of Ras/dERK axis.	53
1.10.5. Pvr in the posterior midgut.	56
<u>1.11. Summary.</u>	56
<u>CHAPTER 2. Methods and Materials</u>	57
<u>2.1. List of buffers</u>	58

<u>2.2. Cells and cell culture.</u>	59
<i>2.2.1. Counting viable cells.</i>	60
<u>2.3. Cell culture assays.</u>	61
<i>2.3.1. dsRNA in S2 cells.</i>	61
<i>2.3.2. Activation of the IMD pathway.</i>	61
<i>2.3.3. Inhibition of dJNK phosphorylation.</i>	61
<i>2.3.4. Activation of the PVR pathway.</i>	62
<i>2.3.5. Inhibition of the PVR pathway.</i>	62
<u>2.4. Fly husbandry.</u>	63
<u>2.5. Fly assays.</u>	63
<i>2.5.1. In vivo RNAi.</i>	63
<i>2.5.2. Transgene expression in the Drosophila intestine.</i>	63
<u>2.6. Mosaic Analysis with a Repressible Cell Marker (MARCM).</u>	65
<i>2.6.1. Generation of pvf2-3 mutant.</i>	65
<i>2.6.2. PCR confirmation of pvr and pvf2-3 recombinants.</i>	65
<i>2.6.2.1. Single fly DNA extraction (for PCR).</i>	65
<i>2.6.2.2. Polymerase chain reaction (PCR).</i>	65
<i>2.6.2.3. Agarose gel electrophoresis.</i>	67
<i>2.6.3. Generation of MARCM clones.</i>	67
<u>2.7. Bacterial infections.</u>	68
<i>2.7.1. Bacterial cultures.</i>	68
<i>2.7.2. Septic injury.</i>	68
<i>2.7.3. Oral infections.</i>	68
<u>2.8. Generation of dsRNA.</u>	69
<i>2.8.1. De novo synthesis of dsRNAs.</i>	69

2.8.2. Amplification of template DNA.	71
2.8.3. Generation of dsRNA.	71
2.8.4. Generation of the whole genome library.	72
<u>2.9. Quantification of gene expression.</u>	72
2.9.1. RNA extraction from S2 cells.	72
2.9.2. RNA extraction from whole flies.	73
2.9.3. Analysis of RNA.	74
2.9.4. cDNA synthesis.	74
2.9.5. Quantitative real-time PCR (qRT-PCR).	75
<u>2.10. Immunochemistry</u>	77
2.10.1. Western blotting.	77
2.10.2. In-cell Western.	79
2.10.2.1. Quantification of ICW.	81
2.10.3. Immunofluorescence microscopy.	82
2.10.3.1. Confocal Microscopy.	86
<u>2.11. Statistical analysis.</u>	86
2.11.1. RNAi screen.	86
2.11.2. Determination of statistical significance.	87
2.11.3. Posterior midgut analysis.	87
2.11.4. Box plots.	88
<u>CHAPTER 3. A whole genome quantitative RNAi screen for modifiers of dJNK phosphorylation in <i>Drosophila</i> immune signaling.</u>	89
3.1. Chapter 3. Introduction.	90
3.2. Chapter 3. Results.	91
3.2.1. Quantification of immune-induced dJNK phosphorylation dynamics in the IMD pathway.	91

3.2.2. <i>Establishment of an In Cell Western (ICW) assay to monitor JNK phosphorylation events in S2 cells.</i>	94
3.2.3. <i>Preliminary RNAi screen for effector on PGN-induced dJNK phosphorylation.</i>	99
3.2.4. <i>In-Cell Western (ICW) assay for PGN-induced dJNK phosphorylation.</i>	104
3.2.5. <i>Quantitative analysis of high-throughput dsRNA screen for regulators of PGN-induced dJNK phosphorylation.</i>	110
3.2.6. <i>Regulators of f-actin levels in S2 cells.</i>	114
3.2.7. <i>Gene ontology of dJNK phosphorylation regulators.</i>	116
<u>CHAPTER 4. Pvr signal axis is a novel suppressor of <i>Drosophila</i> Innate immune response.</u>	118
4.1 Chapter 4. Introduction.	119
4.2 Chapter 4. Results.	120
4.2.1. <i>Validation of Pvr as a suppressor of PGN-induced dJNK Phosphorylation.</i>	120
4.2.2. <i>pvf2 and pvf3 are IMD/dJNK-responsive transcripts.</i>	127
4.2.3. <i>Pvr suppresses PGN-induced Rel signaling.</i>	130
4.2.4. <i>Pvr signaling suppresses PGN-dependent IMD pathway activation.</i>	134
4.2.5. <i>Pnt suppresses Imd pathway signals.</i>	140
4.2.6. <i>Pvr suppresses AMP production in vivo.</i>	143
<u>CHAPTER 5. Autocrine Pvr pathway activity controls intestinal stem cell proliferation in the adult <i>Drosophila</i> midgut.</u>	145
5.1. <u>Chapter 5. Introduction.</u>	146
5.2 <u>Chapter 5.2. Results.</u>	147
5.2.1. <i>Visualization of posterior midgut cells.</i>	147

5.2.2. Posterior midgut ISC express Pvr and Pvf2.	150
5.2.3. The Pvr axis controls midgut homeostasis.	154
5.2.4. Pvr promotes intestinal hyperproliferation.	158
5.2.5. Pvr signals in ISCs are essential for the appropriate development of intestinal cells.	158
5.2.6. Autocrine Pvr signals regulate ISC fate determination.	164
5.2.7. Pvr acts independently of dJNK to control midgut homeostasis.	171
5.2.8. Ras activity is required for Pvr-induced intestinal dysplasia.	176
5.2.9. Extrinsic proliferative cues override intrinsic roles of Pvr in intestinal homeostasis.	179
<u>CHAPTER 6. Discussion.</u>	183
<u>6.1. Quantification of biological signaling events.</u>	185
6.1.1. Fluorescence-based assays.	185
<u>6.1.1.1 Quantification of fluorescence-base assays</u>	186
6.1.2. Establishment of fluorescence-base ICW assay.	187
<u>6.2. Development of high-throughput screens.</u>	191
6.2.1. Assay development.	192
6.2.2. Screen sensitivity and establishment of controls.	192
<u>6.3. Whole genome RNAi screen dJNK phosphorylation.</u>	194
6.3.1. Accuracy of whole genome screens.	194
6.3.1.1. <i>False-positives.</i>	194
6.3.1.2 <i>False-negatives.</i>	196
6.3.2. Biological conservation of dJNK regulators.	197
6.3.2.1. <i>Comparison of RNAi screens for dJNK activity.</i>	198

<u>6.4. Pvr regulation of <i>Drosophila</i> innate immunity.</u>	199
<i>6.4.1. Pvr controls of cell-mediated immunity.</i>	200
6.4.1.1. <i>Pvr regulates IMD pathway signals.</i>	201
<u>6.5. Intestinal immunity.</u>	204
<i>6.5.1. Drosophila intestinal homeostasis.</i>	206
<i>6.5.2. PVR pathway guidance of intestinal homeostasis.</i>	207
6.5.2.1. <i>Public vs. private autocrine Pvr signals.</i>	209
6.5.2.2. <i>Relationship between Pvr and EGFR.</i>	210
<i>6.5.3. Implication of Pvr signals for intestinal aging.</i>	211
<u>6.6. Pvr/PDGFR controls of intestinal development.</u>	211
<u>6.7. Pvr model of cellular proliferation.</u>	212
<u>6.8. Concluding remarks and future perspectives.</u>	213
<u>CHAPTER 7. Literature Cited.</u>	216
<u>CHAPTER 8. Appendices.</u>	268

List of Tables

	Page
CHAPTER 2. Methods and Materials	
Table 2.1. Fly strains.	64
Table 2.2. PCR primers for confirmation of <i>pvr</i> ⁵³⁶³ and <i>pvf2-3</i> recombinants.	66
Table 2.3. List of primers for generating dsRNA.	70
Table 2.4. List of validated qRT-PCR primers.	76
Table 2.5. List of primary antibodies.	84
Table 2.6. List of secondary antibodies.	85
Table 2.7. List of stains.	86
CHAPTER 3. A whole genome quantitative RNAi screen for modifiers of dJNK phosphorylation in <i>Drosophila</i> immune signaling.	
Table 3.1. Genes targeted in preliminary screen for modifiers of PGN induced dJNK phosphorylation in the IMD pathway.	102
CHAPTER 8. Appendices	
Table A1. Enhancers of 15 min PGN-induced P-JNK.	269
Table A2. Suppressors of 60 min PGN-induced P-dJNK.	286
Table A3. Suppressors of 15 min PGN-induced P-JNK.	294
Table A4. dsRNA effects on f-actin levels in S2 cells.	300
Table A5. dsRNA effects on f-actin and P-JNK levels in S2 cells.	302

List of Figures

	Page
CHAPTER 1. Introduction.	
Figure 1.1. <i>Drosophila</i> Innate Immunity.	5
Figure 1.2. Conservation of IMD/TNF pathway components.	13
Figure 1.3 <i>Drosophila</i> IMD pathway.	20
Figure 1.4. JNK/dJNK homology.	23
Figure 1.5. Negative regulation of the IMD pathway.	27
Figure 1.6. siRNA pathway.	30
Figure 1.7. Posterior midgut cells.	40
Figure 1.8. Controls of ISC proliferation and differentiation.	43
Figure 1.9. Structural homology of <i>Drosophila</i> Pvr/Pvfs.	48
Figure 1.10. Canonical Pvr/Ras/Erk pathway.	55
 CHAPTER 3. A whole genome quantitative RNAi screen for modifiers of dJNK phosphorylation in <i>Drosophila</i> immune signaling.	
Figure 3.1. Immune-induced dJNK phosphorylation in <i>Drosophila</i> cell lines.	93
Figure 3.2. dJNK phosphorylation response to PGN exposure.	95
Figure 3.3. Optimization of anti-P-dJNK stain for ICW assay.	97
Figure 3.4. Dynamic regulation of immune-induced dJNK phosphorylation by ICW assay.	98
Figure 3.5. ICW quantification of RNAi effects on P-dJNK dynamics.	100
Figure 3.6. Preliminary RNAi screen for modifiers of PGN-induced dJNK phosphorylation in the IMD pathway.	103
Figure 3.7. Schematic representation of a quantitative RNAi screen for modifiers of PGN-induced dJNK phosphorylation.	105

Figure 3.8.	Whole genome RNAi screen for modifiers of dJNK phosphorylation in the IMD pathway.	106
Figure 3.9.	Representative plate from P-dJNK dsRNA screen.	107
Figure 3.10.	Quantification of relative dJNK phosphorylation levels from representative plate.	109
Figure 3.11.	Whole genome RNAi screen for 15min enhancers and suppressors of dJNK phosphorylation in the IMD pathway.	111
Figure 3.12.	Whole genome RNAi screen for suppressors of dJNK phosphorylation in the IMD pathway.	112
Figure 3.13.	Whole genome RNAi screen for dJNK phosphorylation highlights enhancers of filamentous actin.	115
Figure 3.14.	Analysis of whole genome screen for modifiers of dJNK phosphorylation.	117

CHAPTER 4. Pvr signal axis is a novel suppressor of *Drosophila* Innate immune response.

Figure 4.1.	In-Cell quantification of RNAi effects on dJNK phosphorylation relative to JNK.	121
Figure 4.2.	Secondary analysis of selected modifiers of dJNK phosphorylation.	123
Figure 4.3.	Genetic and physical interaction networks of dJNK phosphorylation modifiers from previous studies.	125
Figure 4.4.	Pvr is a negative regulator of dJNK phosphorylation in the IMD pathway.	126
Figure 4.5.	The PVR pathway suppresses PGN-induced dJNK phosphorylation.	128
Figure 4.6.	<i>pvf2</i> and <i>pvf3</i> are Immune-Induced transcripts.	129
Figure 4.7.	<i>pvf2</i> and <i>pvf3</i> transcripts are dJNK-dependent.	131
Figure 4.8.	Immune-induced <i>pvf2</i> transcription requires an intact IMD pathway.	132
Figure 4.9.	Pvr depletion increases antimicrobial peptide production in S2 cells.	133

Figure 4.10.	Pvr depletion enhances IMD pathway production of antimicrobial peptides.	135
Figure 4.11.	Pvr depletion enhances IMD pathway signals.	136
Figure 4.12.	dERK phosphorylation response to conditioned media exposure.	138
Figure 4.13.	Pvr inhibits antimicrobial peptide production in S2 cells.	139
Figure 4.14.	Pvr-induced dERK activity inhibits antimicrobial peptide production in S2 cells.	141
Figure 4.15.	Pnt depletion enhances IMD pathway signals.	142
Figure 4.16.	Pvr attenuates infection-induced antimicrobial peptide production <i>in vivo</i> .	144

CHAPTER 5. Autocrine PVR pathway activity controls intestinal stem cell proliferation in the adult *Drosophila* midgut.

Figure 5.1.	Visualization of posterior midgut cells.	148
Figure 5.2.	Control of transgene expression in <i>Drosophila</i> .	149
Figure 5.3.	Visualization of posterior midgut ISC/EBs.	151
Figure 5.4.	Pvr is expressed in the <i>Drosophila</i> posterior midgut.	152
Figure 5.5.	Pvr and Pvf2 are expressed in posterior midgut ISCs.	153
Figure 5.6.	Pvr is required for intestinal homeostasis.	156
Figure 5.7.	Pvr pathway activity controls intestinal homeostasis.	157
Figure 5.8.	Pvr activity promotes intestinal mitosis.	159
Figure 5.9.	Pvr controls ISC cell numbers.	160
Figure 5.10.	Pvr controls EB cell numbers.	161
Figure 5.11.	Pvr controls midgut cell development.	162
Figure 5.12.	Generation of <i>pvr</i> ⁵³⁶³ and <i>pvf2-3</i> mutant clones.	165
Figure 5.13.	Mosaic analysis with a repressible cell marker (MARCM).	167

Figure 5.14.	Crossing scheme for generating MARCM clones.	168
Figure 5.15.	Autocrine Pvf/Pvr signals in ISCs establish mature midgut cells.	169
Figure 5.16.	Autocrine Pvf/Pvr signals control ISC identity.	172
Figure 5.17.	Pvr-regulates ISC homeostasis independent of extrinsic dJNK cues.	174
Figure 5.18.	Extrinsic dJNK cues control intestinal homeostasis independently of Pvr.	175
Figure 5.19.	Pvr acts through Ras to control ISC homeostasis.	177
Figure 5.20.	Extrinsic stress signals override Pvr intrinsic homeostatic controls.	180
Figure 5.21.	Pvr signals control survival to <i>Pe</i> oral infection.	182
CHAPTER 6. Discussion.		
Figure 6.1.	Summary model of how the Pvr pathway negatively regulates the IMD pathway.	202
Figure 6.2.	Pvr controls cells mediated immunity.	205
Figure 6.3.	Model of Pvf/Pvr regulation of ISC homeostasis.	208
CHAPTER 8. Appendices.		
Figure A1.	P-JNK screen comparative analysis.	304

List of Symbols, Nomenclature and Abbreviations.

μ – micro

°C – degrees Celsius

Ab – antibody

Act – Actin

AGO2 – Argonaute-2

AMP – Antimicrobial peptide

AP-1 – activator protein 1

ARK – Apaf-1-related killer

APS – Ammonium persulfate

Arm – Armadillo

Att – Attacin

bp – Base pair

Capase – cysteine-aspartic protease

CG – Computed Gene (formerly Celera Genome)

ciAP – cellular inhibitor of apoptosis protein

Cka – Connector of kinase to AP-1

Clk – Clock

CM – conditioned media

CRD – cysteine rich domain

Damm – Death associated molecule related to Mch2

DAP-PGN – diaminopimelic acid-containing peptidoglycan

Dcp-1 – Death caspase-1

Dcr – Dicer

Dcr2 – Dicer-2

DD – Death Domain

Debcl – Death executioner Bcl-2 homologue

Decay – Death executioner caspase related to Apopain/Yama

DED – Death-Effector Domains

dERK – *Drosophila* Extracellular signal-regulated kinase

dFADD – *Drosophila* Fas-associated protein with death domain

dFos – *Drosophila* Fos

dH₂O – distilled water

dHDAC – *Drosophila* histone deacetylase

dIAP1 – *Drosophila* inhibitor of apoptosis 1

dIAP2 – *Drosophila* inhibitor of apoptosis 2

Dif – Dorsal-related immunity factor

dIKK – *Drosophila* IKK

Dipt – Diptericin

DISC – Death-inducing signaling complex

dJNK – *Drosophila* Jun N-terminal Kinase

DI – Delta

dMAPK – *Drosophila* Mitogen-Activated Protein Kinase

dMkk4 – *Drosophila* Mitogen-Activated Kinase Kinase 4

dMkk7 – *Drosophila* Mitogen-Activated Kinase Kinase 7

DNA – Deoxyribonucleic acid

Dnr1 – Defense repressor 1

dNTPs – Deoxyribonucleotide triphosphate

Dredd – Death related ced-3/Nedd2-like protein

drlCE – *Drosophila* interleukin-converting enzyme

dronc – dronc

Dsor1 – Downstream of raf1

dsRBD – double-stranded RNA binding domain

dsRNA – double-stranded RNA

dTab2 – *Drosophila* TAK1-associated binding protein 2

dTAK1 – *Drosophila* TGF- β -activated kinase 1

E. coli – *Escherichia coli*

EB – Enteroblast

EC – Enterocyte cell

EE – Enteroendocrine cell

EGFR – epidermal growth factor receptor

Egr – Eiger

esg – escargot

ERK – extracellular signal-regulated kinases

f-actin – filamentous actin

FADD – Fas-associated protein with death domain

FRET – Fluorescence Resonance Energy Transfer

g – gram

GEF – guanine nucleotide exchange factor

GO – Gene ontology

Grb2 – Growth factor receptor-bound protein

h – hour

HDC ID – Heidelberg *Drosophila* Consortium Identifier

Hep – Hemipterous

Hid – Head involution defective

ICW – In-Cell Western

IKK – I κ B kinase complex

Imd – Immune deficiency

InR – Insulin Receptor

IRAK – IL-1R-associated kinase

Ird5 – Immune response deficient 5

IRF7 – interferon regulatory factor 7

ISC – Intestinal stem cell

I κ B – inhibitor of κ B

JAK – Janus activated kinase

JNK – c-Jun N-terminal kinase

JRA – Jun related antigen

K63 – lysine 63

Key – Kenny

k – kilo

l – liter

lacZ – β -galactosidase gene

LPS – Lipopolysaccharide

Lrg5 – leucine-rich-repeat-containing G-protein-coupled receptor 5

LRR – leucine-rich repeat

m – milli

M – Molar

MAP – mitogen associated protein

MAPK – mitogen associated protein kinase

MAPKK – mitogen associated protein kinase kinase

MAPKK – mitogen associated protein kinase kinase kinase

MARCM – Mosaic Analysis with a Repressible Cell Marker

Mbc – Myoblast city

min – minute

Myd88 – myeloid differentiation factor 88

N – Notch

Nf- κ B – Nuclear factor κ B

NRE – Notch Reporter Element

O/N – overnight

OTE – Off-target effect

P-H3 – phospho-histone 3

p-value – probability value

PAMP – Pathogen associated molecular pattern

PBS – Phosphate buffered saline

PBST – Phosphate-buffered saline with tween-20

PCR – Polymerase chain reaction

PDGF – Platelet-Derived Growth Factor

PDGFR – Platelet Derived Growth Factor Receptor

PDM1 – POU domain protein 1

Pe – *Pseudomonas entomophila*

PGN – Peptidoglycan

PGRP – PGN recognition protein

PGRP-LC – Peptidoglycan receptor protein - long chain

Pirk – poor Imd response upon knock-in

Pnt – Pointed

POSH – plenty of SH3s

Pros – Prospero

PRR – Pattern recognition receptor

Puc – Puckered

Pvf – PDGF- and VEGF-related factor

Pvr – PDGF- and VEGF-related receptor

PvrCA – constitutively active Pvr

PvrDN – dominant negative Pvr

qRT-PCR – quantitative real-time polymerase chain reaction

rcf – relative centrifugal force

Rel – Relish

RHD – Rel homology domain

RIP1 – Receptor-interacting serine/threonine-protein kinase 1

RISC – RNA-induced silencing complex

RNA – Ribonucleic acid

RNAi – RNA interference

rNTP – ribonucleotide triphosphate

ROS – Reactive oxygen species

rpm – rotations per minute

RT – Room temperature

Rt-PCR – Reverse transcription polymerase chain reaction

RTK – receptor tyrosine kinase

s – second

S2 – Schneiders 2 cells

SAPK – stress-activated protein kinases

SDS – sodium dodecyl sulfate

SDS-PAGE – sodium dodecyl sulfate polyacrylamide gel electrophoresis

SEM – Standard Error from the Mean

siRNA – small interfering RNA

SODD – Suppressor of death domain

Sos – Son of sevenless

ssRNA – single-stranded RNA

STAT – Signal transduced and activator of transcription

Tab – TAK1-associated binding protein

Tak1 – Tumor necrosis factor- β activated kinase

TBS – Tris-buffered saline

TBST – Tris-buffered saline with tween-20

TBSTx – Tris-buffered saline with triton-X

TCT – tracheal cytotoxin

TIR – Toll/interleukin-1 receptor

TLR – Toll-like receptors

TNF – Tumor necrosis factor

TNFR – tumor necrosis factor receptor

TRADD – TNF receptor-associated death domain

TRAF – TNF receptor-associated factor

U – Units

UAS – Up-stream Activating Sequence

Upd – Unpaired

UTR – Untranslated region

UV – Ultraviolet

V – Volts

VEGF – Vascular endothelial growth factor

VEGFR – Vascular endothelial growth factor receptor

VM – Visceral muscle

WB – Western blot

Wg – wingless

Wgn – Wengen

Wts – Warts

The following nomenclature was used for Drosophila genes, proteins and pathways using *pvr* as an example:

gene – Lowercase italics (*pvr*)

Protein – First letter capitalized (Pvr)

PATHWAY – All letters capitalized (PVR)

CHAPTER 1

Introduction

1.1. Innate immunity.

Metazoans evolved intricate immune defenses to defend against the relentless threats posed by microbial challengers[1]. Metazoan immune systems use microbial sensing pathways to maintain mutualistic host-microbial interactions, and to repel invasive pathogens with robust antimicrobial defense mechanisms. In higher organisms immune responses are divided into two categories: the adaptive and innate. The adaptive immune response is an evolutionary newcomer restricted to the descendants of vertebrates[2, 3]. The adaptive immune response is composed of highly specialized T and B-lymphocytes that employ *de novo* synthesized antigen receptors rather than germline-encoded receptors[4]. As a result adaptive immune responses are highly specific to the microbial invader and improve upon secondary challenge with the same organism[4, 5]. In contrast, the innate immune system is an ancient and conserved first line of defense against invading microbes present in all extant multicellular organisms. In fact, the vast majority of metazoans species rely exclusively on innate immune defenses for protection against microbial infections[1]. The innate immune system relies on numerous broad strategies to guard against pathogenic microbes including: anatomical barriers, specialized immune cells and humoral and localized immune responses[2].

Host innate immune responses must differentiate self from a vast variety of potential pathogenic challengers with a fixed collection of germline-encoded receptor molecules[6]. This is accomplished through the detection of conserved motifs within essential microbial structural components, called pathogen-associated molecular patterns (PAMPs). Host pattern recognition receptors

(PRR) bind specific classes of microbial PAMPs, and mediate intracellular signals to initiate robust immune defense reactions[7]. In general, PAMPs are microbial-associated structural components that are essential for pathogen viability, thereby limiting the opportunity for immune evasion through adaptive evolutionary changes. In order to differentiate non-infectious self from infectious non-self and to avoid auto-reactive immune responses, PAMPs are pathogen specific molecules not normally found in the host. Examples of PAMPs include, bacterial and fungal cell wall components, and nucleic acids from viruses and bacteria[6]. PRR-mediated detection of PAMPs guides innate immune responses that include opsonization, activation of complement and coagulation cascades, phagocytosis, activation of proinflammatory and antimicrobial signaling pathways and induction of apoptosis (controlled cell death)[2]. Additionally, the innate immune response plays a critical role in shaping adaptive immune responses. For example, the requirement for innate immune activation of antigen-presenting dendritic cells to guide lymphocyte actions is one of many established connections between innate and adaptive responses[8].

The fruit fly, *Drosophila melanogaster*, is premier model to investigate innate immune defenses, as studies in *Drosophila* have revolutionized the field of immunology[9-11]. *Drosophila* is an ideal model to study innate immune defenses because of its genetic malleability, its lack of an adaptive immune response and its conservation of signaling pathways with mammals[8]. For example, in 2011, Jules Hoffmann was recognized for his groundbreaking discovery of Toll immune function in *Drosophila*, receiving the Nobel Prize for Physiology or Medicine with other pioneers in the field of innate immunity.

1.2. *Drosophila* host defenses.

Drosophila melanogaster health is constantly challenged by a huge diversity of pathogenic microbes including bacteria, viruses, fungi, and eukaryotic parasites. In response to the vast array of microbial invaders, *Drosophila* has developed sophisticated innate immune defenses. In *Drosophila melanogaster*, the innate immune defenses include: anatomical barriers, specialized phagocytic hemocytes, humoral response effector molecules such as antimicrobial peptides (AMP), and RNA interference (RNAi) mediated anti-viral defenses (Figure 1.1)[12].

1.2.1. Barrier immunity.

In *Drosophila*, physical structures such as the chitinous cuticle of the exoskeleton, secreted chitinoproteinaceous membranes and epithelium linings, form a barricade between a hostile environment and a sensitive internal milieu. *Drosophila* epithelial barriers include the ectoderm that covers the exterior of the animal, and the endoderm that lines the gut. The formation of tight junctions between polarized epithelial cells establishes the epithelial integrity of the epithelial barriers[13]. Breakdown of these anatomical barriers through mechanical damage or epithelial cell death can lead to infiltration of infectious agents and death[14, 15]. Epithelial surfaces, such as those in the gut, are constantly exposed to potentially deadly microorganisms, and thus maintenance of epithelial integrity is essential for animal survival[16]. For example, continual renewal of the intestinal epithelium is essential for fly longevity and survival from oral infection[17-19]. In addition to forming a physical barrier, epithelial

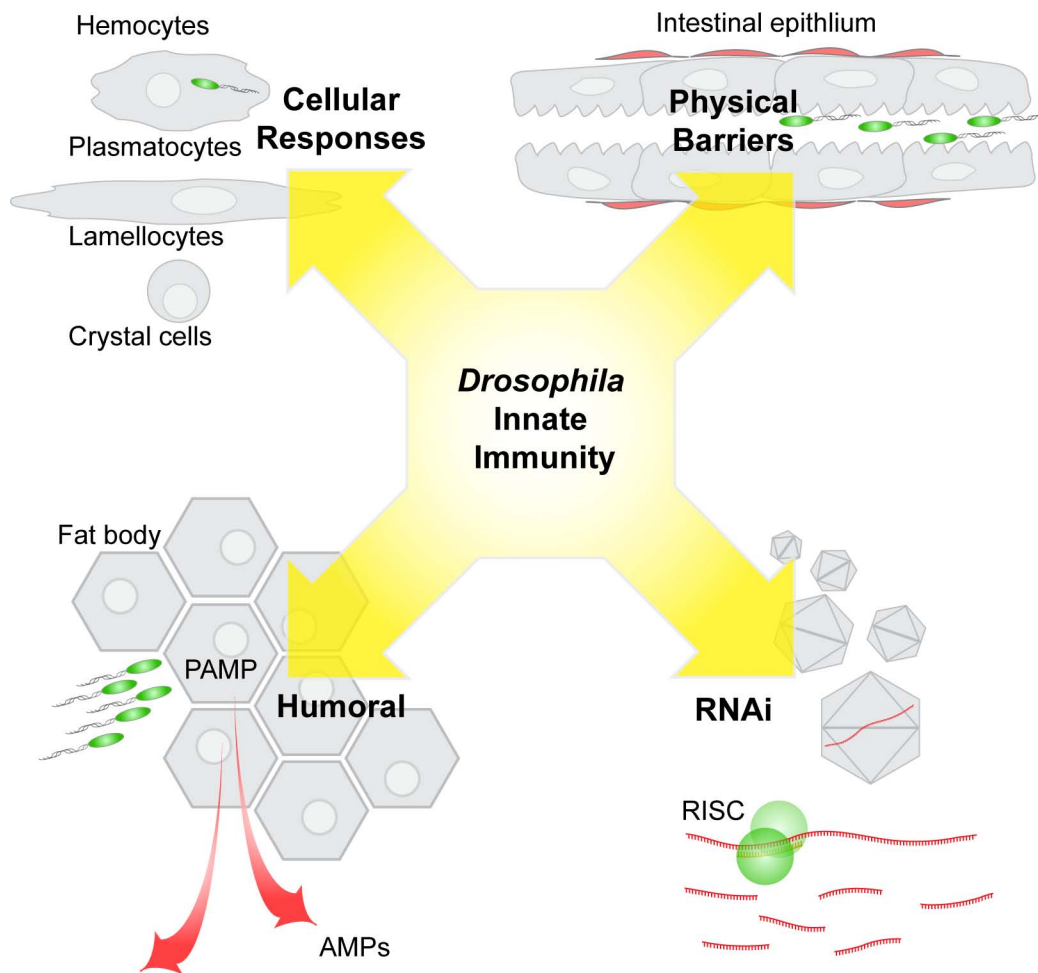


Figure 1.1. *Drosophila* innate immunity.

Drosophila uses multiple innate immune strategies to defend against pathogenic microbes and parasites. The epithelial layers are the first line of defense, forming a physical barrier to prevent microbial invasion. If the epithelium is compromised, *Drosophila* engage a series of innate immune responses to directly combat the invasive microbe, such as the humoral response pathways. The engagement of PRRs pathways with microbe specific PAMPs drives the production of effector molecules, such as the AMPs. *Drosophila* immune cells continue the assault and engulf, melanize and encapsulate foreign pathogens. Finally, the RNAi pathway provides protection from viral infection by degrading viral specific dsRNA in an infected cell. Combined these innate immune strategies provide protection to a vast array of pathogens.

cells directly recognize microbial PAMPs and generate localized immune responses[20, 21]. For example, immune responses in the gut epithelium drive the expression of AMPs and reactive oxygen species (ROS), through activity of the NADPH oxidase enzyme, DUOX[22]. Immune-induced production of ROS is critical for host survival to intestinal infections[23]. Together immune-induced effector molecules generate a hostile milieu for invading microbes.

1.2.2. Cellular immunity.

Drosophila lack lymphoid cells of the mammalian adaptive immune response, and instead relies exclusively on innate immune cells to clear microbial infections[24]. Based on morphological features and physiological functions, *Drosophila* hemocytes (blood cells) are separated into the following types: plasmatocytes, lamellocytes and crystal cells[8]. *Drosophila* hematopoiesis occurs in two spatially and temporally distinct waves. The first wave of hematopoiesis begins in the embryonic procephalic mesoderm, and gives rise to the plasmatocyte and crystal cell lineages[25, 26]. In addition to innate immune responses, embryonic plasmatocytes have specialized roles in embryonic sculpting through the phagocytosis of apoptotic bodies and deposition of extracellular matrix[26-28]. The second wave of hematopoiesis takes place in specialized hematopoietic larval tissues[25, 29]. In healthy larvae, the macrophage-like plasmatocytes constitute approximately 95% of the mature hemocyte population, and phagocytose apoptotic cells and microbial invaders[12, 24]. The small, non-phagocytic crystal cells makeup the remaining 5% of hemocytes, and are primarily involved in melanization, wound response and coagulation[30-32]. Upon larval parasitization, pro-hemocytes preferentially

differentiate into large, flat, lamellocytes that encapsulate foreign materials too large to be phagocytized, such as a parasitic wasp egg[12, 33]. In adult flies hematopoietic organs are absent, and the hemocyte population consists of a mixture of both embryonically- and lymph gland-derived plasmatocytes[29, 34]. In adult flies, the cellular and humoral immune responses cooperate to generate a potent anti-microbial environment to combat microbial invaders[35].

1.2.3. RNAi-mediated antiviral responses.

Flies, worms, and plants cells use the RNAi response to combat viral infections. RNAi is an ancient and conserved post-transcriptional control mechanism with anti-viral properties first described in plants[36, 37]. More specifically, viral double-stranded ribonucleic acids (dsRNAs) generated during the viral infection cycle trigger RNAi pathway activity. During infection the RNAi pathway processes exogenous viral dsRNA into small interfering RNA (siRNA) molecules that guide the RNA-induced silencing complex (RISC) to viral specific nucleotide sequences[38, 39]. The siRNA-RISC machinery degrades viral ssRNA through dsRNA-specific endonuclease activity, and thereby inhibits viral replication. In *Drosophila* an intact RNAi pathway is critical for antiviral defenses, as mutants in this pathway are hypersensitive to viral infection[38, 39]. However, the RNAi pathway is not strictly an innate immune defense mechanism and has additional functions in post-translational controls of gene expression[40].

1.2.4. *Drosophila* humoral immunity.

Septic injury of *Drosophila* with pathogenic microbes triggers the expression of AMPs via the engagement of humoral response pathways. The open

circulatory system of *Drosophila* contains hemolymph (blood) that surrounds immune-responsive tissues, such as the *Drosophila* fat body (the metabolic equivalent of the human liver). Microbial infections triggers fat body cells to secrete effector molecules into the hemolymph generating a global antimicrobial environment. Production of AMPs is a highly dynamic process mediated through numerous PAMP sensing pathways including the Toll and immune-deficiency (IMD) pathways[9, 41]. In *Drosophila*, detection of gram-positive bacteria, fungi and viruses is accomplished through the Toll pathway, whereas detection of gram-negative bacteria is accomplished through the IMD pathway[42]. Low basal levels of AMP are detectable in uninfected flies, however microbial engagement of Toll or IMD pathways drives the rapid synthesis of a broad spectrum AMPs, that again return to basal levels once the pathogen is eliminated[43].

1.2.4.1. *Drosophila* AMPs

The *Drosophila* humoral response wages chemical warfare on microbial combatants generating a noxiously inhospitable environment, of these toxic effectors, AMPs are perhaps the best characterized. AMPs are a universal feature of immune defenses in all living organisms, highlighting their significance in fighting infections[44]. This heterogeneous group of proteins are characterized by their small size, positive charge and microbialcidal activities towards a wide range of pathogens including, fungi and gram negative and positive bacteria. *Drosophila* encodes a variety of AMPs including Attacin (Att), Diptericin (Dipt), Drosocin, Drosomycin, Cecropin, Defensin, and Metchnikowin[8]. The Toll and IMD NF- κ B activities transcribe distinct sets of AMPs. For example, activation of the Toll pathway drives the expression of Drosomycin and Cecropin, while IMD

pathway activity promotes *att* and *dipt* expression[9]. For this reason, the expression levels of *att* and *dipt* are often used as a measure of IMD pathway activation. While their exact antimicrobial mechanisms are not clearly understood, it is proposed that AMPs in general disrupt the integrity of microbial cells walls[45]. Regardless of the precise mechanism it is clear that AMPs have potent antimicrobial properties[46].

1.3. Toll/TLR: *Drosophila* models of innate immunity.

With a century of scientific study, *Drosophila* models are keystones to revolutionary discoveries of numerous biological processes[47]. Compared to mammals, *Drosophila* have several distinct benefits as genetic models, such as a compact genome with fewer instances of gene duplication and redundant gene function. Despite its genetic simplicity, it is estimated that approximately 75% of genes associated with human disease have corresponding homologs in the *Drosophila* genome[48, 49]. *Drosophila* represents an ideal model to study innate immune defenses because of its genetic malleability, its lack of an adaptive immune response and its conservation of signaling pathways. Many key innate immune signaling pathways show remarkable conservation between human and *Drosophila*, despite hundreds of millions of years on separate evolutionary paths.

Perhaps more than any other pathway, the Toll pathway best exemplifies *Drosophila melanogaster* as an invaluable innate immune model. Toll was originally identified in dorso-ventral patterning in the *Drosophila* embryo[50]. Toll is a single-pass transmembrane receptor protein with an intracellular Toll/interleukin-1 receptor (TIR) homology domain, and an ectodomain that

contain multiple leucine-rich repeat (LRR) motifs[51, 52]. The *Drosophila* genome encodes nine Toll genes (Toll 1-9), however only Toll-1 (Toll) has established functions in innate immunity[53]. Early studies showed that overexpression of a constitutively active Toll(10B) induced the expression of the AMP *Cecropin A1* gene in the *Drosophila* mbm2 blood cell line, implicating toll in innate immune signaling[54]. Further research showed that Toll mutants are highly sensitive to gram-positive bacterial, fungal and viral infections[9]. The Toll receptor does not function directly as a PRR, rather Toll recognizes cleaved Spatzle[9, 55, 56]. Spatzle is secreted as an inactive pro-protein that is processed into a mature form, through a series of proteolytic cascades by secreted PRR molecules[57, 58]. Toll recognition of Spatzle drives receptor dimerization and initiation of signaling events mediated through the intracellular TIR domains of the adaptor molecule myeloid differentiation factor 88 (Myd88)[59, 60]. Myd88 then forms a heterotrimeric receptor complex with Tube and the kinase Pelle through death domain (DD)-mediated interactions[61, 62]. Downstream phosphorylation events target the *Drosophila* I κ B homolog cactus for degradation, and activates the NF- κ B transcription factors Dorsal-related immunity factor (Dif) and Dorsal[59, 60, 63-66]. The nuclear translocation of Dif and Dorsal, drives the transcription of a specific set of AMP genes[67, 68]. The discovery that *Drosophila* Toll activates NF- κ B transcription factors, combined with the knowledge that NF- κ B transcription factors also transcribe immune genes in higher eukaryotes, led to the search for mammalian Toll-like receptors (TLR)[9, 69].

Like *Drosophila* Toll, human TLRs are type I transmembrane protein with a conserved extracellular LRR domain and cytoplasmic TIR domain[10]. Humans

and mice encode 10 and 12 TLRs, respectively, that detect an array of lipids, proteins and nucleic acids from a wide range of microbes including bacteria, viruses, parasites and fungi[6, 70-73]. TLRs vary in their cellular localization and respective ligands. TLRs expressed on the cell surface largely recognize microbial membrane components, while those expressed on intracellular vesicles such as the endoplasmic reticulum, lysosomes, and endolysosomes generally detect microbial nucleic acids. Unlike *Drosophila*, human TLRs directly sense PAMPs through their LRR ectodomain, however downstream signaling components remain well conserved between the Toll/TLR pathways. In the MyD88-dependent TLR pathway, detection of TLR ligands drives receptor homo- and heterodimerization and initiates intracellular signals through TIR containing Myd88 adaptor molecules. DD-interactions between MyD88, IL-1R-associated kinase (IRAK) 1 (Pelle homolog), IRAK4 (putative Tube ortholog), and other IRAK molecules form a helical oligomer complex to initiate intracellular signals[74-77]. The TLR pathway, like the *Drosophila* Toll pathway, engages NF- κ B transcription factor activity, and additionally engages c-Jun N-terminal kinase (JNK) and interferon regulatory factor signals[10, 78-80]. These TLR signals are critical for primary innate immune defenses, and further shape secondary adaptive immune responses[81]. More specifically, TLR signals drive inflammatory processes that recruit cells of both the innate and adaptive immune responses to sites of infection through the expression of diffusible chemotactic factors and cell surface adhesion molecules[81]. TLRs are highly expressed on antigen-presenting cell of the adaptive immune system, such as dendritic cells, macrophages and B-cells; and their signals are critical for guiding appropriate adaptive immune responses[82, 83]. For example, TLR-mediated detection of

microbial PAMPs activates dendritic cells and thereby directs T lymphocyte responses[84]. The discovery of TLRs in mammals revolutionized the field of innate immunity and cemented *Drosophila* as a principle model organism in the field of innate immunity. In addition to the Toll/TLR pathway, other immune signaling pathways are evolutionarily conserved between *Drosophila* and human, including the *Drosophila* IMD and the human tumor necrosis factor (TNF) pathways[85].

1.4. TNF and IMD pathways.

The TNF-pathway is often considered homologous to the *Drosophila* IMD pathway, due the similarity of shared signaling components (Figure 1.2). Both TNF and IMD pathways signal through conserved NF- κ B, JNK and caspase modules. While the TNF and IMD pathways share many overt similarities, they are activated by unrelated receptors and distinct ligands. Specifically, the *Drosophila* IMD pathway senses bacterial diaminopimelic acid-containing peptidoglycan (DAP-PGN), while the TNF-receptor responds to soluble TNF homo-trimetric ligand[86, 87]. Extensive *in vitro* studies have illuminated many aspects of TNF pathway signals, however in-depth *in vivo* studies are sparse. Given *Drosophila*'s rich history as a genetically malleable model in innate immune pathways, the *Drosophila* IMD pathway represents a powerful tool to further study conserved signaling events in the human TNF pathway *in vivo*.

1.4.1 TNF pathway.

The TNF pathway is a critical immune pathway in higher organisms[88]. Observations made more than a century ago revealed that bacterial infections

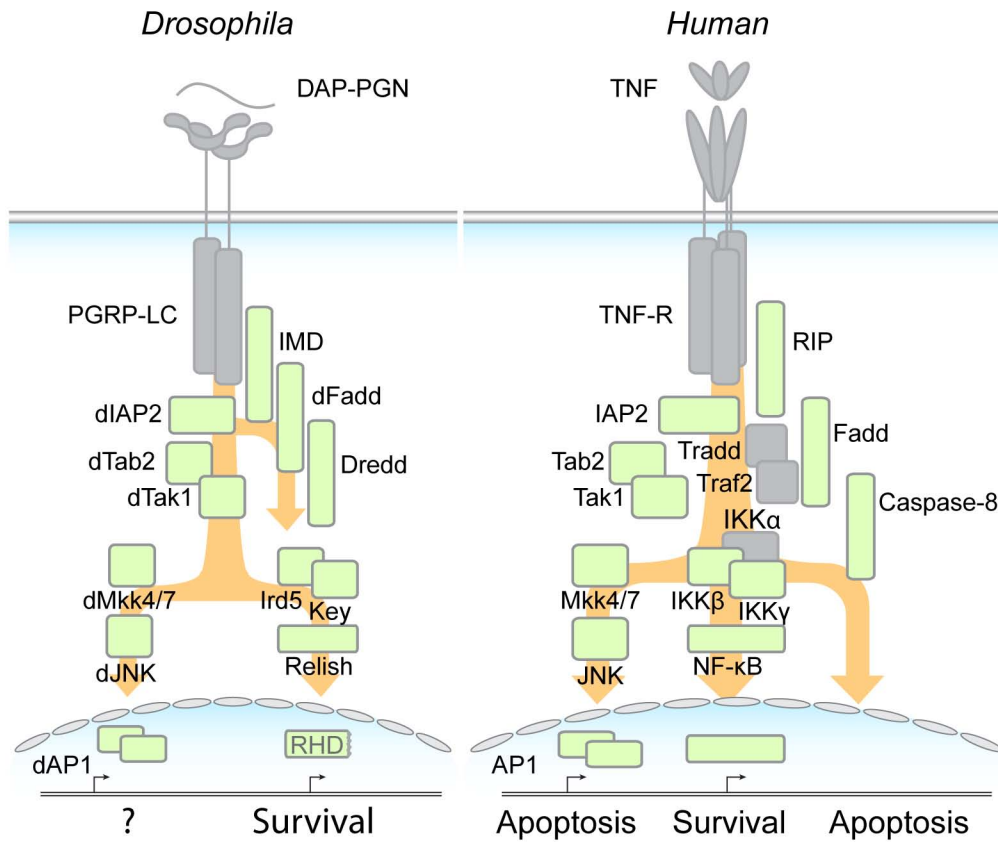


Figure 1.2. Conservation of IMD/TNF pathway components.

The *Drosophila* IMD and Human TNF pathways show remarkable conservation of core signaling components. Conserved members of the IMD/TNF pathways are shown in green, while proteins unique to either pathway are shown in grey. Notable differences include receptor/ligand interactions, while the IMD pathway is engaged by PGN through the PGRP-LC receptor, the TNF-receptor pathway is engaged by TNF.

can lead to tumor regression[89]. Subsequent research showed that infection-induced immune responses exerted these anti-tumor properties through the production of tumor-necrotizing factors, now known as tumor necrosis factor (TNF)[87, 90, 91]. TNF ligand binds the TNF receptor (TNFR), the founding member of the TNFR superfamily that includes 19 ligands and 29 receptor characterized by a cysteine rich domain (CRD) in the extracellular region[89]. TNF is a type II transmembrane protein that self-assembles into non-covalently bound homotrimers, and interacts with TNFR as membrane-integrated or proteolytically cleaved soluble forms[92, 93]. TNFR1 is a type I transmembrane protein with a four CRDs in the extracellular domain, a transmembrane region and an intracellular protein-protein interaction death domain (DD)[94]. The TNFR1 receptor-complex preassembles as a homotrimer of receptor chains at the plasma membrane in the absence of ligand, and ligand-independent signals are blocked through DD associations with the cytosolic negative regulator, suppressor of death domain (SODD)[95, 96]. TNF/TNFR1 interaction at the plasma membrane displaces receptor-associated SODD, and promotes the formation of intracellular signaling complexes mediated through homotypic DD interactions with DD containing adaptor molecules[96, 97]. TNFR1 association with TNF receptor-associated death domain protein (TRADD) serves as a platform for membrane proximal complex (Complex I) proteins TNF receptor-associated factor (TRAF) 2, cellular inhibitor of apoptosis proteins 1 and 2 (cIAP1 and cIAP2), and Receptor-interacting serine/threonine-protein kinase 1 (RIP1)[97-100]. RIP is then labeled with nondegradative K63-linked ubiquitin chains by cIAP1/2 ubiquitin ligase activity, which is essential for recruitment and activation of downstream signaling components[101, 102]. Specifically, the IKK-

activating complex comprised of TGF- β -activated kinase 1 (TAK1), TAK1-associated binding protein (TAB) 2 and 3, is recruited to the core TNFR1 signaling complex through ubiquitin-binding subunits of TAB2[103]. TAK1-mediated phosphorylation of the inhibition of inhibitor of κ B (I κ B) kinase complex (IKK), a heterotrimer of NF- κ B essential modulator (NEMO), IKK α and IKK γ , leads to downstream phosphorylation and subsequent proteasomal degradation of I κ B[104, 105]. I κ B keeps NF- κ B in an inactive form in the cytoplasm. Destruction of I κ B liberates NF- κ B dimers in the cytoplasm, permits its nuclear localization, and initiates the transcription of a distinct set of genes[106]. In a separate signaling module, TAK1, a mitogen associated protein (MAP) kinase kinase kinase (MAPKKK), initiates a kinase cascade through the MAP kinase kinases (MAPKK) 4 and 7, resulting in the phosphorylation and activation the MAP kinase (MAPK) c-Jun N-terminal kinase (JNK)[107, 108]. In turn, JNK phosphorylates and activates the transcription factor AP-1, and transcribes a unique set of JNK-dependent gene transcription[109].

In addition to the NF- κ B, and JNK arms of the TNF pathway, TNFR signals also initiate the formation of a spatially distinct cytoplasmic death-inducing signaling complex (DISC or Complex II) that promotes apoptosis[97, 110]. Complex II forms in the cytoplasm approximately two hours after the first TNF pathway signals are detected. In complex II formation, TRADD recruits the adaptor molecule Fas-associated protein with death domain (FADD) through homotypic DD-mediated interactions, and FADD, in turn, associates with the cysteine-aspartic protease (caspase) 8 through death-effector domains (DED)[97, 98, 110, 111]. In this manner, TNFR signals can lead to the proteolytic

processing and activation of caspase 8, and initiation of an apoptotic cascade.

In the TNF pathway, the relative activities of NF- κ B, JNK and caspase 8 signaling modules act as a fulcrum between cell-survival and -death[112]. More specifically, the engagement of NF- κ B drives the expression of NF- κ B associated-transcripts to promote prosurvival responses[113]. In direct opposition, TNF-induced activation of the caspase and JNK modules propagates proapoptotic signals, which if left unchecked by NF- κ B activities, push the cell towards apoptosis (controlled cell death)[97]. Aside from apoptosis, TNF signals are essential to guide normal immune responses, as NF- κ B activity controls many aspects of lymphocyte biology including development and differentiation[114]. For example, TNF knockout mice lack primary B cell follicles in the spleen and fail to form organized follicular dendritic cell networks and germinal centers[88]. Maturation of humoral responses in TNF knock out mice are severely impaired, and consequently these mice are sensitive to bacterial infections[88]. Abnormal TNF signals are associated with a variety of human diseases including autoimmunity, cancer, diabetes and sepsis[115-120].

1.4.2. IMD pathway.

The discovery that an *imd* mutation impairs the production of antibacterial but not antifungal peptides was the first evidence of multiple innate immune signaling pathways in *Drosophila*[41]. Further characterization of *imd*, uncovered a novel, toll-independent, immune signaling pathway specific to gram-negative bacterial infections[41]. Imd is a death-domain containing protein with homology to RIP of the mammalian TNF pathway[121]. Homozygous *imd* mutant flies display normal

immune responses to gram-positive bacteria and fungi, but are highly susceptible to gram negative bacterial challenges. Alternatively, overexpression of *imd* in flies triggers the production of AMPs in the absence of infection[121].

1.4.1.1. Activation of the IMD pathway.

Drosophila recognize bacterial PGN through members of large family of PGN recognition proteins (PGRPs)[122]. Two PGRPs, PGRP-LC and PGRP-LE synergize to relay DAP-PGN detection to the IMD pathway[86, 123-127]. The *pgrp-lc* gene encodes three alternative splice variants PGRP-LCa, PGRP-LCx and PGRP-LCy, which differ in their extracellular PGRP domains[86, 123]. Membrane bound PGRP-LCx is the primary inducer of the IMD pathway, and *pgrp-lc* mutants rapidly succumb to gram-negative bacterial infections[123]. PGRP-LCx/x homodimers predominantly recognize polymeric DAP-type PGN, while PGRP-LCa/x heterodimers bind tracheal cytotoxin (TCT), a monomeric form of DAP-type PGN. In contrast to PGRP-LC, PGRP-LE is a cytoplasmic sensor for PGN although the mechanism for IMD-pathway activation is not well understood[128]. Together PGRP-LC isoforms and PGRP-LE provide robust detection capabilities to a range of different DAP-type bacteria.

Until recently the precise mechanism of IMD pathway signal transduction was poorly understood, and the following description of IMD pathway signal transduction events represents the best model to date. Recent studies indicate that DAP-type PGN association with PGRP-LCx drives receptor oligomerization, and initiates the formation of a receptor-proximal protein complex through the DD interactions with Imd (RIP1 ortholog)[121, 129]. The death-domain of Imd

interacts with other death-domain containing proteins, including the FADD homolog, termed *Drosophila* FADD (dFADD)[130, 131]. In turn, the caspase-8 homolog Death-related ced-3/Nedd2-like protein (Dredd) interacts with dFADD through homotypic death effector domain (DED) interactions[130]. Physical interaction between Imd, dFadd, Dredd and *Drosophila* inhibitor of apoptosis 2 (dIAP2) form the foundation of an intracellular signaling complex (Figure 1.2)[129-134].

Similar to the TNF-pathway, there is mounting evidence that IMD pathway signal transduction relies on a series of cleavage and ubiquitination events. The caspase-8 homolog Dredd is a cysteine-aspartic protease and is essential for signaling events in the IMD pathway[135, 136]. Unlike caspase-8, Dredd does not promote proapoptotic signals, rather it is thought to be required for the cleavage and subsequent activation of IMD pathway components Imd and Rel. Specifically, Imd is recruited upstream, then Dredd cleaves Imd at the N-terminal caspase cleave site (LEKD) to propagate downstream signals[134]. Cleavage of Imd exposes a consensus IAP-binding motif, allowing association of Imd with the ubiquitin ligase dIAP2[134]. Ubiquitination of signaling adaptors is essential in several steps in the IMD pathway. dIAP2 ubiquitin ligase activity initiates a sequence of ubiquitination events that generate long ubiquitin chains covalently linked at lysine 63 (K63)-linked on Dredd and Imd[133, 134]. dIAP2-mediated ubiquitination networks provide a scaffold for downstream signaling molecules. For example, the ubiquitination of Imd serves as an anchoring point for the TAK1-associated binding protein 2 (Tab2)/TGF- β activated kinase 1(dTak1) complex, whereas ubiquitination of Dredd purportedly facilitates interactions with

Drosophila IKK (dIKK) complex through (Kenny) Key[133, 134]. However, physical interactions between dIKK and ubiquitinated Dredd have yet to be established. These ubiquitination events are required for propagation of downstream phosphorylation events by the mitogen associated protein (MAP) kinase kinase kinase (MAPKKK), dTAK1[134]. IMD pathway signals bifurcate at the level of dTAK1 to coordinately activate both the *Drosophila* JNK (dJNK) and Relish (NF- κ B) modules (Figure 1.3).

1.5. Rel (NF- κ B) signaling module.

The Rel arm of the IMD pathway is well characterized thanks to a number of individual studies and complementary genetic and cell culture RNA interference (RNAi) screens[137]. Rel is a member of the NF- κ B protein family with similarities to human p100/p105, and contains an N-terminal Rel homology domain (RHD) domain and a C-terminal ankyrin repeat domain[138, 139]. Two distinct posttranslational modifications are required for full Relish activation[140]. First, Rel is believed to be activated by the Dredd-dependent endoproteolytic cleavage of the N-terminal Rel-homology domain (RHD) domain from the inhibitory ankrin repeat domain at a caspase cleave site (LQHD)[140-142]. However, *in vitro* cleavage assays have largely failed to show that Dredd directly cleaves Rel, and further molecular clarification is required[136, 142]. Secondly, dTAK1 phosphorylates the dIKK complex, containing Key (mammalian IKK γ ortholog) and immune response deficient 5 (Ird5) (mammalian IKK β ortholog), which in turn phosphorylate Rel (mammalian NF- κ B p105 ortholog)[67, 141, 143, 144]. Interestingly, immune-induced Relish phosphorylation and cleavage are blocked in *ird5* mutant flies, and reconstitution of mutant flies with

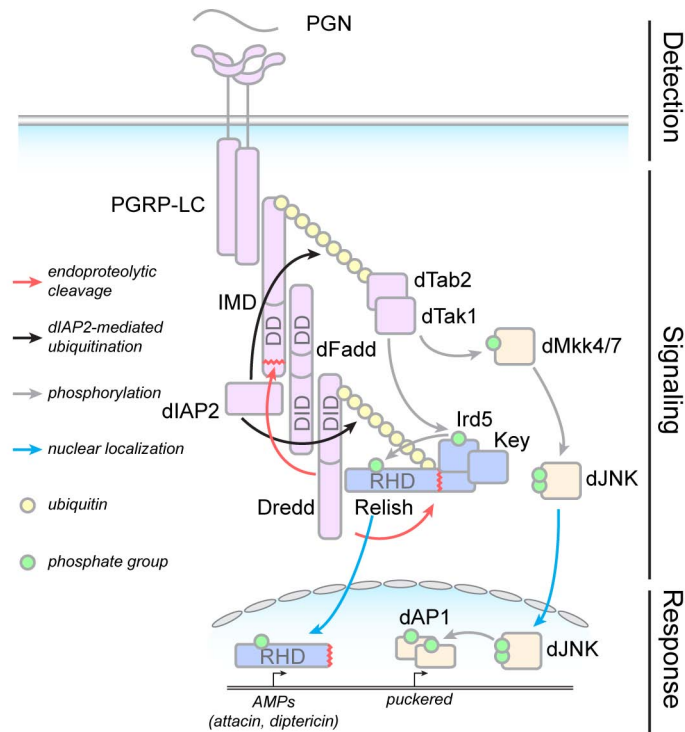


Figure 1.3. *Drosophila* IMD pathway.

Engagement of the IMD pathway begins with the detection of DAP-type PGN by PGRP-LC, and recruitment of the receptor proximal signaling complex. The IMD pathway engages dJNK, Rel and caspase modules through a series of essential phosphorylation (green circles), cleavage (red line) and ubiquitination events (yellow circle). Together these pathways coordinately regulate immune-responsive transcripts, such as the antimicrobial effector molecules *attacin* and *diphtericin*.

catalytically inactive Ird5^{K50A} restores Relish cleavage. This highlights the dual roles of the IKK complex in Rel activation, with dIKK catalytic activity required for Rel phosphorylation and a dIKK kinase-independent structural role that facilitates Rel cleavage. Once cleaved, the N-terminal RHD domain of Rel translocates to the nucleus where it binds Rel target sequence in the promoter region of Rel-dependent genes[142]. While phosphorylation is not a prerequisite for Rel cleavage, it is required for the recruitment of RNA polymerase II and expression of Rel-responsive transcripts, such as the AMP *dipt*[140].

1.6. Drosophila JNK.

The developmental requirements for dJNK and other components of the dJNK arm of the IMD pathway has hampered the study of dJNK signaling events in innate immunity[145, 146]. Relative to the Rel arm of the IMD pathway, the processes that regulate the dJNK arm are poorly understood.

1.6.1. MAPKs.

JNK is member of a large family of MAPK that also includes the extracellular signal-regulated kinases (ERK) and the stress-activated protein kinases (SAPK). MAPKs are a family of phosphotransferases that phosphorylate target proteins at key amino-acid residues affecting their biological activities by altering enzymatic activity, subcellular localization, stability and/or physical interactions. Generally, MAP kinases are activated by dual-phosphorylation at a conserved tripeptide motif (Thr-X-Tyr) in the activation loop (t-loop) domain. This phosphorylation leads to a conformational change in the MAPK structure and reveals the active site in the kinase domain.

Cells respond to physical and chemical changes in environmental conditions through continuous sensing of the intra- and extracellular milieu. Cells monitor the cellular environment for numerous factors including: growth factors, nutritional status, adhesion molecules, cellular interactions, cytokines, and microbial and toxic threats. Signals generated in response to environmental conditions often proceed through the hierarchical activation of MAPK proteins by sequential phosphorylation steps. More specifically, phosphorylation-activated MAPKKK phosphorylate and activate MAPKK, which in turn phosphorylate and activate MAPK (Figure 1.4A). These multiprotein kinase modules allow for the integration of multiple inputs from diverse receptor signals[147]. The MAPK-mediated phosphorylation of transcription factors drives the immediate expression of transcripts encoding important cellular proteins. In this manner, MAPK signaling pathways guide an array of cellular processes including differentiation, proliferation, survival and death[148].

1.6.2. Conservation of dJNK.

The JNK family of MAPKs was first identified as an activator of the transcription factor cJun in the damage response to ultraviolet (UV) radiation[149]. While absent in yeast, JNK homologs are highly conserved in nematodes, flies and mammals[150]. The human genome encodes three JNK isoforms, JNK1, JNK2 and JNK3. JNK 1 and 2 expression is ubiquitous, while dJNK 3 expression is restricted to the brain, testis and heart[151]. Amino acid sequence alignments of *Drosophila* dJNK with human JNK1 shows remarkable evolutionary conservation[145]. Approximately 80% of the amino acids in dJNK are conserved

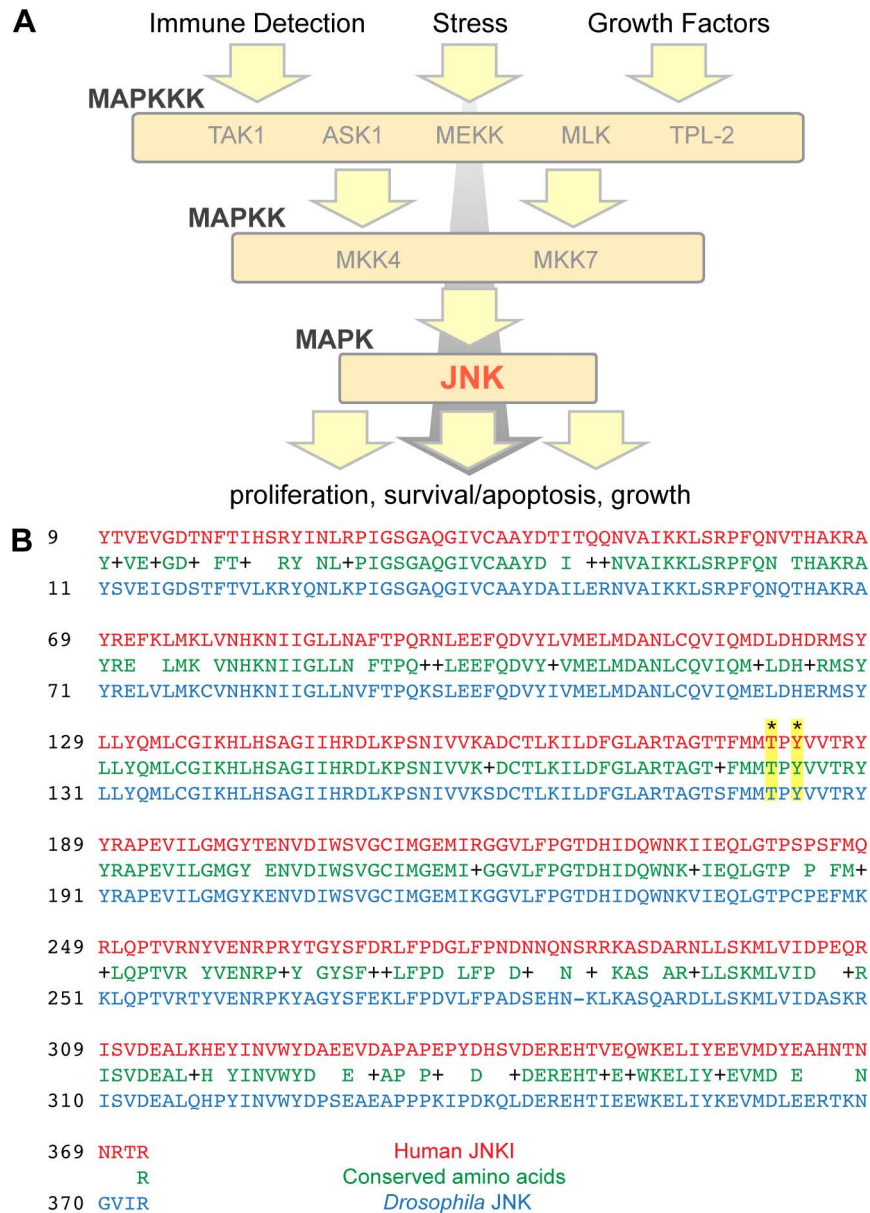


Figure 1.4. JNK/dJNK homology.

A. The human JNK kinase cascade incorporates numerous inputs from diverse environmental stimuli. The kinase cascade is amplified through the MAPK pathways and controls a multitude of biological responses. **B.** Protein sequence alignments of human JNKI (red) with *Drosophila* dJNK (blue) shows conservation of approximately 80% of the amino acids. Conserved phosphorylation sites are shown in yellow box.

in the Human JNK1 sequence (Figure 1.4B). dJNK and JNK are phosphorylated at a conserved threonine and tyrosine amino acid residues in the TXY motif by the orthologous upstream kinases dMKK4/dMMK7 and MKK4/MKK7, respectively[146]. *Drosophila* and human JNKs are so similar that anti-JNK antibodies are frequently cross-reactive to dJNK. Given the evolutionary conservation of JNK protein sequence it is no surprise the many of the functions of JNK are also conserved throughout eukaryotic biology.

1.6.3. Pleiotropic roles of JNK.

Activity of JNK-family members results in diverse cellular responses that depend on the tissue type and the length and strength of the stimulus[152]. In addition to the aforementioned roles in the TNF-signaling pathway, JNK signals also mediate a multiplicity of physiological responses such as cellular proliferation, morphogenetic movements, differentiation, survival and apoptosis[153]. JNK is vital to animal life, the loss of *jnk* in mice or *djnk* in *Drosophila* results in early embryonic death[154-157]. In humans, abnormal JNK pathway activity is associated with the development of a number of human illnesses including Alzheimer's disease, amyotrophic lateral sclerosis, and various types of cancers[148]. Therefore, understanding the regulation of JNK signaling events is paramount given its involvement in human diseases. In this regard the *Drosophila* IMD-pathway represents an important opportunity to study conserved dJNK signaling events in an evolutionary conserved signaling pathway.

1.6.4. JNK in the IMD pathway.

The IMD pathway engages a dTAK1-mediated kinase cascade through the MAP kinase kinases (MAPKKs), dMKK4/7, to ultimately phosphorylate dJNK[158, 159]. Phosphorylated dJNK (P-dJNK) typically activates the *Drosophila* AP-1 transcription factor; a heterodimer of *Drosophila* Jun (dJun) and *Drosophila* Fos (dFos)[145, 151]. AP-1 initiates the transcription of a number of gene products, such as the dual-specificity phosphatase Puckered (Puc)[160]. dJNK phosphorylation is a transient event in the IMD pathway, as P-dJNK is rapidly dephosphorylated by Puc phosphatase activity[159, 161, 162]. In this manner P-dJNK establishes a self-limiting negative feedback loop to prevent hyperactivation. The role of dJNK activity in the IMD-pathway signals remains controversial, as there are conflicting reports as to its precise function in regulating AMP levels. In certain studies dJNK positively regulates early IMD-induced AMP production, while in others dJNK negatively regulates AMP production through the inhibitory action of AP-1[163-165]. Therefore more study is clearly required to resolve these apparently contradictory findings.

1.7. Negative regulation of the IMD pathway.

Hyperactivation of immune signaling pathways can profoundly impact the fitness of an organism. In mammals, the *staphylococcus* enterotoxin B superantigen crosslinks immune cell receptors and causes a positive-feedback immune-hyperactivation that induces a potentially lethal cytokine storm, including TNF[120, 166]. Unlike mammals, hyperactive immune signals do not induce inflammation in *Drosophila*, they do however negatively impact fly fitness and lifespan. For example, female *Drosophila* laid fewer eggs when continually

inoculated with heat-killed bacteria relative to control flies inoculated with media alone[167]. However, the number of eggs laid by a *rel* mutant was unaffected by this immune-hyperactivation, indicating that elevated IMD pathway signals are detrimental to fly fecundity[167]. Furthermore, immune-hyperactivation caused a significant reduction in the life span in adult flies that carried null mutations in three established negative regulators of the IMD pathway (*poor Imd response upon knock-in (pirk)*, *pgrp-sc*, and *pgrp-lb*)[168]. The lifespan of these mutant flies was prolonged in *dredd* mutant flies, directly linking lethality to excessive IMD pathway signals[168].

To prevent the negative consequences associated with hyperactivation, IMD pathway signals are tightly regulated at many levels (Figure 1.5). In addition to the PGRPs that activate IMD and toll pathways, 6 other PGRPs scavenge bacterial PGN[168]. The catalytic activities of scavenger PGRP regulate the IMD pathway at the highest level by restricting the availability of the DAP-type PGN[168]. In the IMD pathway, PGN-responses are also controlled at the level of the PGRP-receptors by a negative feedback regulator, Pirk, first identified in a yeast two-hybrid screen looking for PGRP-LC interacting proteins[169]. Pirk is a Rel-responsive gene transcript that interacts with PGRP-LC and PGRP-LE at conserved signaling domains critical for downstream signals. This association disrupts the receptor proximal signaling complex and traffics PGRP-LC to lysosomal compartments for degradation[170].

In addition to IMD-pathway activation, ubiquitination events play significant roles in the suppression of IMD-pathway signals. RNAi-mediated depletion of

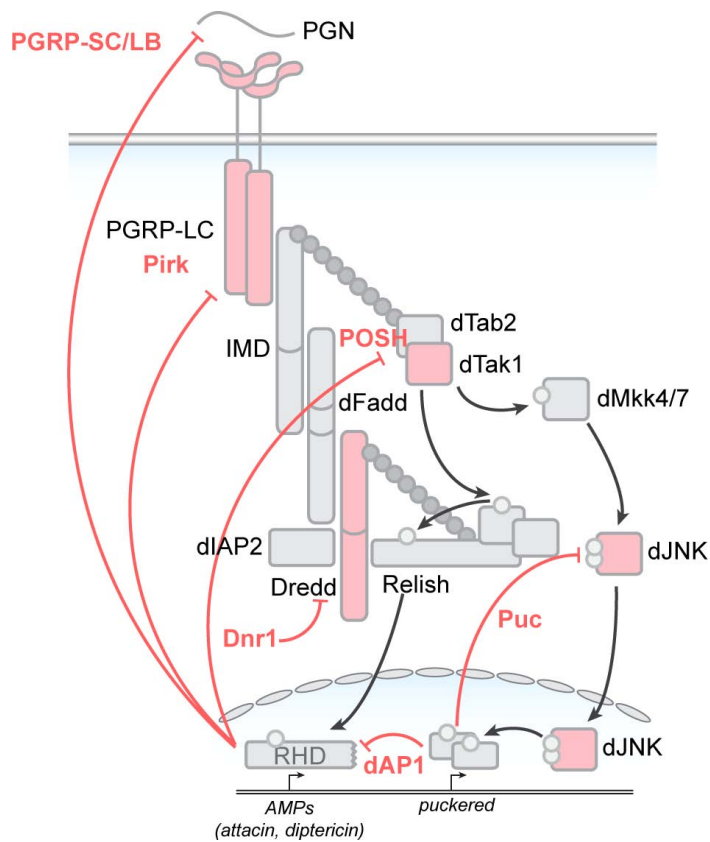


Figure 1.5. Negative regulation of the IMD pathway.

IMD pathway activity is tightly controlled at many levels to prevent pathway hyperactivation, and to maintain dynamic immune responses. Negative feedback loops ensure self-regulatory controls over pathway activation. For example, active dJNK promotes the expression of its own phosphatase, *puc*. Additionally, the dJNK and Rel arms engage negative crosstalk to provide reciprocal control mechanisms. Negatively regulated IMD pathway components are shown in red.

defense repressor 1 (dnr1) results in the constitutive expression of the IMD pathway AMP *diptericin*, even in the absence of immune challenge[137, 171]. Dnr1 contains a conserved RING domain characteristic of E3 ubiquitin ligases that targets Dredd for ubiquitin-mediated degradation[171]. The E3 ligase plenty of SH3s (POSH) is an additional example of ubiquitin/proteasome negative regulation of the IMD pathway. POSH is a Rel-dependent transcript that targets dTAK1 for proteasomal degradation, and thereby establishes a negative feedback loop that limits the duration of both dJNK and Rel activities[172]. In this manner IMD-activation of the Rel arm engages in negative crosstalk to control the JNK arm.

In turn, the dJNK module inhibits Rel-mediated transcriptional activity. Specifically, P-dJNK activation of *Drosophila* AP-1 leads to the formation of a repressosome complex that targets AP-1 binding sites in the promoter regions of certain Rel-responsive genes. For example, the repressosome complex displaces Rel from the Rel-target region in the *attacin-A* promoter, and alters chromatin structure through the recruitment of the histone deacetylase dHDAC1[165, 173]. However, it is not clear if this mechanism is conserved in other Rel-dependent gene transcripts. Together these and other negative feedback loops provide tight control over IMD-induced immune effector molecules, such as the AMPs. Much of what is known about the negative regulation of the IMD Pathway has been established through large-scale RNAi screens in *Drosophila* tissue culture. However all of these screens have focused on the Rel arm of the IMD pathway leaving the dJNK arm poorly resolved. Given the pleiotropic roles of JNK in animal biology and the lack of clarity surrounding

the regulation of dJNK in the IMD pathway, I performed a genome-wide RNAi screen to identify novel regulators dJNK phosphorylation in the IMD pathway.

1.8. RNA interference.

In their landmark paper Fire and Mellow *et al.* (1998) proposed their RNA interference (RNAi) theory in *C. elegans* revolutionizing our perception of gene regulation[40]. While the injection of anti-sense single-stranded RNA (ssRNA) was an established practice to suppress target-gene activity in *C. elegans*, Fire and Mellow *et al.*, made the observation that the introduction of double-stranded RNA dsRNA vastly enhanced target-gene suppression[40]. This work in conjunction with observations made in plants first described RNAi as a novel mechanism for post-translational gene regulation[36, 40, 174].

1.8.1. RNAi: a mechanism of gene suppression.

RNAi is a highly conserved process to regulated gene activity in metazoan biology, and research in *Drosophila* has been central in elucidating the RNAi machinery (Figure 1.6). Research in *Drosophila* was the first to identify the RNase III enzyme Dicer (Dcr) as the molecule responsible for cleavage of exogenous dsRNA molecules into small interfering RNAs (siRNA)[175, 176]. Specifically, Dicer-2 (Dcr2) in association with dsRNA binding domain (dsRBD) proteins co-factors R2D2 and LOQS-PD, recognizes exogenous dsRNA molecules and initiates siRNA biogenesis[177, 178]. The Dcr2 complex produces short double-stranded RNA duplexes of approximately 21 nucleotide (nt) base-pairs (bp) in length with a 2 nt overhang at both 3' ends[179]. The Dcr2 complex then guides the transfer of the newly generated small dsRNA duplex to

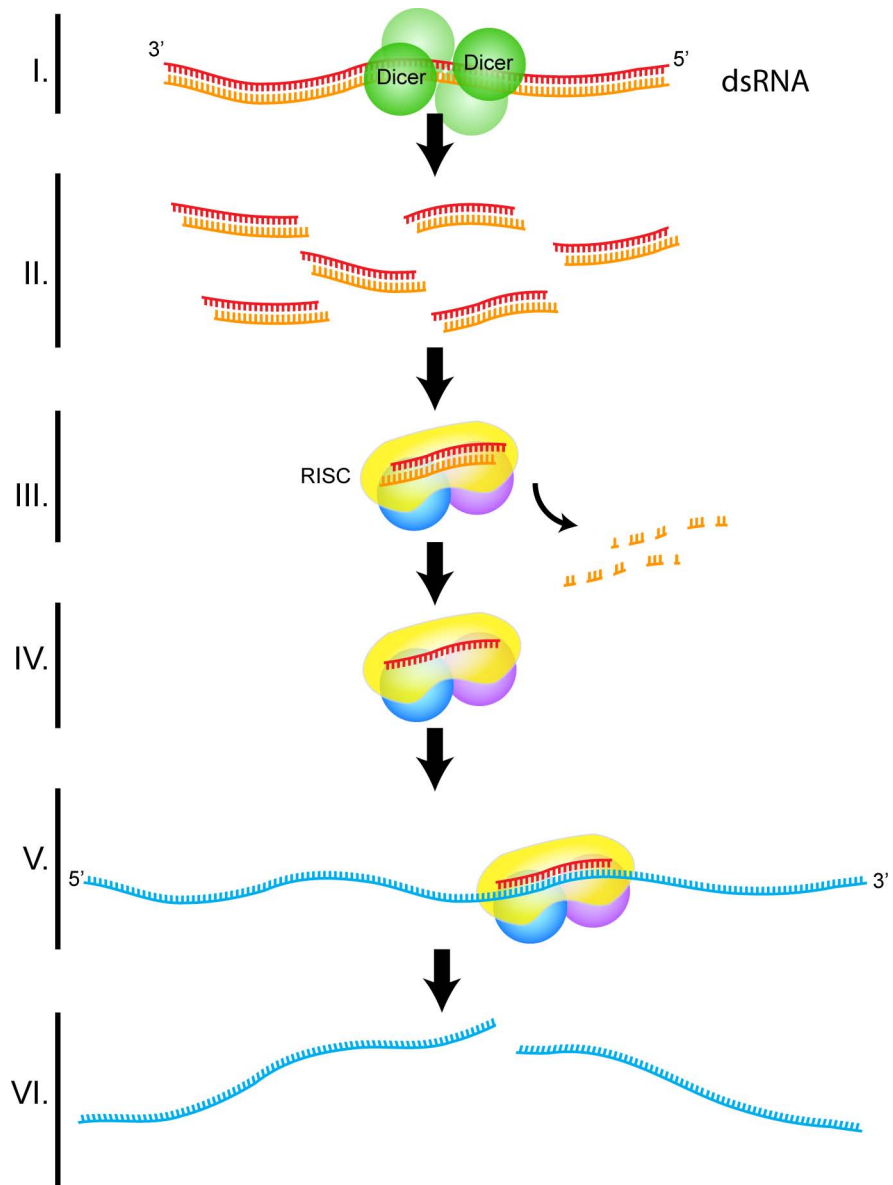


Figure 1.6. siRNA pathway.

The *Drosophila* siRNA pathway processes exogenous dsRNA to control gene activity through the following steps. **I.** Detection of dsRNA by dicer-complex. **II.** Biogenesis 21 nucleotide dsRNAs. **III.** RISC-formation and stand selection. **IV.** Formation of the mature siRNA-RISC complex. **V.** Identification of highly homologous target sequence. **IV.** Degradation of target.

Argonaute-2 (Ago2), a central component of the RNA-induced silencing complex (RISC) complex[175, 180]. The RISC complex further processes the duplexed-RNA into a guide strand that continues to associate with Ago2, while the opposing passenger strand is degraded[181]. The siRNA in association with the mature Ago-RISC complex then guides the cleavage of highly complimentary mRNA targets through the endonuclease activity of Ago2. siRNA-mediated gene silencing described above is a complex process that can be subdivided into distinct steps: dsRNA sensing, siRNA biogenesis, strand selection, loading of the RISC complex, mRNA targeting and effector function. From the perspective of my research the exogenous siRNA pathway provides a valuable tool to specifically target gene transcripts for degradation.

1.8.2. RNAi in Drosophila cell culture.

The capacity of the RNAi pathway to target specific mRNA transcripts for degradation proved to be an attractive biological mechanism for scientists to exploit. RNAi-mediated gene-silencing is now routinely used as an experimental tool both *in vitro* and *in vivo* in a variety of model organisms[56, 182, 183]. Many *Drosophila* tissue culture cells offer an ideal setting for RNAi experiments, and provide distinct advantages over mammalian tissue culture systems. For example, *Drosophila* macrophage-like S2 cells actively uptake long dsRNA molecules (200-800bp) through scavenger-receptor mediated endocytosis, unlike mammalian tissue culture cells, which require transfection-mediated delivery of interfering RNAs[184-186]. Furthermore, dsRNA endocytosis in *Drosophila* macrophage-like S2 cells is a highly efficient process as approximately 95% of cells take up dsRNA molecules with no appreciable effect on other cellular

pathways[186]. By contrast, in mammalian cells long dsRNAs mimic viral infection and consequently engages innate immune defense mechanisms, seriously confounding experimental conclusions[187-190]. In S2 cells, endocytosed dsRNAs naturally enter the siRNA pathway and are processed by cellular machinery to generate diverse array of siRNAs. This vast pool of target-specific siRNAs efficiently knocks-down target gene levels with few off target effects, as potentially cross-reactive siRNA are present at very low concentration, although evidence of off-target effects exists[175, 191]. In mammalian systems off target effects are a much greater concern, and complex algorithms are required to predict optimal siRNA sequences with minimal off-target effects[192-194]. Despite the sophistication of the design algorithms, many siRNAs still fail to deplete the target protein in mammalian cells. Relative to mammals, *Drosophila* is a much simpler genetic model with fewer instances of gene duplication and redundant gene function[43]. Therefore, RNAi knockdown of a target gene in *Drosophila* culture better represents the mutant phenotype. Finally, long dsRNA molecules are easily produced by standard laboratory techniques at low cost. As a consequence large-scale dsRNA libraries have been constructed that cover most, if not all of the *Drosophila* genome[137, 195-198].

1.8.3. Genome-wide RNAi screens in *Drosophila*.

The enormous potential of RNAi to identify previously unknown components of biological pathways was quickly recognized. The sequencing of the *Drosophila* genome in 2000 helped illuminate the *Drosophila* gene set, and thus guided the construction whole genome RNAi libraries[43, 137, 195]. In addition to *Drosophila*, large-scale RNAi libraries are now available for a number of model

systems including human and mouse[199-201]. The distinct benefits associated with RNAi studies in *Drosophila* described previously, are particularly advantageous on the whole genome scale. In the past decade, RNAi screens in *Drosophila* tissue culture have become a common method to identify novel regulators in a variety of biological processes[126, 195, 196, 202]. The results of these RNAi screens has lead to significant discoveries in a wide range of fields, including signal transduction, cell biology, and pathogen-host interactions[203].

1.8.4. RNAi screens of the IMD pathway.

Genome-scale RNAi screens are ideal discovery tools to quickly and easily search for novel components of cell signaling pathways. Not surprisingly, these screens have been instrumental in the identification of numerous regulators of the *Drosophila* IMD pathway[137, 204-206]. The NF- κ B (Rel) arm of the IMD pathway has been the focus of many large-scale RNAi screens, resulting in a comprehensive understanding of the genetic factors that control the innate immune responses to gram negative bacterial infection[137, 204-207]. All of these RNAi screens have relied upon gene reporter assay as an indirect measure of IMD-pathway activity. The first large scale-RNAi screen of the *Drosophila* IMD pathway, relied upon the visualization of *dipt-lacZ* induction in S2 cells treated 7216 individual dsRNAs and exposed to a crude preparation of LPS with contaminating amounts of PGN[137]. More specifically, the β -galactosidase (*lacZ*) gene under the control of the IMD pathway responsive *dipterocin* promoter (*dipt-lacZ*) allowed for quantitative evaluation of RNAi effects on PGN-induced Rel activity. In addition to finding established IMD pathway members, this screen identified numerous novel regulators of Rel activity that control various aspects of

IMD pathway signal transduction. Notably, the gene *sickie* was identified as essential for optimal Relish-activity, while the gene *dnr1* was identified as a novel inhibitor of Dredd[137]. Subsequent RNAi screens of the IMD pathway employed *luciferase* as a reporter to quantify Rel activity relative to an internal control. While these screen all targeted modifiers of AMP production in the IMD pathway there was little overlap of screen results, likely as consequence of significant differences in their experimental approaches. Furthermore, this may have been an intrinsic property of screens with high false negative rates; where moderate modifiers of IMD pathway signaling were disregarded in favor of a low false positive rate. Taken together these screens offered unprecedented insight into the factors that control immune-induced Rel activity in the IMD-pathway. Despite extensive research into the controls of the Rel arm of the IMD-pathway the factors that regulate the dJNK arm activity remained poorly resolved.

1.8.4.1. *In vivo* RNAi screens.

The availability of large-scale RNAi collections of transgenic flies has facilitated whole-genome RNAi screens *in vivo*. While *in vivo* RNAi screens are still in their infancy, many facets of *Drosophila* biology have been targeted including cardiac development, wound closure, and immunity[208-210]. As *Drosophila* has an unequalled pedigree as a premier model organism in innate immunity, it is no surprise that an *in vivo* RNAi screen would target immune signaling pathways. In a recent whole-genome screen, UAS-RNAi lines were monitored for susceptibility or resistance to oral infection with *Serratia marcescens*[210]. This screen identified genes essential for antibacterial host defenses in the gut including *key*, *dfadd* and *dredd*, as well as pathways involved

in the maintenance of intestinal homeostasis, including the JAK/STAT pathway. These data highlight the importance of intestinal immune response pathways for survival to pathogenic microbes.

1.9. Intestinal Immunity.

The alimentary canal in bilateral animals is a series of organs that play essential roles in the mechanical breakdown, enzymatic digestion, and absorption of nutrients from food. During animal embryonic development, invaginations in the outer epithelium (ectoderm) internalize and become the endodermal epithelium that lines the alimentary tract[211]. The alimentary tract is compartmentalized into different organs based on physical features and biological functions. In mammals the small intestine forms principle place of enzymatic digestion and nutrient absorption, and therefore has an expansive surface area maximized through microscopic fingerlike projections termed villi.

The requirement for the gut to absorb nutrients is juxtaposed with the requirement to maintain an impermeable physical barrier between the sensitive internal milieu, and a potentially pathogenic/toxic luminal environment. Additionally, heterogeneous communities of commensal bacteria populate the intestinal tracts of mammals and *Drosophila* alike[212, 213]. These gut-associated bacteria evolved alongside their hosts in a complex reciprocal relationship, and assist in the metabolism of nutrients, modulation of immune responses, and defense against pathogenic microbes[214, 215]. Failure to maintain the intestinal barrier can lead to intestinal infarction, sepsis and death[216]. Intestinal tissue is therefore rapidly renewed with the intestinal

epithelium completely replaced every 2–3 and 3–5 days in mice and humans, respectively[217].

The intestinal immune response of mammals is extraordinarily complex, as the immune cells of the gut encounter more antigen than any other part of the body, and must discriminate between potentially hazardous invasive microbes and harmless antigens or microbes[218]. This is accomplished in mammals through the coordinate efforts of adaptive and innate immune responses[219, 220]. The gut is prone to a number of immune associated diseases as a consequence of its constant association with immune activating microbial agents. For example, breakdown of intestinal homeostasis not only leads to inflammatory diseases such as Crohn's disease and ulcerative colitis, but can also contribute to autoimmune diseases like type 1 diabetes and asthma[221, 222].

Initially, inflammatory diseases were thought to be mediated primarily through adaptive immune response, but recent research in mice has shown that the innate immune pathways significantly contribute to the progression of intestinal diseases, such as inflammatory bowel disease. More specially, engagement of PRRs, such as TLRs and NOD1 and 2 receptors on intestinal epithelial cells communicate changes in the intestinal microflora to the underlying cells of the innate and adaptive immune responses[223, 224]. NF- κ B signals are central to this communication network in the intestinal epithelium, and suppression of these signals can lead to immune responses associated with inflammatory bowel disease[225, 226]. For example, mice with a conditional mutation in the NF- κ B pathway component, NEMO, spontaneously develop colitis[227]. *Drosophila* lack

adaptive immune responses, and are therefore well positioned to directly study the contribution of innate immune responses in the control of intestinal homeostasis.

1.9.1. *Drosophila* intestinal immunity.

Drosophila thrives in the putrid environments of decomposing fruit, completely immersed in bacteria and fungi. Not surprisingly, *Drosophila* has evolved robust immune responses to intestinal pathogens[228]. The *Drosophila* intestinal immune response is tightly tempered to permit colonization by commensal bacteria, while simultaneously guarding against invasive pathogens[168, 229]. The *Drosophila* gut uses an arsenal of physical and chemical defenses to ward off microbial pathogens. The *Drosophila* gut engages in antimicrobial chemical warfare through coordinated activities of immune-induced AMPs and ROS[22, 23]. Immune-induced activation of the IMD pathway is essential for AMP production in the gut, and its activities are tightly regulated to prevent reaction to commensal bacterial populations[168, 170, 229, 230]. During infection, the intestinal epithelium is often damaged through the combined activities of microbial pathogenesis and bystander effects of immune induced ROS production[16, 18, 19]. Therefore, stem cells in the gut are essential for the replacement of dead or dying mature epithelial cells and the maintenance of epithelial integrity.

Infection-induced intestinal damage drives a massive turnover in adult epithelial cells that are replenished through proliferation, and differentiation of intestinal stem cells (ISCs). The recent discovery of stem cells in the posterior

midgut of adult *Drosophila melanogaster* presents a remarkable system to explore factors that regulate stem cell homeostasis[17, 231]. This is due to the unequalled genetic tractability of the *Drosophila* model, and the overarching similarities between *Drosophila* and mammalian intestinal cell types, morphology, developmental patterning and signaling interactions[232-234].

1.9.2. Physiology of the *Drosophila* gut.

The *Drosophila* adult gut serves as an essential interface between the internal milieu and a potentially pathogenic microbial environment. Like the mammalian gut, the *Drosophila* gut is composed of conspicuous morphological regions distinguished by physical appearance, functional characteristics and cellular composition[235]. The *Drosophila* gut, like other insects, is broken down into three main sections: foregut, midgut and hindgut. Within the midgut lies the peritrophic membrane, a thin layer of chitin and glycoprotein that extends the length of the gut lumen. The peritrophic membrane is thought to protect the sensitive gut epithelial cells from abrasive food particle and infectious microbes[236, 237]. The midgut is the primary site of digestion and nutrient adsorption and makes up the majority of the intestinal tract by length[235]. The midgut is further subdivided into physiological regions: anterior midgut, stomach and posterior midgut. The posterior midgut is considered the functional equivalent of the mammalian small intestine and is the primary site of nutrient absorption. The recent discovery of stem cells in the *Drosophila* posterior midgut has resulted in a flurry of research activity[17-19, 231, 238-240].

1.9.2.1. Cellular architecture of the posterior midgut.

The adult *Drosophila* posterior midgut is essentially a simple epithelial monolayer that is renewed through the proliferation and differentiation of ISCs. Posterior midgut ISCs lie in close contact with the underlying basal lamina established by a meshwork of visceral muscle (VM) cells[17, 235]. ISCs self-renew by mitosis and differentiate into non-proliferative, undifferentiated enteroblasts (EBs). EBs are non-dividing intermediate cells, that differentiate into mature epithelial enterocytes (ECs) or secretory enteroendocrine cells (EEs)[234]. Large, polyploid ECs are the predominant terminally differentiated cell type in the gut and overlie the ISC/EBs to form a continuous intestinal epithelial monolayer through which nutrients are absorbed. Secretory EEs are found interspersed throughout the intestinal epithelium and are primarily concerned with secretion of regulatory peptides (Figure 1.7).

1.9.3. Stem cells.

Stem cells are undifferentiated, proliferatively competent cells that provide a constant source of mature cell types essential for normal tissue growth and maintenance[241]. In adult tissues, somatic stem cells replace a multitude of terminally differentiated cells and expand in response to extrinsic cues to confer plasticity on organ size and cell numbers[241]. Stem cell homeostasis is maintained through a delicate balance of stem cell-intrinsic and extrinsic signals that orchestrate proliferation and/or differentiation in response to tissue requirements[232]. When regulatory systems that control stem cell homeostasis fail, impaired tissue function and organ failure result. In the extreme, breakdown of stem cell proliferative controls can lead to aberrant mitosis and the

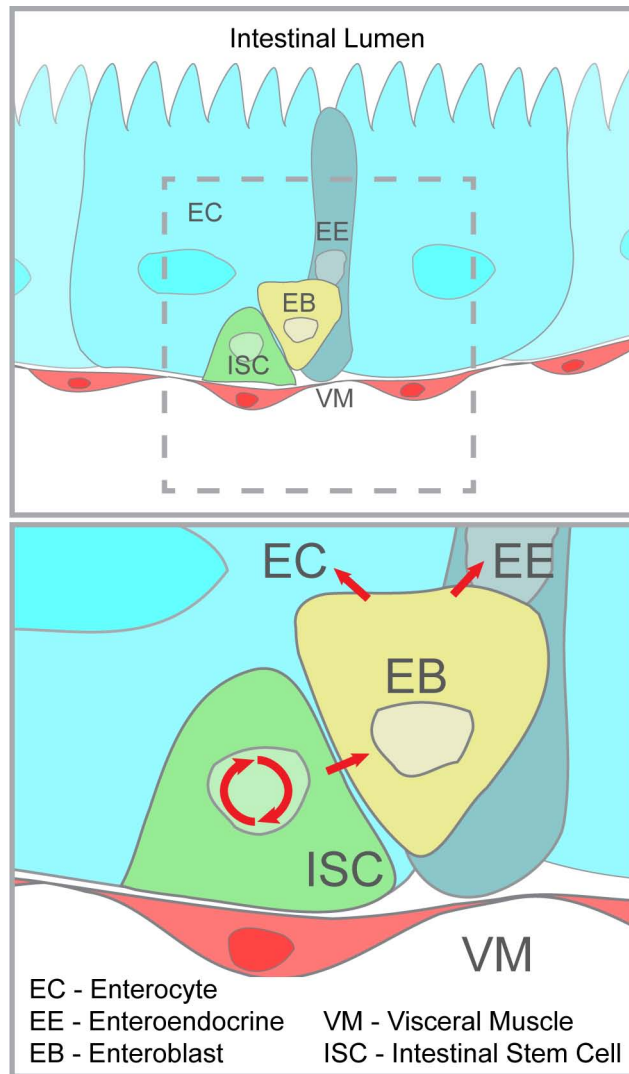


Figure 1.7. Posterior midgut cells.

The posterior midgut is composed ISC (green) that can divide or differentiate into EBs (yellow). EBs are nondividing, pluripotent cells that differentiate in the mature epithelial cells ECs (light blue) or the secretory EEs (dark blue). ISCs are basally located and lie in close contact with a meshwork of VMs (red).

development of cancers[242]. Stem cells and cancers share striking similarities, in that both are pluripotent and have exceptional proliferative potential[241]. Therefore, unraveling the complex signaling networks that control stem cell homeostasis not only aids our comprehension of normal tissue growth and repair, but can also profoundly impact our understanding of cancer development and progression.

1.9.3.1. Posterior midgut ISCs.

ISCs in the posterior midgut follow a predictable differentiation program to replace mature intestinal cell types. Upon ISC division, asymmetric Delta (DI) expression directs differential Notch (N) signals between the newly formed ISC/EB equivalence group to establish developmental fate through lateral inhibition (Figure 1.8)[231, 238]. The basally located DI positive daughter cell within the niche retains stem cell identity, while the opposing N positive daughter cell differentiates into an EB[17, 238]. The intensity of N signals continues to control EB fate decisions, as high N signals in EBs drive differentiation into mature ECs, while low N signals promote the EE cell fate[243, 244].

1.9.4. Drosophila posterior midgut homeostasis.

The developmental architecture discussed above adequately describes the controls that ensure orderly replenishment of dead epithelial cells under steady-state conditions. However, a true genetic evaluation of intestinal integrity must appreciate the intestines as a major interface between an animal and its environment, with intestines continuously exposed to a revolving and unpredictable carousel of pathogenic microbes and toxic molecules. Therefore,

modifiable proliferative mechanisms are crucial to ensure epithelial integrity after the ingestion of cytotoxic agents or enteric pathogens. Not surprisingly, *Drosophila* ISCs use intricate and partially overlapping cell signaling networks that integrate cell-intrinsic and extrinsic cues to coordinate tissue homeostasis and maintain midgut epithelial integrity (Figure 1.8)[245].

1.9.4.1. Posterior midgut equilibrium.

In the absence of extrinsic challenges, ISC turnover proceeds slowly. The rate of ISC turnover in females is twice that of males, completely regenerating the midgut epithelium in approximately two to three weeks[18]. Over the lifespan of the fly the gut epithelium is exchanged upwards of four times in females and twice in males. The steady replacement of dying ECs emphasizes the need for intrinsic developmental mechanisms that maintain intestinal integrity and function[18]. Several ISC-intrinsic signaling pathways have been implicated in the maintenance of ISC homeostasis under unstressed conditions, including the Insulin Receptor (InR), epidermal growth factor receptor (EGFR), and Yorkie/Warts pathway[240, 246-250]. Basal activity of EGFR and InR receptor tyrosine kinase (RTK) pathways are essential for the steady-state turnover of ISCs, although extrinsic cues feed into these pathways to enhance ISC proliferation in response to infection or damage[213, 240, 251, 252]. In this manner, EGFR signals bridge extrinsic and intrinsic cues to regulate gut tissue homeostasis in response to local and systemic conditions[248, 253]. In addition to EGFR, the RTK PDGF and VEGF-receptor related (Pvr) has recently been implicated maintenance of posterior midgut physiology.

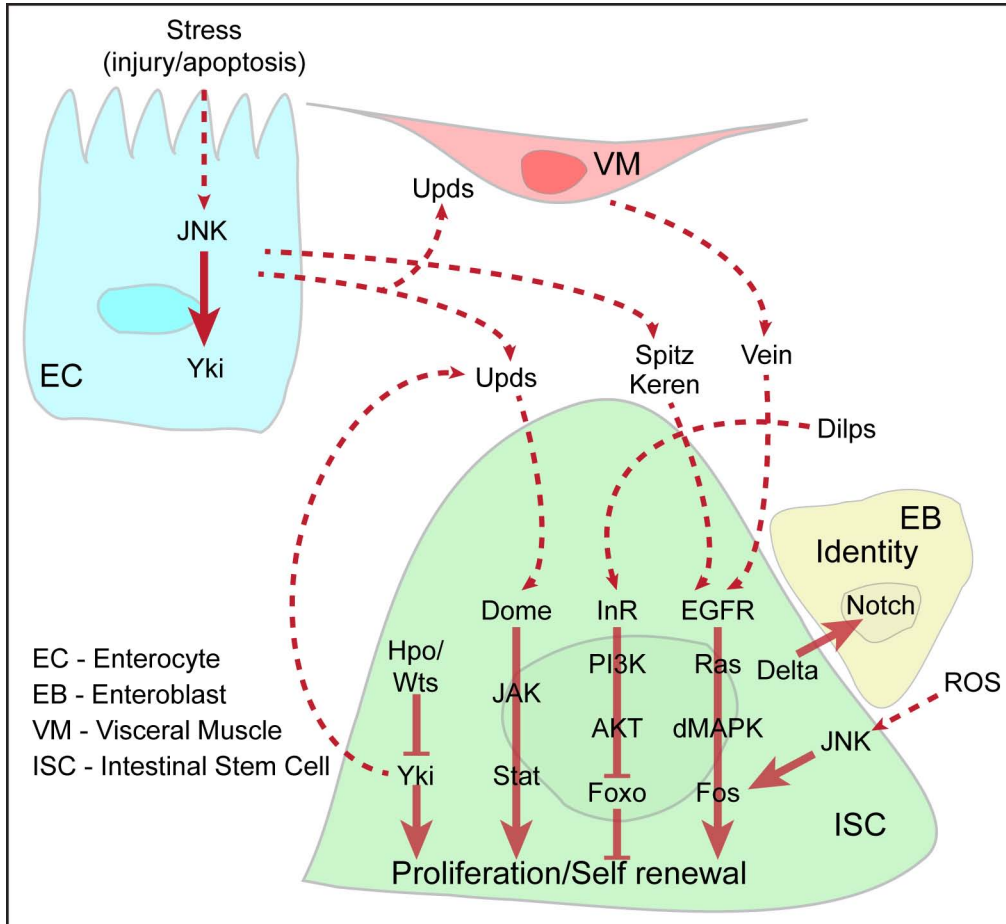


Figure 1.8. Controls of ISC proliferation and differentiation.

Drosophila ISCs incorporate endogenous and exogenous signals to coordinate cellular proliferation and differentiation to maintain gut homeostasis. (Adapted from Biteau *et al.* 2011[232])

1.9.4.2. Midgut response to damage/infection

Exposure to cytotoxic or infectious agents, such as the pathogenic bacterium *Pseudomonas entomophila* (*Pe*), rapidly increases ISC mitoses by 10-100 fold to replace dead and dying epithelial cells[18, 254]. Oral infection of adult flies with low doses of *Pe* results in a rapid expansion of progenitor cells, while high doses of *Pe* damages the intestinal epithelium and kills the host within 1-2 days[15, 255]. Proliferative responses are largely initiated by activation of ISC-extrinsic pathways, such as Jak/Stat, dJNK, and Yorkie/Warts[16, 18, 245-247, 251, 253]. For example, cytotoxic and infectious agents that stress or damage ECs induce the expression of numerous cytokines and growth factors, such as the interleukin-like cytokine Unpaired (Upd) and the EGF-like ligands (Keren and spitz)[18, 248, 253, 256]. Combined, these factors engage their cognate receptor on ISCs to promote JAK/STAT and EGFR pathways, respectively. These extrinsic signals are then integrated in the ISCs to orchestrate appropriate proliferative and differentiation mechanisms[245, 251].

1.9.5. Conservation of *Drosophila* and human homeostatic controls.

Like *Drosophila*, the epithelial cells of the mammalian small intestines undergo dynamic cell turnover mediated by long-lived stem cells[257]. However, the mammalian small intestine is structurally more complex than the simple intestinal epithelial monolayer of *Drosophila* and contains a carpet of finger-like projections that point into the lumen called villi. In addition to the terminally differentiated ECs and EEs found in *Drosophila*, the mammalian villi also contain goblet, and Paneth cells[258]. Crypts at the base of the villi harbor stem cells that generate transient-amplifying cells that undergo rapid cycling until they reach the

crypt-villus junction, where they differentiate into any of the four mature cell types.

The presence of stem cells in the mammalian small intestine remained controversial until the discovery of the Wnt target gene leucine-rich-repeat-containing G-protein-coupled receptor 5 (Lgr5) provided a powerful stem cell marker[259]. However, Lgr5 does not mark the entire ISC population, and the targeted depletion of Lgr5 positive ISCs does not perturb homeostasis of the intestinal epithelium[260]. Like the *Drosophila* posterior midgut ISCs, stem-cell intrinsic signals tightly control mammalian ISC proliferation and identity, and breakdown of these regulatory pathways leads to severe diseases such as cancer[261, 262]. Despite the increased complexity of the mammalian intestine many core homeostatic signaling networks are conserved between *Drosophila* and mammals. The following examples highlight the biologically conserved roles of core JNK/Notch/Wnt signaling pathways in intestinal morphogenesis and homeostasis in *Drosophila* and humans. JNK signals in mammals regulates ISC proliferation and are associated with intestinal cancers in an inflammation-induced colon cancer model in mice[263], while hyperactivation of dJNK signals in *Drosophila* ISCs results in profound intestinal dysplasia[19, 263]. Therefore, the roles of the JNK signaling pathway in controlling intestinal homeostasis appears to be a widely conserved phenomenon[232]. Notch signals are required in the crypts of the mammalian small intestine in order to maintain cells in an undifferentiated, proliferatively competent state. Hyperactivation of Notch signals in the mouse villus drives progenitor cell proliferation, and prevents differentiation in the mature goblet and EE cell types[262, 264]. In *Drosophila*, Dl expression on ISCs establishes asymmetric Notch signals in EBs and directs cellular

developmental fates[17, 231]. Like mammals, *Drosophila* Notch signals in the posterior midgut controls midgut progenitor cell numbers, and differentiation towards mature ECs cell types[17, 231, 238]. Finally, genetic studies in mice identified Wnt signals as a driving force in the regulation of intestinal tissue[265]. Loss of Wnt pathway positive effectors Tcf4 or β -catenin reduces cellular proliferation, resulting in the depletion of the transient amplifying cell population, and the disappearance of the crypt progenitor compartment. In contrast, Wnt pathway hyperactivation drives over-proliferation in the intestinal crypts[265-267]. In contrast, abrogation of Wnt signals in the *Drosophila* posterior midgut ISCs has a less pronounced phenotype, as Wnt pathway mutants show a mild reduction in ISC cell numbers and proliferation[239]. Hyperactivation of Wnt signals through the overexpression of Wnt pathway ligand wingless (wg) result in an accumulation of posterior midgut progenitor cells[239]. While the biological consequences of these signaling pathways may vary between *Drosophila* and mammals, their evolutionarily conserved requirement in the maintenance of intestinal homeostasis is nevertheless remarkable. Due to this conservation, the *Drosophila* posterior midgut provides a unique opportunity to study otherwise inaccessible signaling pathways in mammalian ISCs. For example Pvr, is an ancestrally conserved receptor tyrosine kinase that control aspects of *Drosophila* gut biology, as will be discussed below.

1.10 Pvr.

Pvr is a member of the RTK superfamily conserved throughout the animal kingdom[268]. This family of RTKs is characterized by long-extracellular immunoglobulin-like (Ig) domains, a single-span transmembrane domain, and an

intracellular split tyrosine kinase domain (Figure 1.9A)[269]. In humans this group is divided into subfamilies that include the Platelet Derived Growth Factor Receptor (PDGFR) and Vascular Endothelial Growth Factor Receptor (VEGFR), from where Pvr derives its name[270]. A BLASTp search of the human proteome with *Drosophila* Pvr protein sequence reveals that PDGFR- α has the highest degree of sequence homology with 39% identity. However, the seven extracellular Ig-domains of Pvr shares the greatest structural similarity with the VEGFRs, in contrast to the five Ig-domains present in PDGFRs[271]. Pvr therefore appears to share features with both VEGFR and PDGFR subfamilies and may represent an ancestrally derived RTK[272]. Pvr appears to be the sole representative of the PDGF/VEGF-receptor superfamily, as no other homologs are evident in the *Drosophila* genome. Pvr is engaged by PDGF- and VEGF-related factors (Pvfs) 1, 2 and 3 to initiate intracellular signaling cascades that instruct activities such as morphogenetic cell migrations, embryonic hemocyte development, and epithelial closure[270, 271, 273-280].

1.10.1. *Drosophila* Pvfs.

As the names implies, *Drosophila* Pvfs are distantly related homologs of human VEGF and PDGF. *Drosophila* Pvfs share common domain architectures, that include a PDGF/VEGF domain, a cysteine-rich domain, a transmembrane region, and a signal peptide sequence (Figure 1.9B)[271]. The core PDGF/VEGF growth factor domain is required for receptor binding and activation, and therefore is conserved in all mammalian VEGFs, PDGFs and *Drosophila* Pvfs[268]. Also conserved between mammals and *Drosophila*, is the short N-terminal signal peptide sequence that directs newly synthesized proteins toward

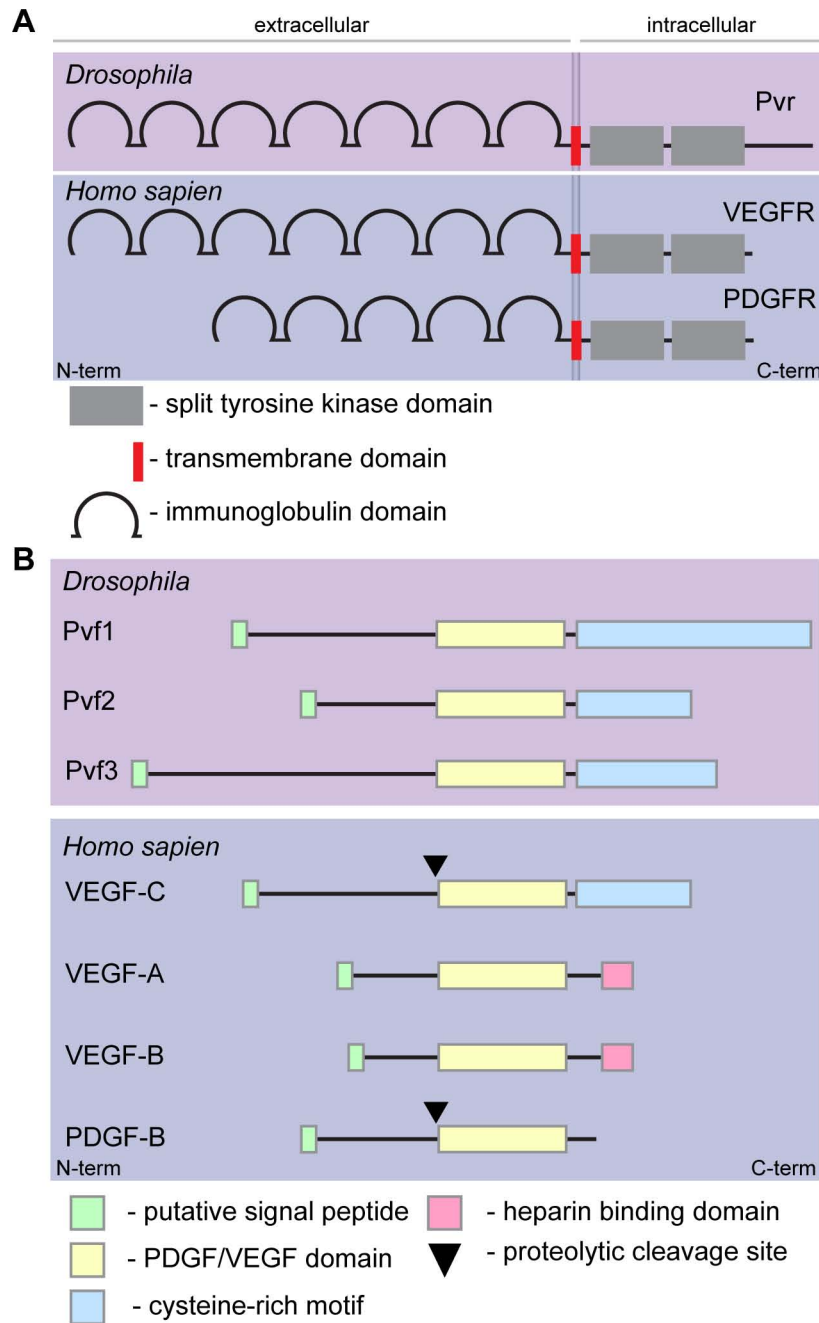


Figure 1.9. Structural homology of *Drosophila* Pvr/Pvfs.

A. *Drosophila* Pvr (top panel) shares conserved features of both the VEGF- and PDGF receptor family (bottom panel). Pvr and VEGFR/PDGFRs share a homologous, intracellular, split tyrosine kinase domain. However, only Pvr and VEGFRs have seven extracellular Ig-domains. **B.** *Drosophila* Pvfs 1, 2 and 3 (top panel) shares conserved features of both the VEGF and PDGF family members (bottom panel). All Pvfs and VEGF/PDGFRs share a homologous PDGF/VEGF domain. However, only Pvfs and VEGF-C contain a cysteine rich domain.

the secretory pathway. There are however distinct structural differences between Pvfs, VEGFs and PDGFs. For example, many VEGF/PDGF members contain peptide cleavage sites, where proteases liberate growth factor domains from the N-terminal membrane anchor; however no such cleavage sites are obvious in the Pvfs. Although *in vitro* evidence from S2 cells suggests that Pvfs are secreted into the tissue culture medium, the precise mechanism for Pvf maturation and cleavage remains unknown[270]. Other aspects of Pvfs more closely resemble VEGFs, such as a shared c-terminal cysteine-rich domain, absent in the PDGFs. These similarities have led to the assertion that the Pvf/PVR pathway is more closely related to VEGF/VEGFR. Pvfs likely homodimerize, as their individual expression patterns appears largely non-overlapping, although it remains unknown if Pvfs form heterodimers[271].

1.10.2. Human PDGF- and VEGF-pathway etiology.

PDGF- and VEGF-pathways control a vast array of cellular activity in mammalian biology including migration, survival, differentiation and proliferation. These pathways play essential roles in development, adult physiology and pathology. Misappropriated VEGFR/PDGFR pathway signals can have disastrous implication on animal survival and can lead to developmental defects and multiple disease pathologies especially cancers. The human VEGF-subfamily family is comprised of five related growth factors (VEGF A, B, C, D and placental growth factor) that form both homo- and heterodimeric polypeptides *in vivo*, however there is little solid evidence for the existence of many heterodimer variants[281]. These growth factors drive receptor dimerization of three established VEGFRs (VEGFR A, B, C), to engage intracellular signals[281]. The

PDGF-subfamily displays similar complexity, with four PDGF growth factors (PDGF A, B, C, D) that engage two PDGFRs (PDGFR- α , and PDGFR- β)[268]. This variation adds depth to possible combinations and permutations of receptor-ligand interactions. This remarkable diversity of PDGF- and VEGF-pathway family members makes the study of these pathways challenging *in vivo*. As a consequence, VEGFs and PDGFs have been extensively characterized in cell culture-based assays. However, *in vitro* tissue culture-based assays cannot fully model the biological complexities of PDGF- VEGF-pathway activities. The *Drosophila* PVR pathway therefore provides an ideal *in vivo* environment to model these conserved signaling pathways.

1.10.3. Pvr biology.

In a gain-of-function genetic screen for border cell migration in *Drosophila* embryos, *pvf1* misexpression significantly abolished cellular protrusions and directed cell movements[282]. The search for the Pvf1 receptor identified Pvr based on the prediction that Pvf1 would engage a PDGFR-related receptor[270]. Consistent with other guidance receptors, polarized Pvr activity is required to guide cell movements[270]. In addition to border cell migration, Pvr also contributes to morphogenetic movement events in organogenesis. For example, the Pvr/Pvf axis guides migration of the developing salivary gland during *Drosophila* embryogenesis[283].

In addition to morphogenetic movements Pvr is also critical for cellular movements in the closure of epithelial wounds in larval stages. Loss of Pvf1/Pvr signals in the larval epithelium results in the failure to heal wounds, characterized

by a gap free of nuclei in the epidermal sheet[278]. Mechanistically, Pvf1 in the hemolymph promotes wound closure through engagement of Pvr-mediated chemotactic signals in the wound-edge epithelial cells[278]. The maintenance of epithelial barriers is a vital aspect of innate immune defenses to hostile external environments.

Pvr is expressed early in embryonic hemocyte development and loss of Pvr produces large hemocytes clusters in the head mesoderm and severe blood cell migration defects[271]. Null mutations in *pvr* are embryonic lethal and show defects in central nervous system patterning due the loss of hemocyte-mediated sculpting of embryonic tissue during development[284]. Interestingly, inhibition of blood cell apoptosis with hemocyte-specific expression of the pan-caspase inhibitor p35 rescues the embryonic lethality of *pvr* mutants. These data suggest that *pvr* may also play a critical role in hemocyte survival[277]. In larval stages, hyperactivation of the PVR pathway significantly elevates hemocyte numbers[277, 285]. This increase is attributed to enhanced hemocyte proliferation rather than survival[274]. Furthermore, uncontrolled Pvr pathway activity in larval hemocyte progenitors alters the developmental program from plasmatocytes to lamellocytes[285]. Collectively these data suggest that *pvr* is essential for many aspects of hemocyte cellular activities including migration, survival, proliferation, and differentiation.

1.10.4. PVR pathway signals.

Despite the importance of the PVR pathway in *Drosophila* biology the biochemical mechanism of Pvr activation and the effector molecule engaged

through downstream signaling events remains poorly resolved. This is in part because downstream pathway components triggered by Pvr signals are highly contextualized to specific tissues and developmental stages.

1.10.4.1. Initiation of RTK signals.

While the precise mechanism of Pvr activation has not been established, we can make predictions based on consensus models set by other RTKs in the PDGF/VEGF superfamily[286-288]. Specifically, a bivalent ligand associates with two RTK molecules to drive receptor dimerization and conformational changes within the intracellular kinase domains[286, 289-291]. These conformational changes expose an ATP-binding site[286, 292, 293]. ATP then binds and promotes auto- and trans-phosphorylation events at tyrosine residues in the receptor dimer or in downstream effector molecules[286, 294, 295]. Phosphorylated tyrosine residues in the intracellular receptor domain act as docking sites for downstream mediators of signal transduction[296, 297]. The engagement of Pvr signals is likely analogous to the aforementioned prototypical RTK activation model. Expression of a constitutively active Pvr (Pvr^{CA}), generated by replacing the extracellular Ig-domain of Pvr with the dimerization domain of bacteriophage λ cI repressor, forces oligomerization of intracellular kinase domains and triggers constitutive activation of downstream molecules, such as *Drosophila* extracellular signal-regulated kinase (dERK)[270, 298]. In contrast, removal of the Pvr intracellular signaling domain produces a dominant negative Pvr (Pvr^{DN}). While ligand-receptor interactions are normal, the loss of the intracellular kinase domains prevents downstream Pvr signals[270]. Ultimately, Pvr^{DN} sequesters the Pvf ligands and prevents endogenous Pvf/Pvr

signals. Together these data support the hypothesis that Pvr oligomerization is essential for initiation of downstream signaling cascades.

1.10.4.2. PVR pathway signal transduction.

Effector molecules downstream of the Pvr receptor are poorly characterized and require greater study. Dissecting the Pvr-pathway has proved challenging, as downstream effector molecules vary throughout tissue types and developmental stages. For example, genetic dissection of the PVR pathway in border cell migration indicates that the *pvr* mutant phenotype is not reproduced by suppression of PI3K or PLC- γ activity using dominant-negative constructs or loss-of-function mutants, respectively[270]. This finding was unexpected because PI3K and PLC- γ are involved in PDGFR guidance and migration in tissue culture[299, 300]. Rather, the Pvr-associated migration signals pass through the non-conventional guanine nucleotide exchange factor (GEF) myoblast city (*mbc*), and *rac* to drive changes in localized filamentous actin levels. However, in the context of embryonic hemocyte survival, overexpression of the PI3K subunit catalytic subunit (p110^{CAAX}), the constitutively active GTPase (Ras^{V12}), or the baculovirus anti-apoptotic protein (p35) rescues the otherwise embryonic-lethal blood cell defects associated with *pvr* mutations[277]. These studies show that varied Pvr actions result from engagement of multiple effector pathways.

1.10.4.3. Pvr-engagement of Ras/dERK axis.

The Ras/MAPK signaling cassette is a frequent downstream target of the PVR pathway in a number of biological activities. Initial observations in border cells showed that the *Drosophila* MAPK, dERK, is phosphorylated in a Pvr

dependent manner[270]. *In vivo* experiments corroborated these observations as the addition of Pvfs, naturally found conditioned culture media from the Kc167 cell line, to *Drosophila* S2 cells strongly induced dERK phosphorylation (P-dERK)[270]. RNAi-mediated depletion of Pvr from S2 cells, or Pvfs 1 and 2 from Kc167 conditioned media prevented the condition media-dependent activation of dERK[270, 301]. These data are interpreted to mean that Kc167 conditioned media contains biologically active Pvfs that engage the Pvr/dERK signaling axis in S2 cell tissue culture[270, 301]. *In vitro* studies of Pvr-regulated cell size in *Drosophila* S2R⁺ tissue culture cells provided further elucidation of the Pvr/Ras/MEK/dERK axis[279, 302]. In these studies the small cell phenotype induced by RNAi-mediated depletion of Pvr is recapitulated by knockdown of the following signaling cascade components: Sos, Grb2, Raf, Ras, MEK and dERK[279]. While these data failed to provide physical linkage between Pvr and the Ras/dERK signaling arm, it provides a good platform for future studies into downstream signaling components in the PVR pathway.

Clarification of the Pvr/dERK axis was established in a high-throughput RNAi screen for RTK-induced dERK-activation[301]. This screen found that Pvr was the primary contributor to basal dERK phosphorylation levels in *Drosophila* S2R⁺ cells[301]. Subsequent investigations showed that Pvf1 and Pvf2 in conditioned media from the *Drosophila* Kc167 cell line hyper-stimulated dERK in S2R⁺ cells through Pvr. An RNAi screen then uncovered canonical Ras/dERK pathway components as essential regulators of conditioned media-induced dERK activation (Figure 1.10)[301]. These data strongly support the hypothesis that Pvr

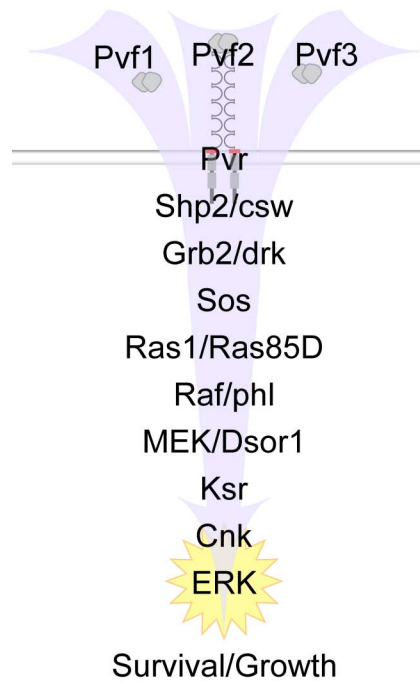


Figure 1.10. Canonical Pvr/Ras/dERK pathway.

Proposed members of the Pvr signaling pathways. Pvf1, 2 and 3 engage Pvr dimerization and initiation of downstream signaling events that result in dERK phosphorylation. Differences between component names in the canonical RTK/Ras/dERK pathway in humans and the Pvr pathway in *Drosophila* are shown as follows: Human/*Drosophila*.

is a potent activator of Ras/dERK signals, and will help to guide studies of other Pvr-associated phenomena.

1.10.5. Pvr in the posterior midgut.

Recent evidence suggests that Pvr plays a role in the control of posterior midgut physiology[303]. In the *Drosophila* gut, Pvr is associated with age-related and oxidative stress-related changes in the posterior midgut[303, 304]. Despite these studies, it is not known if Pvf/Pvr signals in ISCs are required for maintenance of ISC homeostasis throughout adulthood. In addition to oxidative stress and aging, other studies implicate Pvr in intestinal immune responses. For example, microarray analysis of infected *Drosophila* guts showed an increase in the expression of *pvf1* and *pvf2*[256]. Despite the overlapping roles of Pvr and dJNK pathways in the larval wounding response and morphogenetic movements of the male terminalia no studies have investigated the potential epistatic relationship between Pvr and JNK in the posterior midgut.

1.11. Summary.

In this thesis, I will present the results of a whole genome RNAi screen for dJNK phosphorylation in the *Drosophila* IMD pathway. I identified Pvr as a novel negative-feed back regulator of the IMD pathway. More specifically, I showed that PGN-induced dJNK activity drives the expression of Pvr-ligands (Pvf2, 3), and in turn Pvr/Ras/dERK-mediated signals suppress immune-induced AMP production in the IMD pathway. I then translated these findings to the posterior gut model, where I discovered that autocrine Pvr signals control ISC homeostasis, and regulates survival of oral infection.

Chapter 2

Methods and Materials

2.1. List of Buffers.

6X DNA gel loading buffer.

30% glycerol
0.03% bromophenol blue
0.03% xylene cyanol

Phosphate buffered saline (PBS).

140mM NaCl
2.7mM KCl
10mM Na₂HPO₄·7H₂O
1.4mM KH₂PO₄

Polymerase chain reaction (PCR)

DNA template
0.4μM forward and reverse primers
250μM dNTPs (Invitrogen, 10297)
1x ThermoPol Reaction Buffer (NEB)
0.5 units of taq DNA polymerase (NEB, M0273L)

SDS-PAGE: running buffer

25mM Tris
200mM glycine
0.1% SDS (m/v)*
(mass/volume)

SDS-PAGE: sample buffer

62.5mM Tris (pH 6.8)
10% glycerol
2% sodium dodecyl sulfate (SDS)
50mM β-mercaptoethanol (Sigma, M6250)
bromophenol blue

SDS-PAGE: separating gel.

375mM Tris (pH 8.8) (Invitrogen, 15504-020)
8-12% acrylamide (BIO-RAD, 161-0156)
0.1% SDS (m/v) (Sigma, L6026)
0.05% ammonium persulfate (APS) (m/v) (Sigma, A1433)
0.1% Tetramethylethylenediamine (TEMED) (v/v)** (Sigma, T7024)
**(volume/volume)

SDS-PAGE: stacking gel.

125mM Tris (pH 6.8)
4% acrylamide
0.1% sodium dodecyl sulfate (SDS) (m/v)
0.05% ammonium persulfate (APS) (m/v)
0.1% Tetramethylethylenediamine (TEMED) (v/v)

Squishing buffer (SB).

10 mM Tris (pH 8.2)

5 mM NaCl
1 mM EDTA
200 µg/ml Proteinase K (Sigma, P6556)

T7 5x transcription buffer.

400mM HEPES (pH 7.5)
120mM MgCl₂
10mM Spermidine
50mM DTT

T7: dilution buffer.

5mM KHPO₄ (pH 8.0)
4.7mM K₂HPO₄
0.3mM KH₂PO₄
50mM NaCl
0.05mM EDTA
0.5mM DTT
50% Glycerol

T7: transcription buffer.

1x transcription buffer
80mM HEPES (pH 7.5)
24mM MgCl₂
2mM Spermidine
10mM DTT
10% (v/v) 1/7 dilution of T7 enzyme in dilution buffer
6.25mM of each rNTPs (Promega, PR-E6000)
10U/ml Inorganic pyrophosphatase (Sigma, I6143)
40% template PCR DNA

Tris, Acetic acid, EDTA (TAE)

40mM Tris base
1mM Ethylenediaminetetraacetic acid (EDTA)
2mM Glacial acetic acid

Western Blot: transfer buffer.

25mM Tris base
20mM glycine
0.37% SDS (m/v)
20% Methanol (v/v)

2.2. Cells and cell culture.

Drosophila S2 (Edan Foley, from UCSF), S2R+ (*Drosophila* Genomic Resource Center (DGRC)) and Kc167 (DGRC) cell lines were cultured at 25°C in HyQ TNM-FM insect cell culture media (Thermo Scientific/Hyclone, SH3028002)

supplemented with 10% heat inactivated fetal bovine serum (Invitrogen/GIBCO, 12484028), and a solution of penicillin (50U/ml) and streptomycin (50µg/ml) (Invitrogen/GIBCO, 15070063). Serum-free S2 cells were cultured in SFX-InsectTM media (Thermo Scientific/Hyclone, SH30278.01), and a solution of penicillin (5000U/ml) and streptomycin (5000µg/ml). In general, cells were grown in 5ml of culture media in a 75cm² canted neck flask with vent cap (Fisher/Corning, 430641). Cells were grown at 25°C in an incubator (TriTech Research, DigiTherm), and cells were passaged every 3 to 4 days by performing 1:5 dilutions in fresh culture media, depending on cell densities. As a consequence of their increased adherence, serum free S2 cells were detached from the flask with a cell scraper (Fisherbrand, 08-100-241) prior to passage to a new flask.

2.2.1. Counting viable cells.

Cells were unsettled from the flask with repeated aspiration. Dead cells were stained by mixing 10µl of cell suspension with 90µl of trypan blue stain (GIBCO, 15250-061) in one well of 96 well tissue culture plate (Costar Corning, 3596). Viable cells were counted with a hemocytometer (Hausser Scientific Bright Line Counting Chamber/Fisher, 02-671-10), the number of viable cells was determined as the mean of two measurements. The cell concentrations were calculated by multiplying the average number of viable cells by the hemocytometer constant (1×10^4 cells/ml) and the dilution factor (10).

2.3. Cell culture assays.

2.3.1. dsRNA in S2 cells.

Targeted gene knock-down was performed in 1×10^6 S2 cells incubated at 25°C for 16h in 1ml culture media per well of a 12 well tissue culture plate (Corning Costar, 3513), and then treated with 10 μ l (approximately 10 μ g/ml) of dsRNA. Control wells were treated with non-targeting GFP dsRNA. Plates were rocked gently to mix dsRNA and cells were incubated for a further 3-4 days to deplete the target gene(s). dsRNA was generated in an *in vitro* transcription reaction as will be described in detail[137].

2.3.2. Activation of the IMD pathway.

S2 cells and serum free S2 cells were plated at a density of 1×10^6 cells in 1ml of tissue culture media in a 12 well plate, and incubated for 16h under standard conditions. The IMD pathway was activated by adding 10 μ l of 100x LPS (5mg/ml) (L2637, Sigma) that contains contaminating amounts of PGN, to each well (50 μ g/ml), while control wells were left untreated. Cells were collected at the indicated time points.

2.3.3. Inhibition of dJNK phosphorylation.

S2 cells were plated at 1×10^6 cells/ml in 1ml of tissue culture media per well of a 12 well tissue culture plate, and incubated for 16h. PGN-dependent dJNK activation was inhibited with the addition of 25 μ M SP600125 for 1h prior to PGN-exposure, relative to DMSO treated controls. The IMD pathway was activated with addition of 50 μ g/ml PGN contaminated LPS, and S2 cells were collected in

culture media and transferred to 1.5ml microfuge tubes. The cell suspension was centrifuged at 1000 relative centrifugal force (rcf) for 5min to pellet the cells.

2.3.4. Activation of the PVR pathway.

PVR pathway activation was performed as described previously[301]. Specifically, Kc167 cells were grown in 5ml of insect cell culture media for 3-4 days at 25°C. Conditioned media (CM) was collected with Kc167 cells and centrifuged in 15ml conical tube (Corning, 430052) at 1000rcf for 5min, to pellet the Kc167 cells. Cleared conditioned media was transferred to a 15ml conical tube and stored at 4°C. S2 cells were plated at a density of 1×10^6 cells/ml in 1ml of tissue culture media per well of a 12 well plate, and incubated at 25°C for 16h. Prior to the addition of CM, 0.5ml of media was removed from each well of the 12 well plates and replaced with 0.5ml of CM (1:1 dilution) or fresh tissue culture media, as a control. Plates were rocked gently, and S2 cells were collected in 1.5ml microfuge tube at the indicated time points. In experiments testing PVR pathway inhibition of PGN-induced AMP production, 1×10^6 cells S2 cell were simultaneously exposed to a 1:1 dilution of CM with 50µg/ml LPS for 6h in one well of a 12 well plate. Cells were collected in culture media and centrifuged in a 1.5ml microfuge tube at 1000rcf for 5min to pellet the cells.

2.3.5. Inhibition of the PVR pathway.

Pvr dependent dERK phosphorylation was inhibited in 1×10^6 S2 cells in 1ml of culture media per well of a 12 well plate for 16h at 25°C. 0.5ml of media was removed and of 50µM PD98059 was added for 1h prior to the addition of 0.5 ml CM exposure, to activate the PVR pathway. S2 cells were collected in tissue

culture media and transferred to 1.5ml microfuge tube. Cells were pelleted by centrifugation for 5min at 1000rcf and the supernatant was discarded.

2.4. Fly husbandry.

Drosophila fly stocks were maintained on standard corn meal medium (Nutri-Fly Bloomington Formulation, Genesee Scientific) in a 25°C incubator (BioCold Environmental, BC26-IN), unless otherwise stated (Table 2.1). Flies were transferred to fresh vials every two weeks.

2.5. Fly assays.

2.5.1. In vivo RNAi.

For *in vivo* knock down of Pvr, *UAS-PvrIR* flies were crossed with *hs-gal4* flies or *w¹¹¹⁸* flies as a control. *hs-gal4* flies were obtained from Dr. Sarah Hughes and *UAS-PvrIR* flies were obtained from the Vienna *Drosophila* RNAi Center. 1 day old progeny flies were heat-pulsed eight times at 37°C for 1h to initiate the expression of the RNAi construct and returned to 25°C for 5h over 48 hours.

2.5.2. Transgene expression in the Drosophila intestine.

Transgenes were expressed in ISC/EBs under the temperature sensitive control of the ;*esg-GAL4*, *tub-GAL80^{ts}*, *UAS-GFP*; (*esg^{ts}*) expression system as described in detail in Chapter 5[231]. Briefly, under permissive temperatures (25°C) the temperature sensitive mutant allele of the GAL4 inhibitor, GAL80^{ts} (25°C), binds GAL4 and blocks GAL4 transactivator activity at UAS-sites. However, at nonpermissive temperatures (29°C), GAL80^{ts} is inactive, and GAL4 activity promotes transgene expression at UAS-sites. Therefore, flies were raised

Table 2.1. Fly strains.

Fly	Genotype	Source
<i>DI-GAL4</i>	<i>w;;DI-GAL4</i>	Xiankun Zeng[305]
<i>esg-gal4,tub-GAL80^{ts},UAS-GFP</i>	<i>w; esg-gal4,tub-GAL80^{ts},UAS-GFP;</i>	Bruce Edgar[231]
<i>FRT(40A)</i>	<i>w; P{neoFRT}40A;</i>	Bloomington, 8215
<i>GBE+Su(H)-LacZ</i>	<i>;;GBE+Su(H)-LacZ</i>	Susan Bray[306]
<i>hs-gal4</i>	<i>;hs-gal4;</i>	Sarah Huges
<i>hs-flp,UAS-mCD8:GFP;40A(FRT)</i>	<i>P{UAS-mCD8::GFP.L}LL4, p{hs-flp}22,y[1] w[*]; P{neoFRT}40A;</i>	Bloomington, 28832
<i>pvf2-3</i>	<i>w; pvf2-3/Cy;</i>	Homemade
<i>pvr⁵³⁶³</i>	<i>w; pvr[5363];</i>	Bloomington, 9399[284]
<i>hs-GAL4</i>	<i>;hs-GAL4;</i>	Sarah Hughes
<i>hs-flp,UAS-mCD8:GFP;pvf2-3^Δ, 40A(FRT)</i>	<i>P{UAS-mCD8::GFP.L}LL4, p{hs-flp}22,y[1] w[*];pvf2-3, P{neoFRT}40A/Cy;</i>	Homemade
<i>pvf2-lacZ</i>	<i>w;pvf2-lacZ;</i>	Mi-Ae[304]
<i>Su(H)GBE-GAL4</i>	<i>w;Su(H)GBE-GAL4/Cy;</i>	Xiankun Zeng[305]
<i>tub-GAL80,FRT(40A);tub-GAL4</i>	<i>y[1],w[*]; P{tubP-GAL80}/Cy; P{w[+mC]=tubP-GAL4}LL7/Mkrs</i>	Homemade
<i>UAS-bsk^{DN}</i>	<i>w[1118]P{w[=mC]=UAS-bsk.DN}2</i>	Bloomington, 6409[307]
<i>UAS-GFP</i>	<i>w;UAS-GFP;</i>	
<i>UAS-hep^{CA}</i>	<i>w[*]; P{w[+mC]=UAS-Hep.Act}2;</i>	Bloomington, 9306[307]
<i>UAS-pvf1</i>	<i>w;;UAS-Pvf1</i>	Pernille Rorth[282]
<i>UAS-pvf2</i>	<i>W;UAS-pvf2;</i>	Marie Lagueux[274]
<i>UAS-pvr^{CA}</i>	<i>w; UAS-pvr^{CA};</i>	Pernille Rorth[282]
<i>UAS-pvr^{DN}</i>	<i>w; UAS-pvr^{DN};</i>	Pernille Rorth[282]
<i>UAS-PvrIR1</i>	<i>w;; UAS-PvrIR</i>	VDRC, 13502
<i>UAS-PvrIR2</i>	<i>w;UAS-PvrIR;</i>	VDRC, 977
<i>UAS-Ras85D^{N17}</i>	<i>P{w[=mC]=UAS-Ras85D.N17}TL1, w[1118]</i>	Bloomington, 4845[308]

under standard conditions (25°C) until 3-5 days post eclosure, to prevent transgene expression during development. Flies were then shifted to 29°C to induce transgene expression for 10 days, unless otherwise stated.

2.6. Mosaic Analysis with a Repressible Cell Marker (MARCM).

2.6.1. Generation of *pvf2-3* mutant.

pvf2-3 flies were generated by targeted excisions of the intervening genomic region between *P{XP}Pvf2^{d00645}* and *PBacPvf3^{f04842}* (Exelixis Collection) transposable-elements by standard genetic techniques by Edan Foley[309].

2.6.2. PCR confirmation of *pvr* and *pvf2-3* recombinants.

pvr⁵³⁶³ and *pvf2-3* mutant alleles were recombined onto a *neoFRT(40A)* containing chromosome to generate *y,w,hs-flp,UAS-mCD8:GFP;pvr⁵³⁶³,neoFRT(40A)/Cy* and *y,w,hs-flp,UAS-mCD8:GFP;pvf2-3,neoFRT(40A)/Cy* flies. Recombinant flies were confirmed with PCR and complementation assays.

2.6.2.1. Single fly DNA extraction (for PCR).

A single fly was placed in 1.5ml microfuge tube and crushed for 5-10s with a pipette tip in 50µl squishing buffer (SB). Fly homogenate was incubated in a 37°C water bath for 30min, and then transferred to an 85°C heating block for 10min to inactivate the proteinase K. Digested material was centrifuged at 16000rcf for 1min, placed on ice, and 1µl of cleared supernatant was used in a PCR reaction.

Table 2.2. PCR primers for confirmation of *pvr*⁵³⁶³ and *pvf2-3* recombinants.

Primer name	Target	Sequence
<i>pvf2-3</i> forward	<i>pvf2-3</i>	5'-AATGATTCGCAGTGGGAAGGCT-3'
<i>pvf2-3</i> reverse	<i>pvf2-3</i>	5'-GACGCATGATTATCTTTTACGTGAC-3'
<i>pvr</i> forward	<i>pvr</i>	5'-GTACACGTACATGGAGCTGGC-3'
<i>pvr</i> reverse	<i>pvr</i>	5'-CTCATCGAAGTGACGGCTGAC-3'
FRT(40A) forward	FRT	5'-ATCTGGACGAAGAGCATCAGGG-3'
FRT(40A) reverse	FRT	5'-CGATACCGTAAAGCACGAGGAAG-3'

2.6.2.2. Polymerase chain reaction (PCR).

The presence of the *pvf2-3* and *pvr*⁵³⁶³ mutations was determined by PCR with mutation specific primers (Table 2.2). Specifically, 1µl of genomic DNA template, 0.4µM forward and reverse primers, 250µM dNTPs (dATP, dTTP, dCTP and dGTP mix (Invitrogen, 10297)), ThermoPol Reaction Buffer, and 0.25 units of taq DNA polymerase (NEB, M0273L) was added to dH₂O to a final volume of 25µl in a PCR tube (Axygen, PCR-02-C). PCR was run in Mastercycler ep gradient S thermocycler (Eppendorf, 950010151) under the following conditions: 1 cycle at 96°C for 2min, 40 cycles at 96°C for 20s, 55°C for 20s, 72°C for 2min, 1 cycle at 72°C for 5min, and a 4°C hold. DNA gel loading buffer was added and the samples were stored at 4°C.

2.6.2.3. Agarose gel electrophoresis.

Agarose (2% v/w) (Invitrogen, 16500-100) was dissolved in boiling TAE buffer and approximately 0.5µg ethidium bromide was added. Cooled TAE agarose gel was submerged in TAE in an agarose gel electrophoresis cell (BioRad, 170-4489EDU), and 5µl of template DNA PCR in DNA loading buffer was added to each well with 100bp ladder (Invitrogen, 15628-019) and 1kb ladder (New England BioLabs, N3232L) as molecular size markers. The gel was run at 100 Volts (V) until bromophenol blue band migrated 2/3rds the length of the gel. The gel was visualized on with an ImageQuant 300 (GE, 63-0056-52) UV lightbox with a digital camera.

2.6.3. Generation of MARCM clones.

*hs-flp,UAS-mCD8:GFP;pvr*⁵³⁶³,*FRT(40A)/Cy*; and *hs-flp,UAS-mCD8:GFP*;

pvf2-3,FRT(40A)/Cy; flies were crossed with *tub-gal80,FRT(40A);tub-gal4* flies and MARCM clones were generated in the progeny by standard techniques[310]. Briefly, 3-5 day old adult flies were heat shocked at 37°C for 2h and returned to 25°C, to induce flp-recombination. GFP positive clones were visualized at two weeks, or at 3 days post *Ps. Entomophila* infection (OD=5) by confocal microscopy. MARCM clones will be described in detail in Chapter 5.

2.7. Bacterial infections.

2.7.1. Bacterial cultures.

Escherichia coli (*E. coli*) DH5 α and *Pseudomonas entomophila* (*Pe*) (Bruno Lemaitre), were cultured overnight in Lysogeny Broth (LB) (Becton Dickinson, 244520) at 37°C at 200rpm. For long term storage, glycerol stocks were generated by mixing 500 μ l of overnight (O/N) culture with sterile 500 μ l 30% glycerol solution and freezing at -80°C.

2.7.2. Septic injury.

DH5 α *E. coli* bacteria were cultured overnight in 5ml LB at 37°C with constant agitation. 1ml of bacteria was pelleted in a microfuge tube at 6000rcf for 5min. Infection was monitored in flies that were either uninjured (control), or pricked with a tungsten needle dipped in the pellet of DH5 α *E. coli* bacteria (infection).

2.7.3. Oral infections.

Flies were collected 3-5 days after eclosure and transgenes were induced with *esg*^{ts} at 29°C for 10 days. *Pe* were grown overnight at 30°C in LB, and the

absorbance of a 1:10 dilution of bacteria in LB was measured at 600nm with a spectrophotometer. The total number of OD units was calculated, the bacteria were pelleted by centrifugation at 6000rcf for 15min. Bacterial pellets were resuspended in a sucrose solution (5% sucrose, 0.5% PBS) to either 5OD₆₀₀ or 100OD₆₀₀. Flies were starved for 2 hours and then fed a high dose 100OD₆₀₀ (survival curve) or a low dose 5OD₆₀₀ (MARCM) of *Pe* in sucrose solution. Flies were fed the high dose of *Pe* for 16h at 29°C and transferred to fresh food vials where the number of surviving flies were counted over time. For MARCM infections studies, flies were heat shocked at 37°C for 2 hours, to induce flp-recombination, and recovered at 25°C for 16h prior to oral infection with a low dose of *Pe* for 4h at 25°C. Flies were transferred to fresh food vials for 3 days at 25°C prior to dissection.

2.8. Generation of dsRNA.

2.8.1. De novo synthesis of dsRNAs.

Template DNA was amplified from genomic DNA using gene-specific primers with a GGGCGGGT anchor sequence at the 5' end (Table 2.3). Specifically, 1µl of cDNA or genomic DNA preparations, 0.4µM forward and reverse gene-specific primers, 200µM dNTPs (dATP, dTTP, dCTP and dGTP mix (Invitrogen, 10297)), ThermoPol Reaction Buffer, and 0.5 units of Taq DNA polymerase (NEB, M0273L) were added to dH₂O to a final volume of 50µl in a PCR tube (Axygen, PCR-02-C). PCR was run in Mastercycler ep gradient S thermocycler (Eppendorf, 950010151) under the following conditions: 1 cycle of 96°C for 2min, 40 cycles of 96°C for 30s, 55°C for 30s 72°C for 1min, 1 cycle at 72°C for 5min, and a 4°C hold.

Table 2.3. List of primers for generating dsRNA.

Primer name	Sequence
GFP forward	5'-GGGCGGGTACGTAAACGGCCACAAG-3'
GFP reverse	5'-GGGCGGGTCTCAGGTAGTGGTTGTC-3'
Kenny forward	5'-GGGCGGGTTCAGCGTACTCTTACTGGTCT-3'
Kenny reverse	5'-GGGCGGGTCACTCGTTTGAGTTCGTACCA-3'
dTak1 forward	5'-GGGCGGGTGAAGTCCACATAGGCTGCCTG-3'
dTak1 reverse	5'-GGGCGGGTCACTAATGTATCGATGACGGT-3'
Pvr 1 forward	5'-GGGCGGGTGATGACTACATGGAGATGAGCC-3'
Pvr 1 reverse	5'-GGGCGGGTATACCTTCGTTGCTCCTTCTCG-3'
Pvr 2 forward	5'-GGGCGGGTCTCCTGATTTTGCGGATCTC-3',
Pvr 2 reverse	5'-GGGCGGGTGTCTTGGGATCGTTTCTTGA-3'
Universal primer	5'-TAATACGACTCACTATAGGGAGACCACGGGCGGGT-3'

The template DNA was amplified in a second round of PCR with a universal primer bearing the T7 RNA polymerase promoter sequence followed by the anchor sequence. Specifically, 2 μ l of PCR template, 0.4 μ M, 200 μ M dNTPs, ThermoPol Reaction Buffer, and 0.5 units of Taq DNA polymerase (NEB) were added to dH₂O to a final volume of 50 μ l in a PCR tube. PCR was run in thermocycler under the following conditions: 1 cycle of 94°C for 2min, 5 cycles of 94°C for 30s, 42°C for 30s, 35 cycles of 94°C for 30s, 60°C for 30s 72°C for 1min, 1 cycle at 72°C for 10min, and a 4°C hold. Template DNA was placed at -20°C for long-term storage.

2.8.2. Amplification of template DNA.

Template DNA was amplified to generate consistent laboratory stocks of commonly used dsRNAs. Specifically, 2 μ l of DNA template PCR, 0.4 μ M universal primer, 250 μ M dNTPs, ThermoPol Reaction Buffer, and 0.5 units of taq DNA polymerase (NEB) were added to dH₂O to a final volume of 50 μ l in a PCR tube (Axygen, PCR-02-C). PCR was run in thermocycler under the following conditions: 1 cycle at 96°C for 2min, 40 cycles at 96°C for 15s, 55°C for 15s, 72°C for 1min, 1 cycle at 72°C for 5min, and a 4°C hold. Template DNA was stored at 4°C.

2.8.3. Generation of dsRNA.

dsRNA was amplified from template PCR DNA using T7 RNA polymerase. The T7 reaction was composed of the following proportions: 4/20 5x transcription buffer, 5/20 25mM rNTPs, 1/20 200U/ml inorganic pyrophosphatase, 2/20 T7 polymerases in dilution buffer (from a 1/7 dilution of the original T7 concentrate)

and 8/20 DNA template. dsRNA was generated in a thermocycler at 37°C for 6h and annealed by cooling at 1°C/min from 90°C to 30°C. RNA was diluted 1:1 in dH₂O and stored at -20°C.

2.8.4. Generation of the whole genome library.

The dsRNA library employed in this screen is an extension of a partial-genome library described previously[137]. The remainder of the library was purchased from Open Biosystems RDM4220. The dsRNA was amplified from 5µl of template DNA in 166 96 well PCR plates covering a total of 15852 *Drosophila* genes. Specifically, 7.5µl of a T7 master mix containing the following proportions: 4/12, 5x transcription buffer, 5/12, 25mM rNTPs, 1/12, 200U/ml inorganic pyrophosphatase, 2/12, T7 polymerase (from a 1/7 dilution of T7 concentrate), was added to the 5µl of template DNA resulting in a total volume of 12.5µl. Plates were sealed with sealing foil, incubated at 37°C for 6h, and stored at -80°C. Plates were placed in a thermocycler, and heated to 90°C and cooled to 30°C at 1°C/min. RNAi was diluted 1:1 by adding 12.5µl of dH₂O to each well.

2.9. Quantification of gene expression.

2.9.1. RNA extraction from S2 cells.

Approximately 1x10⁶ S2 cells were aspirated from 1 well of a 12 well plate in 1ml of tissue culture media, transferred to 1.5ml microfuge tube, and centrifuged at 12000rcf for 1min, to pellet cells. The supernatant was aspirated, and the remaining cell pellet was gently resuspended in 200µl of TRIzol reagent (Invitrogen, 15596-026). Samples were incubated at RT for 5min to allow for dissolution of lipids, proteins, and nucleic acids. Homogenates were centrifuged

at 12000rcf for 10min at 4°C, to pellet non-dissolved cell debris and DNA. Cleared homogenate was transferred to a new 1.5ml microfuge tube, and 40µl of chloroform was added. Samples were vortexed vigorously for 15s, and incubated at RT for 3min. Samples were centrifuged at 12000rcf for 15min at 4°C to separate top aqueous phase (water, and RNA) from the bottom organic (TRIzol, and chloroform) phase. The upper aqueous phase was carefully removed and transferred to new 1.5ml microfuge tube, and 100µl isopropyl alcohol was added to precipitate RNA. Samples were vortexed vigorously and incubated at RT for 10min (or O/N at -20°C to maximized RNA yield). Samples were centrifuged at 12000rcf for 15min at 4°C, and the supernatant was carefully aspirated off, avoiding the clear RNA pellet. RNA pellet was washed with 100µl 70% ethanol, and centrifuged at 7500rcf for 5min at 4°C. The supernatant was aspirated off the washed RNA pellet, and the pellet was dried at RT until the opaque RNA pellet turned translucent. RNA was resuspended in 20µl sterile filtered dH₂O, and stored at -20°C.

2.9.2. RNA extraction from whole flies.

Approximately 10-20 anesthetized flies were transferred to 1.5ml microfuge tube, and emulsified with a pestle in 400µl TRIzol reagent. 600µl of TRIzol reagent was added to the homogenates and samples were incubated at RT for 5min to allow for dissolution of lipids, proteins, and nucleic acids. Homogenates were centrifuged at 12000rcf for 10min at 4°C to pellet non-dissolved fly debris and DNA. Cleared homogenate was transferred to a new 1.5ml microfuge tube, and 200µl of chloroform was added. Samples were vortexed vigorously for 15s, and incubated at RT for 3min. Samples were centrifuged at 12000rcf for 15min at

4°C to separate top aqueous phase (water, and RNA) from the bottom organic (TRIzol, and chloroform) phase. Upper aqueous phase was carefully removed and transferred to new 1.5ml microfuge tube, and 500µl isopropyl alcohol was added to precipitate RNA. Samples were vortexed vigorously and incubate at RT for 10min (or O/N at -20°C to maximize RNA yield). Samples were centrifuged at 12000rcf for 15min at 4°C, and supernatant was carefully aspirated, avoiding the clear RNA pellet. The RNA pellet was washed with 500µl 70% ethanol, and centrifuged at 7500rcf for 5min at 4°C. Supernatant was aspirated of the washed RNA pellet, and the pellet was dried at RT until the opaque RNA pellet turned translucent. RNA was resuspended in 20-40µl sterile filtered dH₂O depending on the size of the RNA pellet and stored at -20°C.

2.9.3. Analysis of RNA.

To determine the concentration of RNA, 2µl of RNA was diluted in 98µL dH₂O and the absorbance at 260nm (A_{260}) and 280nm (A_{280}) wavelength was measured using a spectrophotometer (Jenway, Genova). The purity of RNA was determined with the A_{260} to A_{280} ratio; an A_{260}/A_{280} value of 2.1 is considered pure for RNA. The concentration of RNA was determined with the following calculation based on the knowledge that 1OD A_{260} =40µg/ml:

$$\text{Sample } A_{260} \times \text{Dilution factor (50)} \times 40\mu\text{g/ml} = \text{Sample } A_{260} \times 2\mu\text{g}/\mu\text{l} = X \mu\text{g}/\mu\text{l}$$

2.9.4. cDNA synthesis.

Complementary DNA (cDNA) was synthesized with qScript cDNA Synthesis Kit (Quanta Biosciences, 95047) following the manufacturers recommendations. Briefly, 1µg of RNA, 2µl 5x qScript reaction mix, and 0.5µl of qScript reverse transcriptase was added to dH₂O (a final volume of 10µl per reaction). cDNA was synthesized in a thermocycler with the following program: 22°C for 5min, 42°C for 30min, and 85°C for 5min. cDNA was diluted 1:16 with dH₂O and stored at -20°C.

2.9.5. Quantitative real-time PCR (qRT-PCR).

Transcript levels were monitored in flies and tissue culture with qRT-PCR using PerfeCTa SYBR Green FastMix (Quanta Biosciences, 95072). Briefly, 2.5µl of a cDNA dilution, and 2.5 µl of a 1.6mM mix of forward and reverse gene-specific primers (final concentration of 0.4µM) was added to 5µl of 2x PerfeCTa SYBR Green FastMix per reaction, for a final reaction volume of 10 µl (Table 2.4). Each reaction was replicated in triplicate. Reactions were performed in a twin.tech 96 well real-time PCR plate (Eppendorf, 951022027), and plates were covered with heat sealing film (Eppendorf, 30127854) with a heat sealer (Eppendorf, 951023078). A realplex² (Eppendorf, 950021209) qRT-PCR machine was used to perform the following PCR reaction: 1 cycle of 95°C for 2min, 40 cycles of 95°C for 15s and 60°C for 1min. SYBR green fluorescence was monitored at the end of each 60°C step, and the transcript fluorescence was given a cycle threshold (Ct) value as it crossed the CalQplex threshold set by the Eppendorf realplex 2.2 software. To ensure the qRT-PCR reaction amplified of only one gene transcript a melting curve was performed as follows: 95°C for 15s,

Table 2.4. List of validated qRT- PCR primers.

Primer name	Target	Sequence
<i>act</i> forward	<i>actin</i>	5'-TGCCTCATCGCCGACATAA-3'
<i>act</i> reverse	<i>actin</i>	5'-CACGTCACCAGGGCGTAAT-3'
<i>att</i> forward	<i>attacin</i>	5'-AGTCACAACCTGGCGGAC-3'
<i>att</i> reverse	<i>attacin</i>	5'TGTTGAATAAATTGGCATGG-3'
<i>dipt</i> forward	<i>diptericin</i>	5'-ACCGCAGTACCCACTCAATC-3'
<i>dipt</i> reverse	<i>diptericin</i>	5'-ACTTTCCAGCTCGGTTCTGA-3'
<i>pvf1</i> forward	<i>pvf1</i>	5'-GCGCAGCATCATGAAATCAACCG-3'
<i>pvf1</i> reverse	<i>pvf1</i>	5'-TGCACGCGGGCATATAGTAGTAG-3'
<i>pvf2</i> forward	<i>pvf2</i>	5'-TCAGCGACGAAACGTGCAAGAG-3'
<i>pvf2</i> reverse	<i>pvf2</i>	5'-TTTGAATGCGGCGTCGTTCC-3'
<i>pvf3</i> forward	<i>pvf3</i>	5'-AGCCAAATTTGTGCCGCCAAG-3'
<i>pvf3</i> reverse	<i>pvf3</i>	5'-CTGCGATGCTTACTGCTCTTCACG-3'

60°C for 15s, 60°C to 95°C over 20min, and 95°C for 15s. Initially, qRT-PCR primers were validated by generating a 4 step dilution series of cDNA: 1:4, 1:16, 1:64 and 1:256. Primers were considered ideal if they produced linear range of cDNA amplification, with an efficiency of approximately 1.0 and a slope of -3.3. Relative gene expression values were determined with the delta delta Ct ($\Delta\Delta^{Ct}$) method as follows. First the delta Ct (Δ^{Ct}) was determined for a gene X standardized to an internal actin control between qRT-PCR runs.

$$\text{Gene X Ct} - \text{actin Ct} = \Delta^{Ct}$$

Three replicate measurements were taken for each gene, and experimental outliers were discarded from further analysis. A measurement was considered an outlier if it deviated significantly from the other two measurements. Measurements were averaged, and this value represents the cycle difference between a variable gene X and an invariable internal house-keeping gene. Second, the Δ^{Ct} value is standardized to an experimental control; an untreated S2 cell cDNA for example.

$$\text{Gene X } \Delta^{Ct} - \text{reference control } \Delta^{Ct} = \Delta\Delta^{Ct}$$

The $\Delta\Delta^{Ct}$ value represents cycle difference with experimental treatment. Finally, the fold change in transcript values was determined, assuming each PCR cycle represents a doubling of transcript numbers.

$$\text{Fold change from control} = 2^{-\Delta\Delta^{Ct}}$$

This value represents the fold change in gene X expression with experimental treatment, and permits pairwise comparisons between treatment groups.

2.10. Immunochemistry.

2.10.1. Western blotting.

Generally, cells were grown to a density of 1×10^6 cells/ml in 1ml of culture media in a 12 well plate. Cells were unsettled from the well surface and transferred to a 1.5ml microfuge tube, and centrifuged for 3min at 1000rcf in a microfuge (Thermo Electron Corporation, MICROMAX). Supernatant was then removed by aspiration and the cell pellet was resuspended in sample buffer, vortexed and incubated at 95°C for 5min. Proteins were separated by sodium dodecyl sulphate - polyacrylamide gel electrophoresis (SDS-PAGE) using the Mini-PROTEAN 3 system (BioRad, 165-3301). Generally, SDS-PAGE gels contained a 4% polyacrylamide stacking gel, and 10% or 12% acrylamide resolving gel depending on the size of the target protein. Proteins were run at a constant 100V until the sample buffer dye entered the resolving gel at which time the voltage was increased to 150V, until the bromophenol blue dye ran to the bottom of the gel.

Proteins in the SDS-PAGE gel were placed in transfer buffer with 6 sheets of equal sized pieces of chromatography paper (Fisherbrand, 05-714-4), and nitrocellulose membrane (BioRad, 162-0115). The nitrocellulose membrane and SDS-PAGE gel were sandwiched together between three sheets of soaked chromatography paper, with the nitrocellulose membrane placed on the cathode side of the transfer apparatus. Proteins were transferred by semidry transfer with a Trans-Blot[®] SD Semi-Dry Transfer Cell (BioRad, 170-3940) at 20v for 20min.

Membranes were rinsed once in PBS, and blocked in 4ml blocking buffer (1:1 mixture of LI-COR blocking buffer (LI-COR Biosciences, 927-40000) and PBS) for 1h at RT with gentle shaking. All subsequent stain and wash steps were performed with gentle agitation on an orbital shaker. Blocking buffer was decanted from the membrane, and primary antibodies were added with 0.05% tween 20. Primary antibody in blocking buffer was returned to the membrane and incubated O/N at 4°C. Primary antibody was removed and stored at 4°C for additional use. Membranes were washed with wash buffer (PBS, 0.05% tween 20) at RT for 5min. Membranes were washed an additional 3 times, discarding the wash buffer between wash steps. Membranes were incubated at RT for 1h in the dark, with secondary antibodies added to 4ml of wash buffer containing 1:5 dilution of blocking buffer. Membranes were washed with 4 times in wash buffer (PBS, 0.05% tween 20) for 5min per wash at RT. Membrane were rinsed once in PBS to remove residual wash buffer.

Membranes were visualized with an Aeries automated imaging system (LI-COR Biosciences) following the manufacturers recommendations. Briefly, the membranes were scanned at 800nm and 700nm wavelengths, using 200µm resolution, 3.0 mm focus offset, and an initial intensity setting of 7.0 for both the 700nm and 800nm channels. Laser intensities were increased or decreases to maximize protein signal without saturation. Proteins levels were quantified with Aeries 1.0 software (LI-COR Biosciences).

2.10.2. In-cell Western.

dsRNA (1.5µl of 1:1 dilution of dsRNA:dH₂O) was added to 100µl of serum-free tissue culture media in a 96 well plate, and placed on an orbital shaker (JIOTECH, SK-300) for 5min at 30 rpm to mix dsRNA and culture media.

S2 cells were grown with 5ml serum-free growth media (Hyclone, SFX-Insect™) in a 75cm² flask, for 3-4 days until completely confluent. Cells were unsettled from flasks with a cell scraper, and viable cells were counted as described previously. The cell suspension was centrifuged at 1000rcf in a centrifuge (Eppendorf, 5810R) for 5min to pellet S2 cells. Cleared conditioned media (CM) supernatant was separated from S2 pellet and set aside. CM was diluted with fresh serum-free medium in a 3:2 ratio, and used to resuspend cell pellet to 3x10⁶ S2 cells/ml. 50µl of serum-free S2 cells were added at a concentration of 3x10⁶ S2 cells/ml in 60% conditioned medium to each well. The final S2 cell concentration was 1.5x10⁵ cells/well in 20% CM. Plates were rocked gently to evenly distribute the cells. Each 96 well plate required approximately 5ml of concentrated S2 cell concentrate and 3ml of CM. Plates were incubated at 25°C for 3 days in a humidified incubator.

After 3 days, cells were stimulated with LPS contaminated with PGN, by adding 2µl of 100x LPS (5mg/ml) (L2637, Sigma) to 48µl serum-free culture media, and 50µl was added per well to a final concentration of 50ug/ml LPS. Cells were stimulated with the LPS, at which point the medium was removed by inverting the plate over a collection container. In all subsequent steps media/buffers were removed from the plate by carefully inverting the plate, to

avoid disturbing the cells by pipetting. The remaining adherent cells were washed once with 200µl PBS per well, and then fixed with 150µl fixing solution (PBS, 3.7% formaldehyde (Sigma, F1635)) for 15min at room temperature (RT) (plates were rocked 10 times, do not shake). The fixed cells were permeabilized by submerging the 96-well plate in PBSTx (PBS, 0.1% Triton X-100 (Fisher, BP151-500)) and incubated for 6min on an orbital shaker with gentle shaking (30rpm). Wash steps were repeated an additional 3 times. Wells were blocked in 150µl per well blocking buffer (LI-COR, 927-40000) for 1hour. Primary antibody, anti-Phospho-SAPK/JNK (T183/Y185) mouse monoclonal antibody (Cell Signaling, 9255S), was diluted to 1:200 in blocking buffer, and 50µl of antibody dilution was added to each well. Fixed cells were incubated with the primary antibody stain for 16h at 4°C, shaking gently. Primary antibody was removed, and collected (antibody can be reused). Plates were submerged in wash buffer (PBS, 0.1% Tween 20 (Fisher, BP337-500)) and cells were washed with gentle agitation on orbital shaker for 6min. Wash steps were repeated an additional 3 times. Secondary antibody Alexa Fluor 750 goat anti-mouse IgG (Molecular Probes, A21037) was diluted to 1:1000 with a 1:1000 dilution of Alexa Fluor 680 phalloidin (Molecular Probes, A22286) in 0.1% Tween 20, and 50µl was added to each well. Plates were incubated in the dark for 1h at RT with gentle shaking. Plates were submerged in wash buffer and cells were washed with gentle agitation on an orbital shaker for 6min in the dark. Wash steps were repeated an additional 3 times. Plates were submerged one additional time in PBS to remove residual wash buffer. Plates were inverted and gently blotted on paper towel to remove remaining PBS. Plate bottoms were cleaned with 75% ethanol before visualization.

2.10.2.1. Quantification of ICW.

Plates were visualized with Aerius automated infrared imaging system (LI-COR). Specifically, the plates were scanned at 800nm and 700nm wavelengths, using 200µm resolution, 3.0 mm focus offset, and an intensity setting of 9.5 for the 800nm channel and 5.5 for the 700nm channel. For the high-throughput screen the processes was automated with the Bio-Stack Automated Microplate Stacking System (Bio-Tek) controlled through Aerius 1.0 software (LI-COR).

2.10.3. Immunofluorescence microscopy.

Adults flies were anesthetized with CO₂, submerged in 95% ethanol to reduce surface tension, and transferred to 500µl PBS in one well of a 9 well glass depression plate (Corning, 7220-85) for dissection. Genitalia and thorax were removed from the abdomen with dissecting scissors (FST, 15100-09). The gut was gently separated from the abdomen and superfluous malpighian tubules and trachea elements were detached. Isolated guts were placed in PBS on ice for no longer than 1h prior to fixation for 20 min at RT in 500µl fixative solution (PBS, 4% formaldehyde) in one well of a 12 well tissue culture plate. All subsequent washing steps were performed in 24 well tissue culture plate (Corning Costar, 3526) with gentle agitation on an orbital shaker unless stated otherwise. Guts were rinsed once in PBS for 5min at RT and blocked overnight in 200µl PBSTBN (PBS, 0.05% tween-20, 5% bovine serum albumin and 1% normal goat serum) in one well of 96 well tissue culture plate at 4°C. Guts were stained for 3h at RT in PBSTBN with a combination of primary antibodies (Table 2.5) with gentle agitation on an orbital shaker. Guts were then washed once in 1ml PBSTB (PBS,

0.05% tween-20, 5% BSA) for 45min at RT. Gut were stained for 1h at RT in PBSTBN with Hoechst (1:1000; Molecular Probes, 33258) to visualize the total cell nuclei, and with the appropriate secondary antibodies (Table 2.6 and Table 2.7). Guts were washed once in 1ml of PBSTB for 45min at RT, and then rinsed in 1ml PBS at 4°C O/N prior to visualization. Microcopy slides (Fisherbrand, 12-522-5) were cleaned with 70% ethanol and nail polish was used to create a bridge slightly smaller than the cover glass (Fisherbrand, 12-544B). Guts were mounted in 4 drops of fluoromount (Sigma, F4680) and cover class was placed over the bridge. Slides were stored at 4°C.

2.10.3.1. Confocal microscopy.

Drosophila posterior midgut immunofluorescence was visualized by spinning-disk confocal microscopy in the Faculty of Medicine and Dentistry Core Imaging Facility, at the University of Alberta. Specifically, I used the spinning disk confocal microscope integrated by Quorum Technologies based on an IX-81 microscope stand (Olympus), laser excitation from a Laser Merge Module (LMM5, Spectral Applied Research), and a CSU-X1 spinning disk confocal scan head (Yokogawa Electric Corporation). Images were recorded on an EMCCD (C9100-13, Hamamatsu Photonics), using Quorum WaveFX imaging software (Quorum Technologies Inc). All gut images were collected as a Z-series and processed with Fiji software to generate a single Z-stacked image[311]. Colocalization between individual color channels was determined using Imaris software

Table 2.5. List of primary antibodies.

Antibody target	Type	Source	Assays	Concentration
Armadillo	M, MC	DSHB, N2 7A1	IF	1:100
Delta	M, MC	DSHB, C594.9B-c	IF	1:100
Prospero	M, MC	DSHB, (MR1A)-c	IF	1:00
P-JNK	M, MC	Cell Signaling, 9255S	WB, ICW	1:2000/1:400
JNK	R, PC	Santa Cruz Biotechnology, sc-571	WB, ICW	1:4000/1:400
Actin	M, MC	Sigma, A3853	WB	1:5000
Actin	R, PC	Cell Signaling, 4968S	WB	1:2000
P-ERK	R, PC	Millipore, 05-797R	WB	1:8000
PH3	R, PC	Millipore, 06-570	IF	1:1000
P-ERK	M, MC	Millipore, 05-797R	WB	1:8000
Pvr	Rt, PC	Pernille Rorth[282]	WB/IF	1:1000/1:100
Relish	M, MC	Silverman [140]	WB	Undiluted
P-Relish	R, PC	Silverman, [140]	WB	1:1000
β -galactosidase	M, MC	Sigma	IF	1:500
β -galactosidase	R, PC	MP-biosciences, 08559761	IF	1:2000
PDM1	Rt, PC	Xiaohang Yang	IF	1:2000

MC- monoclonal, **PC-** polyclonal

M- Mouse, **R-** Rabbit, **Rt-** Rat

WB- Western Blot, **ICW-** In-Cell Western, **IF-** Immunofluorescence microscopy

DSHB- Developmental Studies Hybridoma Bank

Table 2.6. List of secondary antibodies.

Antibody	Source	Assay	Concentration
AlexaFluor 568 G anti-M IgG	Molecular Probes, A11004	IF	1:1000
AlexaFluor 568 G anti-R IgG	Molecular Probes, A11011	IF	1:1000
AlexaFluor 647 G anti-R IgG	Molecular Probes, A21244	IF	1:1000
Alexa Fluor 647 G anti-M IgG	Molecular Probes, A21235	IF	1:1000
AlexaFluor 680 G anti-M IgG	Molecular Probes, A21057	WB	1:10000
AlexaFluor 680 G anti-R IgG	Molecular Probes, A21076	WB/ ICW	1:10000/1:1000
AlexaFluor 680 G anti-Rt IgG	Molecular Probes, A21096	WB	1:10000
AlexaFluor 750 G anti-M IgG	Molecular Probes, A21037	WB/ ICW	1:10000/1:1000
AlexaFluor 750 G anti-R IgG	Molecular Probes, A21039	WB	1:10000
Cy3 D anti-Rt	Jackson ImmunoResearch, 711-165-152	IF	1:1000

M-Mouse, **R**-Rabbit, **G**-Goat, **D**-Donkey, **Rt**-Rat

WB- Western Blot, **ICW**-In-Cell Western, **IF**-Immunofluorescence microscopy

Table 2.7. List of stains.

Stain	Source	Assay	Concentration
Hoechst	Molecular Probes, H3569	IF	1:1000
AlexaFluor phalloidin 568	Molecular Probes, A12380	IF	1:1000
AlexaFluor phalloidin 680	Molecular Probes, A22286	ICW	1:1000

ICW-In-Cell Western, **IF**-Immunofluorescence microscopy

(Bitplane Inc.) colocalization algorithms. Images were processed in Photoshop CS5 (Adobe) and figures were prepared with Illustrator CS5 (Adobe).

2.11. Statistical analysis.

2.11.1. RNAi screen.

For the RNAi screen, the raw fluorescent trimmed mean level was determined for P-JNK and f-actin channels in each well with Aeries 1.0 software, and the relative P-JNK:f-actin value was calculated. I applied z-score analysis to normalize P-JNK:f-actin values across the entire screen. Z-scores were calculated by subtracting the plate median value from the sample value and dividing by the plate standard deviation. The z-score assumes normal distribution and represents the standard deviation of every P-JNK:f-actin value from the plate median for each dsRNA treatment. Z-scores above 2.58 or below -2.58 represent the 99% confidence interval and z-scores above 1.96 or below -1.96 represent the 95% confidence interval. The f-actin z-scores were also calculated for every well on each plate and dsRNA treatments resulting in f-actin z-scores below -2.58 (99% CI) were excluded from further analysis to eliminate actin modifiers and lethal dsRNAs. I considered dsRNAs that modified P-JNK:actin z-scores outside the 95% confidence interval as hits in the screen.

2.11.2. Determination of statistical significance.

Statistical significance was determined on data sets with a minimum of three independent experimental values with a two-tailed Students t-test with two-samples of equal variance relative to control values with Microsoft Excel software. p-values of less than 0.05 are indicated with a single asterisk (*), and p-values of

less than 0.01 are indicated with a double asterix (**). Error bars are shown as the standard error of the mean (SEM) calculated in Microsoft Excel software with the following formula:

$$\text{SEM} = \text{standard deviation} / \sqrt{(\text{sample size})}$$

2.11.3. Posterior midgut analysis.

GFP positive cells in posterior midguts were counted relative to the total cell population stained with Hoechst in each image with the Imaris software spot counter algorithm. To determine statistical significance I performed a two-tailed Students t-test with two-samples of equal variance relative to control values. p-values of less than 0.01 are indicated with **.

2.11.4. Box plots.

Box plots were used to show the differences in data distribution between experimental groups without making assumptions about their statistical significance. Specifically, the centerline indicating the median value in each data set is flanked by upper and lower quartiles represented by the top and bottom of the box, respectively. The top and bottom whiskers show the maximum and minimum values, respectively.

CHAPTER 3

A whole genome quantitative RNAi screen for modifiers of dJNK phosphorylation in *Drosophila* immune signaling.

A version of this chapter has been published.

Bond, D.*, Primrose, D.A.*, and Foley, E. (2008). Quantitative evaluation of signaling events in *Drosophila* S2 cells. *Biological Procedures Online* 10, 20-28.

* Authors contributed equally

Bond, D., and Foley, E. (2009). A quantitative RNAi screen for JNK modifiers identifies Pvr as a novel regulator of *Drosophila* immune signaling. *PLoS Pathogens* 5, e1000655.

3.1 Chapter 3. Introduction.

Drosophila melanogaster responds to gram-negative bacterial challenges through the IMD pathway, a signal transduction cassette that is driven by the coordinated activities of dJNK, NF- κ B and caspase modules. While many modifiers of NF- κ B activity were identified in cell culture and *in vivo* assays, the regulatory apparatus that determines dJNK inputs into the IMD pathway is relatively unexplored. In this chapter, I present the first quantitative screen of the entire genome of *Drosophila* for novel regulators of dJNK activity in the IMD pathway. I identified a large number of gene products that negatively or positively impact on dJNK activation in the IMD pathway. Furthermore, given the pleiotropic involvement of JNK in eukaryotic cell biology, I believe that many of the novel regulators identified in this screen are of interest beyond immune signaling.

3.2. Chapter 3. Results.

3.2.1. Quantification of immune-induced dJNK phosphorylation dynamics in the IMD pathway.

The IMD pathway serves as the principal immune defense pathway to fight gram-negative bacterial infections. As a part of this defense strategy, *Drosophila* engage the dJNK-signaling arm through a kinase-cascade of transient phosphorylation events [158, 159, 312]. It is important that the cell line(s) used in assays faithfully reproduce the salient features of the event(s) being assayed. To determine how well dJNK signaling events in the IMD pathway are recapitulated in *Drosophila* tissue culture cells, I tested the *Drosophila* embryonic S2, S2R+ and Kc167 cell lines for PGN-induced dJNK phosphorylation (P-dJNK). The nontransformed, macrophage-like S2 cell line is derived from an Oregon R wildtype strain embryo, while the S2R+ (receptor plus) cell line is a derivative of the original S2 cell line found to express the Wg receptor, Dfrizzled-2[313, 314]. The Kc167 cell line is a clone of the original Kc line established from embryonic hemocytes, and has plasmatocyte-like properties[315]. The S2, S2R+ and Kc167 transcriptomes show distinct expression patterns in microarray studies[315].

I treated the S2, S2R+ and Kc167 cell lines with a commercially available preparation of *E.coli* lipopolysaccharide (LPS) contaminated with peptidoglycan (PGN); routinely used to activate the IMD pathway[124]. I prepared lysates from S2, S2R+, and Kc167 cells treated with PGN over a time course and probed with phospho-specific dJNK and dJNK antibodies, as a control, in a Western blot assay (Figure 3.1A)[172]. I simultaneously visualized dJNK and P-dJNK antibody stains with secondary antibodies covalently bound with separate, non-

overlapping fluorescent molecules, with peak emission spectra at 680nm and 750 nm, respectively. A distinct benefit of fluorescence-based methods over traditional chemiluminescence detection in Western blot analysis is the ability to accurately quantify the relative levels of multiple proteins in linear fashion over a high dynamic range.

I found the S2 cell line ideal for studying transient dJNK phosphorylation events, because S2 cells most accurately recapitulate key traits of the IMD pathway in flies, and as such are frequently used to model the IMD pathway *in vitro*[137] (Figure 3.1A). In contrast, dJNK is not phosphorylated in S2R+ cells exposed to PGN and is more weakly phosphorylated in PGN-treated Kc167 cells (Figure 3.1B). It remains unclear why the S2R+ cell line, a derivative of the S2 cell line, is nonresponsive to PGN-induced dJNK phosphorylation. In these experiments I monitored P-dJNK levels relative to total dJNK levels. IMD pathway activation showed no observable impact on dJNK levels, and therefore transient dJNK phosphorylation does not result from fluctuations in total cellular dJNK. To determine if PGN-induced dJNK phosphorylation events in S2 cells recapitulate the response to gram-negative bacteria, I collected lysates from untreated cells or cells treated with PGN or dilutions of an overnight culture of *E.coli* (Figure 3.1C). The PGN-induced dJNK phosphorylation was consistent with S2 cells directly contaminated with bacterial cultures. Exposure of S2 cells to PGN resulted in a 17 fold increase in P-dJNK:actin relative to untreated cells, compared to a 7 and 22 fold increases for 1/100 and 1/10 dilutions of overnight *E.coli* cultures, respectively (Figure 3.1D). These data show that commercial

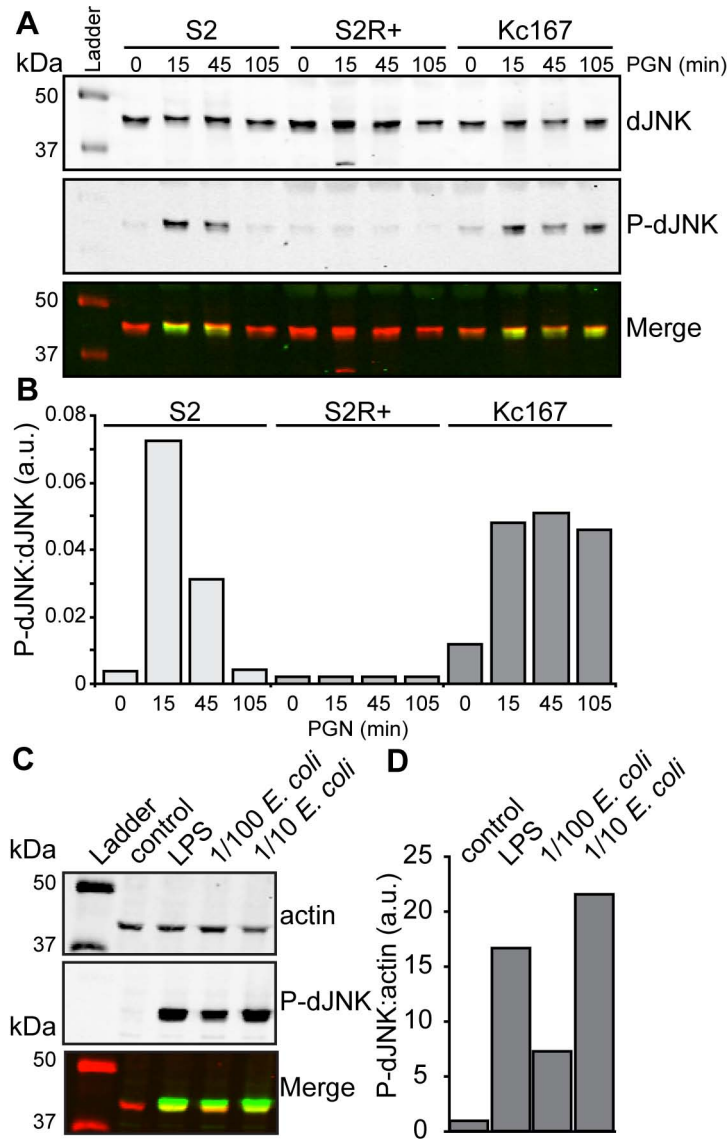


Figure 3.1. Immune-induced dJNK phosphorylation in *Drosophila* cell lines.

A. Western blot of S2, S2R+ and Kc167 cells treated with PGN for the indicated periods. Lysates were probed with anti-dJNK (top panel) and anti-P-dJNK antibodies (middle panel). P-dJNK (green) and dJNK (red) channels were false colored and merged (bottom panel). **B.** Quantification of relative dJNK phosphorylation in (A). dJNK phosphorylation levels were quantified and reported relative to dJNK levels for S2 (columns 1-4), S2R+ (columns 5-8), and Kc167 cells (columns 9-12) for each of the indicated time points. **C.** Western blot of S2 cells treated with PGN or a dilution of an overnight culture of *E. coli*, as indicated. Lysates were probed with anti-actin (top panel) and anti-P-dJNK antibodies (middle panel). P-dJNK (green) and actin (red) channels were false colored and merged (bottom panel). **D.** Quantification of relative dJNK phosphorylation in (C). dJNK phosphorylation levels were quantified and reported relative to actin levels for each of the experimental lysates.

preparations of PGN are a reliable alternative to raw bacterial preparations to engage dJNK activity.

To more accurately determine the dynamics of PGN-induced dJNK phosphorylation, I prepared lysates from S2 cells treated with PGN over a time course and probed with phospho-specific dJNK and actin antibodies, as a control, in a Western blot assay (Figure 3.2A). I observed transient dJNK phosphorylation upon engagement of the IMD pathway (Figure 3.2A). I then quantified P-dJNK levels relative actin levels and I observed PGN-induced dJNK phosphorylation:actin levels peaks at 5min and returns to near basal levels by 60min in S2 cells (Figure 3.2B).

3.2.2. Establishment of an In Cell Western (ICW) assay to monitor dJNK phosphorylation events in S2 cells.

Western blot analysis is an effective method to quantify dJNK phosphorylation events of small sample numbers. However, Western blot analysis is impractical for experiments with large sample numbers, such as genome-scale RNAi screens. To resolve these shortcomings, I developed a quantitative high-throughput In Cell Western (ICW) assay to monitor dJNK phosphorylation events in the IMD pathway. Specifically, I grew S2 cells in 96 well tissue culture plates, stimulated with PGN, and incubated with P-dJNK specific monoclonal antibodies. I detected P-dJNK with fluorescently labeled secondary antibodies and I counterstained the cells with fluorescently tagged phalloidin. Phalloidin binds filamentous actin (f-actin) and serves as a control for cell numbers per well. I then quantified P-dJNK and f-actin levels in each well

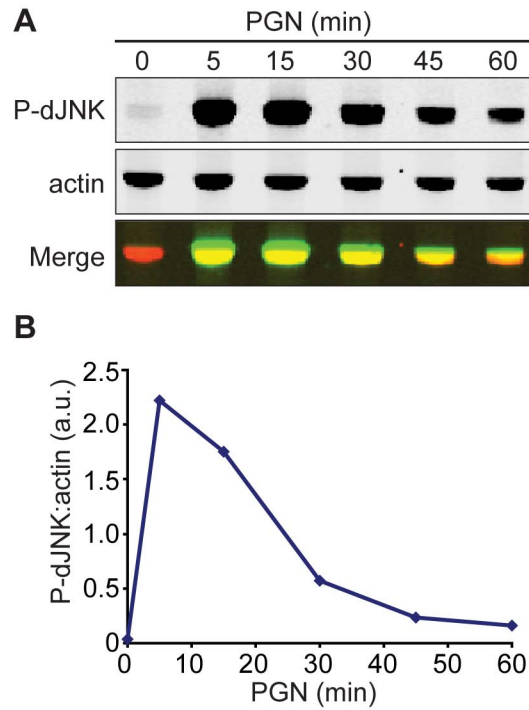


Figure 3.2. dJNK phosphorylation response to PGN exposure.

A. Representative Western blot analysis of S2 cell lysates treated with PGN for the indicated period. Lysates were probed with anti-P-dJNK (top panel) and anti-actin (middle panel) antibodies. P-dJNK (green) and actin (red) channels were false colored and merged (bottom panel). **B.** Quantification of relative dJNK phosphorylation in (A). P-dJNK phosphorylation levels were quantified and reported relative to actin levels for each of the indicated time points.

separately. To determine the ideal P-dJNK antibody concentration, I monitored PGN-induced dJNK phosphorylation with a dilution series of primary antibody by ICW (Figure 3.3A). Quantification of anti-P-dJNK antibody dilutions showed an appreciable loss of dJNK phosphorylation levels past the 1/800 dilution step (Figure 3.3B). I concluded therefore, that a 1/400 dilution of anti-PJNK antibody is optimal to accurately quantify PGN-induced dJNK phosphorylation events in an ICW assay.

To evaluate dJNK phosphorylation dynamics in an ICW assay, I visualized P-dJNK relative to f-actin at various times after PGN treatment. The ICW assay accurately reproduces the expected PGN-induced dJNK phosphorylation profile initially observed by Western blot (Figure 3.4A). IMD pathway stimulation drives intense dJNK phosphorylation in the ICW assay with P-dJNK:f-actin levels peaking at 15min and returning to basal levels by 120min (Figure 3.4B). However, PGN-exposure had no observable impact on f-actin levels. Importantly for the purposes of an RNAi screen, non-targeting GFP dsRNA had no impact on P-dJNK levels, and indicates that dsRNA treatment alone does not effect the dynamics of immune-induced dJNK phosphorylation. Together, these data show that the ICW assay is a potentially useful tool for monitoring PGN-induced dJNK phosphorylation events in a high throughput RNAi screen.

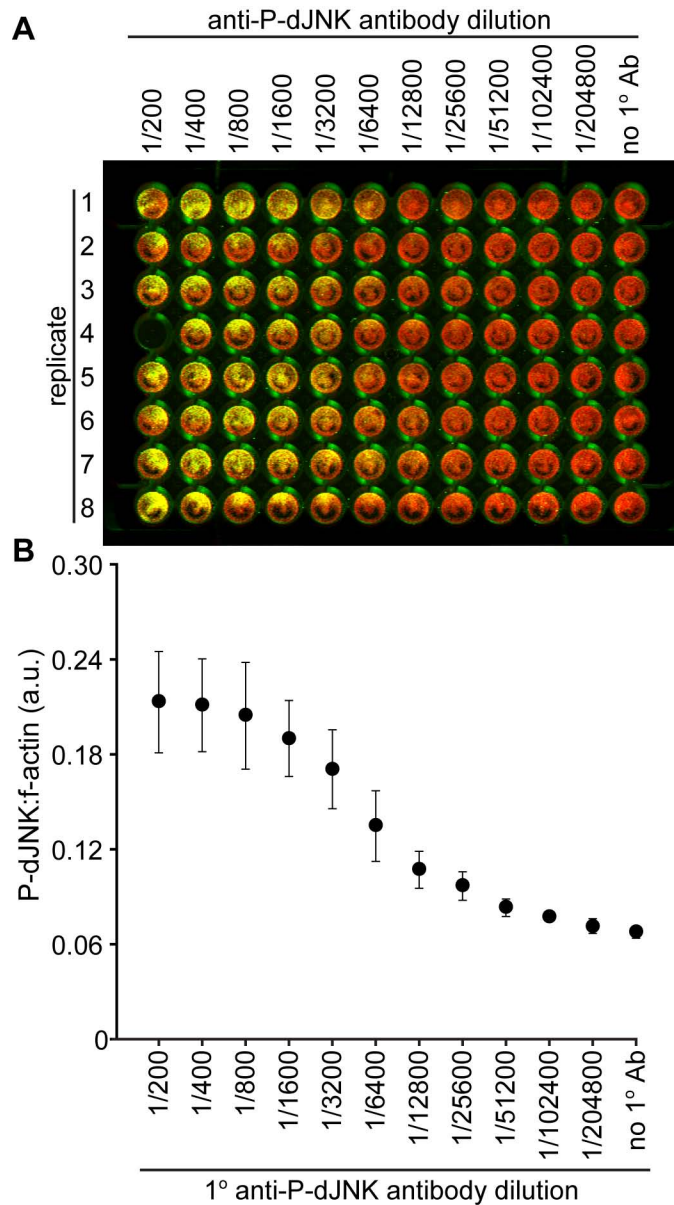


Figure 3.3. Optimization of anti-P-dJNK stain for ICW assay.

A. ICW of dJNK phosphorylation in S2 cells after exposure to PGN for 15min. Cells were stained with dilutions of anti-P-dJNK primary antibodies or no primary antibody, as indicated. P-dJNK (green) and f-actin (red) channels were false-colored and merged. **B.** P-dJNK values from (A) were quantified and normalized to f-actin values in each well. Error bars represent the standard deviation of replicate observations. Pipetting error in lane 4 in (A) was removed from the analysis in (B).

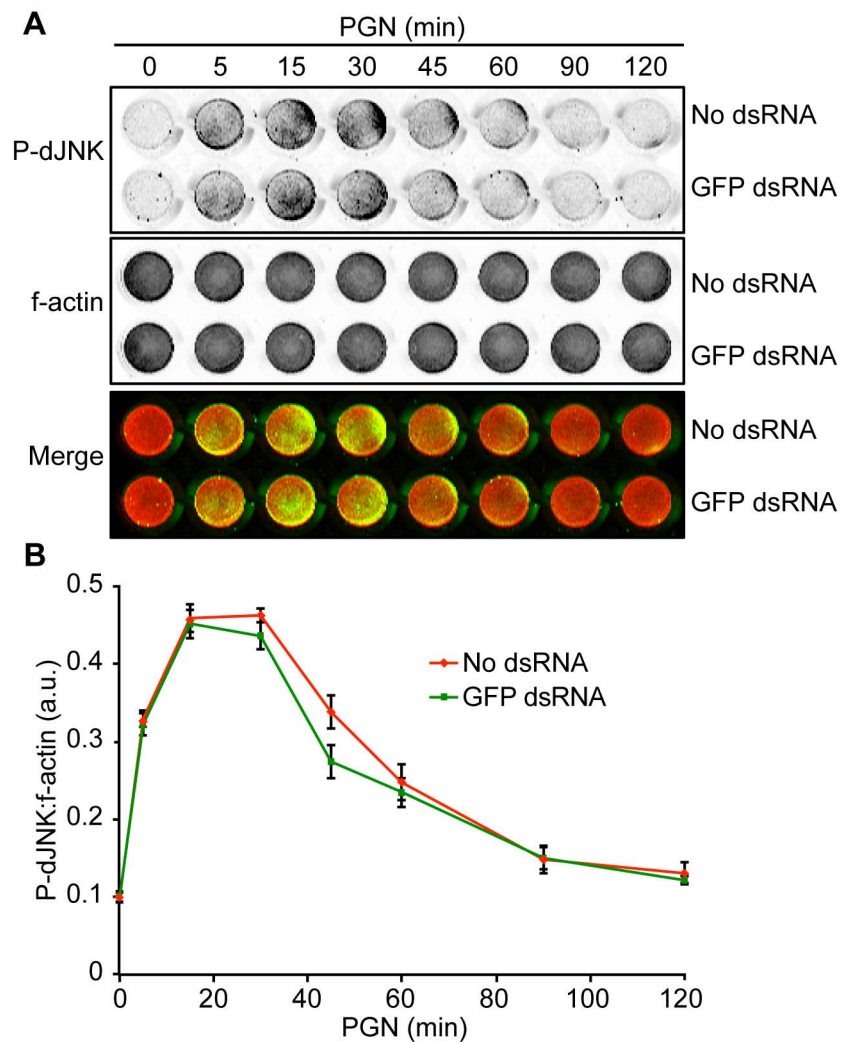


Figure 3.4. Dynamic regulation of immune-induced dJNK phosphorylation by ICW assay.

A. ICW of S2 cells treated with PGN for the indicated periods. Cells were stained with Alexa-fluor 680-labeled phalloidin to detect f-actin (top panel) and anti-P-dJNK antibodies visualized by Alexa-fluor 750-labeled secondary antibodies (middle panel). P-dJNK (green) and f-actin (red) channels were false-colored and merged (bottom panel). **B.** P-dJNK protein levels from (A) were quantified and normalized to f-actin levels in for each time point. Error bars represent the SEM of three independent experiments.

3.2.3 Preliminary RNAi screen for effector on PGN-induced dJNK phosphorylation.

To determine how known enhancers or suppressors control the dynamics of dJNK activation in the IMD pathway, I monitored PGN-induced dJNK phosphorylation in S2 cells with dsRNA targeting dTak1 or Key respectively. I then measured the ratio of P-dJNK to f-actin at various times after PGN treatment by ICW. Consistent with the data presented previously, I observed transient dJNK phosphorylation in response to exposure of S2 cells to PGN (Figure 3.5A). I detected maximal phosphorylation signal 15min after exposure to PGN and P-dJNK levels returned to basal levels within an additional 45min. dTAK1 is an essential MAPKKK for dJNK phosphorylation in response to PGN and loss of dTAK1 blocks PGN-dependent dJNK phosphorylation[312]. Interestingly, I observed a complete block to PGN-mediated dJNK phosphorylation in S2 cells treated with dsRNA targeting dTAK1 (Figure 3.5A and B). Key is part of the IKK complex that activates Rel[67]. A subset of Rel-responsive transcripts contributes to dJNK inactivation and loss of Key leads to prolonged dJNK phosphorylation in S2 cells exposed to PGN[159]. Similarly, I observed sustained dJNK phosphorylation in S2 cells treated with Key dsRNA and exposed to PGN (Figure 3.5A and B). I showed that the ICW assay detects modifiers of the IMD/dJNK pathway in a predictable manner through the RNAi-based inactivation of IMD/dJNK signal transduction elements. Thus, I conclude that the plate-based assay described above reproduces all known features of dJNK activation by the Imd pathway and represents an ideal tool for direct quantification of dJNK phosphorylation events. Furthermore, I established dTAK1

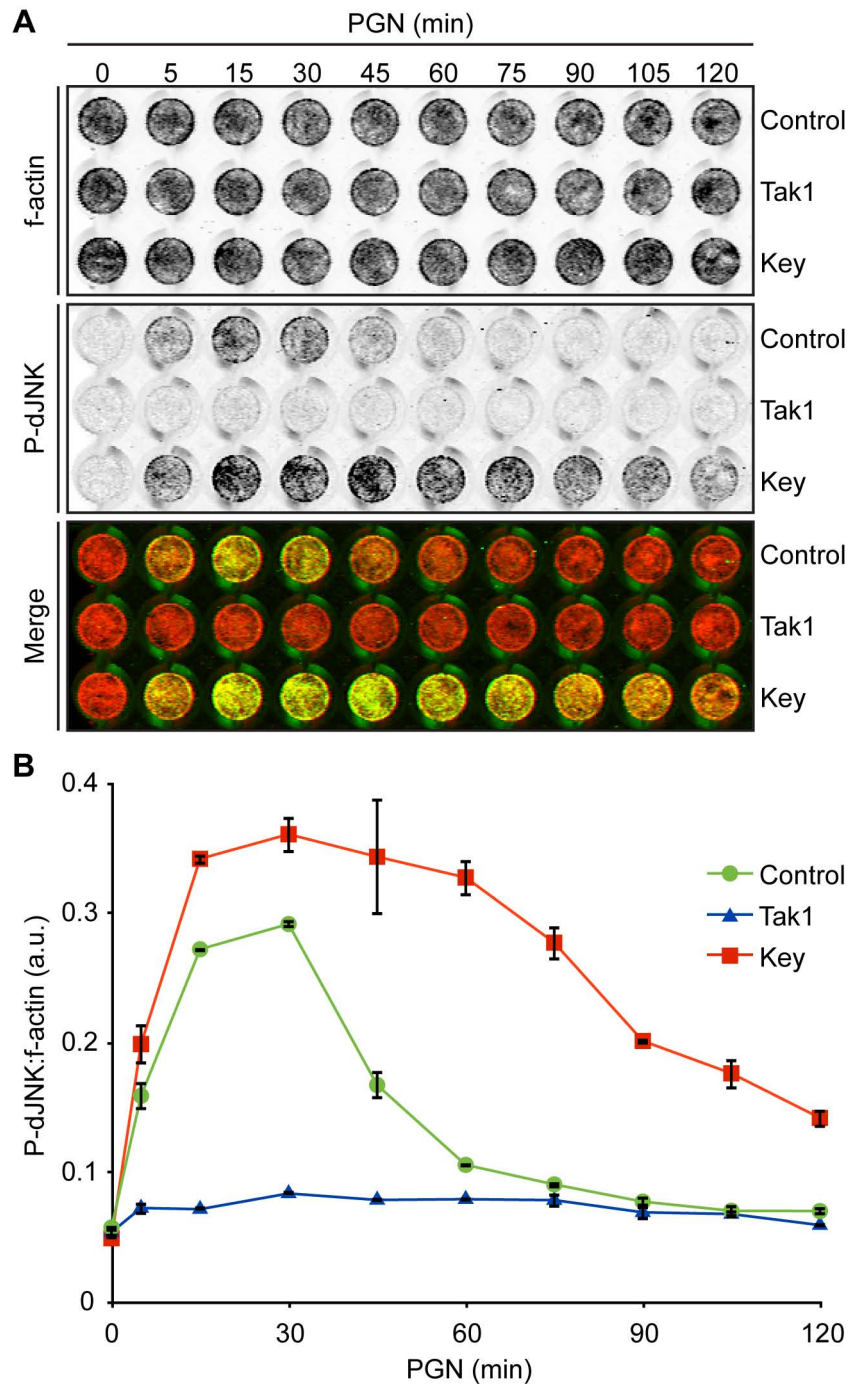


Figure 3.5. ICW quantification of RNAi effects on P-dJNK dynamics.

A. ICW of S2 cells or S2 cells incubated with Tak1 or Key dsRNA and treated with PGN for the indicated periods. Cells were probed anti-P-dJNK antibodies (middle panel) and phalloidin to detect f-actin (top panel). P-dJNK (green) and f-actin (red) channels were false-colored and merged (bottom panel). **B.** P-dJNK protein levels from (A) were quantified and normalized to f-actin levels in for each time point. Error bars show SEM from triplicate replicates from a representative assay.

and Kenny dsRNAs as valuable P-dJNK enhancer and suppressor controls, respectively, for a whole genome RNAi screens.

RNAi screens are a powerful discovery tool to identify previously unknown regulators of cellular pathways[126, 137, 195, 196]. To determine if the ICW assay would be a suitable platform to carry out a high-throughput RNAi screen, I performed a preliminary RNAi screen with a selection of dsRNAs (Table 3.1). Specifically, I treated S2 cells with 28 individual dsRNAs that targeted numerous signaling pathways with a particular focus on established IMD and dJNK signal transduction pathways. I then visualized P-dJNK and f-actin stains in untreated control cells or cells exposed to PGN for 15min or 120min by ICW, to capture dsRNAs that regulate the both intensity and duration of dJNK phosphorylation (Figure 3.6A). Organization of P-dJNK/f-actin values from lowest to highest illuminated distinct groups dJNK phosphorylation modifiers: I. enhancers of P-dJNK levels, II. neutral on P-dJNK levels and, III. suppressors of P-dJNK levels (Figure 3.6B). Established IMD pathway components were commonly found as enhancers or suppressors consistent with their predicted roles in IMD pathway activity. For example, I identified the IKK-complex components *Key/Ird5* as the strong suppressors of dJNK phosphorylation, consistent with their established roles as Rel-activators[67, 141]. I also identified PGRP-LC as a critical enhancer of dJNK phosphorylation, in keeping with its role as the PGN receptor in the IMD pathway[123]. Finally, I showed that depletion of the essential anti-apoptotic protein DIAP1 resulted in a loss of S2 cells presumably due to apoptotic death, as seen by a loss of both P-dJNK and f-actin signals[316]. Given its accuracy at

Table 3.1. Genes targeted in preliminary screen for modifiers of PGN-induced dJNK phosphorylation in the IMD pathway.

Serum free S2 cells were depleted of the genes listed with target-specific dsRNAs, and PGN-mediated dJNK phosphorylation was monitored by ICW.

Gene	Symbol	Gene ontology	Pathway	Ref
<i>dFas associated death domain</i>	<i>dfadd</i>	Immune signaling	IMD	[131]
<i>defense repressor 1</i>	<i>dnr1</i>	Immune signaling	IMD	[137]
<i>Drosophila inhibitor of apoptosis 2</i>	<i>diap2</i>	Immune signaling	IMD	[205]
<i>Drosophila TNF receptor associated 1</i>	<i>dTRAF1</i>	Apoptosis	Eiger/JNK	[317]
<i>Drosophila TNF receptor associated 1</i>	<i>dTRAF2</i>	Apoptosis	Eiger/JNK	[317]
<i>Peptidoglycan recognition protein LC</i>	<i>PGRP-LC</i>	Immune signaling	IMD	[126]
<i>immune response deficient</i>	<i>ird5</i>	Immune signaling	IMD	[143]
<i>kenny</i>	<i>key</i>	Immune signaling	IMD	[318]
<i>immune deficiency</i>	<i>imd</i>	Immune signaling	IMD	[41]
<i>Drosophila inhibitor of apoptosis 1</i>	<i>Diap1</i>	Anti-apoptosis	Ubiquitination	[316]
<i>Misshapen</i>	<i>msn</i>	Development/ Apoptosis	Eiger/JNK	[319, 320]
<i>Apaf-1-related killer</i>	<i>Ark</i>	Apoptosis	Caspase	[321]
<i>Drosophila Jun N-terminal kinase</i>	<i>djnk</i>	Development/ Immune signaling	IMD/JNK	[145, 146]
<i>Drosophila mitogen associated kinase kinase 7</i>	<i>dmkk7</i>	Development/ Immune signaling	IMD/JNK	[146, 322]
<i>TGF-β activated kinase</i>	<i>dtak1</i>	Immune signaling	IMD	[323]
<i>death executioner Bcl-2 homologue</i>	<i>debcl</i>	Apoptosis	Pro- apoptosis	[324]
<i>strica</i>	<i>strica</i>	Apoptosis	Caspase	[325]
<i>head involution defective</i>	<i>hid</i>	Apoptosis	Ubiquitination	[326]
<i>Wengen</i>	<i>wgn</i>	Apoptosis	Eiger	[327]
<i>Eiger</i>	<i>egr</i>	Apoptosis	Eiger	[320]
<i>Drosophila ice</i>	<i>drice</i>	Apoptosis	Caspase	[328]
<i>Dredd</i>	<i>dredd</i>	Immune signaling	IMD	[35]
<i>dronc</i>	<i>dronc</i>	Apoptosis	Caspase	
<i>death executioner caspase related to Apopain/Yama</i>	<i>decay</i>	Apoptosis	Caspase	[329]
<i>Death associated molecule related to Mch2</i>	<i>Damm</i>	Apoptosis	Caspase	[330]
<i>Death caspase-1</i>	<i>Dcp-1</i>	Apoptosis	Caspase	[331]
<i>relish</i>	<i>rel</i>	Immune signaling	IMD	[138]

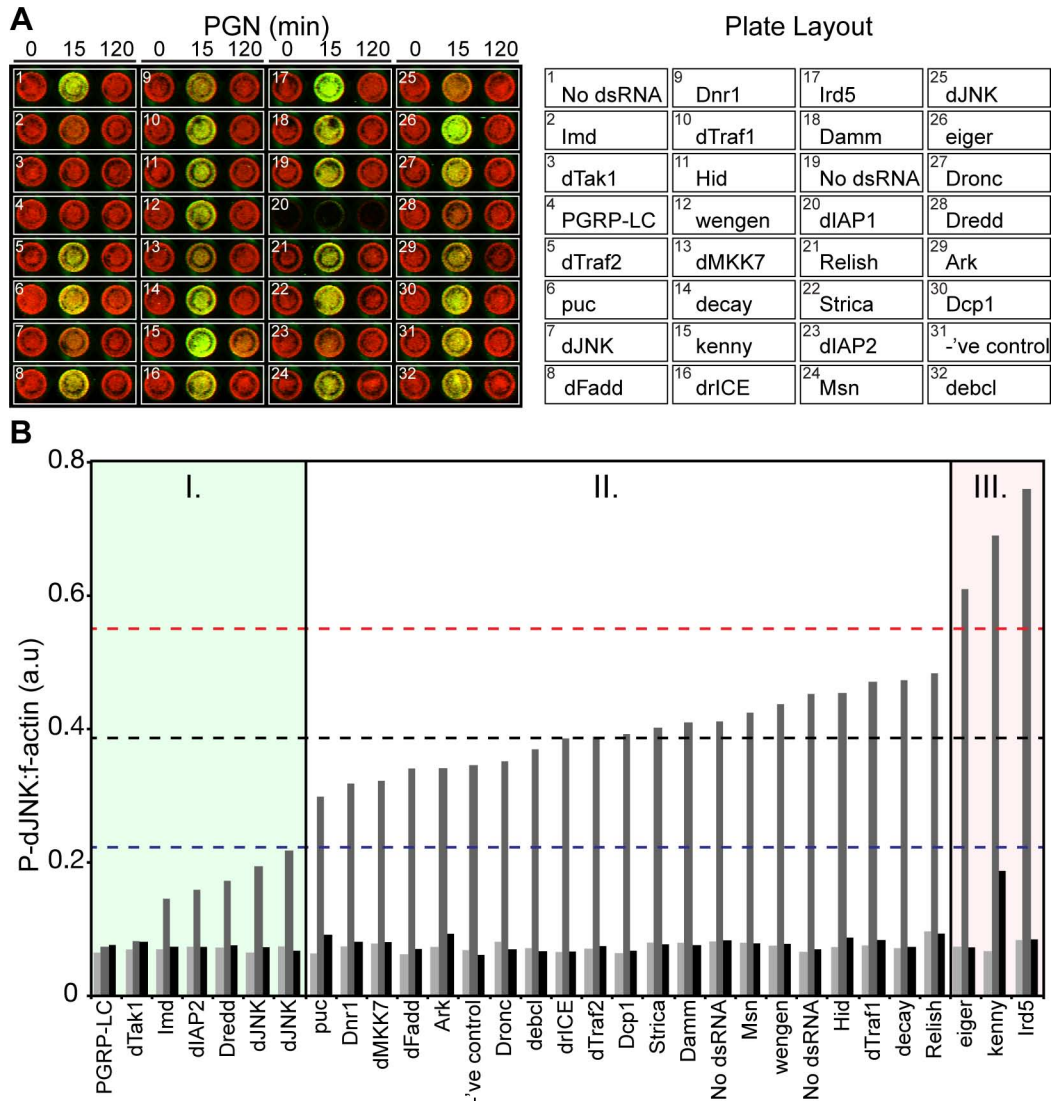


Figure 3.6. Preliminary RNAi screen for modifiers of PGN-induced dJNK phosphorylation in the IMD pathway.

A. Quantification of P-dJNK:f-actin in an ICW assay of S2 cells incubated with dsRNA and treated with PGN for the indicated periods. Cells were probed with anti-P-dJNK antibodies and counterstained with phalloidin to detect f-actin. P-dJNK (green) and f-actin (red) channels were false-colored and merged. Organization of preliminary screen plate is shown (right panel). **B.** P-dJNK protein levels from (A) were quantified and normalized to f-actin levels for each well. dsRNAs were organized from lowest to highest 15min P-dJNK:f-actin value. The black dashed line shows the median value, whereas red and blue lines indicate one standard deviation above and below the median, respectively. Results are grouped into dsRNAs that deplete proteins essential for (I), neutral on (II), or suppressors of (III) dJNK phosphorylation in the IMD pathway. dIAP1 was excluded from analysis due to extensive lethality.

identifying established IMD pathway members, the ICW assay is a valuable tool to identify novel regulators of dJNK phosphorylation.

3.2.4. In-cell Western assay for PGN-induced dJNK phosphorylation.

Based on my preliminary studies described above, I developed a quantitative high-throughput dsRNA screen to identify novel regulators of dJNK signaling in the IMD pathway. With the assistance with others, I generated 15,852 unique dsRNA molecules from a DNA template library that covers all the annotated genes in the *Drosophila* genome[137, 198]. A schematic representation of the ICW method is shown in Figure 3.7. In this assay, I treated *Drosophila* S2 cells with 15,852 dsRNAs and I monitored the subsequent extent of PGN-induced dJNK phosphorylation relative to f-actin by ICW analysis as described previously. To identify genes that modulate the intensity and duration of dJNK phosphorylation, I screened the entire genome at 15min and 60min PGN treatment (Figure 3.8). I reasoned that depletion of gene products that are required for optimal PGN-induced dJNK phosphorylation would decrease dJNK phosphorylation at 15min and I defined such gene products as enhancers of dJNK phosphorylation. Likewise, I reasoned that depletion of gene products involved in the attenuation of dJNK phosphorylation would increase the relative intensity and/or duration of dJNK phosphorylation at fifteen and/or 60min and I defined such gene products as suppressors of dJNK phosphorylation.

A representative 96-well plate from the screen shows P-dJNK (Figure 3.9A) and f-actin stains (Figure 3.9B) merged (Figure 3.9C) after a 15min exposure to PGN. To determine the influence of individual dsRNAs on PGN-induced dJNK

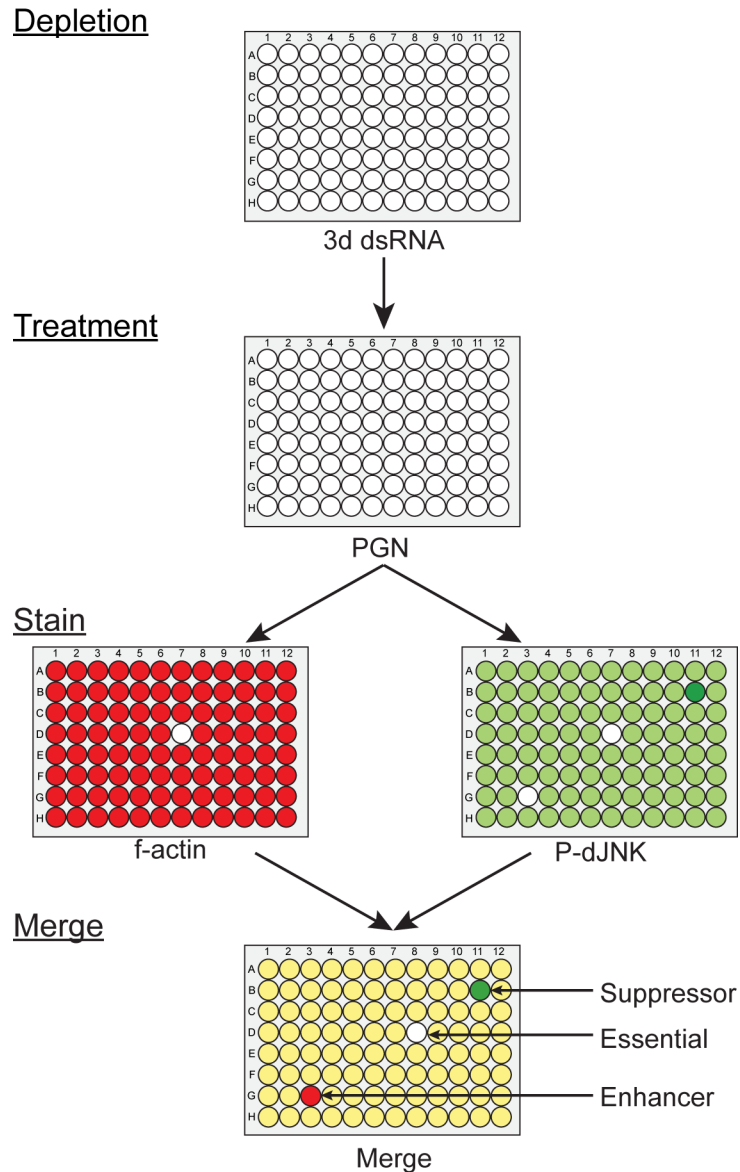


Figure 3.7. Schematic representation of a quantitative RNAi screen for modifiers of PGN-induced dJNK phosphorylation.

S2 cells were incubated with dsRNA in 96 well plates for 3 days prior to exposure to PGN. Cells were stained with an antibody specific for P-dJNK and were counterstained with phalloidin to visualize f-actin. dJNK phosphorylation levels were quantified relative to f-actin levels. Loss of activators (enhancers) of dJNK phosphorylation decreases dJNK phosphorylation. In contrast, loss of inhibitory gene products (suppressors) increases dJNK phosphorylation. Essential gene products are visible as wells with no dJNK or f-actin staining.

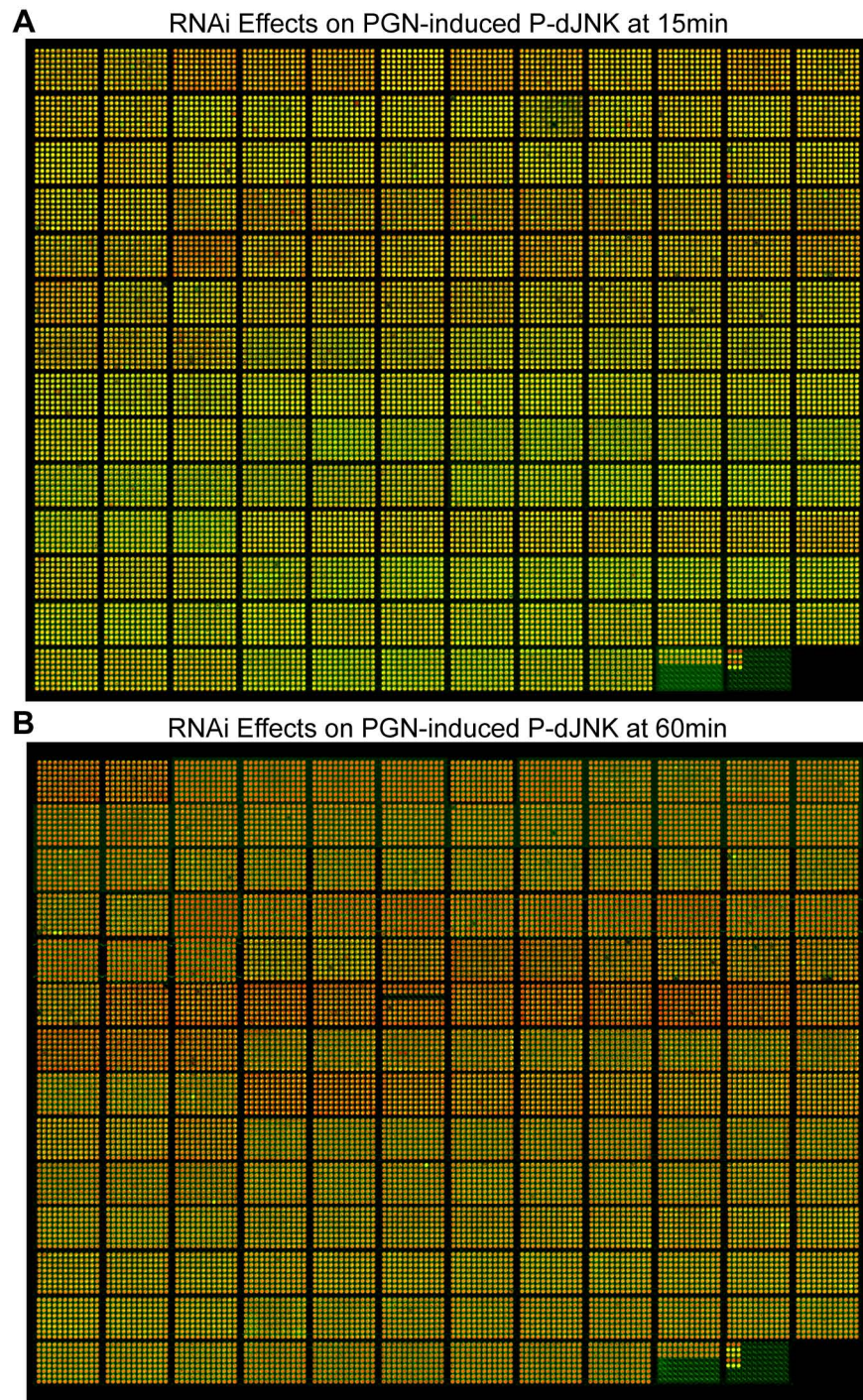


Figure 3.8. Whole genome RNAi screen for modifiers of dJNK phosphorylation in the IMD pathway.

ICW of S2 cells incubated with 15852 distinct dsRNAs and treated with PGN for 15min (A) or 60min (B). Cells were stained with anti-P-dJNK and counterstained for f-actin. P-dJNK (green) and f-actin (red) channels were false colored and merged. S2 cells were untreated or treated with dsRNA targeting Key or Tak1 in triplicate as suppressor and enhancer controls respectively (bottom right corner).

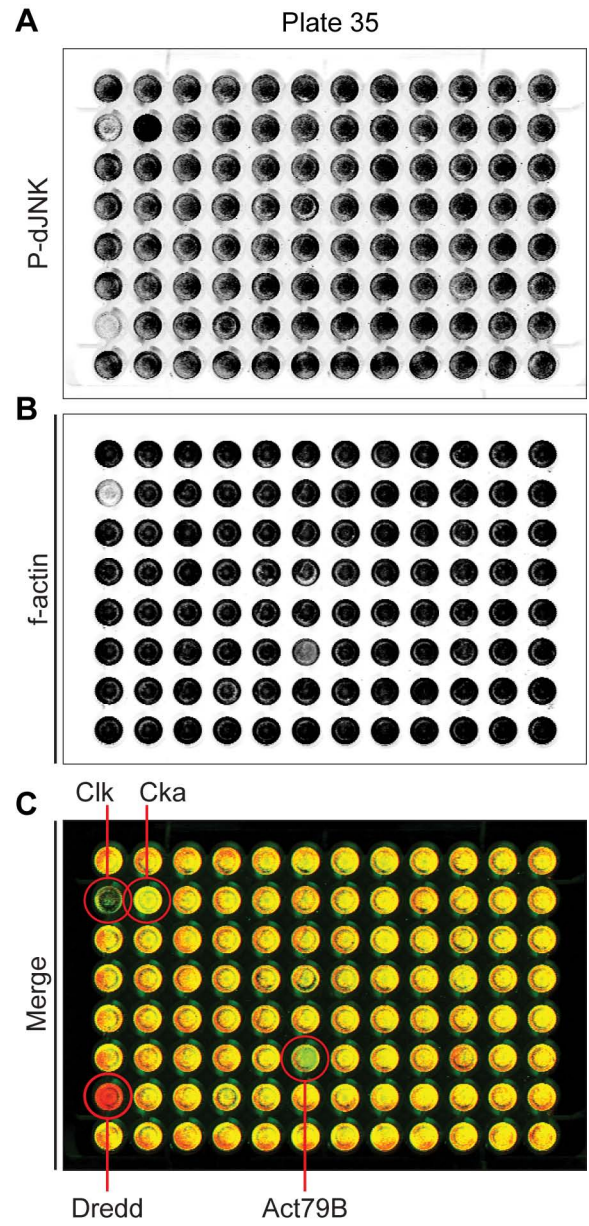


Figure 3.9. Representative plate from P-dJNK dsRNA screen. S2 cells incubated with 96 distinct dsRNAs were treated with PGN for 15min. Cells were stained for P-dJNK (A) and counterstained for f-actin (B). To visualize relative P-dJNK levels, P-dJNK (green) and f-actin (red) channels were false colored and merged (C). ICW assay identified dsRNAs that deplete enhancers (Dredd) and suppressors (Cka) of dJNK phosphorylation, as well as proteins essential for cell viability (Clk) and actin levels (Act79B).

phosphorylation, I measured the raw P-dJNK and f-actin levels in each of the 96 wells (Figure 3.10A). On this plate I identified Dredd as an enhancer of dJNK phosphorylation consistent with its role as an essential upstream regulator of IMD pathway signals[132, 133, 135, 332]. In addition, I found Cka, an essential scaffold protein in the dJNK signaling pathway in embryo development, as a suppressor of PGN-induced dJNK phosphorylation[333]. However, this is the first report linking Cka to dJNK activity in the IMD pathway. As expected, I identified the dsRNA that targets actin isoform Act79B as a regulator of f-actin levels. I also discovered Clk, a master transcriptional regulator of the *Drosophila* circadian clock, as an essential gene for S2 cell viability. I considered Clk an essential gene because its depletion led to the complete loss of both f-actin and P-dJNK signals. To eliminate dsRNAs, like Clk, that negatively affected cell viability or cell adherence, I excluded dsRNAs that greatly reduced cell numbers as determined by an absence of f-actin fluorescence (z -score < -2.58 , or 99% CI) from subsequent analyses. If a dsRNA significantly reduces f-actin levels then the normalized P-dJNK:f-actin ratio will give the false impression that the dsRNA controls dJNK activity. I then calculated the P-dJNK:f-actin z -score for all remaining wells to determine the statistical significance of dsRNA-treatment on PGN-induced dJNK phosphorylation and to allow for inter-plate comparisons (Figure 3.10B). The z -score is a statistic that indicates the number of standard deviations from the median for a given sample. From the z -score I can assign a probability (p -value) that the sample is a hit based on a two-tailed standard distribution. For example a z -score of ± 1.96 is equivalent to a p -value of 0.05, or the 95 percentile, while a z -score of ± 2.58 is equivalent to a p -value of 0.01, or the 99 percentile. Furthermore, a Z score with a positive value identifies a

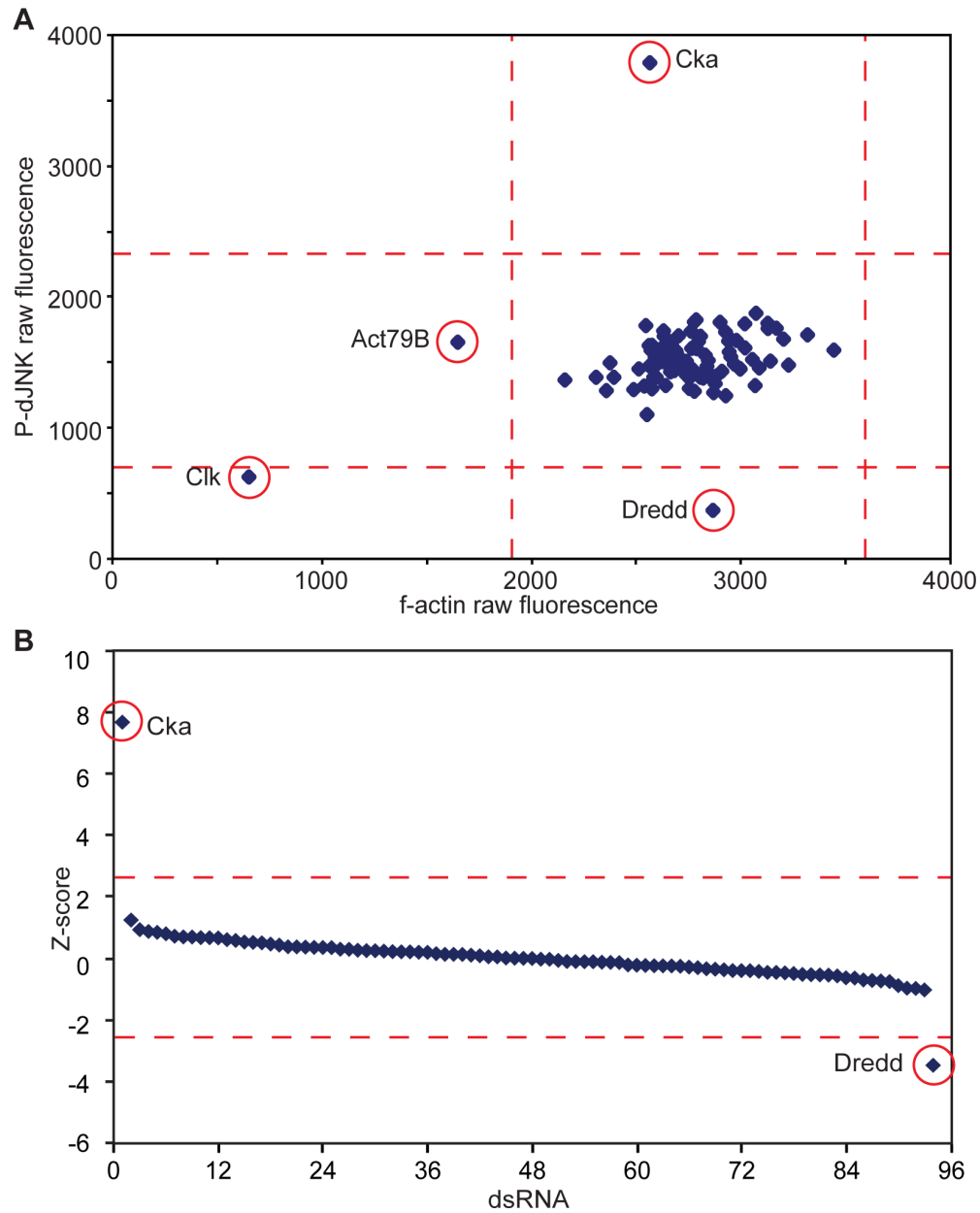


Figure 3.10. Quantification of relative dJNK phosphorylation levels from representative plate.

A. Raw dJNK phosphorylation values were graphed against raw f-actin values. Red dashed lines indicate ± 2.58 standard deviations from the median for both P-dJNK and f-actin values. dsRNA targeting the established dJNK modifiers Dredd and Cka decrease or increase dJNK phosphorylation levels respectively with no effect on f-actin levels. **B.** Statistical analysis of PGN-induced dJNK phosphorylation relative to f-actin from plate 35. P-dJNK values were standardized to f-actin values for each of the 96 dsRNA treatments. Red dashed lines represent z-score values of ± 2.58 . dsRNA that targeted Cka and Dredd were identified as significant modifiers of PGN-induced dJNK phosphorylation. Clk and Act79B in (A) were excluded from analysis in (B) due to loss of f-actin signal.

suppressor of dJNK phosphorylation, while a Z score with a negative value identifies an enhancer of dJNK phosphorylation. By these criteria, I successfully identified Cka and Dredd as statistically significant modifiers of dJNK phosphorylation with z-scores of 7.70, (p-value $<10^{-10}$) and -3.48 (p-value <0.0005), respectively. These data indicate that the ICW assay is an effective method to detect modifiers of PGN-induced dJNK phosphorylation in S2 cells.

3.2.5. Quantitative analysis of a high-throughput dsRNA screen for regulators of PGN-induced dJNK phosphorylation.

To visualize the impact of 15,852 dsRNAs on PGN-induced dJNK phosphorylation at 15min and 60min, I measured the raw fluorescence level of P-dJNK and f-actin for each dsRNA at each time point. I then calculated the fold change from the median plate value for each of the 96 wells per plate. Graphical analysis of the fold change values in phosphorylation against f-actin PGN exposure shows a distinct clustering of dsRNAs (Figure 3.11A, 3.12A). At 15min PGN-exposures most dsRNAs had no effect on P-dJNK levels relative to the plate median, however a subset of dsRNAs decreased or increased P-dJNK levels with no appreciable impact on f-actin (center left or center right, respectively, Figure 3.11A). An additional subset of dsRNAs drastically reduced the raw fluorescent levels of both P-dJNK and f-actin, indicating that these genes are likely essential for S2 cell viability (lower left corner, Figure 3.11A). Graphical analysis of P-dJNK and f-actin fold change values at 60min PGN-exposures showed clear enhancement of PGN-induced dJNK phosphorylation within a subset of dsRNAs (upper right quadrant, Figure 3.12A). However, dsRNAs that

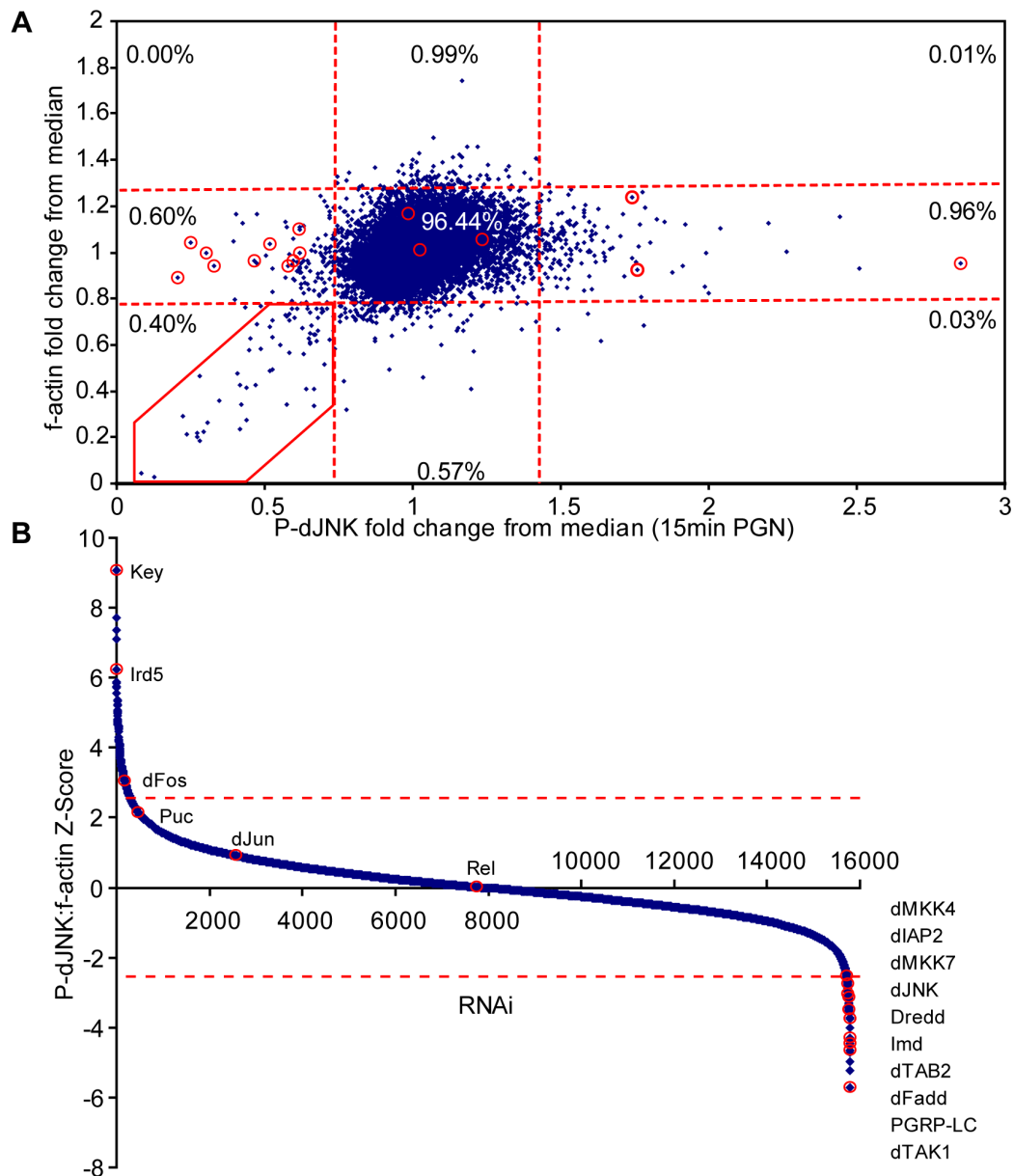


Figure 3.11. Whole genome RNAi screen for 15min enhancers and suppressors of dJNK phosphorylation in the IMD pathway.

A. Scatter plot of P-dJNK:f-actin values in S2 cells treated with 15852 distinct dsRNAs and exposed to PGN for 15min. Cells were stained for P-dJNK and f-actin and raw dJNK phosphorylation and f-actin fluorescence values were measured by quantitative ICW assay. P-dJNK and f-actin values were calculated as a fold change from the median in each plate. Red dashed lines indicate the top or bottom 1%. **B.** Quantification of relative dJNK phosphorylation in A. The relative P-dJNK:f-actin z-score was determined for each dsRNA. The red dashed lines represent z-score values of + or - 2.58. Red circles in panels A and B show the position of established IMD pathway members. dsRNAs that modified f-actin levels in (A) were excluded from further analysis in (B).

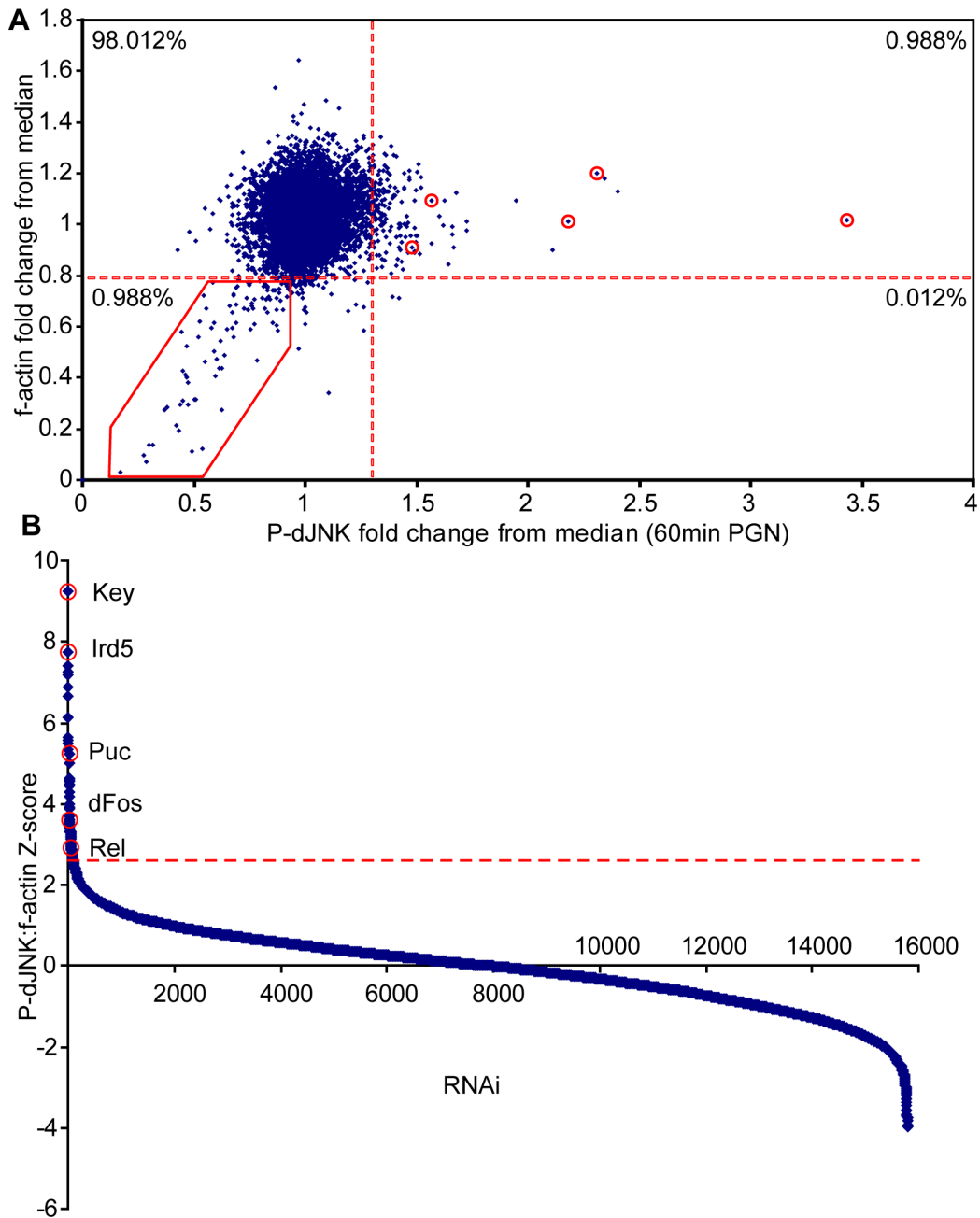


Figure 3.12. Whole genome RNAi screen for suppressors of dJNK phosphorylation in the IMD pathway.

A. Scatter plot of P-dJNK:f-actin values in S2 cells treated with 15852 distinct dsRNAs and exposed to PGN for 60min. Cells were stained for P-dJNK and f-actin and raw dJNK phosphorylation and f-actin fluorescence values were measured by quantitative ICW assay. P-dJNK and f-actin values were calculated as a fold change from the median in each plate. The red dashed lines indicate the top 1%. **B.** Quantification of relative dJNK phosphorylation in A. The relative P-dJNK:f-actin z-score was determined for each dsRNA. The red dashed lines represent z-score values of + 2.58. Red circles show the position of core IMD pathway components. f-actin modifiers were excluded from further analysis in (B).

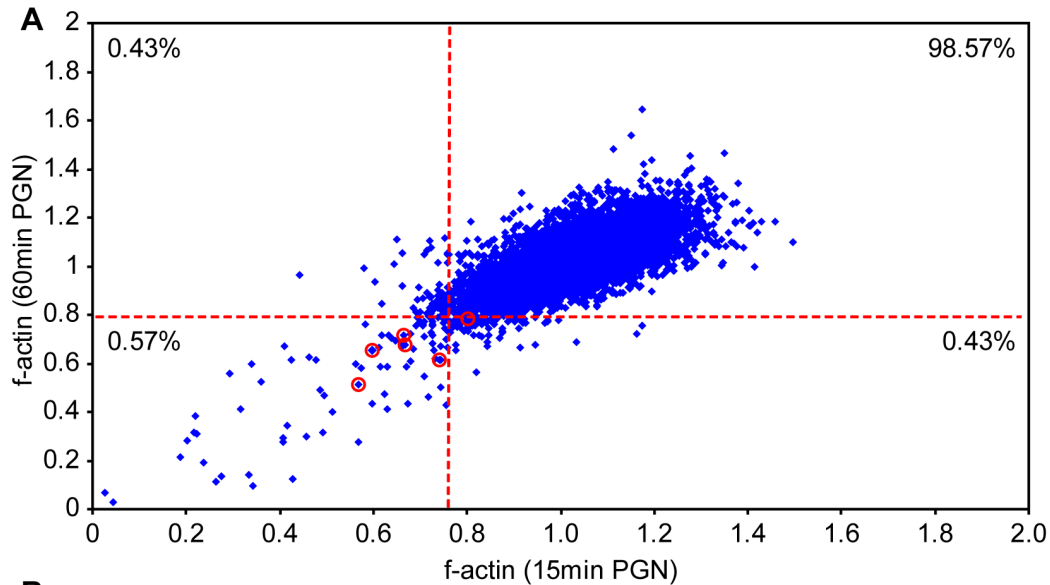
decrease P-dJNK levels are noticeably absent as PGN-induced phosphorylation returns to near basal levels by 60min (upper left quadrant). These analyses clearly identify dsRNAs that modify PGN-induced dJNK phosphorylation in the IMD pathway, however fail to provide a meaningful statistical evaluation of the screen results.

To provide quantitative statistical analysis to the P-dJNK screen results, I determined the z-score for all non-lethal dsRNA treatments, as described previously. I graphed all the z-scores from highest to lowest for both 15min and 60min PGN-exposures (Figure 3.11B, 3.12B). dsRNA-mediated depletion of enhancers or suppressors of PGN-dependent dJNK phosphorylation resulted in reduced or elevated P-dJNK z-scores, respectively. At 15min PGN treatment, I identified 292 and 594 suppressors of dJNK phosphorylation in the 99th (z-score > 2.58) and 95th (z-score > 1.96) confidence intervals, respectively (Table A1). Furthermore, at 60min PGN treatment, I identified 110 and 280 suppressors of prolonged dJNK phosphorylation in the 99th and 95th confidence intervals, respectively (Table A2). Finally, I found 73 and 222 enhancers of dJNK phosphorylation in the 99th and 95th percentiles, respectively, at the 15min PGN treatment (Table A3). The z-scores for all dsRNAs tested are found at http://www.mmi.med.ualberta.ca/staff_students/Bond_Thesis_Screen_Data.pdf. I disregarded the P-dJNK enhancers at 60min PGN-exposure because the level of PGN-induced dJNK phosphorylation was not sufficiently elevated over background P-dJNK levels. I identified Key as the strongest suppressor of dJNK phosphorylation at both 15min and 60min with z-scores of 9.05 and 9.23, respectively. Conversely, I identified dTAK1 as the strongest enhancer of dJNK

phosphorylation at 15min PGN-exposure with a z-score of -5.7 . As the Key/Rel axis of the IMD pathway attenuates dJNK activation and dTAK1 is essential for dJNK phosphorylation, these data are consistent with the known roles of Key and dTAK1 in the IMD pathway[159]. These findings give confidence that I also identified novel regulators of dJNK phosphorylation in the IMD pathway.

3.2.6. Regulators of f-actin levels in S2 cells.

While the primary objective of the RNAi screen was to identify novel regulators of dJNK phosphorylation, it is likely that I serendipitously identified regulators of the formation of actin filaments as a consequence of using phalloidin as a counterstain. I therefore calculated the fold changes from the median in phalloidin stain as a measure of f-actin levels in each of the 96 wells per plate. I then graphed all of the f-actin values for each dsRNA tested at both 15min and 60min (Figure 3.13A). In support of the accuracy of this re-analysis, I identified 5 of the 6 actin genes present in the dsRNA library in the lower 1 percent of f-actin modifiers for both the 15min and 60 minute time points (Figure 3.13B). However, this data set of f-actin modifiers also included dsRNAs lethal to S2 cell viability. Therefore, I selected f-actin modifiers that had no significant impact on dJNK phosphorylation at 15min, to distinguish dsRNA that specifically regulate f-actin levels from dsRNAs that may effect S2 cell viability (Table A4, A5). These data remain largely unexplored, however they provide a potentially useful resource for future studies into factors that regulate cellular f-actin levels.



B

Gene	PGN (min)	
	15	60
Actin 42A	0.742958	0.611865
Actin 57B	0.808539	0.789314
Actin 5C	0.664536	0.713959
Actin 79B	0.598418	0.654224
Actin 87E	0.668471	0.675951
Actin 88F	0.569152	0.513721

Figure 3.13. Whole genome RNAi screen for dJNK phosphorylation highlights enhancers of filamentous actin.

A. Scatter plot of f-actin levels from S2 cells incubated with 15852 individual dsRNAs and treated with PGN for 15min and 60min. S2 cells were stained with phalloidin and the raw fluorescence value was calculated as a fold change from median for each 96-well plate. Red lines indicate lower 1% percent for 15min and 60min. Red circles show dsRNAs that target actin. **B.** Filamentous actin levels calculated as a fold change from the plate median for six individual actin dsRNAs tested in the whole genome screen. Values are shown for 15min and 60min exposures to PGN.

3.2.7. Gene ontology of dJNK phosphorylation regulators.

To gain a broad perspective on the screen results, I grouped all suppressors of dJNK phosphorylation with z-scores above 2.58 (99th percentile confidence interval) at fifteen and sixty minutes and all enhancers of dJNK phosphorylation with z-scores below -2.58 at fifteen minutes according to their known biological functions (Figure 3.14A). I identified many genes involved in innate immune signaling, in addition to a large number of genes with previously uncharacterized functions. As a testament to the saturation of this screen, I identified fifteen IMD pathway components as modulators of PGN-induced dJNK phosphorylation with z-scores above 1.96 or below -1.96 (Figure 3.14B). I note that in each case the z-score is consistent with the established role of the fifteen genes as either suppressors or enhancers of dJNK phosphorylation (Figure 3.14C).

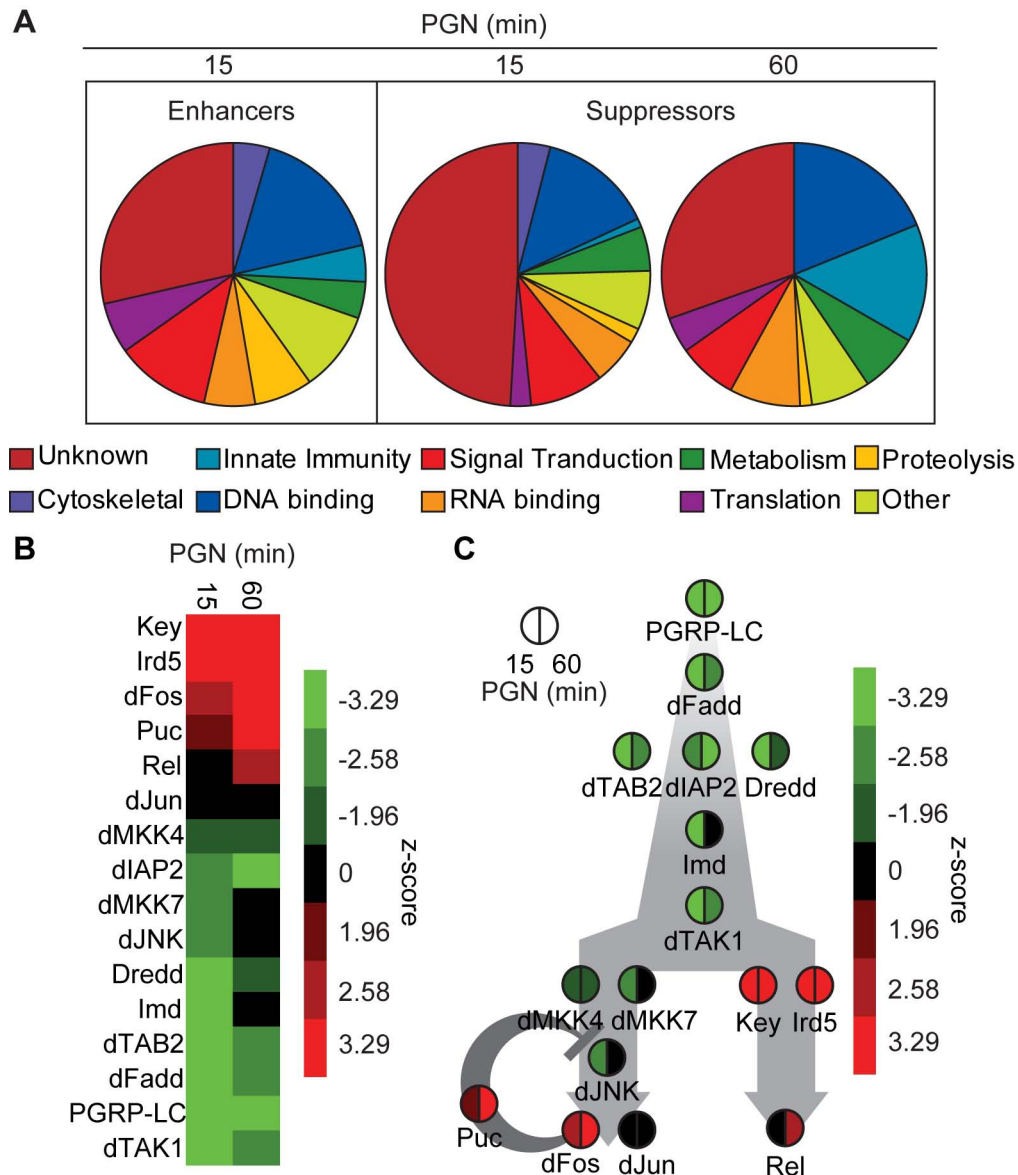


Figure 3.14. Analysis of whole genome screen for modifiers of dJNK phosphorylation.

A. Modifiers of the dJNK phosphorylation response to PGN were grouped according to biological functions. The biological functions for enhancers of dJNK phosphorylation with a z-score below -2.58 at 15min PGN exposure are presented (left panel). Additionally, the biological functions for suppressors of dJNK phosphorylation with a z-score above 2.58 at 15min and 60min PGN-exposure are presented (right panel). **B.** Heat map of z-score values for S2 cells depleted of known Imd pathway components and exposed to PGN for 15min or 60min. Core IMD pathway components were identified in the screen as either suppressors (z-scores above 1.96) or enhancers (z-scores below -1.96) of PGN-induced dJNK phosphorylation respectively. **C.** Schematic of IMD pathway with heat map values from (B). 15min and 60min values are shown on the left and right of the circle respectively. All known IMD pathway components were identified in the P-dJNK screen with the exception on dJun.

CHAPTER 4

The Pvr signal axis is a novel suppressor of Drosophila innate immune responses.

A version of this chapter has been published.

Bond, D., and Foley, E. (2009). A quantitative RNAi screen for JNK modifiers identifies Pvr as a novel regulator of *Drosophila* immune signaling. *PLoS Pathogens* 5, e1000655.

4.1. Chapter 4. Introduction.

Given the conserved and pleiotropic roles of JNK in eukaryote biology, I performed a quantitative high-throughput RNAi screen to identify novel regulators of dJNK activity in the *Drosophila* IMD pathway. In this screen, I identified numerous novel negative and positive regulators of dJNK signaling including the receptor tyrosine kinase Pvr pathway. Knockdown of Pvr and PVR pathway components with dsRNA enhanced PGN-induced P-dJNK levels at 15min with minimal impact on P-dJNK levels at 60min. I therefore hypothesized that the PVR pathway negatively regulates dJNK phosphorylation in the IMD pathway. In this chapter, I show that dsRNA-mediated depletion of Pvr in S2 cells significantly enhances PGN-induced IMD pathway responses through both dJNK and Rel (NF- κ B) signaling arms. In agreement with the RNAi studies, I found that engagement of Pvr pathway signals actively suppress IMD pathway responses in S2 cells. Additionally, I discovered that PGN-induced IMD pathway activation promotes the expression of Pvr-ligands *pvf2* and *pvf3* in a dJNK dependent manner. These data uncover a previously unknown negative-feed back loop, whereby immune-induced activation of dJNK results in the production of *pvf2* and *pvf3* and engagement of the Pvr pathway, which in turn suppresses immune responses. I extended these studies to an *in vivo* infection model to determine the role of the Pvr pathway in regulating *Drosophila* innate immune responses. I found that RNAi-mediated depletion of Pvr, *in vivo*, resulted in elevated immune responses in adult flies under aseptic conditions and upon systemic challenge with gram-negative bacteria. Together these data indicate that the Pvr signal transduction pathway constitutes a novel negative regulator of the *Drosophila* IMD pathway.

4.2. Chapter 4. Results.

4.2.1. Validation of Pvr as a suppressor of PGN-induced dJNK phosphorylation.

To test the validity of the dsRNA screen, I selected a representative cohort of P-dJNK enhancers and suppressors for secondary analysis. To resolve if these dsRNA specifically regulate dJNK phosphorylation or total dJNK protein levels, I monitored PGN-induced P-dJNK relative to dJNK in independent secondary ICW assays. I reasoned that normalizing P-dJNK directly to dJNK provides a more direct measure of relative dJNK phosphorylation levels compared to the phalloidin stain. I therefore adapted the ICW assay to examine the dynamics of PGN-induced dJNK phosphorylation relative to dJNK (Figure 4.1A, B). S2 cells were untreated or treated with dsRNA targeting dJNK, and Tak1 or Key, as enhancer and suppressor controls respectively. I observed that dJNK dsRNA significantly reduced total dJNK protein levels, while dJNK levels were unchanged in cells exposed to dTak and Key dsRNA, relative to untreated control cells. However, dJNK dsRNA did not effect the PGN-induced dJNK phosphorylation profile when P-dJNK was measured relative to total dJNK protein levels by ICW, relative to control cells. Consistent with previous results, treatment of S2 cells with dsRNA targeting Tak1 and Key resulted in a loss of PGN-induced dJNK phosphorylation or elevated and prolonged dJNK phosphorylation, respectively. These data show that ICW analysis of P-dJNK relative to dJNK discriminates between dsRNAs that regulate total dJNK protein levels or dJNK phosphorylation, in secondary assays.

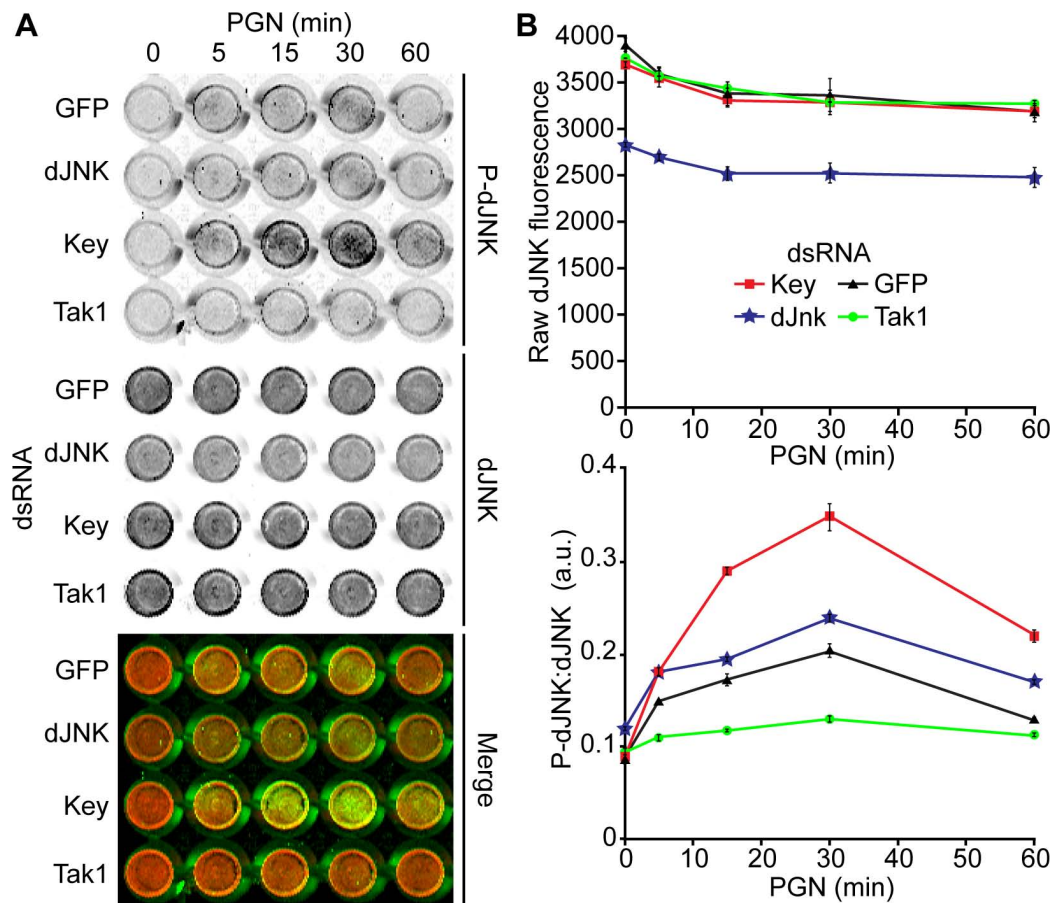


Figure 4.1. In-Cell quantification of RNAi effects on dJNK phosphorylation relative to JNK.

A. ICW of S2 cells or S2 cells incubated with dJNK, Tak1 or Kenny dsRNA and treated with LPS for the indicated periods. Cells were stained with anti-JNK (top) and anti-P-JNK antibodies (middle). P-dJNK (green) and f-actin (red) channels were false-colored and merged (bottom). **B.** Raw dJNK fluorescence values from A are shown for each time point (top graph). P-dJNK protein levels from A were quantified and normalized to dJNK levels for each time point. The P-dJNK:dJNK ratio are shown for every time point in each treatment group (bottom graph). Error bars represent the standard error of three independent experiments.

I selected a subset of three enhancers and eight suppressors of PGN-induced dJNK phosphorylation for secondary analysis based on a number of criteria. More specifically, I chose genes with established roles in signal transduction not previously known to modify dJNK activity in the IMD pathway, as I reasoned that these genes would most likely represent novel dJNK regulatory networks. These genes were selected throughout the range of P-dJNK suppressors and enhancers, with z-scores greater than 1.96 or less than -1.96 (95% confidence interval), respectively. I then monitored the effect of dsRNA treatment for all genes in the cohort on dJNK phosphorylation relative to f-actin at zero, 15min and 60min PGN-exposure. I compared the eleven putative modifier dsRNAs to two dsRNAs (CG11318 and Toll) that had no effect on dJNK phosphorylation in the primary screen. The value of these dsRNA controls is that like the test dsRNAs they are processed by the exogenous RNAi-pathway and target genuine cellular mRNAs, however they have no effect on dJNK phosphorylation levels.

Secondary dsRNA analysis was consistent with the screen results as nine of the eleven dsRNAs significantly modified dJNK phosphorylation relative to f-actin compared to control dsRNA (Figure 4.2A). Even though I excluded actin modifiers from my primary data analysis, I considered the possibility that a fraction of the phenotypes observed might be indirectly caused by effects on f-actin or total dJNK protein levels, as opposed to dJNK phosphorylation. To test this hypothesis, I depleted each gene in the cohort and monitored PGN-induced dJNK phosphorylation relative to total dJNK by ICW, with the aforementioned ICW assay (Figure 4.2B). I observed that the P-dJNK:dJNK analysis essentially

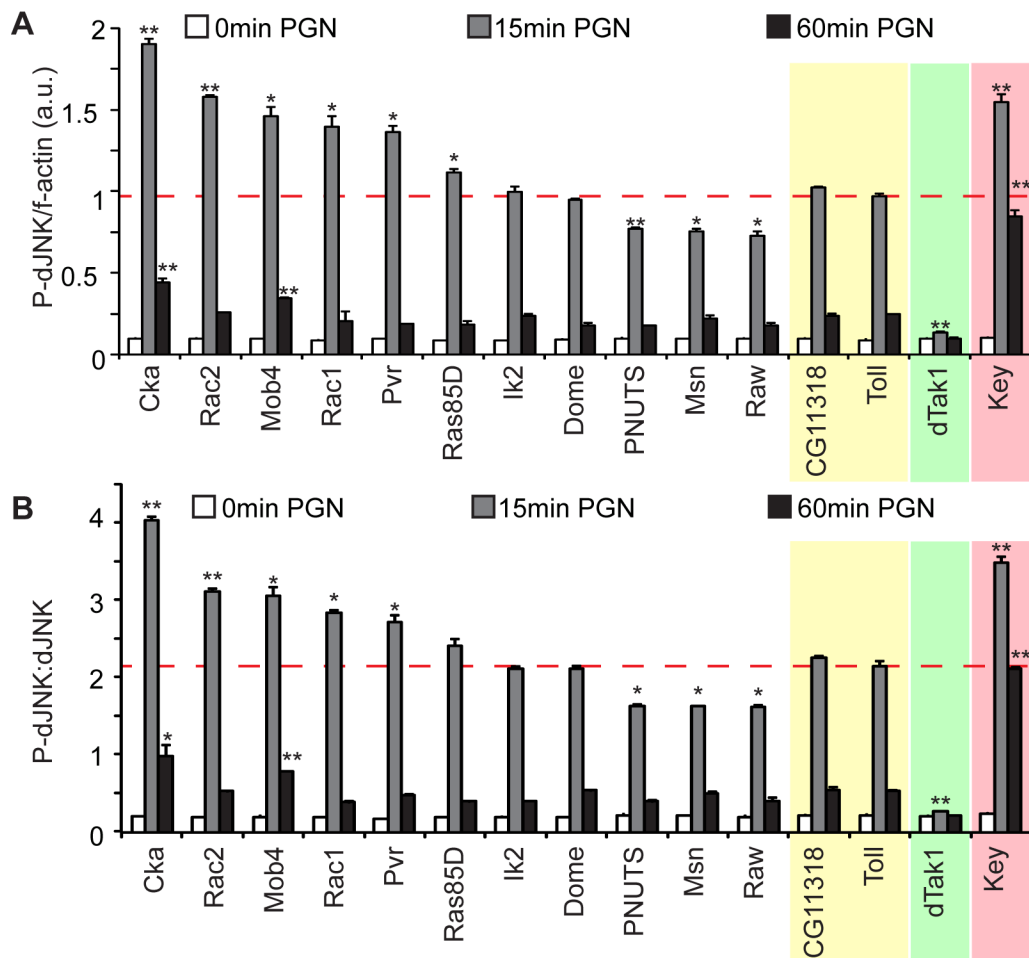


Figure 4.2. Secondary analysis of selected modifiers of dJNK phosphorylation.

Quantification of PGN-induced dJNK phosphorylation relative to f-actin (A) or total JNK (B). S2 cells were incubated with the indicated dsRNAs and exposed to PGN at 0min, 15min or 60min as indicated. Key (red box) and dTak1 (green box) dsRNA were used as modifier dsRNA controls, whereas Toll and CG11318 dsRNA (yellow box) were used as non-modifier dsRNA controls. Cells were stained with anti-P-dJNK antibody and dJNK phosphorylation was standardized to f-actin (A) and total dJNK (B). Data are presented as the mean of two independent experimental values and error bars indicate + SEM. The red dashed line represents the mean dJNK phosphorylation value for Toll dsRNA and dsRNAs that significantly modulated dJNK phosphorylation from this value are indicated (*=p-value < 0.05, **=p-value < 0.01). Secondary dsRNA analysis recapitulates the dJNK phosphorylation values from the primary screen in nine of the eleven dsRNA tested.

mirrored the P-dJNK:f-actin analysis for each gene in the cohort. Thus, I have confidence that my screen primarily identified regulators of PGN-dependent dJNK phosphorylation rather than total cellular JNK levels. To map relationships between the identified modulators of PGN-induced dJNK phosphorylation, I mined genetic and physical interaction databases to develop an interaction network for all hits in my primary screen. I restricted the interaction network to include direct physical or genetic interactions exclusively between genes identified in the primary screen that formed nodes. Within this direct interaction network I identified a group with a high density of interactions that spanned the IMD and the dJNK signaling pathways (Figure 4.3). Interestingly, I identified the receptor tyrosine kinase, Pvr, as a major node within this branch. The PVR pathway integrates signals from three Pvr-ligands, Pvfs 1, 2 and 3 to engage intracellular signaling events that control a multitude of cellular responses including migration, survival and proliferation. However, these data also implicate Pvr as a novel suppressor of PGN-induced dJNK phosphorylation in the IMD pathway. These findings are consistent with previous screens that identified Ras/dERK signaling components as suppressor of the IMD pathway[137, 205].

To confirm Pvr as a suppressor of dJNK phosphorylation in the IMD pathway, I depleted S2 cells of Pvr with two independent non-overlapping dsRNAs and monitored relative dJNK phosphorylation upon exposure to PGN at zero, 15min and 60min. I confirmed that both dsRNAs deplete Pvr by monitoring Pvr protein levels relative to actin in S2 cell lysates using Pvr specific antibodies (Figure 4.4A). Treatment of S2 cells with Pvr dsRNA 1 or 2 reduced relative Pvr protein levels to 1.6% and 15.6% of the control, respectively. In addition, depletion of Pvr

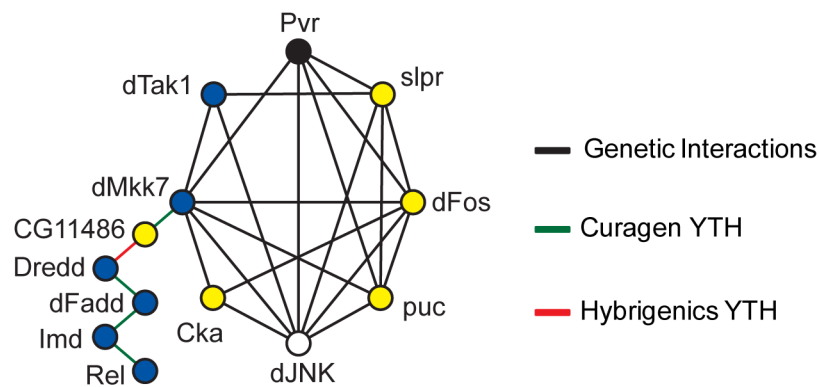


Figure 4.3. Genetic and physical interaction networks of dJNK phosphorylation modifiers from previous studies.

Modulators of dJNK phosphorylation with z-scores greater than 1.96 or less than -1.96 were grouped in an interaction network using genetic and physical interaction databases. Within this network I identified *Pvr*/IMD pathway interactions. *Pvr* (black circle) and *dJnk* (white circle) are connected directly and indirectly through a number of intermediate genes (yellow circles). The *Pvr* and *dJnk* interaction network also connects to IMD pathway (blue circles).

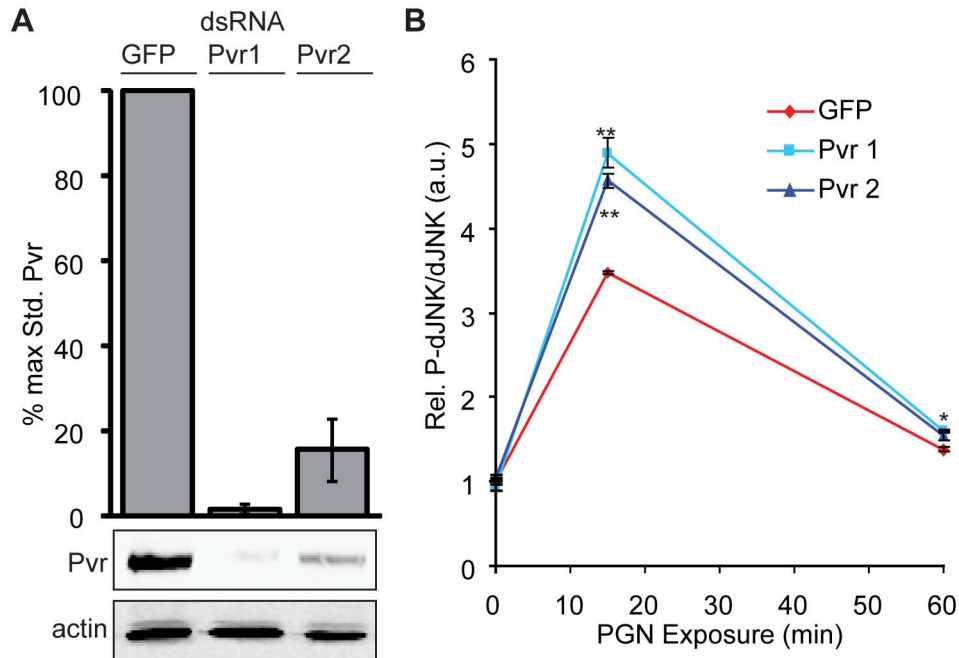


Figure 4.4. Pvr is a negative regulator of dJNK phosphorylation in the IMD pathway.

A. Quantitative Western blot analysis of lysates from S2 cells treated with either Pvr or GFP dsRNA. Lysates were probed with anti-Pvr (top blot) and anti-actin (bottom blot) antibodies. Pvr levels were quantified relative to actin (top graph). Data are presented as the mean of three independent experiments and error bars indicate + SEM. Both Pvr dsRNA molecules deplete Pvr in S2 cells. **B.** ICW quantification of PGN-induced dJNK phosphorylation. S2 cells were treated with GFP dsRNA as a control or two independent non-overlapping dsRNA targeting Pvr as indicated. Cells were exposed to PGN and dJNK phosphorylation was monitored relative to total dJNK. P-dJNK:dJNK values at 0h PGN exposure with GFP dsRNA were assigned a value of 1 and the remaining P-dJNK:dJNK values are reported relative to these data. Data is expressed as the mean of two independent experiments and the error bars represent +/- SEM. Significant differences in P-dJNK values are indicated (*=p-value < 0.05, **=p-value < 0.01). Depletion of Pvr increases PGN-induced dJNK phosphorylation at 15min, indicating that Pvr negatively regulates dJNK activation in the IMD pathway.

by either dsRNA significantly increased PGN-induced dJNK phosphorylation at 15min (Figure 4.4B). Thus, I conclude that Pvr suppresses PGN-dependent dJNK phosphorylation.

4.2.2. *pvf2* and *pvf3* are IMD/dJNK-responsive transcripts.

Pvr is primarily known for its role in *Drosophila* ERK signaling and cell migration. To investigate the involvement of the PVR pathway in attenuation of dJNK activation, I charted the dJNK:f-actin z-scores for each member of the Pvr/dERK axis based on the primary screen data (Figure 4.5A). As a comparison, I charted the dJNK:f-actin z-scores for members of the wingless (Wg) pathway; a signal transduction pathway with no known interaction with the IMD/dJNK module (Figure 4.5B). As expected, my data do not indicate any major interactions between the wingless and IMD/dJNK pathways. In contrast, my data consistently indicate that the Pvr/dERK pathway negatively regulates dJNK activation. Ablation of the Pvr ligands Pvf2 and Pvf3, Pvr, established dERK adaptors, Ras, dERK, and the transcription factor Pnt known to induce transcriptional responses to dERK signaling, resulted in considerably increased PGN-mediated dJNK phosphorylation[334].

As negative feedback loops control the IMD pathway at many levels, I asked if IMD pathway activation results in expression of Pvr ligands. Treatment of S2 cells with PGN resulted in a minor decline in the expression of *pvf1* and significant increases in the levels of *pvf2* and *pvf3* expression (Figure 4.6). Induction of *pvf2* and *pvf3* reached maximal levels within one hour of PGN treatment and reverted to basal levels by six hours. These expression patterns

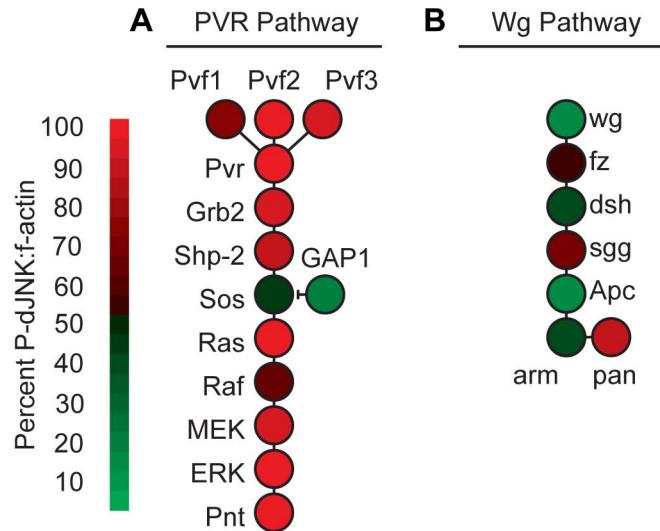


Figure 4.5. The PVR pathway suppresses PGN-induced dJNK phosphorylation.

Heat map analysis of known PVR pathway genes shown in **A**. compared to known Wg pathway genes shown in **B**. from the whole genome dsRNA screen results at 15min PGN-exposure. 15min PGN-induced dJNK:f-actin z-scores were ordered from highest to lowest and organized according to percentile intervals. Genes colored more red indicate suppressors of PGN-induced dJNK phosphorylation while genes colored more green indicate enhancers of PGN-induced dJNK phosphorylation. PVR pathway components were consistently identified as suppressors of PGN-induced dJNK phosphorylation.

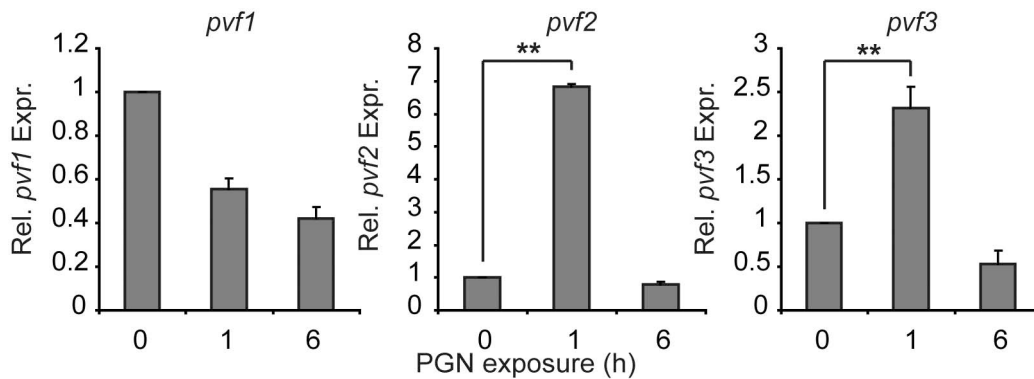


Figure 4.6. *pvf2* and *pvf3* are Immune-Induced transcripts.

Quantitative real-time PCR analysis of standardized *pvf1,2* and *3* expression in S2 cells treated with PGN for the indicated times. The uninduced expression levels for *pvf1,2* and *3* were given a values of 1 and the remaining *pvf1,2* and *3* expression values are reported relative to these values. Data are presented as the mean of three independent experiments and error bars indicate the + SEM. Significant differences in expression values are indicated (**=p-value < 0.01).

are reminiscent of other IMD/dJNK-responsive transcripts. To test if *pvf2* and *pvf3* are dJNK-responsive transcripts, I pre-incubated S2 cells with the dJNK inhibitor SP600125 or DMSO as a solvent control, and monitored the subsequent levels of *pvf2* and *pvf3* expression in response to PGN. My data showed that SP600125 completely blocked the PGN-dependent expression of *pvf2* and *pvf3* (Figure 4.7). Likewise, I observed a significant reduction in PGN-dependent *pvf2* induction in cells depleted of PGRP-LC (Figure 4.8A) or dMKK4/dMKK7 (Figure 4.8B), confirming a requirement for the IMD/dJNK cassette in *pvf2* induction by PGN. In summary, these data show that activation of the IMD pathway results in the dJNK-dependent expression of the Pvr ligands Pvf2 and Pvf3 and that the Pvr/dERK pathway attenuates dJNK activation.

4.2.3. Pvr suppresses PGN-induced Rel signaling.

Given that Pvr suppresses dJNK signaling in the IMD pathway, I asked if Pvr also modulates Rel signaling events. To determine if Pvr depletion affects Rel signaling in the IMD pathway, I depleted S2 cells of Pvr with two independent non-overlapping Pvr dsRNAs and monitored PGN-induced AMP expression. Specifically, I monitored expression of the Rel-responsive AMPs *dipt* and *att*. Depletion of Pvr by either dsRNA profoundly strengthened PGN-induced expression of *att* and *dipt* in comparison to control S2 cells (Figure 4.9A and B). Additionally, Pvr depletion significantly increased the basal expression levels of both *att* and *dipt*, in the absence of PGN stimulation. In fact, the basal levels of *att* or *dipt* expression in cells treated with Pvr dsRNA are approximately equal to the PGN-induced expression levels in cells treated with GFP control dsRNA. These data show that loss of Pvr in S2 cells results in an increase in both the

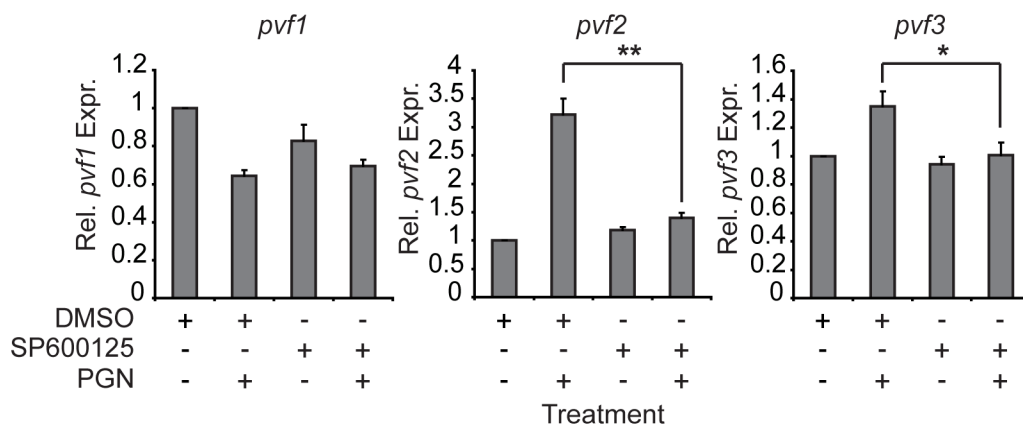


Figure 4.7. *pvf2* and *pvf3* transcripts are dJNK-dependent.

Quantitative real-time PCR analysis of standardized *pvf1,2* and *3* expression in S2 cells or S2 cells treated with SP600125. S2 cells were incubated with SP600125 or DMSO, as a control, for 1h prior to exposure to PGN for 1h, as indicated. The uninduced expression levels for *pvf1,2* and *3* were given values of 1 and the remaining *pvf1,2* and *3* expression values are reported relative to these values. Data are presented as the mean of three independent experiments and error bars indicate the + SEM. Significant differences in P-JNK values are indicated (*=p-value < 0.05, **=p-value < 0.01).

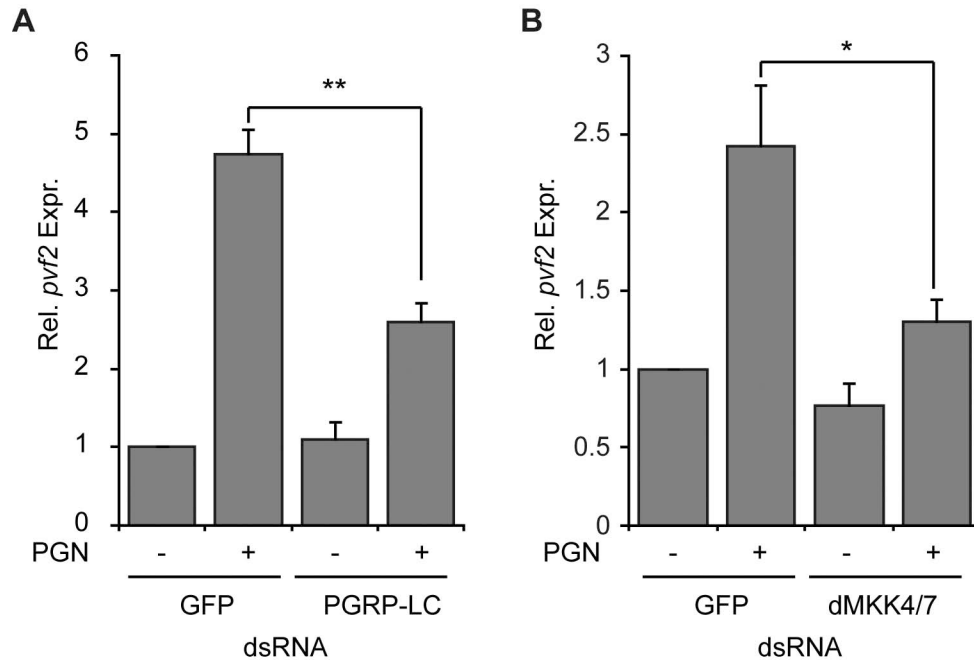


Figure 4.8. Immune-induced *pvf2* transcription requires an intact IMD pathway.

A. Quantitative real-time PCR analysis of standardized *pvf2* expression in S2 cells incubated with GFP or PGRP-LC dsRNA and treated with PGN as indicated. Data are presented as the mean of three independent experiments and error bars indicate the + SEM. Significant differences in *pvf2* expression levels are indicated (**=p-value < 0.01). **B.** Quantitative real-time PCR analysis of standardized *pvf2* expression in S2 cells incubated with GFP or a combination of dMKK4/7 dsRNA and treated with PGN as indicated. Data are presented as the mean of three independent experiments and error bars indicate the + SEM. Significant differences in *pvf2* expression levels are indicated (*=p-value < 0.05).

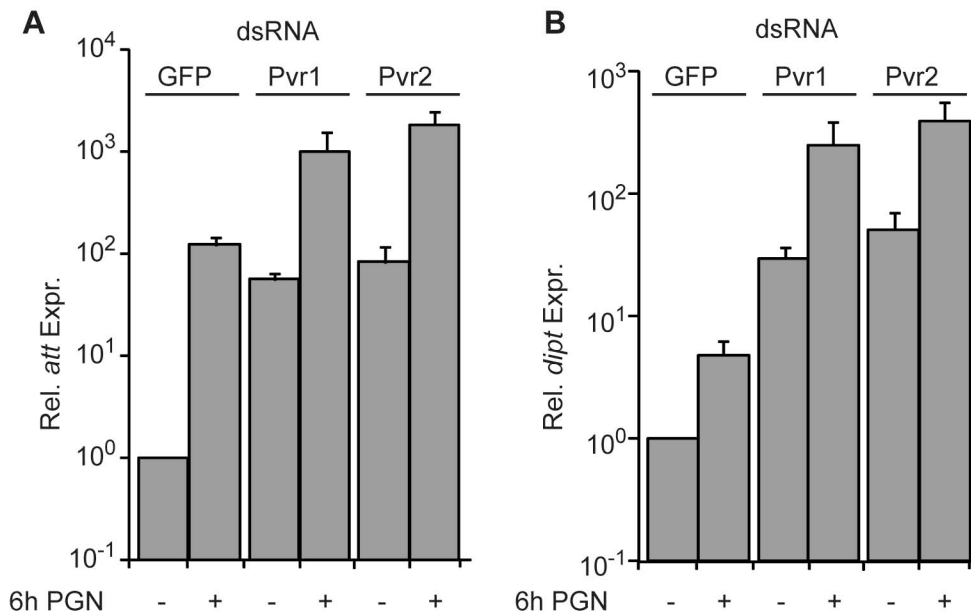


Figure 4.9. Pvr depletion increases antimicrobial peptide production in S2 cells.

A. Quantitative real-time PCR analysis of standardized *att* expression in S2 cells incubated with either GFP or two distinct Pvr dsRNA. S2 cells were treated with PGN were indicated. *att* expression levels of unstimulated S2 cells treated with GFP dsRNA were assigned a value of 1 and the remaining *att* expression values are reported relative to these values. Data are presented as the mean of two independent experiments and error bars indicate the + SEM. **B.** Quantitative real-time PCR analysis of standardized *dip*t expression in S2 cells incubated with either GFP or two distinct Pvr dsRNA. S2 cells were treated with PGN for 6h were indicated. *dip*t expression levels of unstimulated S2 cells treated with GFP dsRNA were assigned a value of 1 and the remaining *dip*t expression values are reported relative to these values. Data are presented as the mean of two independent experiments and error bars indicate + SEM.

uninduced and the PGN-induced expression of AMPs.

To confirm that the increased AMP expression observed upon Pvr loss proceeds through Rel, I then examined the expression of *att* in S2 cells that were simultaneously treated with Pvr and Rel dsRNA. As expected, depletion of Pvr increased the PGN-mediated expression of *att* (Figure 4.10A). In contrast, PGN-mediated expression of *att* was greatly reduced in cells treated with a combination of Rel and Pvr dsRNA. Thus, my data indicate that the bulk of Pvr RNAi-dependent increases in *att* expression proceed through the IMD/Rel module. In agreement with a role for the PVR pathway in reducing *att* expression, I also observed increased *att* induction in cells treated with Ras85D dsRNA (Figure 4.10B). As Pvr loss leads to enhanced Rel-mediated AMP expression, I then asked if Pvr affects Rel cleavage or Rel phosphorylation. Whereas depletion of Pvr greatly sensitized S2 cells to PGN-dependent induction of dJNK phosphorylation (e.g. compare lanes 5 and 11, Figure 4.11A), I did not detect alterations in the pattern of PGN-induced Rel cleavage in S2 cells treated with Pvr dsRNA (Figure 4.11A). In contrast, I detected prolonged and increased PGN-responsive phosphorylation of Rel (P-Rel) in S2 cells treated with Pvr dsRNA (Figure 4.11B). These data indicate that Pvr negatively regulates the PGN-induced phosphorylation of both dJNK and Rel in the IMD pathway.

4.2.4. Pvr signaling suppresses PGN-dependent IMD pathway activation.

Given my findings that Pvr depletion increases AMP expression, I asked if activation of Pvr suppresses the IMD pathway. I monitored dERK phosphorylation to visualize Pvr signaling, as Pvr engagement results in

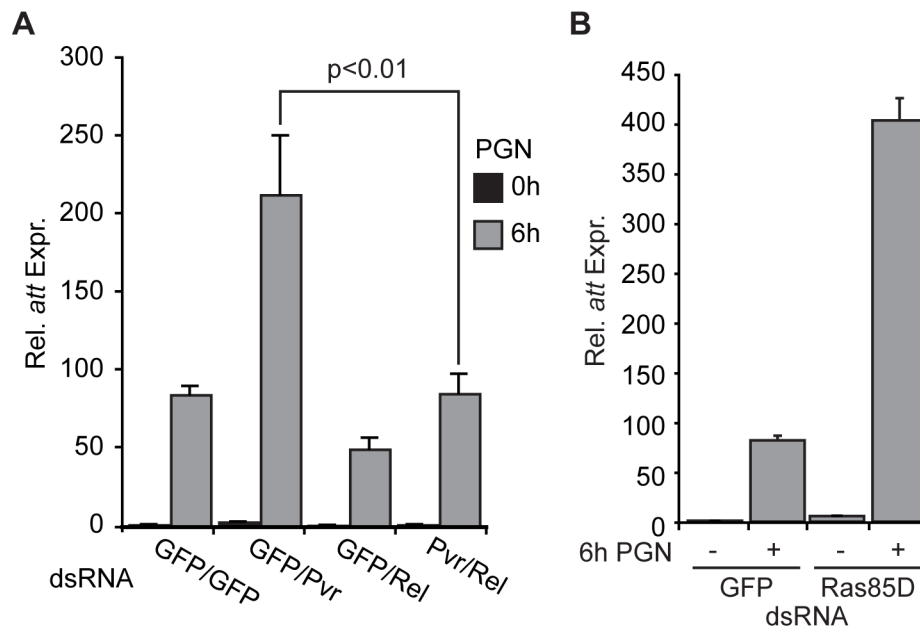


Figure 4.10. Pvr depletion enhances IMD pathway production of antimicrobial peptides.

A. Quantitative real-time PCR analysis of standardized *att* expression in S2 cells incubated with GFP or Pvr dsRNA in combination with Rel dsRNA. S2 cells were treated with the indicated dsRNAs and unstimulated or stimulated with PGN for 6h as indicated. *att* expression levels of unstimulated S2 cells treated with GFP dsRNA were assigned a value of 1 and the remaining *att* expression values are reported relative to these values. Data are presented as the mean of three independent experiments and error bars indicate the + SEM. Significant differences in *att* expression values are indicated with a p-value. **B.** Quantitative real-time PCR analysis of standardized *att* expression in S2 cells incubated with GFP or Ras85D dsRNA and treated with PGN as indicated. Data are presented as the mean of two independent experiments and error bars indicate the + SEM.

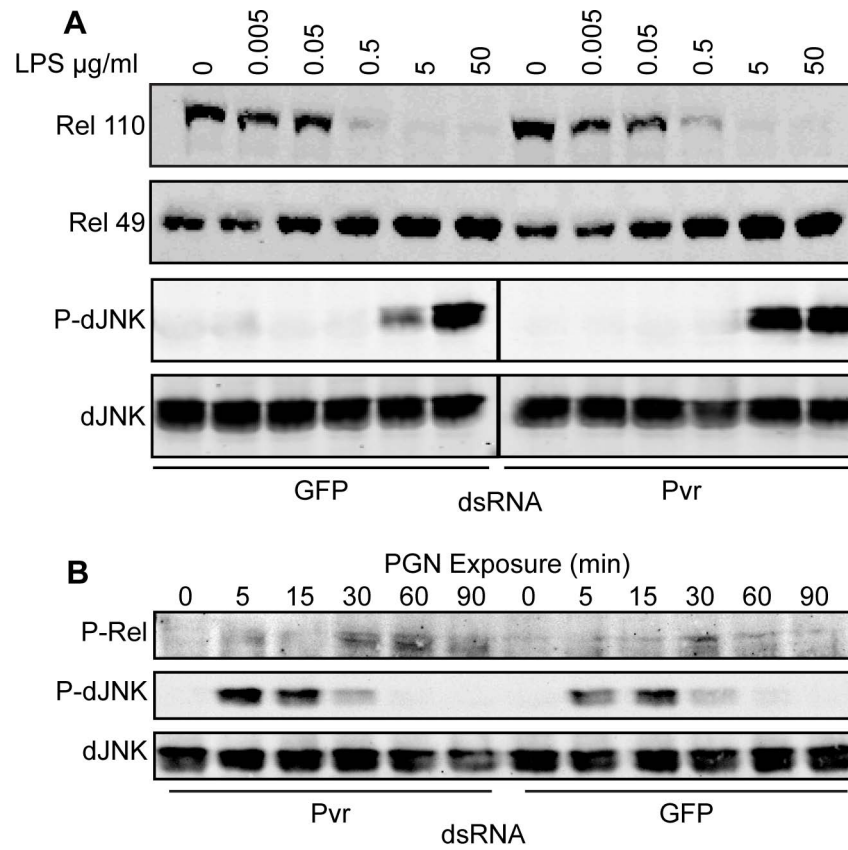


Figure 4.11. Pvr depletion enhances IMD pathway signals.

(A) Western blot analysis of lysates from S2 cells incubated with GFP dsRNA (lanes 1-6) or Pvr dsRNA (lanes 7-12). S2 cells were untreated or treated with PGN for 15min in increasing ten-fold gradations of LPS from $5 \times 10^{-3} \mu\text{g/ml}$ to $50 \mu\text{g/ml}$. Lysates were probed with anti-Rel (top panels), anti-P-JNK (middle) and anti-JNK (bottom panel). **B.** Western blot analysis of lysates from S2 cells incubated with Pvr dsRNA (lane 1-6) or GFP dsRNA (lanes 7-12) and treated with PGN for the indicated period. Lysates were probed with anti-P-Rel (top panel), anti-P-JNK (middle) and anti-JNK (bottom panel).

activation of dERK in S2 cells. Previous reports demonstrated that Pvr ligands in conditioned medium (CM) from the *Drosophila* Kc167 cell line activates Pvr signaling in S2 cells[301]. To determine the phosphorylation profile of dERK, I treated S2 cells with Kc167 CM and I monitored phosphorylated dERK (P-dERK) with a P-MAPK specific antibody (Figure 4.12A). Kc167 CM treatment leads to transient dERK phosphorylation that peaks between 15-30min and returns to basal levels by 3hs in S2 cells (Figure 4.12B). These data show that Kc167 CM is a potent inducer of dERK phosphorylation. In agreement with a previous report, I found that Pvr is required for Kc167 CM-induced dERK phosphorylation in S2 cells (Figure 4.13A). Quantification of relative dERK phosphorylation levels showed that Pvr dsRNA treatment decreased CM-induced dERK phosphorylation 21 fold (Figure 4.13B). To examine the effect of Pvr signaling on AMP expression, I treated S2 cells with GFP or Pvr dsRNA and monitored PGN-induced *att* expression levels 6h after exposure to CM (Figure 4.13C). Consistent with the role of Pvr as a suppressor of Rel signaling, I found that CM significantly decreased PGN-induced *att* expression. The phenotype is not an indirect effect of CM on PGN or other aspects of the IMD pathway, as dsRNA-mediated depletion of Pvr from S2 cells abrogated the suppressive effects of CM on *att* expression (Figure 4.13). Thus, I conclude that activation of Pvr blocks PGN-responsiveness in S2 cells.

As Pvr signaling often proceeds through dERK and the bulk of the Ras/MEK1/dERK pathway yielded Pvr-like phenotypes in my primary screen, I then tested if the Ras/MEK1/dERK axis is required for CM suppression of PGN-induced *att* expression[270, 301]. MEK1 is a MAPKK downstream of Ras/Raf

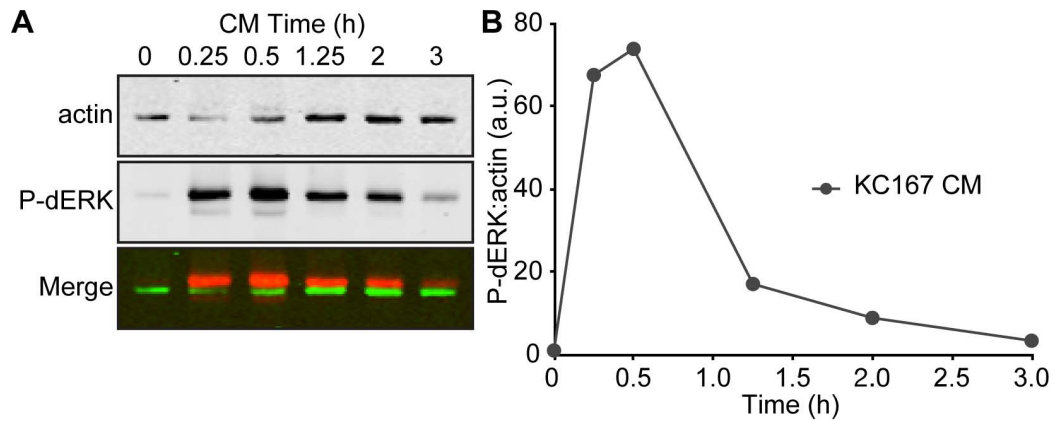


Figure 4.12. dERK phosphorylation response to conditioned media exposure.

A. Representative Western blot analysis of S2 cell lysates treated with conditioned media from Kc167 cells for the indicated periods, as indicated. Lysates were probed with anti-actin (top panel) and anti-actin (middle panel). To visualize relative dERK phosphorylation (red) and actin (green) channels were false colored and merged (bottom panel). **B.** Quantification of relative dERK phosphorylation in A. dERK phosphorylation levels were quantified and reported relative to actin levels for each of the indicated treatment groups and time points.

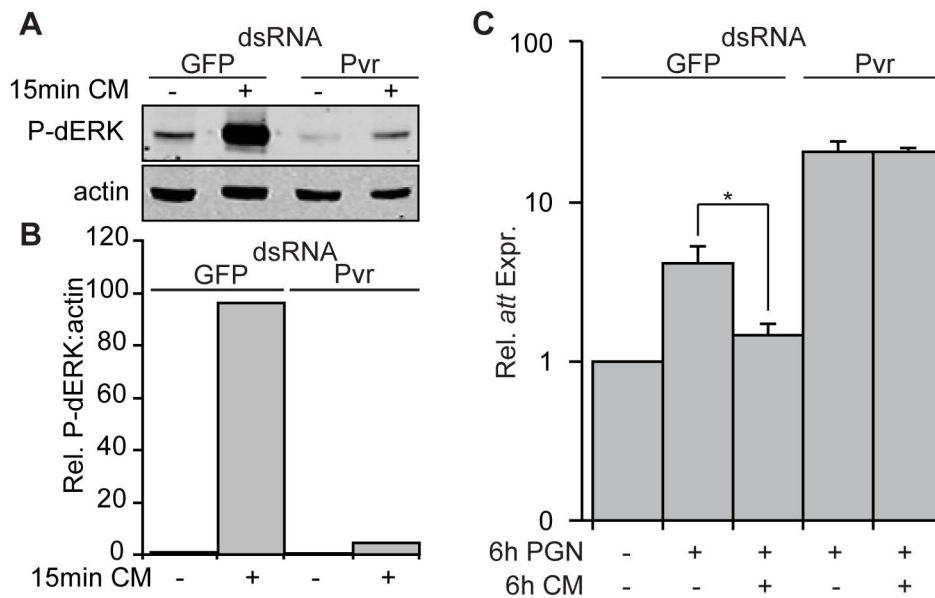


Figure 4.13. Pvr inhibits antimicrobial peptide production in S2 cells.

A. Western blot analysis of lysates from S2 cells incubated with GFP dsRNA (lane 1-2) or Pvr dsRNA (lanes 3-4). S2 cells were exposed to Kc167 cell conditioned media (CM) were indicated to induce dERK phosphorylation. Lysates were probed with antibodies specific for P-dERK (top panel), and actin (bottom panel). Data is representative of three individual experiments. **B.** Relative quantification of P-dERK levels from (A). P-dERK levels were standardized to actin levels for each treatment group. The unstimulated GFP dsRNA treated P-dERK:actin value was given a value of 1 and the remaining P-dERK:actin values are reported relative to this value. **C.** Quantitative real-time PCR analysis of *att* expression in S2 cells incubated with GFP dsRNA (columns 1-3) or Pvr dsRNA (columns 4-5). S2 cells were treated with Kc167 CM, and PGN as indicated. *att* expression levels in unstimulated S2 cells treated with GFP dsRNA was assigned a value of 1 and the remaining *att* expression values are reported relative to these values. Data are presented as the mean of three independent experiments and error bars indicate + SEM. The significance of CM treatment on the decrease in *att* expression relative to the untreated samples is indicated (*=p-value < 0.05). CM does not suppress *att* expression in the absence of Pvr.

(also known as Dsor1) that is critical for the phosphorylation of dERK in *Drosophila*[335]. Treatment of S2 cells with the MEK1 inhibitor PD98059 decreased CM-induced dERK phosphorylation 3.2 fold relative to S2 cells treated with CM alone (Figure 4.14A and B). To test the effect of dERK inhibition on CM-mediated suppression of *att* expression, I pretreated S2 cells with PD98059 prior to exposure to PGN and CM (Figure 4.14C). CM suppressed the PGN-induced expression of *att* by 7.7 fold. However, I detected significant restoration of PGN-induced *att* expression in S2 cells treated with CM and PD98059. These data indicate that signal transduction through a Pvr/MEK1/dERK axis attenuates activation of the IMD pathway.

4.2.5. Pnt suppresses IMD pathway signals.

The Pvr/dERK axis plays an integral role in the negative regulation of IMD pathway signals, however it remained unclear how dERK exerts downstream effects. In the primary dsRNA screen I identified the transcription factor Pointed (Pnt) as one of the strongest suppressors of PGN-induced dJNK phosphorylation. Pnt is an established downstream effector of Ras signals in *Drosophila* eye development[336], and is implicated in Pvr-mediated hemocyte proliferation[285]. I found that depletion of Pnt increased PGN-induced dJNK phosphorylation intensity in S2 cells (Figure 4.15A and B). However, dsRNA knockdown of Pnt had no observable effect on PGN-induced Rel cleavage. These data recapitulate the observations made in S2 cells depleted of Pvr (Figure 4.15C). To determine if Pnt influenced the activity of the Rel-arm of the IMD pathway, I treated cells with GFP control or Pnt dsRNA and monitored PGN-induced AMP production. Specifically, I monitored expression of the Rel-responsive AMP *att*. Depletion of

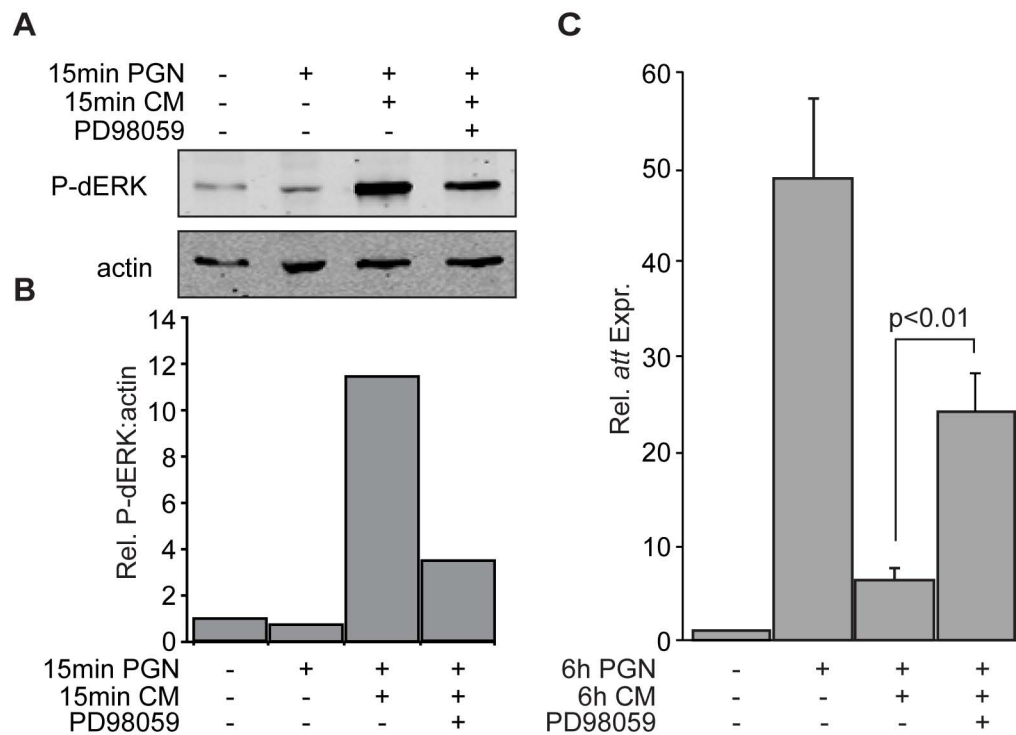


Figure 4.14. Pvr-induced dERK activity inhibits antimicrobial peptide production in S2 cells.

A. Western blot analysis of lysates from S2 cells treated with the MEK1 inhibitor PD98059 or DMSO, as a control, for 1h followed by exposure to PGN, and Kc167 CM for 15min, as indicated. Lysates were probed with anti-P-dERK (top panel), and anti-actin (bottom panel) antibodies. **B.** Relative quantification of P-dERK levels in panel A. P-dERK levels were standardized to actin levels for each treatment group. The untreated P-dERK:actin value was given a value of 1 and the remaining P-dERK:actin values are reported relative to this value. **C.** Quantitative real-time PCR analysis of *att* expression levels in S2 cells (column 1-3) or S2 cells treated with PD98059 (column 4). S2 cells were incubated with Kc167 CM, and PGN as indicated. *att* expression levels in unstimulated S2 cells were assigned a value of 1 and the remaining *att* expression values are reported relative to these values. Data are presented as the mean of three independent experiments and error bars indicate + SEM. Inhibition of MEK1 activation with PD98059 significantly restored *att* expression in response to Kc167 CM.

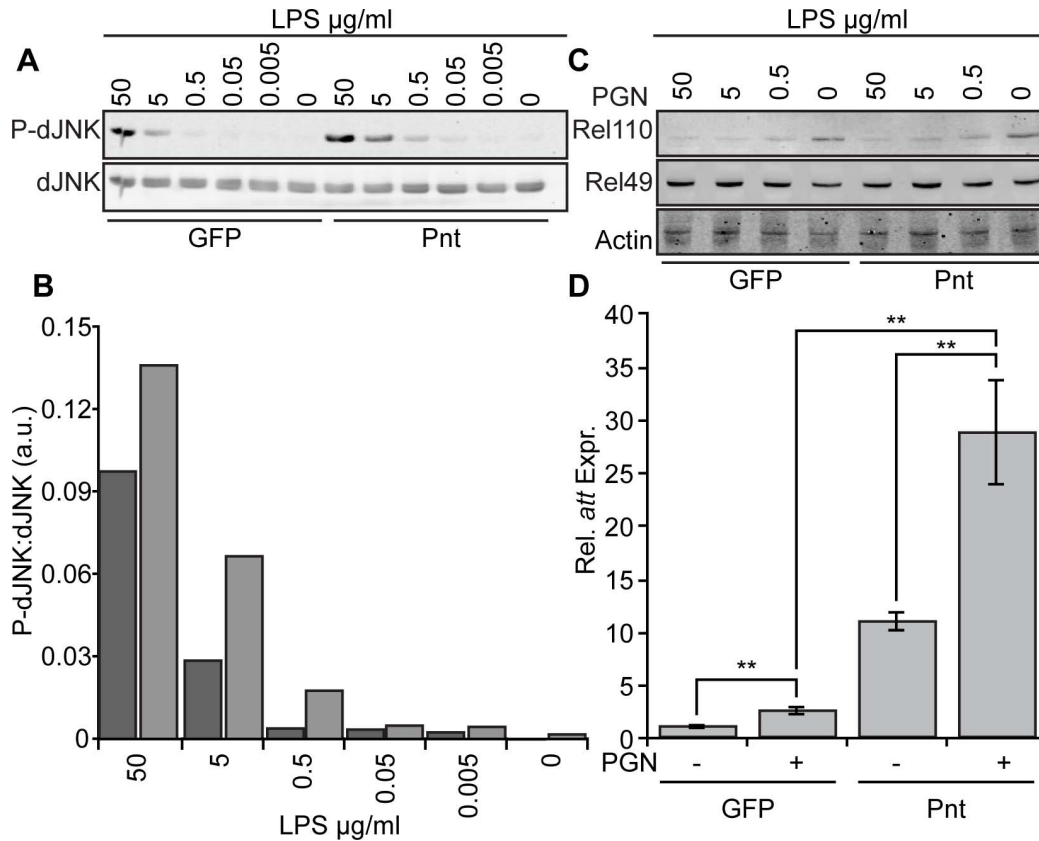


Figure 4.15. Pnt depletion enhances IMD pathway signals

A. Western blot analysis of lysates from S2 cells incubated with GFP dsRNA (lanes 1-6) or Pnt dsRNA (lanes 7-12). S2 cells were untreated or treated with PGN in decreasing ten-fold gradations of LPS from 50 $\mu\text{g/ml}$ to 5 $\times 10^{-3}\mu\text{g/ml}$. Lysates were probed with anti-P-JNK (top panel) and anti-JNK antibodies (bottom panel). **B.** Relative quantification of P-JNK levels from (A). P-JNK levels were standardized to JNK levels for each treatment group and the P-JNK:JNK values are shown. **C.** Western blot analysis of lysates from S2 cells incubated with GFP dsRNA (lane 1-4) or Pnt dsRNA (lanes 5-8) and treated with PGN for the indicated period. Lysates were probed with anti-Rel (top, middle panels) and anti-actin **D.** Quantitative real-time PCR analysis of standardized *att* expression in S2 cells incubated with GFP or Pnt dsRNA and treated with PGN as indicated. Data are presented as the mean of three independent experiments and error bars indicate the \pm SEM. The significant differences in *att* values are indicated (**=p-value<0.01).

Pnt significantly increased PGN-induced expression of *att* levels in comparison to control S2 cells (Figure 4.15D). Additionally, Pnt depletion significantly increased the basal expression levels of *att* in the absence of PGN stimulation. In these experiments I observed that the basal levels of *att* expression in S2 cells treated with Pnt dsRNA were higher than the PGN-induced expression levels in cells treated with GFP control dsRNA. These data show that dsRNA mediated depletion of Pnt closely mirrors the Pvr-depletion phenotype in *Drosophila* S2 cells. Together with my previous findings, these data suggest that PVR pathway signals proceed through the Ras/MEK1/dERK/Pnt axis to disrupt IMD pathway immune responses.

4.2.6. Pvr suppresses AMP production *in vivo*.

I then asked if Pvr suppresses IMD pathway activity *in vivo*. To reduce Pvr activity in whole animals, I expressed Pvr dsRNA hairpin constructs (Pvr-IR) in adult flies (refer to section 2.5.1.). I then compared the immune response of infected wild type flies to flies that express Pvr-IR. Specifically, I monitored the expression of the Rel-responsive transcript *att* in uninfected flies (control) and flies that were pricked with a needle coated in *E. coli* (infection). Strikingly, I noticed that *in vivo* depletion of Pvr significantly enhanced infection-mediated *att* expression in three separate experiments in two separate Pvr-IR fly lines (Figure 4.16). These data show that depletion of Pvr from adult flies results in increased IMD pathway activity and further support a role for Pvr as a negative regulator of IMD pathway activity, *in vivo*.

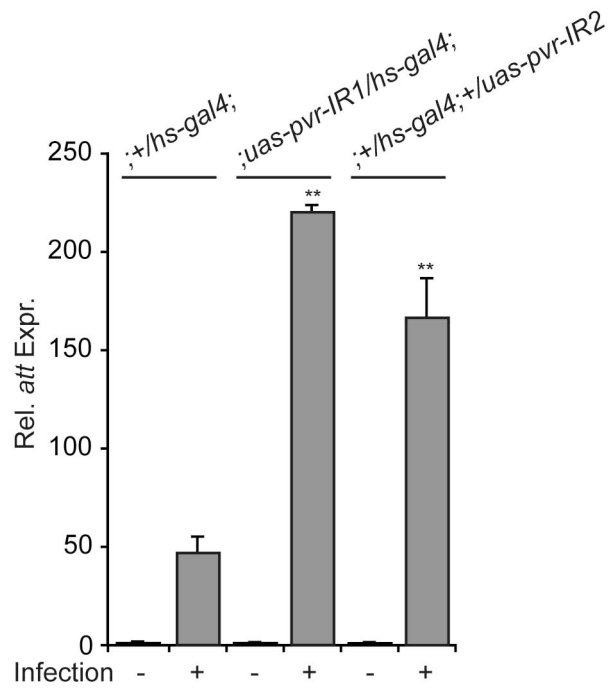


Figure 4.16. Pvr attenuates infection-induced antimicrobial peptide production *in vivo*.

Quantitative real-time PCR analysis of *att* expression in *hs-gal4/+* control flies (columns 1-2), *hs-gal4/UAS-Pvr-IR* flies (columns 3-4) and *hs-gal4/+ ; UAS-Pvr-IR/+* flies (columns 5-6). Flies were uninfected or infected through septic injury with *E. coli* as indicated. *att* expression levels of uninfected controls were assigned a value of 1 and the remaining *att* expression values are reported relative to this value. Data are presented as the mean of three independent experiments and error bars indicate the + SEM. Significant differences in *att* expression are indicated (**=p-value < 0.01).

CHAPTER 5

Autocrine PVR pathway activity controls intestinal stem cell proliferation in the adult Drosophila midgut.

A version of this chapter has been published.

Bond, D., and Foley, E. (2012). Autocrine PDGF- VEGF- receptor related (Pvr) pathway activity controls intestinal stem cell proliferation in the adult Drosophila midgut. The Journal of Biological Chemistry.

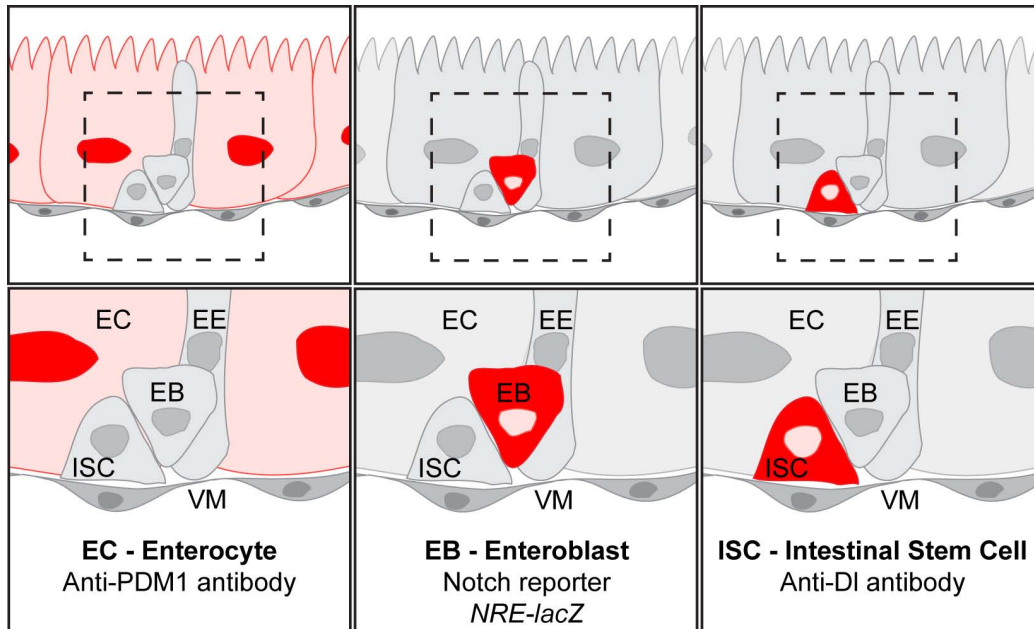
5.1. Chapter 5. Introduction.

In my previous studies I uncovered the PVR pathway as a novel negative feed-back regulator of IMD pathway immune responses. To determine the significance of these findings in a relevant immune model system, I investigated the role of PVR-pathway signals in the *Drosophila* posterior midgut (functional equivalent of the human small intestine)[232, 233, 337]. In the posterior midgut a dynamic pool of undifferentiated somatic stem cells proliferate and differentiate to replace dead or dying mature cell types and maintain the integrity and function of adult tissues. ISCs in the *Drosophila* posterior midgut are a well established model to study the complex genetic circuitry that governs stem cell homeostasis. Exposure of the intestinal epithelium to environmental toxins and other noxious agents results in the expression of cytokines and growth factors that drive the rapid proliferation and differentiation of ISCs. In the absence of stress-signals, ISC homeostasis is maintained through intrinsic pathways. In this study, I uncovered the PVR pathway as an essential regulator of ISC homeostasis. I found that ISCs coexpress Pvr and Pvf2 and that hyperactivation of the PVR pathway distorts the ISC developmental program and drives intestinal dysplasia. In contrast, I showed that ISCs mutant in the PVR pathway are defective in homeostatic proliferation and differentiation resulting in a failure to generate mature cell types. Additionally, I determined that extrinsic stress signals generated by enteropathogenic infection are epistatic to the hypoplasia generated in Pvf/Pvr mutants. My findings illuminate an evolutionarily conserved signal transduction pathway with essential roles in metazoan biology and direct involvement in numerous disease states.

5.2. Chapter 5. Results.

5.2.1. Visualization of posterior midgut cells.

In the posterior midgut, basally located ISCs differentiate into non-dividing undifferentiated EBs that in turn differentiates into mature ECs, the predominant intestinal epithelial cells, or secretory EEs. These cells types are easily visualized by fluorescence microscopy with cell-type specific antibodies (Figure 5.1). Additionally, cell type specific promoters paired with the GAL4/UAS system permit temporal and spatial control over transgene expression. This is accomplished through the GAL4/UAS system adapted from yeast, where the yeast transcriptional trans-activator (GAL4) binds up-stream activating sequence (UAS) to drive gene expression[338]. Cloning tissue or cell-type specific promoters upstream of the GAL4 sequence permits spatial control over UAS-transgene expression in transgenic animals. The coexpression of GAL4 with a temperature sensitive allele of the GAL4-inhibitor (*GAL80^{ts}*) adds temporal control over the GAL4/UAS system. Physical association of *GAL80^{ts}* with GAL4 blocks GAL4-activity at permissive temperatures (<25°C), however at nonpermissive temperatures (>29°C), *GAL80^{ts}* is inactive and GAL4 is free to restore transcriptional activity at UAS sites (Figure 5.2). This technique permits exquisite control of transgene expression in the desired cell or tissue type at any time during the *Drosophila* life span. In these studies I specifically expressed transgenes in ISC/EBs under the control of the *esg^{ts}* (*esg-GAL4, UAS-GFP, tub-GAL80^{ts}*) TARGET system[231, 339]. This marks ISC/EBs green and simultaneously induces expression of UAS-bearing targets. To determine the expression pattern of *esg^{ts}* in the posterior midguts, adult flies were transferred to nonpermissive temperatures for *GAL80^{ts}*, and GFP expression was monitored in



EC- enterocyte, **EE**-enteroendocrine, **EB**-enteroblast,
ISC-intestinal stem cell, **VM**-visceral muscle

Figure 5.1. Visualization of posterior midgut cells.

Cartoon representation of *Drosophila* posterior midgut cross-section visualized with cell type specific antibody stains and transgenic reporter fly lines. ECs and ISCs are visualized by immunofluorescence microscopy with anti-POU domain protein 1 (PDM1) (left panels) and anti-DI (right panels) antibody stains, respectively. EBs are visualized with anti- β -gal antibodies targeting β -gal produced by *NRE-lacZ* transgene (middle panel).

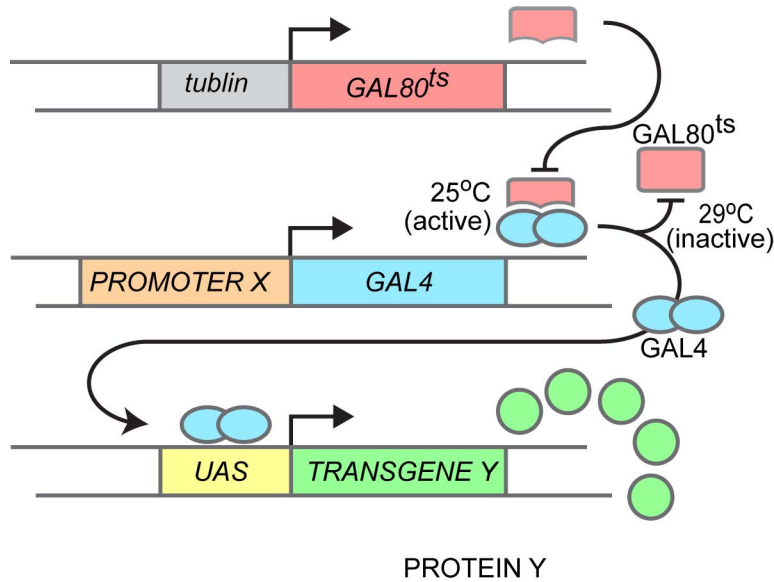


Figure 5.2. Control of transgene expression in *Drosophila*.

Control of transgene expression in *Drosophila* is accomplished with the GAL4/UAS system. Briefly, cloning tissue or cell type specific promoters (Promoter X) upstream of the *GAL4* gene provides control over transgene expression at upstream activating sequences (UAS). The transactivator GAL4 binds to the UAS driving the expression the desired transgene (Transgene Y). Additional temporal control of the UAS-GAL4 system is provided by the temperature sensitive allele of the GAL4-inhibitor, *GAL80^{ts}*. Under permissive temperatures (25°C) *GAL80^{ts}* physically blocks GAL4 activity, while at nonpermissive temperatures (29°C) *GAL80^{ts}* disassociates from GAL4 leading to GAL4-mediated transcription if UAS-transgenes.

isolated guts by fluorescence microscopy (Figure 5.3). Gut morphology was additionally assessed with Hoechst, to visualize the total cell population, and with anti-Armadillo (Arm) antibodies, to mark intercellular boundaries. *Drosophila* Arm is the homolog of human β -catenin, and is a central component of the multiprotein complex that form the adherence junctions between cells. In agreement with previous studies, *esg*^{ts} drives GFP/transgene expression in a subset of small, basally located, posterior midgut cells reminiscent of ISC/EB populations (Figure 5.3)[231]. The *esg*^{ts} system permits me to bypass the embryonic, larval and pupal stages and restrict *esg*-mediated transgene expression to adult flies.

5.2.2. Posterior midgut ISCs express Pvr and Pvf2.

To determine if Pvr is expressed in the posterior midgut, I stained posterior midguts from 3-5 day old adult wildtype *Drosophila* with an anti-Pvr antibody (Figure 5.4). Pvr antibody stain appears enriched in a subpopulation of cells with relatively small nuclei consistent with the ISC/EB cell population. To determine the precise identity of this Pvr enriched cell population, I visualized Pvr in the midguts of adult flies that express cell type specific GFP reporters. I used a Notch reporter element (NRE)-GAL4 driver line and a Delta-Gal4 driver line to express GFP in EBs (NRE>GFP⁺) and ISCs (*dl*>GFP⁺), respectively. I then performed colocalization analysis on GFP and anti-Pvr fluorescence in the respective lines to assess the degree of overlap between the cell type specific markers and Pvr (Figure 5.5A). I found a marked colocalization of Pvr with *dl*>GFP positive ISCs and essentially no overlap with NRE>GFP positive EBs. In short, it seems ISCs express Pvr. Primary antibody stains frequently create a

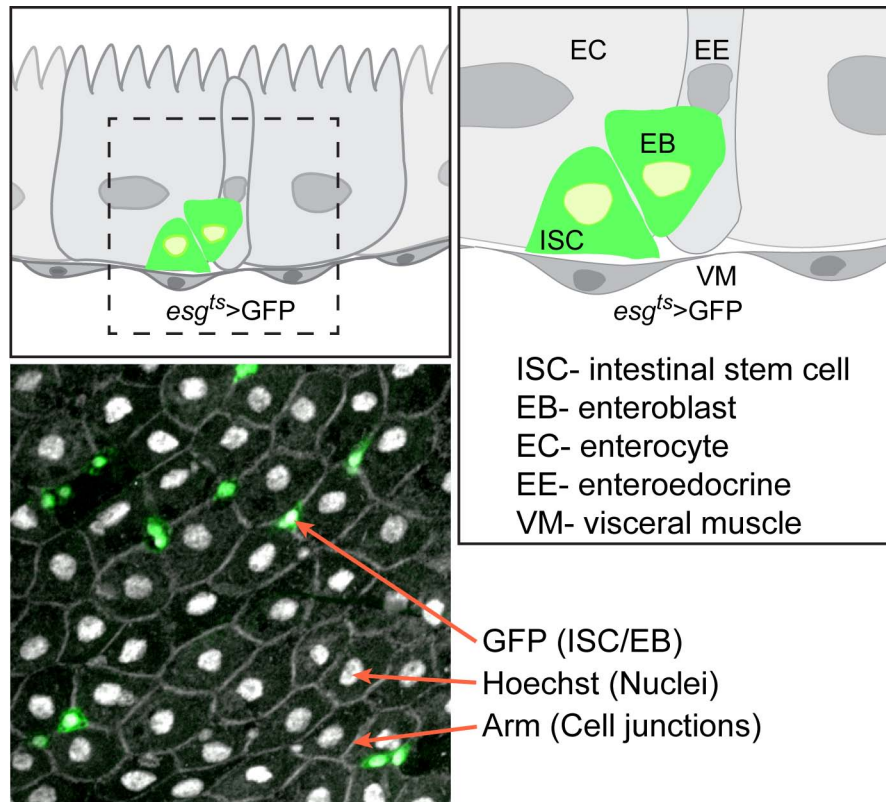


Figure 5.3. Visualization of posterior midgut ISC/EBs.

Cartoon representation of a cross section of the *Drosophila* posterior midgut (top left panel). Hashed box in the top left panel shows the area enlarged in the top right panel. The position of $esg^{ts}>GFP$ positive ISC/EBs cells (green) are shown relative to the VM, EC and EE cells (top panels). Fluorescence microscopy $esg^{ts}>GFP$ posterior midguts from adult flies shows ISC/EB cell populations (green). Gut architecture was visualized with Hoechst stain, to label total cell population, and with anti-Arm antibodies, to mark cell junctions, as indicated (orange arrows).

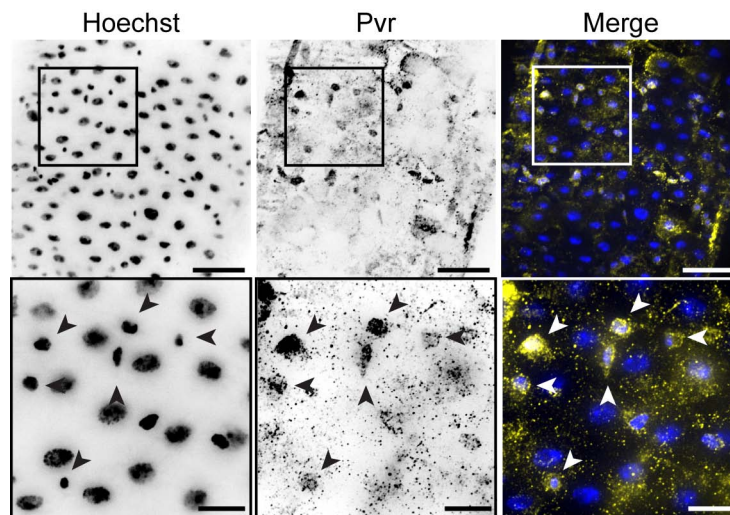


Figure 5.4. Pvr is expressed in the *Drosophila* posterior midgut. Wildtype midguts were stained with Hoechst (column 1) and anti-Pvr antibodies (column 2). Hoechst (blue) and anti-Pvr (yellow) channels were false colored and merged in column 3. The box in the low magnification image (top row) represents the area visualized in the high magnification image (bottom row). Scale bars represent 25 μ m and 10 μ m for low and high magnifications, respectively. Images are representative of 7 guts visualized per three replicate experiments. Arrowheads indicate cells enriched in Pvr stain.

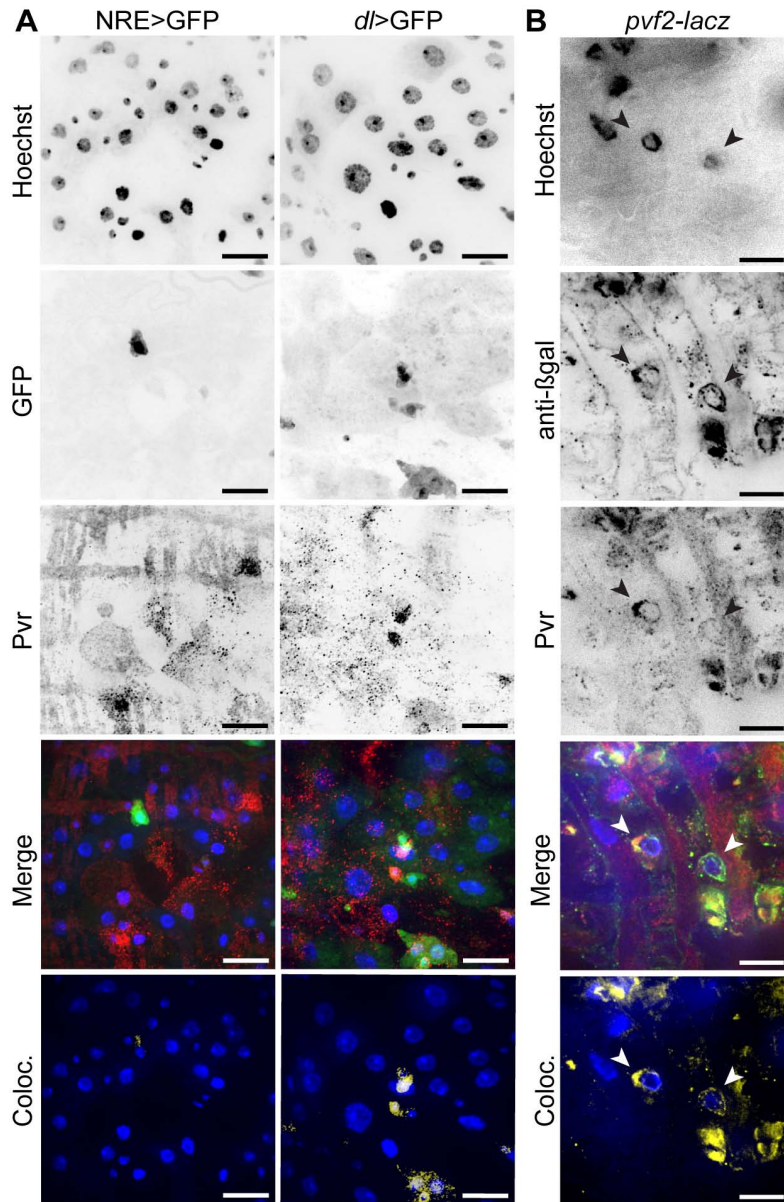


Figure 5.5. Pvr and Pvf2 are expressed in posterior midgut ISCs.

A. Pvr localization in adult midguts that express cell type specific GFP reporters. GFP (row 2) was visualized in EBs (column 1) or ISCs (column 2). Midguts were stained with Hoechst (row 1) and anti-Pvr antibody (row 3). Hoechst (blue), GFP (green) and Pvr (red) channels were false colored and merged in row 4. Pixels where GFP and Pvr signals overlap were false colored (yellow) and merged with Hoechst (blue) (row 5). Scale bars represents 15 μ m.

B. Pvr and the *pvf2-lacZ* reporter colocalize in posterior midgut ISCs (white arrowhead). Guts were isolated from *pvf2-lacZ* flies and stained with Hoechst (panel 1), anti- β gal (panel 2), and anti-Pvr anti-bodies (panel 3). Hoechst (blue), anti- β gal (green), and Pvr (red) channels were false colored and merged in panel 4. Pixels where *pvf2*-reporter (β gal) and Pvr signals overlap were false colored (yellow) and merged with Hoechst (blue) (panel 5). Scale bars represent 10 μ m. Images in A and B are representative of 7 guts visualized per two replicate experiments.

striated pattern in guts visualized by immunofluorescence microscopy, consistent with cross reactivity with the filamentous actin found in the visceral muscle.

Previous studies with a *pvf2-lacZ* reporter fly line that expresses β -gal under control of the *pvf2* promoter uncovered Pvf2 expression in midgut ISCs[303]. To determine if Pvr and Pvf2 expression overlap, I stained posterior midgut ISCs from *pvf2-lacZ* flies with anti-Pvr and anti- β gal antibodies (Figure 5.5B). In these studies, I observed a strong overlap between Pvr and Pvf2 in individual cells of the posterior midgut. Thus, I conclude that posterior midgut ISCs co-express Pvr and Pvf2.

5.2.3. The Pvr axis controls midgut homeostasis.

As posterior midgut ISCs co-express Pvr and a *pvf2-lacZ* reporter, I monitored the impact of Pvr signals on gut homeostasis. To accomplish this, I specifically hyperactivated or inhibited Pvr signals in ISCs with the targeted expression of constitutively active Pvr (Pvr^{CA}) and dominant negative Pvr (Pvr^{DN}) transgenes, respectively. In Pvr^{CA} the dimerization domain of bacteriophage λ cI repressor replaces the extracellular Ig-domain of Pvr forcing oligomerization of intracellular kinase domains and triggering constitutive activation of downstream molecules, such as dERK[270]. In contrast, deletion of the Pvr intracellular signaling domain produces a dominant negative Pvr (Pvr^{DN}) that sequesters Pvr ligands and blocks intracellular PVR pathway signals[270].

I reared flies at the restrictive temperature, until 3-5 days of adulthood and then shifted flies to 29°C to drive Pvr^{CA} or Pvr^{DN} expression in ISC/EB cells for 10

days (Figure 5.6). Control *esg>GFP* positive cells display a typical ISC/EB partnership of small, evenly spaced and frequently paired cells. Cross sections revealed that wildtype *esg>GFP* positive cells were typically in close association with the basal lamina as expected for progenitor cells. In stark contrast, *Pvr^{CA}* activation resulted in a striking expansion of *esg^{ts}>GFP* positive cell clusters with distinctly altered cellular morphology. *Pvr^{CA}* promoted the expression of *esg>GFP* in an increased number of small cells, and larger polyploid cells reminiscent of the ISC/EB and EC cell populations, respectively. Analysis of cross-sections from *Pvr^{CA}* midguts revealed that *esg^{ts}>GFP* positive cells extended through the gut epithelium from the basal lamina to the intestinal lumen. In striking contrast, *Pvr* inhibition through the expression of *Pvr^{DN}* resulted in considerably fewer *esg>GFP* positive cells that were rarely paired. In midgut cross-sections, these *esg>GFP* cells were strictly associated with the basal lamina.

These observations prompted me to explore the impact of Pvf-ligand expression on the posterior midgut. For these studies, I expressed Pvf1 and Pvf2 in adult gut ISC/EBs with *esg^{ts}*, as described above (Figure 5.7). As anticipated, wildtype *esg^{ts}>GFP* positive cells appear small, often paired, and evenly distributed throughout the posterior midgut. In contrast, *esg^{ts}*-mediated expression of Pvf1 or Pvf2 elevated *esg^{ts}>GFP* positive cell numbers. High magnification images showed clear changes in the morphology of *esg^{ts}>Pvf1* and *esg^{ts}>Pvf2* midgut cells, relative to control midgut cell. As with *Pvr^{CA}*, expression of either Pvf1 and Pvf2 promotes the expansion of *esg^{ts}>GFP* positive cell clusters composed of both large and small nucleated cells reminiscent of EC and

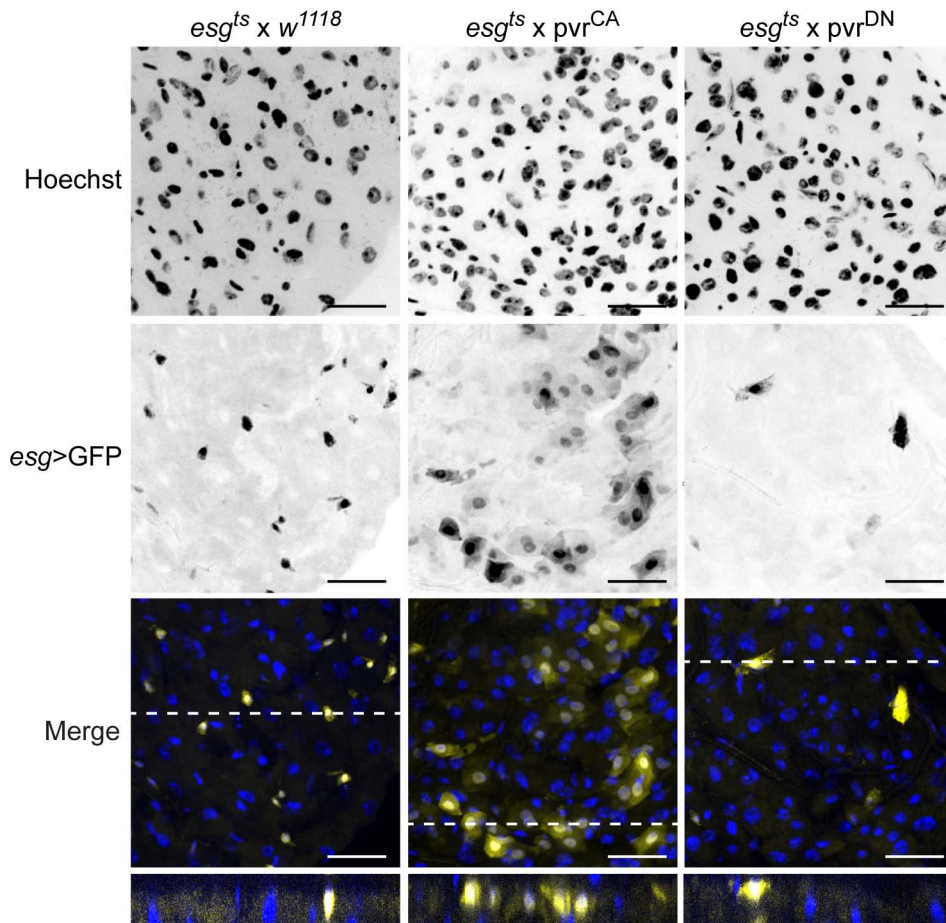


Figure 5.6. Pvr is required for intestinal homeostasis.

Immunofluorescence microscopy of posterior midguts upon expression of Pvr^{CA} (column 2) and Pvr^{DN} (column 3) in ISC/EBs relative to control midguts (column 1). Guts were stained with Hoechst (row 1) and ISC/EBs were visualized by GFP expression (row 2). Hoechst (blue) and GFP (yellow) channels were false colored and merged (row 3). White dashed lines represent the area shown in cross-section in row 4. Scale bars represent 25 μm. Images are representative of 7 guts visualized per four replicate experiments.

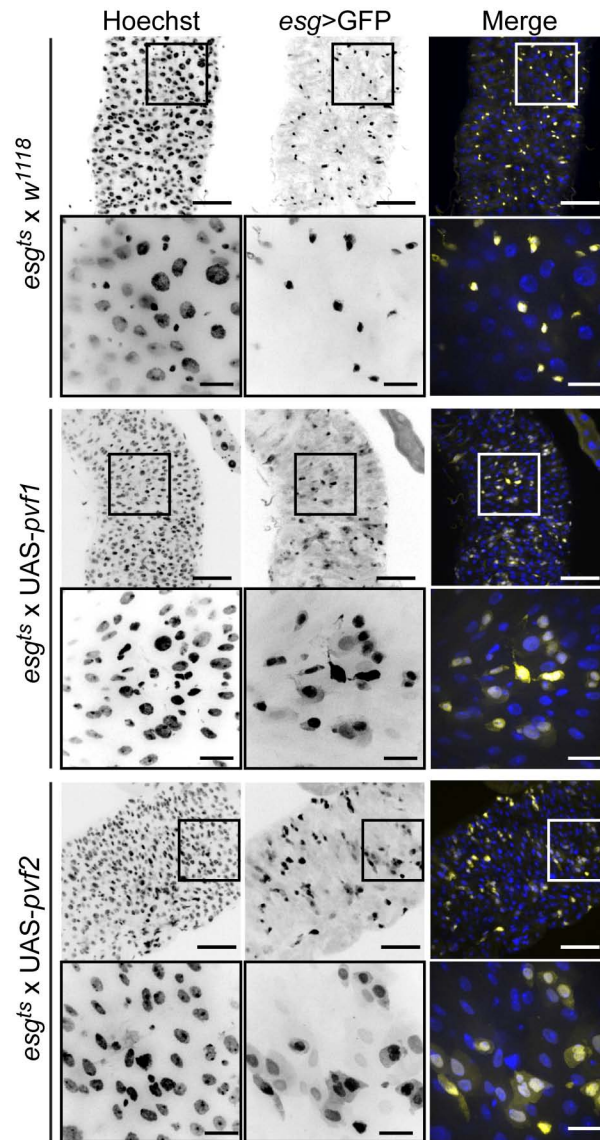


Figure 5.7. Pvr pathway activity controls intestinal homeostasis.

Visualization of posterior midgut morphology upon *UAS-pvf1* (rows 3 and 4) and *UAS-pvf2* (rows 5 and 6) expression in ISC/EBs relative to control midguts (rows 1 and 2). Guts were stained with Hoechst (column 1) and ISC/EBs were visualized by GFP expression (column 2). Hoechst (blue) and GFP (yellow) channels were false colored and merged in column 3. The boxed areas in the low magnification rows 1, 3, and 5 indicate the areas shown in high magnification in rows 2, 4, and 6, respectively. Scale bars represent 50 μ m and 15 μ m for low and high magnification images, respectively. Images are representative of 7 guts visualized per three replicate experiments.

ISC/EB cell populations, respectively. Combined, these data suggest that Pvr signals regulate midgut homeostasis.

5.2.4. Pvr promotes intestinal hyperproliferation.

My initial tests established that Pvr^{CA} drives the expansion of *esg^{ts}>GFP* positive cells in posterior midguts. To quantify the extent of this expansion, I calculated the percentage of *esg^{ts}>GFP* positive cells in midguts that expressed Pvr^{CA}, relative to control midguts (Figure 5.8A). In line with previous studies, I found that 21% of all cells in the posterior midgut of wild-type *esg^{ts}>GFP* flies were GFP positive[340]. Pvr^{CA} expression in ISCs/EBs doubled the average percent of *esg^{ts}>GFP* positive cells (42% *esg^{ts}>GFP* +ve) in the posterior midgut. To determine if increased ISC divisions were responsible for greater *esg^{ts}>GFP* cell numbers, I visualized ISC mitosis with an anti-phospho-histone 3 (PH3) antibody (Figure 5.8B). Histone 3 is highly phosphorylated during mitosis, and is therefore a common marker for actively dividing ICS in the posterior midgut[240, 341]. I found that Pvr^{CA} expression in ISCs/EBs significantly enhanced the number of mitotic cells in the *Drosophila* gut (Figure 5.8C).

5.2.5. Pvr signals in ISCs are essential for the appropriate development of intestinal cells.

My preliminary observations hint at a possible requirement for Pvr signals in intestinal homeostasis. To explore this possibility further, I determined the identity of individual midgut cells in *esg^{ts}* flies that express Pvr^{CA} or Pvr^{DN}. For these experiments, I used anti-DI antibodies, anti-PDM1 antibodies and Notch-reporter element (NRE-lacZ) transgenic flies to mark ISCs, ECs and EBs (Figure 5.9, 5.10,

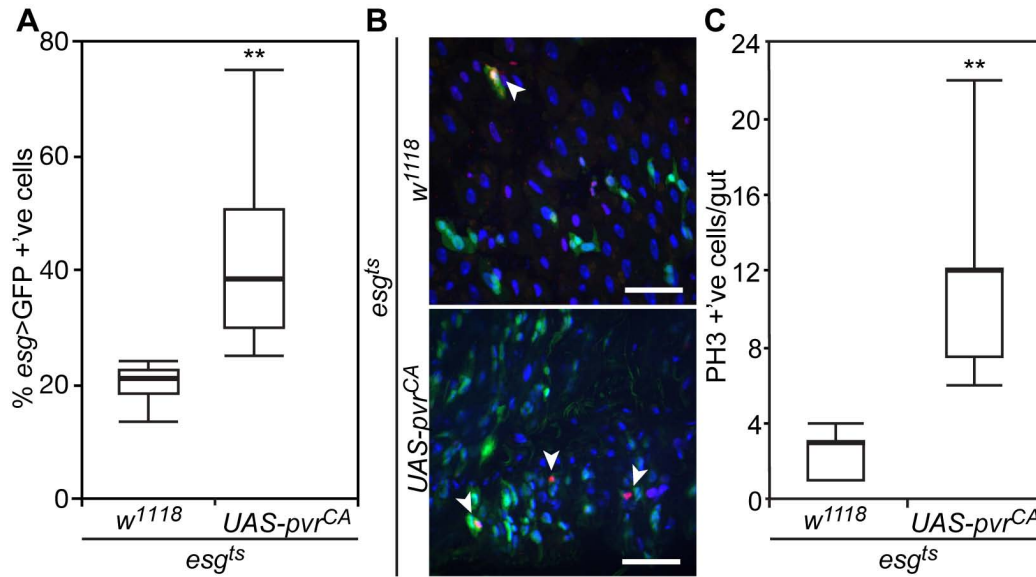


Figure 5.8. Pvr activity promotes intestinal mitosis.

A. Quantification of GFP-positive cells in posterior midguts upon expression of Pvr^{CA} under the control of *esg^{ts}*, relative to control guts as indicated (n=10 guts from three independent experiments). All cells were stained with Hoechst and GFP positive cells were calculated as a percentage of total cells per field. **B.** Representative immunofluorescence images of posterior midguts upon expression of Pvr^{CA} (bottom panel) in ISCs/EBs relative to control midguts (top panel). Guts were stained with Hoechst and anti-PH3, and ISC/EBs were visualized by GFP expression. Hoechst (blue), PH3 (red) and GFP (green) channels were false colored and merged. Arrow heads point to PH3-positive cells. Scale bars represent 25 μ m. **C.** Quantification of PH3-positive cells in whole guts upon expression of Pvr^{CA} (n=12 guts in two independent experiments) under the control of *esg^{ts}*, relative to control guts as indicated (n=14 guts in two independent experiments). All cells were stained with Hoechst and anti-PH3 and the number of pH3-positive cells was calculated per gut. In A and C, box plots show the median number of GFP and PH3 positive cells (thick line) respectively, flanked by the first quartile (bottom edge) and third quartile values (top edge), while top and bottom whiskers indicate the highest and lowest data points for each data set. ** indicates p<0.01.

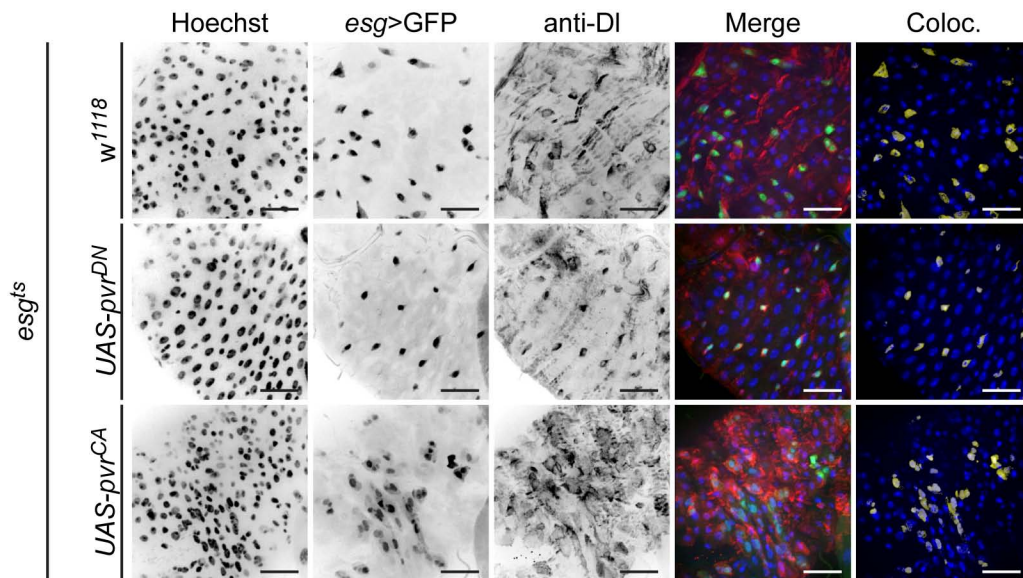


Figure 5.9. Pvr controls ISC cell numbers. In all panels, posterior midguts were visualized upon *pvr^{DN}* (row 2) or *pvr^{CA}* (row 3) transgene expression under the control of *esg^{ts}*, relative to control midguts (row 1). Guts were stained with anti-DI antibodies to mark ISCs. All cells were stained with Hoechst (column 1) and *esg^{ts}* positive cells were visualized with GFP fluorescence (column 2). Hoechst (blue), GFP (green), and DI-positive ISCs (red) channels were false colored and merged in row 4. Pixels where GFP and cell type specific marker signals overlap were false colored (yellow) and merged with Hoechst (blue) (row 5). Scale bars represent 25 μ m. Images are representative of 7 guts visualized per two replicate experiments.

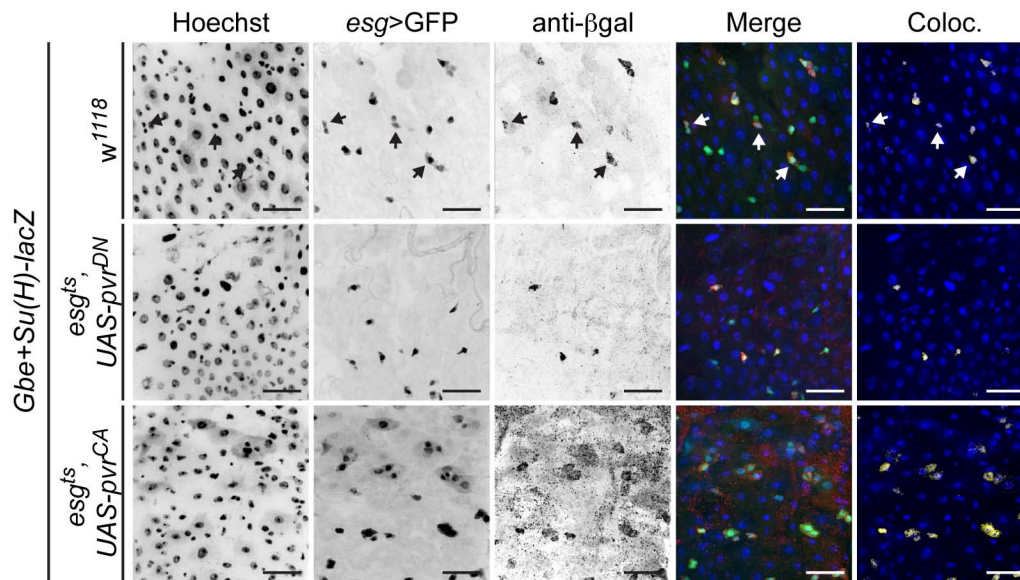


Figure 5.10. Pvr controls EB cell numbers.

In all panels, posterior midguts were visualized upon *pvr^{DN}* (row 2) or *pvr^{CA}* (row 3) transgene expression under the control of *esg^{ts}*, relative to control midguts (row 1). Guts were stained with anti-βgal antibodies to mark EBs. All cells were stained with Hoechst (column 1) and *esg^{ts}* positive cells were visualized with GFP fluorescence (column 2). Hoechst (blue), GFP (green), and βgal-positive EBs (red) channels were false colored and merged in row 4. Pixels where GFP and cell type specific marker signals overlap were false colored (yellow) and merged with Hoechst (blue) (row 5). Arrows indicate EBs within ISC/EB equivalence groups. Scale bars represent 25μm. Images are representative of 7 guts visualized per two replicate experiments.

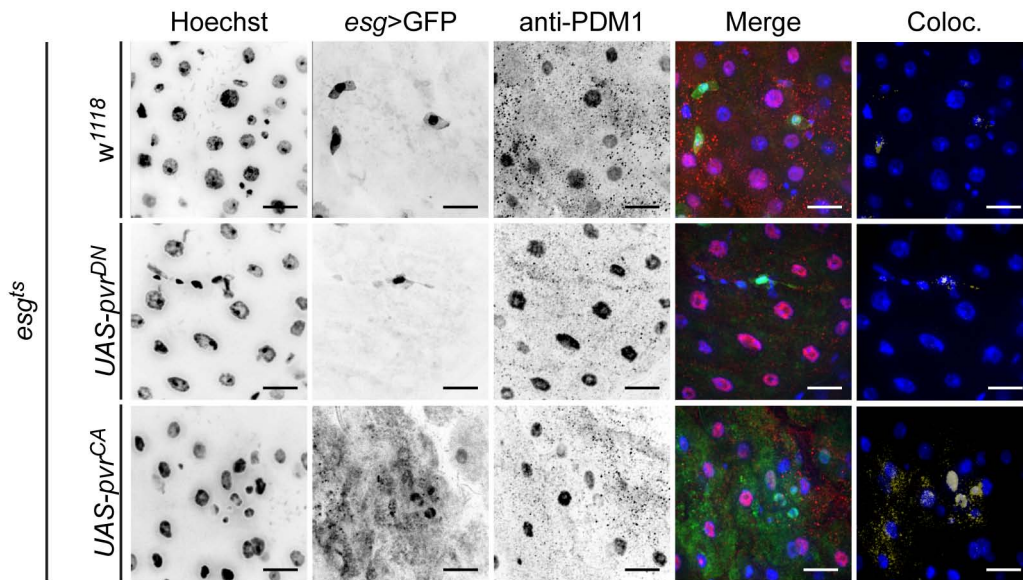


Figure 5.11. Pvr controls midgut cell development.

In all panels, posterior midguts were visualized upon *pvr^{DN}* (row 2) or *pvr^{CA}* (row 3) transgene expression under the control of *esg^{ts}*, relative to control midguts (row 1). Guts were stained with anti-PDM1 antibodies to mark ECs. All cells were stained with Hoechst (column 1) and *esg^{ts}* positive cells were visualized with GFP fluorescence (column 2). Hoechst (blue), GFP (green), and PDM1-positive (red) channels were false colored and merged in row 4. Pixels where GFP and cell type specific marker signals overlap were false colored (yellow) and merged with Hoechst (blue) (row 5). Scale bars represent 15 μ m. Images are representative of 7 guts visualized per two replicate experiments.

5.11), respectively. As expected, I observed the archetypal DI/Notch equivalence group in wildtype guts. *esg^{ts}*>GFP-positive cells were most often DI positive ISCs, and when *esg^{ts}*>GFP positive cells were paired the partnership was completed with a NRE>lacZ-positive EB cell, as indicated with arrows (Figure 5.10). Further examination of *esg^{ts}*>GFP positive cells showed no overlap with the nuclear localized anti-PDM1 EC marker (Figure 5.11).

My observations on wildtype midguts are in stark contrast to the observed distribution of ISC, EB and EC specific markers with *esg^{ts}*-mediated expression of Pvr^{CA}. Hyperactivation of Pvr signals expanded the *esg^{ts}*>GFP population with a corresponding increase in the co-expression of ISC, EB, and EC cell type specific markers in midguts. Specifically, I found that Pvr^{CA} increased the total number of DI positive ISCs, while a significant population of *esg^{ts}*>GFP positive cells were DI negative (Figure 5.9). Additionally, I found that Pvr activation increased the number of EBs within *esg*>GFP positive cell clusters (Figure 5.10). These EB cells were frequently observed in close proximity to other EBs and non-EB *esg^{ts}*>GFP positive cells. Finally, I observed a strong overlap of PDM1 and *esg^{ts}*>GFP upon Pvr^{CA} expression. In summary, hyperactivation of Pvr in presumptive progenitor cells results in increased *esg^{ts}*>GFP in ISCs, EBs and unexpectedly ECs. These data demonstrate that hyperactive Pvr signals disrupt midgut homeostasis and promote intestinal dysplasia.

In contrast, expression of the Pvr^{DN} transgenes with *esg^{ts}* resulted in a marked reduction of *esg^{ts}*>GFP positive cells, relative to control guts. Furthermore, suppression of Pvr signals greatly diminished the number of GFP

positive paired cells with a strong bias towards maintenance of DI positive ISCs within the *esg^{ts}>GFP* populations (Figure 5.9). These data indicate that Pvr signals are required for cells to progress beyond the ISC fate and establish the ISC/EB equivalence group.

5.2.6. Autocrine Pvr signals regulate ISC fate determination.

Studies of the true mutant phenotype are always more desirable than misexpression studies with artificial transgenes. To directly test the requirement for Pvr in the homeostatic control of ISC development, I examined the midgut architecture of *pvr* and *pvf* mutant flies. For these studies I selected the *pvr⁵³⁶³* null mutant with a 61bp deletion between amino acid residues 114-134 resulting in a frameshift that causes a premature translation termination and a complete loss of Pvr functionality[284]. A gene duplication event likely generated the *pvf2* and *pvf3* genes in a tandem genomic arrangement and hints at overlapping and potentially redundant functions among the two ligands. This prompted us to generate a genomic deletion that specifically ablates *pvf2* and *pvf3* (*pvf2-3Δ*, hereafter abbreviated as *pvf2-3*, Figure 5.12A,B). Dr. Foley and I generated the *pvf2-3* flies through transposase mediated excision of the intervening genomic region between two P-element transposons inserted into the transcriptional start site of *pvf2* and the first exon of *pvf3*[309]. Work by Brendon Parsons in the lab validated that the deletion ablates *pvf2* and *3* without any other genes being affected. Consistent with redundant developmental requirements for *pvf2* and *pvf3*, the *pvf2-3* deletion was homozygous lethal and phenotypically similar to *pvr⁵³⁶³* null mutant embryos, while the single mutant flies were homozygous viable. As both *pvr⁵³⁶³* and *pvf2-3* mutations are homozygous lethal, it is

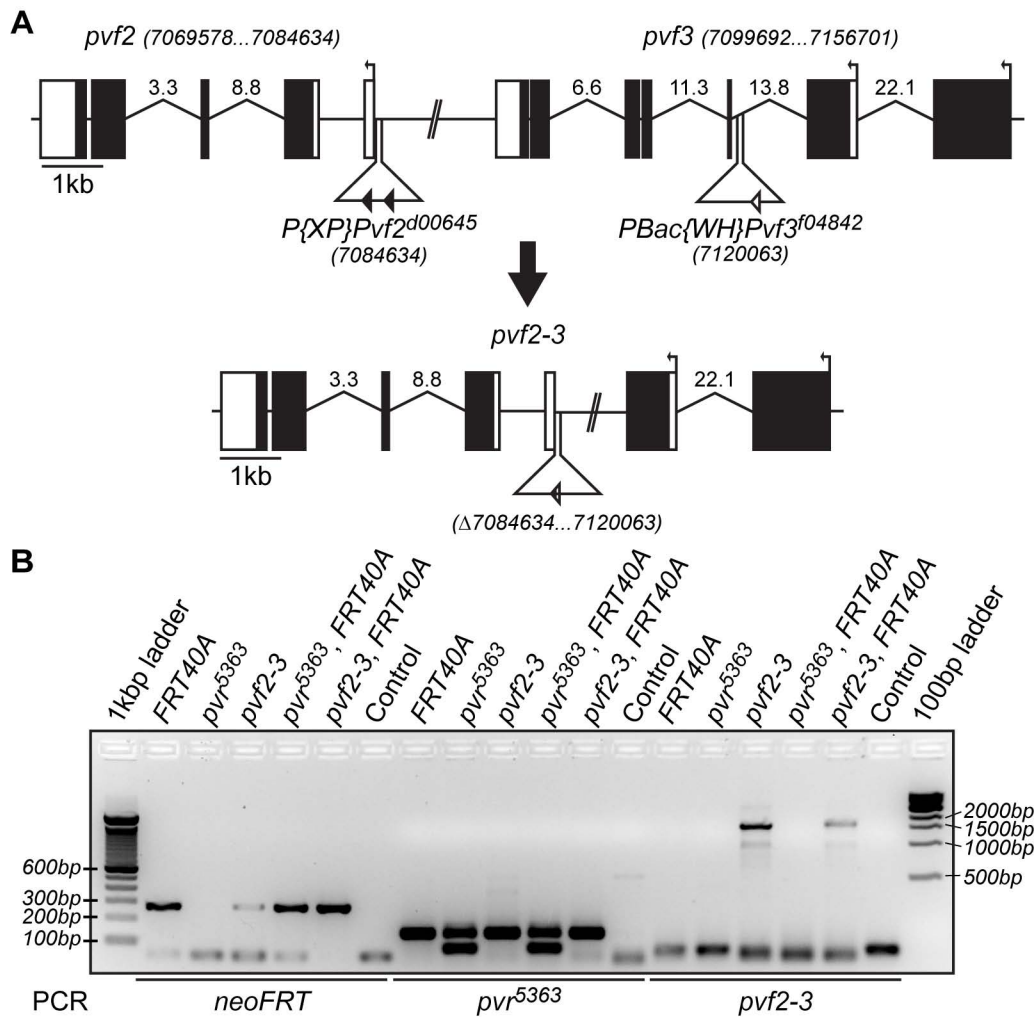


Figure 5.12. Generation of *pvr*⁵³⁶³ and *pvf2-3* mutant clones.

A. Diagram of $P\{XP\}Pvf2^{d00645}$ and $PBac\{WH\}Pvf3^{f04842}$ *P* element insertions into *pvf2* and *pvf3* genes, respectively (top diagram). *P* element excision by recombination removed the promoter region and the transcriptional start site of *pvf2*, and *pvf3* after the first exon to generate *pvf2-3* deletion mutant (bottom diagram). Black and white boxes represent translated and untranslated sequence, respectively. Transcription initiation sites are indicated with arrows and the *P* element recombination sites depicted with triangles. The scale bar indicates 1kbp, and long intronic regions are shown as bent lines with their sizes labeled above.

B. Generation of *pvf2-3*, *FRT40A* and *pvr*, *FRT40A* recombinants for MARCM. Single fly PCR of *FRT40A* (lanes 2-7), *pvr*⁵³⁶³ (lanes 8-13), *pvf2-3* (14-19). The individual genotypes are indicated. Ladders are shown in lane 1 (100bp) and lane 20 (1kbp) and with labeled with respective bands sizes. PCR of the gene region flanking the 63bp deletion found in *pvr*⁵³⁶³ generates a band of ~160bps in wildtype *pvr* and ~100bps in the *pvr*⁵³⁶³. PCR of DNA from heterozygous *pvr*⁵³⁶³ flies show 2 bands at ~100bps and ~160bps (lanes 9 and 11).

impossible to study complete nulls in adult flies. To circumvent this issue, I generated homozygous mutant ISC clones for the *pvr*⁵³⁶³ and *pvf2-3* in otherwise heterozygous adult guts through mitotic recombination using the mosaic analysis with a repressible cell marker (MARCM) technique (Figure 5.13)[310]. More specifically, *pvr*⁵³⁶³ and *pvf2/3* mutations were recombined onto chromosomes containing FRT(40A) recombination sites, and mutant clones were generated in progenitor cells with heatshock induced FLP-recombinase expression (Figure 5.14). FLP expression results in the crossing over of sister chromosome arms, and with the next cell division one wildtype and one homozygous *pvr*⁵³⁶³ or *pvf2/3* mutant cell are created. Homozygous control or mutant clones were marked with the expression of membrane bound GFP (Figure 5.15A). Adult flies were visualized 2 weeks after induction of MARCM clones to allow for developmental transition from progenitor to progeny, resulting in groups of clonally derived cells. Under standard conditions the gut epithelium is renewed every 12 days in wild type female flies[18]. As expected, wildtype MARCM clones contain large groups of cells with mixed cellular morphology that primarily consist of large ECs derived from ISC proliferation and differentiation. In contrast, I observed a dramatic collapse in cell numbers in clones mutant for *pvr* or *pvf2-3*. Both, *pvr*⁵³⁶³ and *pvf2-3* clones were severely handicapped in their proliferative potential and appeared significantly smaller (1-3 cells per clone) than their wildtype counterparts (>10 cells per clone) (Figure 5.15B). Furthermore, the ISC developmental program in *pvr*⁵³⁶³ and *pvf2-3* mutant cells appeared completely disrupted as I found no large polyploid ECs within the clones.

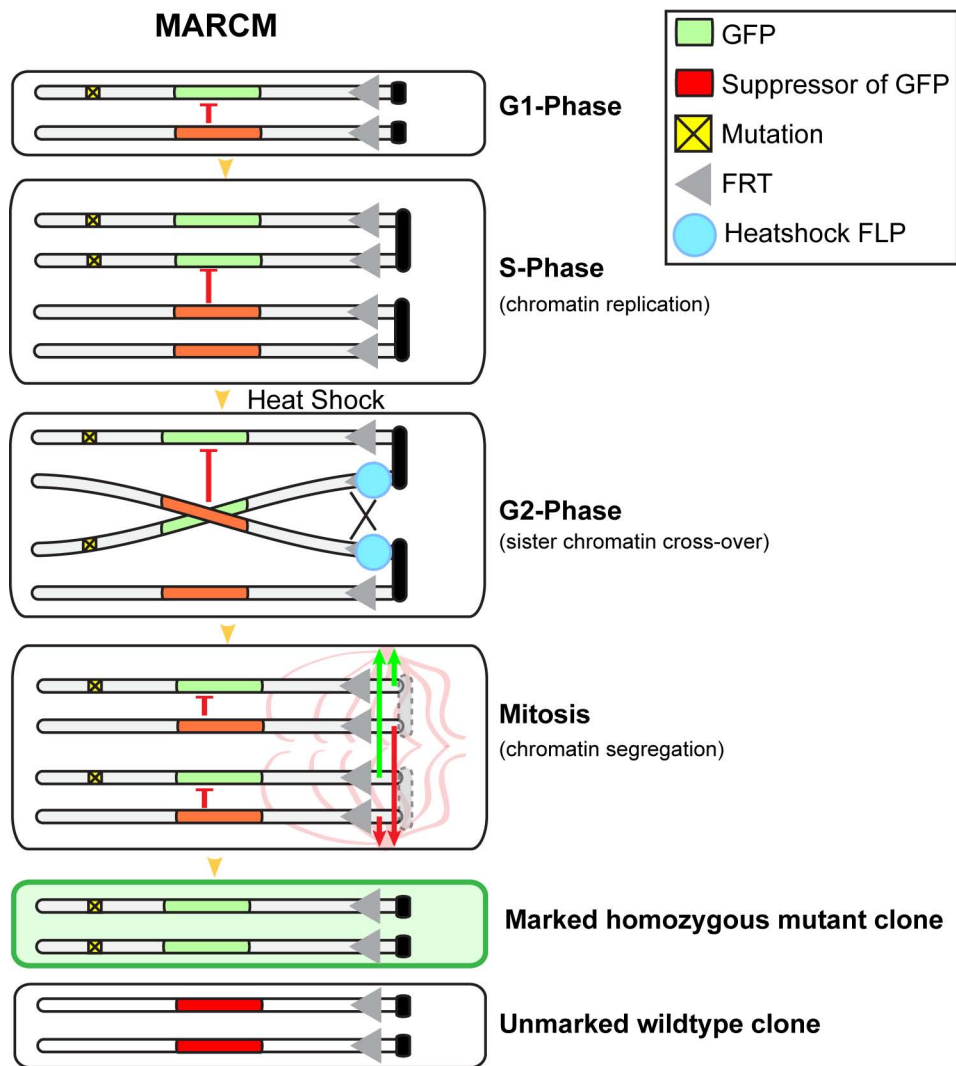


Figure 5.13. Mosaic analysis with a repressible cell marker (MARCM).

The MARCM technique generates homozygous mutant clone cells in an otherwise heterozygous background. Mutant clones are generated through recombination of chromosome arms during the G2-phase by a heatshock inducible FLP recombinase at FRT sites. During the next mitosis the inhibitor of GFP is segregated into one daughter cell allowing GFP-transgene expression in the opposing homozygous mutant daughter cell.

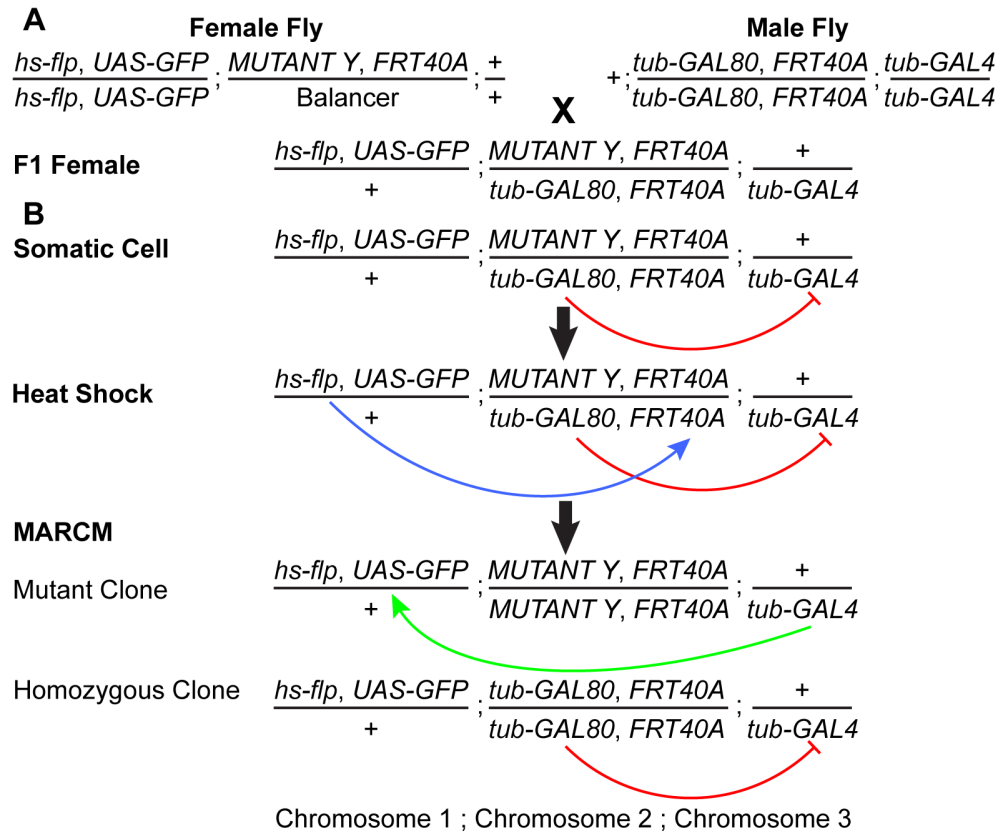


Figure 5.14. Crossing scheme for generating MARCM clones.

A. Genotypes are as follows: wildtype chromosome (+), heat-shock *flp* recombinase (*hs-flp*), upstream activation sequence promoting green fluorescence protein (*UAS-GFP*), mutant Y (*pvr⁵³⁶³* or *pvf2-3*), balancer chromosome stabilizes mutant Y in heterozygous state (balancer), flipase recognition target at position 40A on the second chromosome (*FRT40A*), tubulin promoter drives constitutive expression of the inhibitor of GAL4, GAL80 (*tub-GAL80*), and tubulin promoter drives constitutive expression of GAL4 (*tub-GAL4*). In the F1 progeny, the heterozygous *mutant Y, FRT40* chromosome is juxtaposed with the *tub-GAL80, FRT40A* chromosome. GAL80 expression blocks GAL4 activity and consequently cells do not express *UAS-GFP*. Heat-shock induced FLP recombinase expression causes crossover of chromosomal arms at FRT sites during G2-phase in the cell cycle. The *mutant Y, FRT 40* chromosome segregates from the *tub-GAL80, FRT40A* chromosome during the next cell division, and the resultant homozygous mutant cell is devoid of GAL80. Consequently, GAL4 activity is restored in the mutant cell, driving GFP expression in all subsequent progenitor cells.

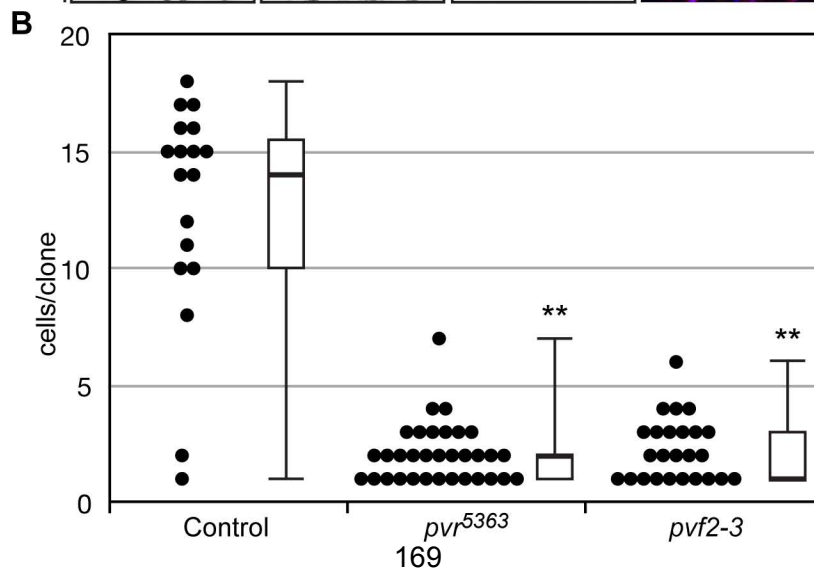
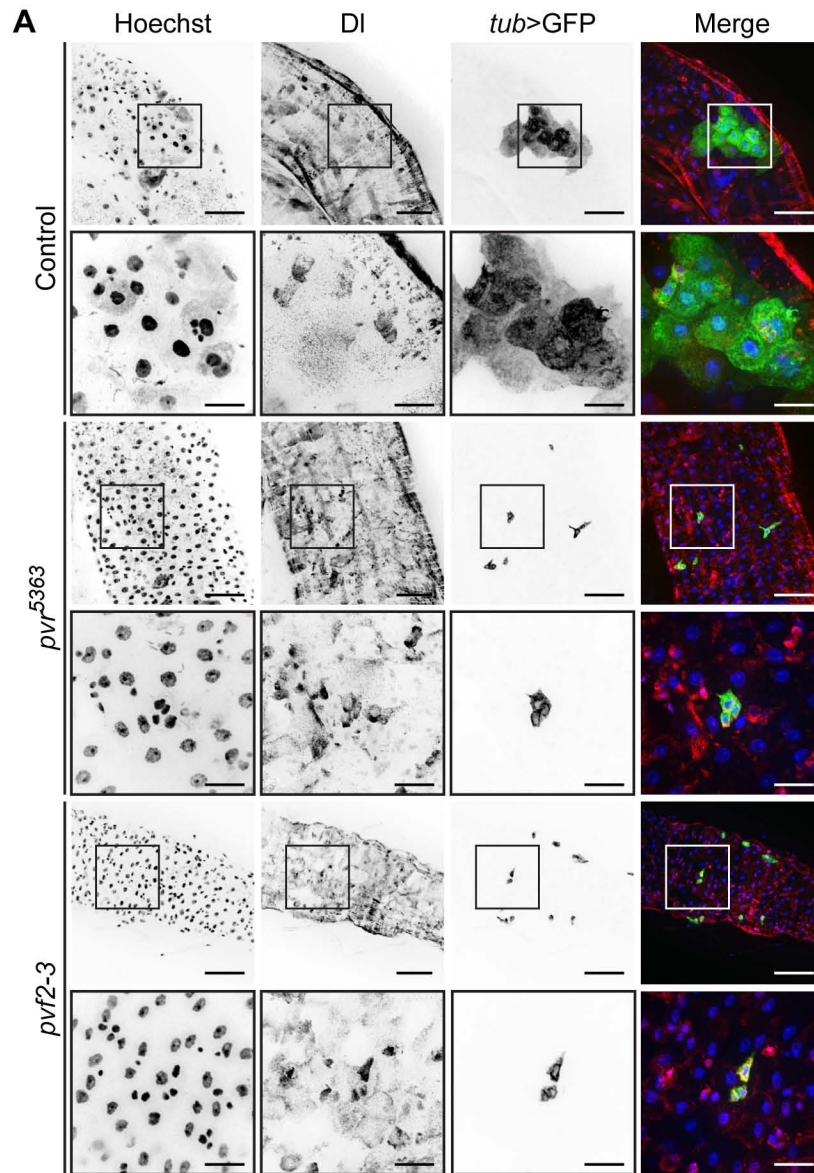


Figure 5.15. Autocrine Pvf/Pvr signals in ISCs establish mature midgut cells.
A. *pvr*⁵³⁶³ (rows 3 and 4) and *pvf2-3* (rows 5 and 6) MARCM clones in the posterior midgut compared to wild type control midguts (rows 1 and 2). Guts were stained with Hoechst (column 1), and anti-DI antibodies (column 2). MARCM clones were visualized by *tub>GFP* expression in row 3. Hoechst (blue), DI (red), and *tub>GFP* (green) channels were false colored and merged in column 4. The boxed areas in the low magnification rows 1, 3, and 5 indicates the area shown in high magnification in rows 2, 4, and 6, respectively. Scale bars represent 50 μ m and 15 μ m for low and high magnifications, respectively. **B.** Quantification of GFP positive cells in *pvr*⁵³⁶³ (n=33 clones) and *pvf2-3* (n=25 clones) MARCM clones compared to control clones (n=18 clones). Black circles represent individual data points. Box plots show the median number of cells/clone (thick line) flanked by the first (bottom edge) and third quartile (top edge) values, while whisker represent peripheral values in each data set. Double asterisk indicates $p > 0.01$.

Consistent with an essential requirement for the PVR pathway in homeostatic intestinal development, I found that all *pvr*⁵³⁶³ and *pvf2-3* mutant clones are comprised entirely of DI positive ISCs (Figure 5.16). These data establish that signals through the Pvf/Pvr axis are essential for ISCs to progress along their developmental program to generate mature cell types in the posterior midgut. Interestingly, proximal Pvf-production by surrounding heterozygous cells fails to compensate for the loss of Pvf2 and Pvf3 in *pvf2-3* mutant clones. These findings suggest that Pvf's are produced and sensed by individual ISCs in an autocrine fashion to regulate Pvr-mediated homeostatic signals. In summary, my findings establish that Pvf/Pvr intrinsic signals are essential for ISC homeostatic proliferation and differentiation, and that loss of Pvr leads to midgut hypoplasia.

5.2.7. Pvr acts independently of dJNK to control midgut homeostasis.

We showed previously that immune-induced dJNK activation promotes *pvf2* and *pvf3* expression and that PVR pathway activation regulates dJNK signals in a negative feed-back loop[280]. As dJNK signals feed into ISC proliferative controls[16, 18, 19], I assessed the genetic relationship between Pvr and dJNK signals in ISC proliferation. To assess if Pvr^{CA} dysplastic cues proceed through dJNK, I used *esg*^{fs} to simultaneously hyperactivate Pvr and inhibit dJNK, with a nonactivatable dominant negative T181A mutation in dJNK (dJNK^{DN})[342], in ISCs. As a corollary, I simultaneously inhibited the PVR pathway and activated the dJNK pathway to determine if dJNK associated proliferative cues require Pvr.

In the first set of experiments, I expressed Pvr^{CA} and dJNK^{DN} together or independently in 3-5 day old adult flies for 10 days, alongside wildtype control

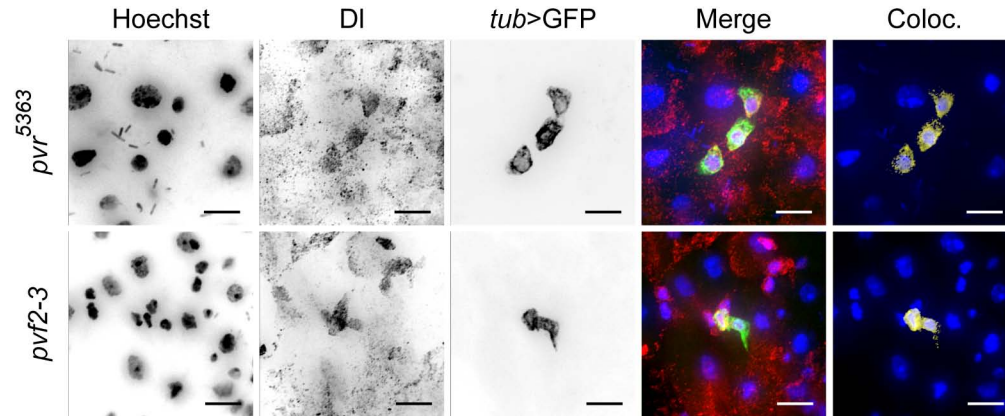


Figure 5.16. Autocrine Pvf/Pvr signals control ISC identity.

High magnification images of *pvr*⁵³⁶³ (row 1) and *pvf2-3* (row 2) MARCM clones in Figure 5.15. Guts were stained with Hoechst (column 1) and anti-DI antibodies (column 2). MARCM clones were visualized by *tub*>GFP expression (column 3). Hoechst (blue), DI (red), and *tub*>GFP (green) channels were false colored and merged in row 4. Scale bars represent 10µm. Images are representative of *pvr*⁵³⁶³ (n=33) and *pvf2-3* (n=25) clones visualized from 7 guts per genotype.

flies (Figure 5.17). To assess midgut morphology, I stained guts with anti-Arm antibodies to mark cell junctions and with anti-Prospero antibodies to label EEs[17]. I then visualized ISC/EBs by *esg^{ts}>GFP* fluorescence. Consistent with my previous findings, *Pvr^{CA}* expression drives the expansion of *esg^{ts}>GFP* positive cells in the posterior midgut. In contrast, inhibition of dJNK signals with *dJNK^{DN}*, mildly reduced total *esg^{ts}>GFP* positive cell numbers, relative to control guts. Simultaneous *esg^{ts}*-mediated expression of *Pvr^{CA}* and *dJNK^{DN}* phenocopied the proliferation of *esg^{ts}>GFP* positive cells observed with *Pvr^{CA}* expression alone. From these data I conclude that *Pvr^{CA}* signals promote the expansion of *esg^{ts}>GFP* positive cells in the posterior midgut independently of dJNK activity.

To determine if dJNK-induced ISC proliferation is the outcome of downstream PVR pathway activation, I used the *esg^{ts}* driver system to express *dMKK7^{CA}*. *dMKK7^{CA}* is a constitutively active MAPKK where S326D and T330D mutations mimic an activated phosphorylated kinase that engages dJNK independent of external stimuli[307]. I coexpressed *dMMK7^{CA}* and *Pvr^{DN}* with *esg^{ts}* to simultaneously promote dJNK activity while blocking the PVR pathway in ISC/EBs, respectively (Figure 5.18). I also individually expressed *dMKK7^{CA}* and *Pvr^{DN}* with *esg^{ts}*, alongside wildtype flies, as controls. Hyperactive dJNK activity in ISCs rapidly induces gut hyperplasia and eventually kills the affected fly, therefore *dMMK7^{CA}* expression was limited to 3 days in all flies[19]. In agreement with previous studies, constitutive dJNK activation induced profound changes in the number and morphology of *esg^{ts}>GFP* positive cells, relative to control midguts. However, when *dMKK7^{CA}* and *Pvr^{DN}* are coexpressed with *esg^{ts}* the proliferative signals generated through constitutive dJNK activation overwhelm

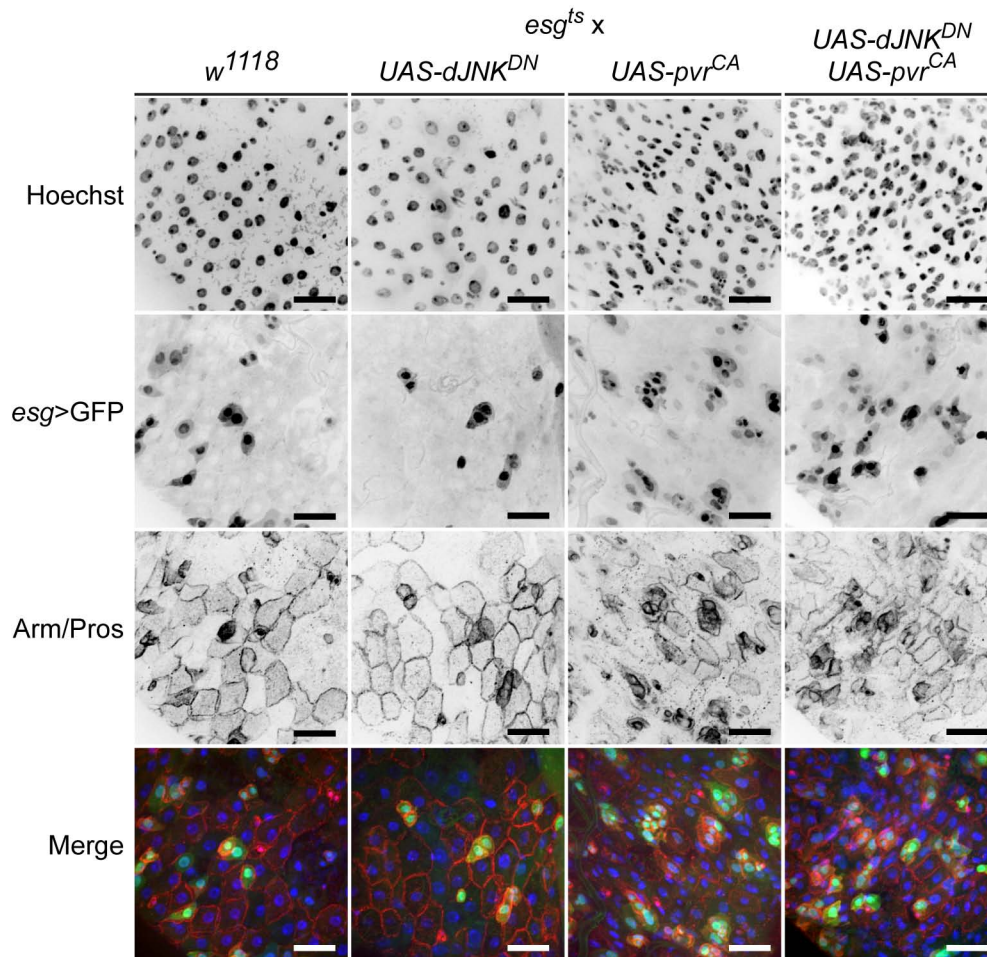


Figure 5.17. Pvr-regulates ISC homeostasis independent of extrinsic dJNK cues.

dJNK^{DN} (column 2), and *pvr^{CA}* (column 3) transgenes were expressed individually or together (column 4) in ISC/EBs and posterior midgut morphology was visualized relative to control midguts (column 1). Guts were stained with Hoechst (row 1), and anti-Arm/Pros antibodies (row 3), while ISC/EBs were visualized with *esg^{ts}*>GFP expression (row 2). Hoechst (blue), GFP (green), and anti-Arm/Pros channels (red) channels were false colored and merged in row 4. Scale bars represent 25 μ m. Images are representative of 7 guts visualized per two replicate experiments.

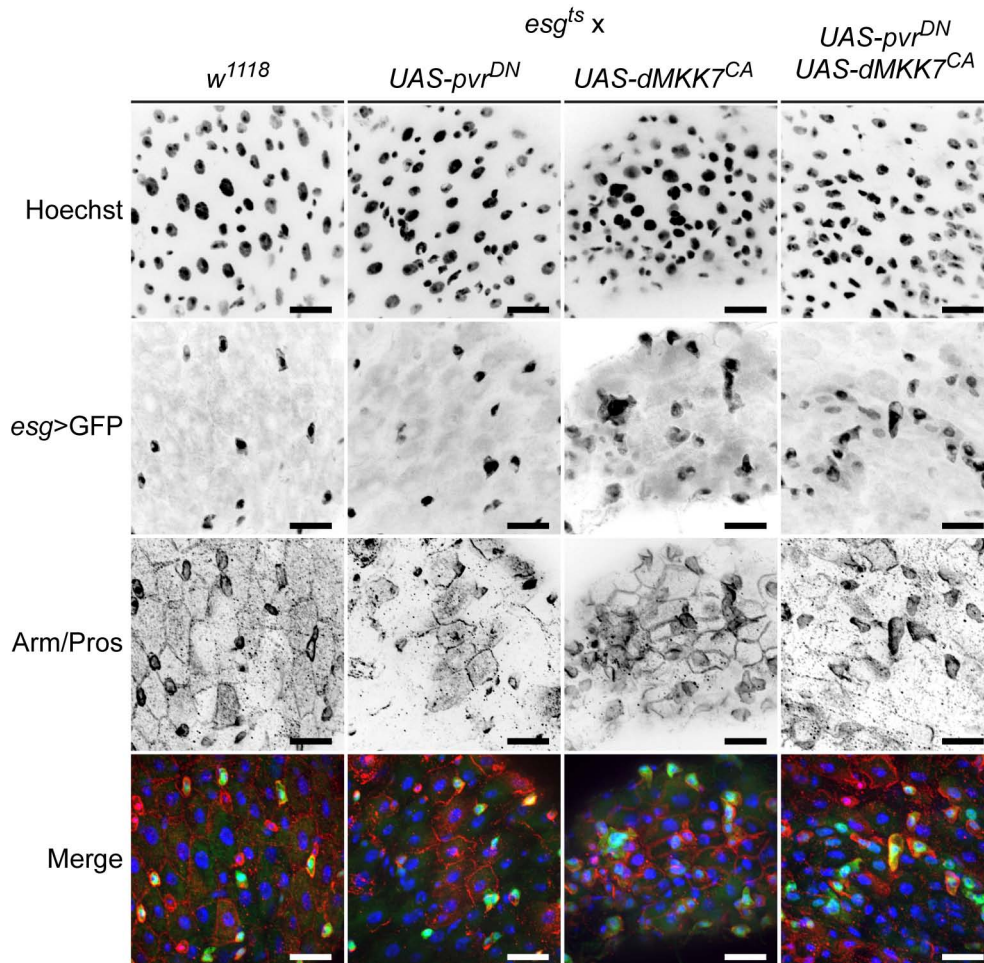


Figure 5.18. Extrinsic dJNK cues control intestinal homeostasis independently of Pvr.

pvr^{DN} (column 2) and *dMMK7^{CA}* (column 3) transgenes were expressed individually or together (column 4) by *esg^{ts}* and posterior midgut morphology was visualized relative to control midguts (column 1). Guts were stained with Hoechst (row 1) and anti-Pros/Arm antibodies (row 3), while ISC/EBs were visualized with *esg^{ts}*>GFP (row 2). Hoechst (blue), GFP (green), and anti-Arm/Pros channels (red) channels were false colored and merged in row 4. Scale bars represent 25 μ m. Images are representative of 7 guts visualized per two replicate experiments.

any suppressive effects of Pvr^{DN}. I conclude that Pvr and dJNK pathways act independently to regulate ISC proliferation in the posterior midgut. However, I cannot exclude the possibility that Pvr and dJNK pathways promote ISC proliferation through shared downstream effectors.

5.2.8. Ras activity is required for Pvr-induced intestinal dysplasia.

Previous studies showed that constitutive Ras activity in ISCs promotes hyperproliferation and posterior midgut dysplasia[250]. My data suggest that hyperactive Pvr dysplastic cues are independent of the dJNK pathway, and given the established connection between Pvr/Ras signaling, I asked if Pvr intracellular signals proceed through the Ras pathway. To assess the downstream requirement for Ras in Pvr controls of intestinal homeostasis, I simultaneously expressed Pvr^{CA} with a dominant negative allele of mammalian Ras with a S17N mutation (Ras^{N17}), which is stronger than the *Drosophila* allele at blocking downstream signals[308]. For these experiments, I expressed Pvr^{CA} and Ras^{N17} transgenes together or independently in 3-5 day old adult flies for 10 days, alongside wildtype control flies (Figure 5.19A). I monitored posterior midgut morphology with anti-Arm antibody stain, ISC/EBs with *esg*>GFP, and the total intestinal cell population with Hoechst fluorescence. I then quantified ISC/EBs with *esg*>GFP and total cell populations with Hoechst in each field and I calculated the percent *esg*>GFP positive cells (Figure 5.19B). Consistent with my previous findings Pvr^{CA} expression promoted cellular dysplasia and significantly increased the percentage of *esg*>GFP positive cells relative to wildtype controls in posterior midguts. Expression of Ras^{N17} alone with *esg*^{ts} had a mild reducing effect on ISC/EB cell numbers. Furthermore, I found that coexpression of Ras^{N17}

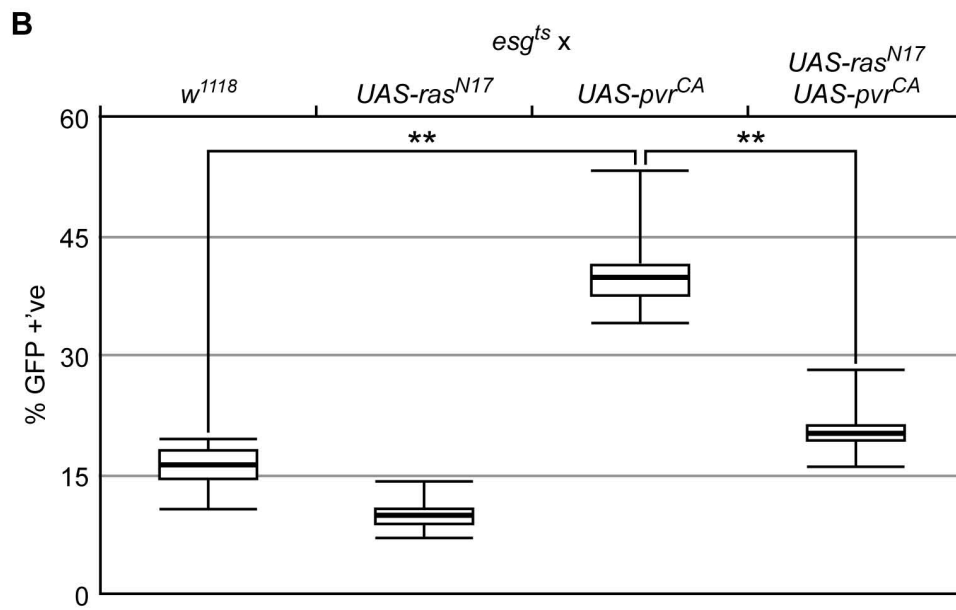
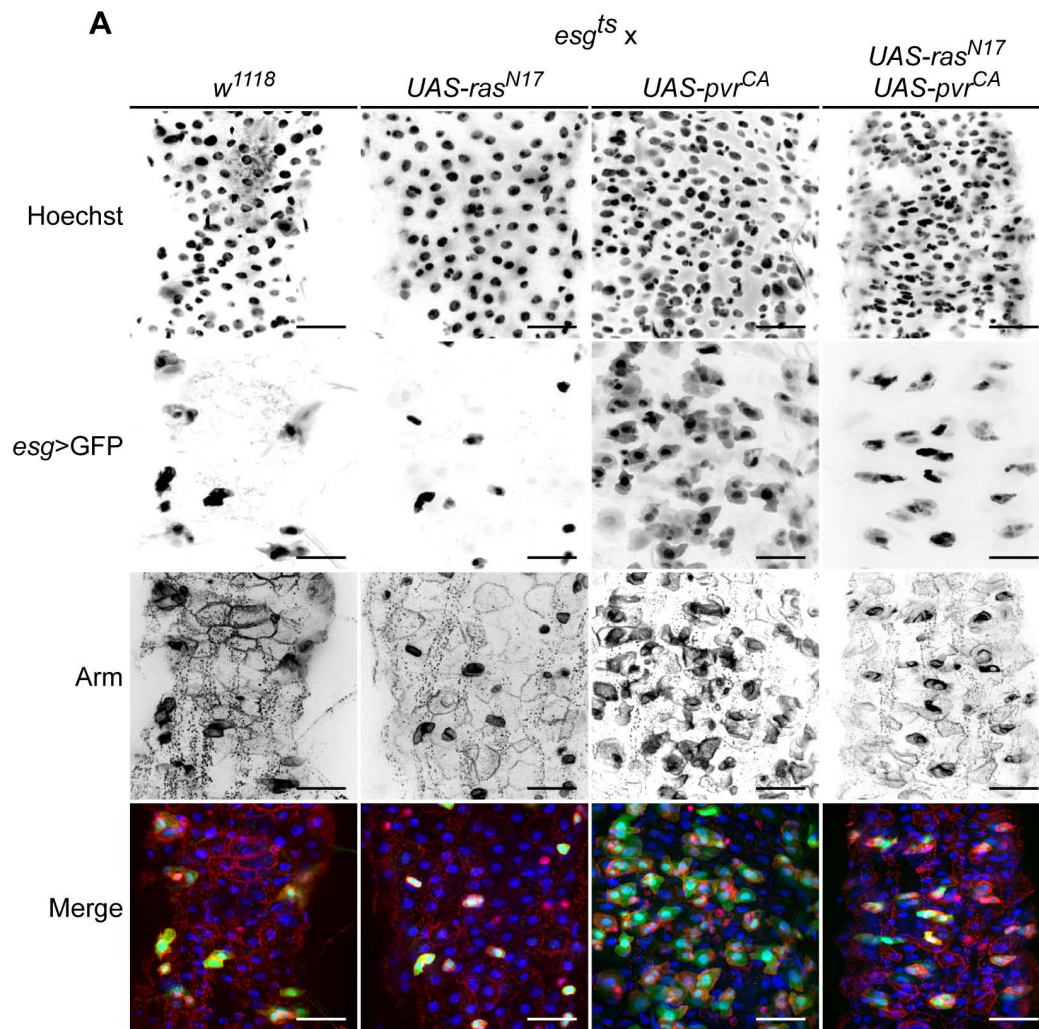


Figure 5.19. Pvr acts through Ras to control ISC homeostasis.

A. *ras*^{N17} (column 2), and *pvr*^{CA} (column 3) transgenes were expressed individually or together (column 4) by *esg*^{ts} and posterior midgut morphology was visualized relative to control midguts (column 1). Guts were stained with Hoechst (row 1), and anti-Arm antibodies (row 3), while ISC/EBs were visualized with *esg*^{ts}>GFP expression (row 2). Hoechst (blue), GFP (green), and anti-Arm (red) channels were false colored and merged in row 4. Scale bars represent 25µm.

B. Quantification of GFP positive cells in A. Percent GFP positive cells were calculated in posterior midguts that expressed *Pvr*^{CA} (n=5 guts), *Ras*^{N17} (n=8 guts) or *Pvr*^{CA} and *Ras*^{N17} together (n=8 guts) with *esg*^{ts}, relative to controls (n=6 guts). Box plots show the median percent GFP positive cells (thick line), flanked by the first quartile (bottom edge) and third quartile values (top edge), while top and bottom whiskers indicate the highest and lowest data points for each data set. ** indicates p<0.01.

and Pvr^{CA} significantly abrogated the Pvr^{CA} dysplastic phenotype. These findings indicate that Ras is a downstream signaling component in the Pvr-dependent regulation of intestinal homeostasis.

5.2.9. Extrinsic proliferative cues override intrinsic roles of Pvr in intestinal homeostasis.

My data established that dJNK proliferative signals overwhelm the Pvr^{DN} phenotype in posterior midgut ISCs. As dJNK activates ISC proliferation in response to acute stress such as microbial challenge, I asked if oral infection-mediated ISC proliferation also overrides the hypoplastic phenotypes of *pvr*⁵³⁶³ and *pvf2-3*. Oral infection of adult *Drosophila* with low concentrations of the enteropathogenic bacterium *Pe* promotes the rapid proliferation and differentiation of ISCs to replenish damaged ECs, and maintain posterior midgut epithelial continuity[15, 16]. I therefore tested if *Pe* oral-infection induces expansion of *pvr*⁵³⁶³ and *pvf2-3* mutant clones in the posterior midgut. I generated GFP-marked wildtype, *pvr*⁵³⁶³ and *pvf2-3* clones, and fed adult flies low concentrations of *Pe* in sucrose or sucrose alone, as a control (Figure 5.20). In uninfected guts wildtype, *pvr*⁵³⁶³ and *pvf2-3* clones were small, sparsely distributed and mostly single cells after 3 days[18]. This reflects the generally low homeostatic proliferation rate of ISCs in the absence of challenge. As expected, *Pe* infection increased the size and cellular architecture of GFP-marked wildtype clones, with an anticipated expansion of large polyploid ECs that accounts for the majority of cells within the clone. These data overlap with previous reports that ISCs rapidly proliferate and differentiate into mature cell types to maintain tissue homeostasis upon *Pe* infection. Strikingly, *pvr*⁵³⁶³ and *pvf2-3* mutant clones were

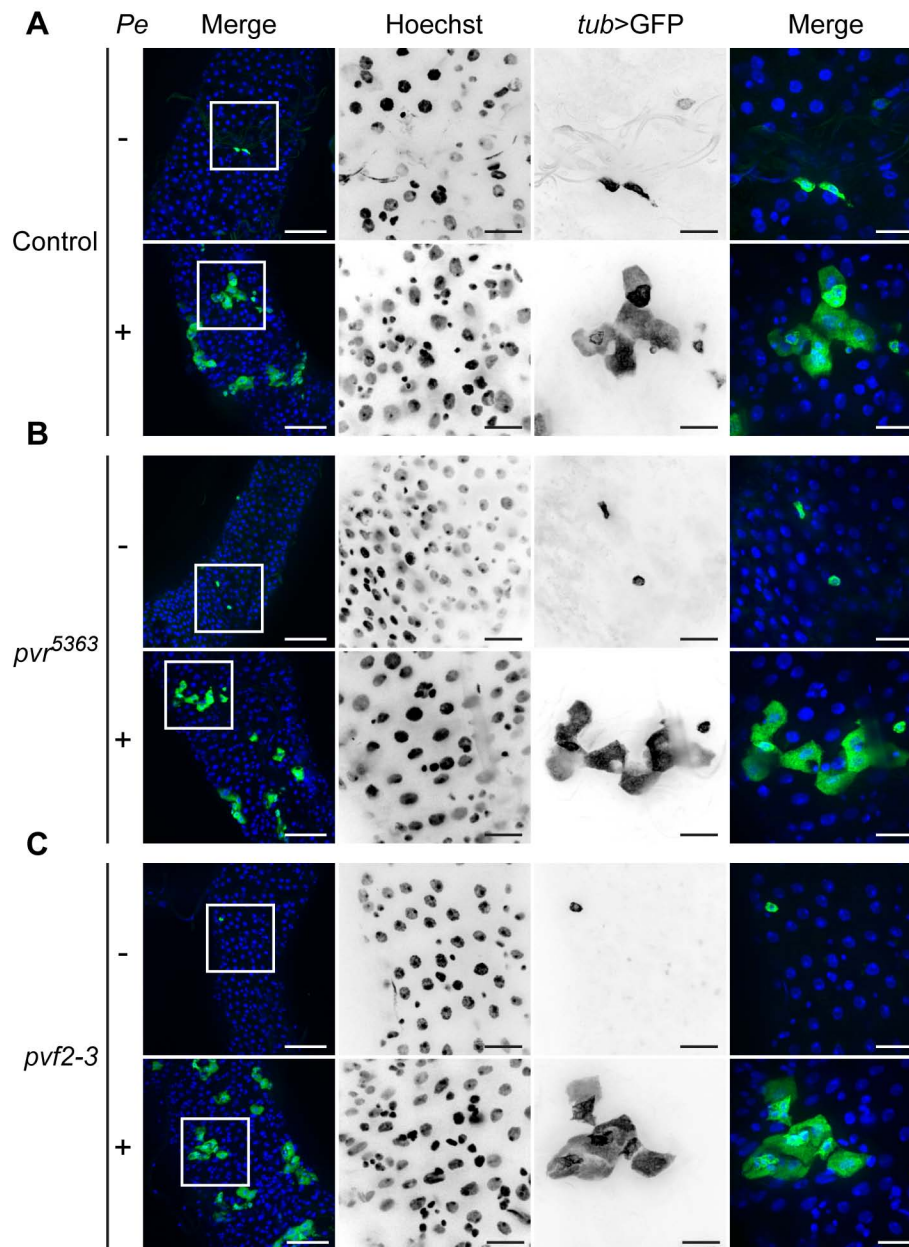


Figure 5.20. Extrinsic stress signals override Pvr intrinsic homeostatic controls.

Infection-induced proliferative signals override Pvr-regulation of ISCs. A. Wildtype (rows 1 and 2), *pvr*⁵³⁶³ (rows 3 and 4), and *pvf2-3* (rows 5 and 6) MARCM clones in uninfected and *Pe*-infected adult posterior midguts as indicated. Guts were stained with Hoechst (column 2), and clones were visualized with *tub*>GFP in column 3. Hoechst (blue), DI (red), and *tub*>GFP (green) channels were false colored and merged in column 1 and 4. The boxed areas in the low magnification column 1 indicates the area shown in high magnification in column 2-4. Scale bars represent 50 μ m and 15 μ m for low and high magnifications, respectively. *pvr*⁵³⁶³ and *pvf2-3* mutant clones expand in response to *Pe*-infection. Images are representative of 7 guts visualized per two replicate experiments.

indistinguishable from wildtype clones. In each case, I observed a clear expansion of GFP positive clones that primarily consist of large ECs derived from ISC proliferation and differentiation. I conclude that extrinsic stress-induced proliferative signals override the hypoplastic defects in ISCs attributed to the loss of intrinsic Pvf/Pvr signals upon intestinal infection.

As Pvr dampens innate immune responses[280] and epithelial renewal programs remain intact in the midgut of infected *pvr* mutants, I reasoned that loss of PVR pathway activity may enhance host responses to bacterial challenge. To determine if Pvr signals impact survival rates after oral infection with a lethal dose of *Pe*[254], I expressed Pvr^{CA} and Pvr^{DN} transgenes in ISC/EBs of 3-5 day old adult flies for 10 days. I then orally infected flies with *Pe* and counted the number of surviving flies over time (Figure 5.21). I found that wildtype and *esg^{ts}>Pvr^{CA}* flies rapidly succumbed to *Pe* oral infection. Remarkably, inhibition of Pvr signals with *esg^{ts}*-mediated expression of Pvr^{DN} improved survival to *Pe* infection. For example, half the wildtype and *esg^{ts}>Pvr^{CA}* flies succumb to infection within 64h of infection, while I observed no appreciable decrease in *esg^{ts}>Pvr^{DN}* fly viability. These data show that inhibition of Pvr signals enhance fly survival to oral infection with *Pe*, despite the apparent requirement for Pvr in ISC proliferation under normal conditions. However, these findings are consistent with my previous data that show Pvr is a potent inhibitor of the IMD-pathway, and inhibition of Pvr, *in vivo*, enhances the basal and immune-induced expression levels of AMPs.

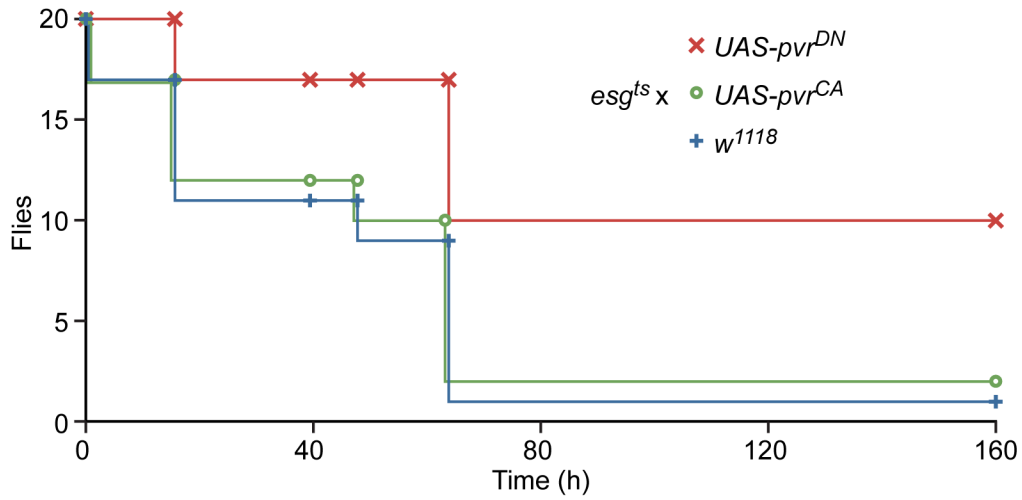


Figure 5.21. Pvr signals control survival to *Pe* oral infection.

Survival curve of adult flies that express *pvr*^{CA} or *pvr*^{DN} transgenes with *esg*^{ts} in EB/ISCs upon oral infection with *Pe*, relative to control *w*¹¹¹⁸ flies. Flies were infected orally with *Pe* and surviving flies were counted at the indicated times. Pvr inhibition enhances survival to *Pe* infection.

CHAPTER 6

Discussion

6. Discussion.

The model organism *Drosophila melanogaster* has labored as a reliable servant to biologists for the better part a century. Humankind owes great thanks to this little fly for the enormous contributions to our understanding of biological events ranging from development to immunology. The strength of the *Drosophila* model is based, in part, on its unequaled genetic accessibility. Mutagenesis screens in *Drosophila* identified many novel regulators of developmental pathways[154-156]. Upon identifying an embryo with unusual morphology researchers are said to have proclaimed in German "Das ist ja toll!", which roughly translates as "That's great". Unknown to them at the time, Toll was to revolutionize the field of immunology[9, 11]. The finding that *toll* mutants are highly susceptible to fungal and gram-positive bacterial infections combined with the knowledge that Toll engages NF- κ B signaling, a family of proteins with conserved immunological functions, prompted the search for human Toll-like receptors[10]. The discovery of the TLR changed our understanding of pathogen/host interactions, and cemented *Drosophila* as a premier model organism of innate immune responses[9].

Based on this history, I began to study the *Drosophila* IMD pathway because of its overt similarities to the human TNF pathway. The IMD and TNF pathways engage conserved NF- κ B, caspase and JNK signaling modules, with remarkable overlap in core signaling components. Despite substantial research into the regulation NF- κ B and caspase modules, the JNK arm remained poorly resolved. This is surprising given the pleotropic roles of JNK signals in animal biology, and its association with numerous human diseases. As hyperactivation of JNK/dJNK

signals leads to apoptosis in humans and *Drosophila* respectively, I hypothesized that a network of conserved regulatory elements carefully controls dJNK activity in the IMD pathway. To test this, I performed the first whole-genome RNAi screen for dJNK activation. Given the evolutionary conservation of the JNK signal transduction pathway, I believe that this study is of direct relevance to JNK activity in other aspects of animal biology.

6.1. Quantification of biological signaling events.

The ability of an assay to accurately reproduce the pertinent features of biological events is critical to the success or failure of genome scale RNAi screens due to the huge number of samples. As RNAi screens are expensive and labor intensive, extensive preliminary studies are prerequisite to optimize assay conditions. In my studies, I developed a high-throughput ICW assay to quantify PGN-induced JNK phosphorylation events in the IMD pathway. This assay was used to monitor 15,852 dsRNA effects on P-dJNK/f-actin levels, at both 15min and 60min PGN-exposures in serum-free S2 cells.

6.1.1. Fluorescence-based assays.

Traditionally, Western blots were probed with target-specific antibodies linked to chemiluminescent enzymes, and light emitting enzyme/substrate reactions were captured on film[343]. For example, enhanced chemiluminescence (ECL) detection relies on horseradish peroxidase-coupled antibodies that react with luminol, emitting light as a byproduct. However light production is constrained by substrate/enzyme kinetics, and therefore is linear over a narrow range of protein concentrations that varies with film exposure times. For this reason ECL is not

ideal for quantitative measurements of protein levels. Fluorescence-based assays have numerous advantages over traditional enzyme-based assays for quantifying protein levels, including a wide linear dynamic range of protein detection. Additionally, the use of infrared labels with non-overlapping emission spectra allows for the simultaneous detection of multiple proteins on a single blot. In my studies, I used secondary antibodies bound to infrared fluorophores with peak emission spectra at 680nm or 750nm wavelengths. These secondary antibodies allow for precise measurements of two separate epitopes on a single blot, even when the protein bands overlap or when the epitopes are located on a single protein. This was particularly valuable for quantifying P-dJNK levels relative to control JNK or actin levels, as these signals overlap one another. This multiplex approach facilitates normalization or comparative analyses of numerous targets on a single blot. On the other hand, chemiluminescence is a one-color technique that can only detect one protein at a time. To achieve the same measurements with traditional enzymatic techniques the blot would need to be stripped and reprobed, adding time and variability to the experiment.

6.1.1.1 Quantification of fluorescence-based assays

Infrared detection of target proteins represents a technological step forward over traditional chemiluminescence Western blot techniques that require film. The use of film has particular drawbacks, such as limited ability to detect signal saturation, and the reliance on indirect, non-linear densitometric measurements to quantify protein levels. In contrast, infrared fluorescence does not rely on enzyme/substrate kinetics, but instead infrared dyes coupled directly to the detecting antibody. Consequently the signal to sample ratio is linear over a

broader range of protein concentrations. Blots are visualized with an infrared scanner that excites the bound fluorophores with a laser, and measures the subsequent emission wavelength. The imaging software produces a real-time digital image that clearly displays underexposed or saturated signals, issues that can be immediately address by altering laser intensities. Fluorescent dyes come in an array of emission and excitation wavelength but the infrared fluorescent dyes are particularly advantageous for Western blot analysis due to low membrane auto-fluorescence in the infrared spectrum. These features allow for sensitive and reliable quantification of protein levels in the infrared imaging system. I used the above fluorescence-based Western blot technique extensively throughout this project to quantify dJNK phosphorylation events in the *Drosophila* IMD pathway. I then adapted this assay to the ICW method; a critical initial step in performing a whole-genome RNAi screen.

6.1.2. Establishment of fluorescence-based ICW assay.

The infrared Western blot technique is an excellent method to quantify protein levels in cell lysates. However, Western blots are impractical for the large number of samples associated with genome-wide RNAi screens, as they require lengthy sample preparation, protein electrophoresis, protein electroblotting, and incubation of the membranes with antibodies. With this in mind, I established a plate-based assay to monitor immune-induced dJNK signaling events in the IMD pathway that could accommodate a large number of experimental samples commensurate with genome-scale screens. An additional benefit to fluorescence-based ICW assays is the ability to simultaneously monitor multiple targets. This property allows for the inclusion of internal controls to normalize

target protein levels. In this study, I stained S2 cells with fluorescently labeled phalloidin to monitor actin levels as an internal control. The inclusion of f-actin controls permitted the normalization of P-dJNK levels across the 96 well plate and allowed for a more robust analysis of RNAi screen results, as genes that modified cell viability or numbers were excluded from further analysis.

There are numerous considerations to bear in mind regarding reagent choice in the plate-based assays[344]. Unlike Western blots, where several bands are easily distinguished on a single blot, the plate-based assay measures the total signal from each well on the plate, which makes the choice of antibody for the assay critical. The antibody should be specific for a single target and have low background. If the antibody binds more than one target it will generate off-target signals not representative of the genuine target protein level. In the ICW assay, I used a mouse anti-P-JNK antibody that generated a single P-dJNK band with little background fluorescence, in Western blots.

ICW assay optimization not only produces more accurate experimental outcomes, but also reduces reagent costs, as antibodies may represent the largest single reagent expense in a genome-scale screen. To determine the ideal concentration that balanced strong signal detection with low background fluorescence, I titrated the anti-P-dJNK antibody over an extended dilution series. I determined that the ideal concentration for detection of P-dJNK was 1:400. This antibody concentration balanced strong signal detection with low background fluorescence. Given the amount of antibody required for a whole genome RNAi screen it is important to have a consistent reagent, and for this reason I used a

mouse monoclonal anti-P-JNK antibody from a single production lot. An additional benefit of monoclonal antibodies is that the epitope is often mapped. As this antibody was raised against human P-JNK, I thought it pertinent to address the specificity of the antibody against *Drosophila* P-dJNK. I therefore performed a preliminary screen in which I depleted established modifiers of dJNK phosphorylation in the IMD pathway. All known modifiers of dJNK phosphorylation had the predictable and consistent effects on P-dJNK levels, and I therefore concluded that this antibody is specific for P-dJNK in samples of fixed S2 cells.

The cell line(s) used in the assay must faithfully reproduce the salient features of events being assayed. I therefore tested the *Drosophila* embryonic S2, S2R+ and Kc167 cell lines, and I found the S2 cell line ideal for studying PGN-induced dJNK phosphorylation in the IMD pathway. Analogous to dJNK activation *in vivo*, exposure of S2 cell to PGN induced transient phosphorylation of dJNK that peaked at 15min and returned to basal levels by 120min. In contrast, JNK is not phosphorylated in S2R+ cells exposed to PGN and is only weakly phosphorylated in PGN-treated Kc167 cells.

The S2, S2R+ and Kc167 transcriptomes show distinct expression patterns in microarray studies[315], likely contributing to the varied dJNK phosphorylation profiles. However, it is currently unknown how these transcriptional differences contribute to dJNK activity. I find it interesting that the PGN-induced dJNK-responses were severely attenuated in the S2R+ cells, a variant of the S2 cell line. The S2 cell line does not express the Wingless (Wg) pathway receptors, and

therefore does not respond to Wg pathway signals. However, the S2R+ (receptor plus) cell line was identified as a S2 cell derivative with a gain of function in the Wg pathway receptors Dfrizzled-2 and Dfrizzled-1. Engagement of the Wg pathway in S2R+ cells may account for the loss of PGN-induced dJNK responses[314]. In my screen I did not identify Wg pathway components as modifiers of PGN-induced dJNK phosphorylation, not surprising, as the S2 cell line does not engage Wg pathway signals. It is also worth noting, that Kc167 cells also showed abrogated PGN-induced dJNK phosphorylation responses. I find this particularly relevant in light of our findings that PVR pathway activation negatively regulates PGN-induced P-dJNK levels, as Kc167 cells are known to express Pvr ligands Pvf1 and Pvf2. It is possible that higher basal Pvr activity in Kc167 cells results in increases in the suppression of IMD pathway signals. It is also conceivable that the Wg pathway may interfere with normal dJNK activation, as the Kc167 cell line is a well-established model for Wg pathway studies[202]. If Wg pathways signals in S2R+ and Kc167 cells inhibit PGN-induced dJNK phosphorylation, then RNAi-mediated depletion of Wg pathway components should, in theory, restore dJNK activation. However, this line of investigation has yet to be undertaken.

The cells used in the ICW assay should be adherent to establish a confluent cellular monolayer. To prevent cell loss, I used S2 cells grown in a serum-free tissue culture medium. I found that S2 cells grown in serum-free medium are considerably more adherent than S2 cells grown in conventional cell culture medium containing fetal bovine serum, although the cause of this is unknown. While this finding seems superficial, it was a critically important advance in

establishing a reliable ICW assay in S2 cells. The efficacy of RNAi-mediated depletion of target protein in serum free S2 cells grown under serum-free conditions appears comparable, if not slightly better than S2 cells grown under standard conditions, although I did not make direct experimental comparisons.

I believe that S2 cells present an ideal system investigating JNK signal transduction pathway, as S2 cells are readily accessible to large-scale RNAi screens, reproduce key elements of the innate immune response and serve as a convenient gateway for whole animal studies in the genetically tractable *Drosophila* model. Furthermore, I conclude that the ICW technique represents a robust method for direct quantification of dJNK activation in serum-free S2 cell tissue culture assays. The promise of the ICW assay to accurately quantify biological signaling events goes beyond dJNK phosphorylation events in S2 cells. In our lab this assay has been adapted to a variety of signaling events, from caspase engagement in S2 cell apoptosis to TNF induced JNK activity in the human HeLa cell lines[206].

6.2. Development of high-throughput screens.

A well-defined objective is essential to the design and performance of a successful high-throughput RNAi screen[345]. In cases where molecular pathways are well established, the goal of the screen might be to identify missing components. Alternatively, RNAi screens can provide a global overview of genes involved in less well-established biological processes. My objective for the dJNK screen was the former, as the dJNK signaling module was poorly resolved relative to the remainder of the IMD pathway.

6.2.1. Assay development.

The most important element to the success of an RNAi screen is the assay used to monitor the biological processes of interest. Ideally, the assay should be simple to perform, and highly reproducible, given the huge number of samples tested. The ICW assay that I developed to monitor dJNK phosphorylation events in S2 cells fits these criteria, however there are intrinsic properties of the pathway being studied that need to be considered. This highlights the importance of preliminary investigations into the nature of the biological event(s) being screened. I used the ICW assay to monitor dynamic dJNK phosphorylation events in S2 cells treated with PGN over a time course. I found that the ICW assay closely reproduced other measures of dJNK activity in the IMD pathway, and I established that P-dJNK peaks at 5-15min and returns to basal levels by 60min-120min. These data informed the time points I selected for the genome-wide screen. I monitored PGN-induced P-dJNK level at 15min to identify genes that enhance or suppress P-dJNK levels, and at 60min to identify genes that suppress or terminate dJNK phosphorylation.

6.2.2. Screen sensitivity and establishment of controls.

The assay sensitivity is an important consideration when adapting a protocol to a genome scale RNAi screen. Ideally the treatment values should widely differ from controls, and thereby provide high signal-to-noise ratio and large dynamic range[345]. In preliminary evaluations of dJNK phosphorylation events by ICW, I consistently observed a 3-6 fold increase in normalized P-dJNK levels with 15min PGN-treatment relative to untreated controls. This large dynamic range in P-

dJNK levels allows ample opportunity to measure RNAi-mediated changes by ICW. If the signal-to-noise ratio is too low then RNAi effects are not identified over the background noise. As an example, I began the RNAi screen for modifiers of dJNK phosphorylation with an untreated group of S2 cells in addition to the 15min and 60min PGN time points. I initially screened 2496 dsRNAs for effects on basal P-dJNK levels in S2 cells, however I abandoned this line of investigation, as RNAi effects could not be distinguished from background noise. This was likely a reflection of the low basal level of dJNK phosphorylation in S2 cells that caused an insufficient signal-to-noise ratio. As a further example, I chose not to examine dsRNAs that decreased PGN-induced P-dJNK responses at the 60min time point, as initial investigation showed that well-to-well variability overwhelmed genuine modifiers of dJNK phosphorylation. These two examples showcase the importance of a large dynamic range in order to overcome the inherent variability associated with RNAi screen.

Furthermore, when selecting controls for a genome scale screen it is important to choose positive controls with high signal and negative controls with low noise[203]. In my preliminary investigations I tested IMD pathway components Key and dTak1 as established suppressors and enhancers of PGN-induced dJNK phosphorylation, respectively. In agreement with previous studies, I showed that Key dsRNA significantly increased and prolonged dJNK phosphorylation, while dTAK1 dsRNA abrogated P-dJNK levels[159, 164, 312]. I serendipitously identified Key (2.9 and 3.43 fold increase in P-dJNK levels at 15min and 60min, respectively), and dTak1 (3.03 fold decrease in P-dJNK levels)

as the strongest modifiers of PGN-induced P-dJNK levels in the screen, highlighting their accuracy as positive and negative controls, respectively.

6.3. Whole genome RNAi screen of dJNK phosphorylation.

Signal transduction through the JNK family of MAP kinases is a central element of vertebrate and invertebrate innate immune responses to infectious microbes[146, 346, 347]. In addition, JNK activation contributes to the regulation of essential cellular processes, such as differentiation, apoptosis and directed cell movements[348-350]. The pleiotropic developmental and homeostatic requirements for JNK activity combined with functional redundancies among JNK pathway member isoforms hampered large-scale evaluations of JNK in model systems. For these reasons, I performed a genome-wide RNAi screen for regulators of immune-induced dJNK phosphorylation in the IMD pathway.

6.3.1. Accuracy of whole genome screens.

To some degree there is variability in every experimental assay. Variability in RNAi screens can be introduced through the quality of the reagents, the nature of the assay, the accuracy of the assay, the specificity of the dsRNA, environmental conditions, data sampling, and so on. Consequently, large-scale screens can be plagued with high false-positive and -negative rates, thereby incorrectly implicating a gene in, or disregarding a genuine regulatory component from, a given biological process, respectively.

6.3.1.1. False-positives.

Arguably, false-positives are preferable to false-negatives, as genes initially

implicated as hits in the primary screen can be excluded upon secondary analysis. However, these false positives can obscure genuine hits and require rigorous, time consuming, and expensive secondary assays. False-positives are an inherent property of high-throughput screens, and arise from numerous sources including experimental variability (noise), assay bias, and off-target effects (OTE)[203]. OTE occur when RNAi depletes a gene other than the intended target due to promiscuous RNAi sequences. While, OTE effects are well known in mammalian RNAi screen, OTE are less well studied in *Drosophila* RNAi screens[351]. While it was once thought that dsRNA OTE were less prevalent in *Drosophila* tissue culture, recent studies have concluded that OTE contribute to false-positive rate in *Drosophila* high-throughput screens[205, 351]. To mitigate OTEs dsRNAs should be designed to avoid conserved sequences in multiple proteins, and screen results should be confirmed in secondary assays with non-overlapping dsRNAs for each candidate gene.

As my objective was to identify and characterize specific novel regulators of dJNK phosphorylation, rather than producing a global network of dJNK modifiers, I performed targeted secondary assays. I selected a cohort of eleven modifiers of dJNK phosphorylation, including 8 suppressors and 3 enhancers for secondary analysis based on their predicted/known molecular functions in other signaling pathways. These genes represented a full range of z-scores within the 95% CI (z-score= +/-1.96) from the preliminary screen. In secondary ICW assays, I determined that 9 of the 11 dsRNAs retained the predicted phenotype. These data suggest a low false positive rate for this screen, however a more comprehensive analysis of the entire screen hits would be required to determine

the true false positive rate. Furthermore, as the secondary assays were performed with the same dsRNA sequences used in the primary screen I cannot discount the possibility that some of these rescreened dsRNA represent OTE. Nevertheless, the genome-scale ICW assay generated reproducible RNAi phenotypes recapitulated in secondary assays.

6.3.1.2 *False-negatives.*

False negative rates are difficult to measure in genome-wide screens of poorly understood biological events, as identification of false negatives requires previous knowledge that a gene is involved in a given process[352]. RNAi screens of well-established signaling pathways can estimate false-negative rates based on the failure to identify known signaling components. Together these studies suggest that the false negative rate for genome-wide RNAi screen is between 16% to 50% in *Drosophila* tissue culture[352]. This lack of understanding surrounding the false-negative rate is because experimentally setting out to monitor false-negatives (known components of a biological process) is contrary to the purpose of an RNAi screen.

I consider the false negative rate for IMD pathway members a pertinent measure of the success of my screen. In contrast to previous RNAi screens of signal transduction pathways, my assay did not rely on indirect reporter assays[137, 204, 205]. Instead, I measured the contribution of each annotated gene within the fly genome to the IMD-responsive phosphorylation of dJNK. I believe that the direct quantitative nature of my assay combined with the ease of RNAi in S2 cells greatly minimizes the likelihood of false negatives in the primary

screen. Indeed, preliminary analysis of my primary screen data identified the bulk of the IMD signal transduction pathway (PGRP-LC, Imd, dFADD, Dredd, dTAB2, dIAP2, dTAK1, dMKK4/7, dJNK, dFos, Puc, Key, Ird5 and Rel) as essential modifiers of JNK activation in the IMD pathway. In each case, the phenotype was consistent with the established molecular function of the respective IMD pathway element as either negative or positive modifiers of JNK activation. In this screen I correctly identified 15 of the predicted 16 core signaling components in the IMD pathway, equating to a remarkably low false negative rate of 6%. Thus, I am satisfied that false negatives do not obfuscate interpretation of my data in any meaningful manner. Ironically, the only anticipated hit I failed to identify was dJun[164]. This is surprising, as it is believed that dJun/dFos heterodimers form the dAP-1 transcription factor, and AP-1 transcription factor activity drives the expression of the dJNK phosphatase, Puc[165]. However, it is possible that dJun is dispensable for the regulation of dJNK phosphorylation in the IMD pathway, and dAP-1 may alternatively form as a homodimer of dFos molecules[353].

6.3.2. Biological conservation of dJNK regulators.

I identified core elements of the JNK activation cassette such as *misshapen* (*msn*, dM4K ortholog), *dMKK4* (MKK4 ortholog) and *dMKK7* (MKK7 ortholog) as required for activation of dJNK in the IMD pathway. However, I consider it likely that I have serendipitously identified general regulators of the JNK pathway with roles that extend beyond immune signaling. For example, I identified Cka as a powerful suppressor of dJNK phosphorylation, and RNAi-mediated depletion of Cka resulted in elevated/prolonged PGN-induced dJNK phosphorylation in secondary assays. Cka is scaffold protein that brings dMMK7, dJNK and

dJun/dFos together, and is required for the phosphorylation of the downstream AP-1 transcription factor[333]. My findings are consistent with this model, as failure to activate AP-1 would limit the expression of the dJNK phosphatase, Puc, and thereby prolong dJNK phosphorylation. Cka has essential roles outside of IMD signaling, as null mutations in *cka* are embryonic lethal due to defects in dorsal closure, however this is the first report of Cka involvement in immune signaling[333, 354].

6.3.2.1. Comparison of RNAi screens for dJNK activity.

A recent RNAi-based survey of four hundred eighty two *Drosophila* genes identified seventy seven core JNK pathway regulators[355]. Specifically, this screen relied upon a dJun-FRET (Fluorescence Resonance Energy Transfer) reporter that provided continuous fluorometric readout of dJNK activity. dJNK-mediated phosphorylation of dJun sequences in the dJun-FRET reporter causes a conformational change that alters the amount of FRET from CFP to YFP, in transfected Kc167 cells. In this manner, the authors detected gene products that modified the basal level of dJNK activation in a number of genetically compromised backgrounds[355]. There are significant differences between the two screens. Specifically, I used phosphorylation specific antibodies to directly monitor dJNK phosphorylation levels, whereas this screen relied upon dJun reporter activity. Furthermore, whereas I monitored whole genome RNAi effects on PGN-induced P-dJNK levels in S2 cells, the former screen monitored basal dJun reporter activity in Kc167 cells treated with RNAs that simultaneously targeted two separate genes. Of the 77 JNK pathway regulators identified in the dJun-FRET screen, I excluded 6 of these JNK modifiers from analysis as they

caused a significant depletion of f-actin. Of the remaining 71 gene products, 23 were significant modifiers of PGN-mediated dJNK phosphorylation (Figure A1). Most notably, both screens independently identified dERK as a suppressor of dJNK activity. I speculate that differences maybe cell line dependent, as I previously established that there are significant differences in immune-induced P-dJNK levels between the S2 and Kc167 cells lines. Despite the large differences between both screens, I noticed a considerable overlap in my identification of dJNK modifiers including Pvr pathway components Ksr, Slpr and dERK.

6.4. Pvr regulation of *Drosophila* innate immunity.

The *Drosophila* RTK Pvr shows considerable similarity to members of the mammalian PDGF and VEGF receptor families and Pvr is considered an evolutionary ancestor of PDGF/VEGF receptors [270]. Pvr is activated in a partially redundant manner by three PDGF/VEGF-type ligands, Pvf1-3 [270, 271, 274, 356]. Initial studies implicated Pvr as a guidance receptor for cell migratory cues in embryonic hemocyte migration, oocyte border cell migration, thorax closure and dorsal closure of male terminalia [270, 271, 276, 356, 357]. The molecular basis for Pvr-mediated cell movements requires clarification. While functional redundancies appear to exist between individual Pvf ligands, several studies indicate a potential preference for Pvf-1 in the guidance of cell migration [275, 356]. In thorax closure and border cell migration, migratory cues proceed through the Pvr adaptor proteins Mbc, Ced-12 and Crk [276, 357]. In the case of thorax closure and rotation of male genitalia it appears that Pvr induces the corresponding morphogenetic cell movements through the JNK pathway. Thus, Pvr appears to be a positive regulator of JNK activity in the context of cell

movements. This is logical given the extensive involvement of JNK in the coordination of cell migration during development. However, my data strongly indicate that Pvr is a negative regulator of JNK activity during immune signaling. However, I did not detect any requirements for Mbc, Ced-12 or Crk in the regulation of PGN-induced JNK phosphorylation in the IMD pathway. These data suggest that distinct adaptor molecule configurations may discriminate between the impacts of Pvr on immune responses and cell migration.

6.4.1. *Pvr controls of cell-mediated immunity.*

In addition to requirements for Pvr in cell migration, a parallel body of literature indicates a distinct function for Pvr in the regulation of hemocyte proliferation and distribution. Hemocytes in *pvr* mutant embryos are reduced in numbers and lack of normal hemocyte distribution[271]. The disruptions to embryonic hemocyte migration in *pvr* mutants were originally interpreted to indicate that Pvr detects migratory guidance cues in hemocytes[271]. More recent studies demonstrated that expression of the anti-apoptotic p35 molecule in the hemocytes of *pvr* mutants rescues the majority of the migratory phenotype[277]. Further studies confirmed that the bulk of the *pvr* hemocyte phenotype is the result of cell death and that there are only minor guidance requirements for Pvr in hemocyte migration[277]. Pvr activates the ERK pathway, which induces hemocyte proliferation[277, 279]. Consistent with a role for Pvr in hemocyte proliferation, overexpression of Pvf2 drives massive larval hemocyte proliferation *in vivo* and incubation of the embryonic *mbn-2* hemocyte line with Pvr antibodies blocks cellular proliferation in a dose-dependent manner[274]. In contrast, overexpression of Pvf-1 did not substantially alter hemocyte

proliferation *in vivo* and a recent study indicated that proliferative signals for hemocytes are preferentially provided by Pvf2 and Pvf3[274, 279]. In this context, I consider it particularly striking that my data reveal that signal transduction through the IMD pathway results in dJNK-mediated expression of Pvf2 and Pvf3 in the hemocyte-like S2 cell line. These data suggest that immune-induced IMD pathway signals generate timely hemocyte proliferative cues through the expression of Pvf2 and Pvf3.

6.4.1.1. Pvr regulates IMD pathway signals.

My study reveals a novel role for the Pvr/ERK pathway in the attenuation of the IMD pathway and illuminates our understanding of the network of regulatory checks and balances that fine tune the level of IMD/dJNK activity. My data are most consistent with a model whereby activation of the IMD pathway results in dJNK-dependent expression of the Pvr ligands Pvf2 and Pvf3. Pvr then signals through Ras/dERK/Pnt to negatively regulate the IMD pathway (Figure 6.1). On a molecular level, my data show that Pvr signaling dampens the dTAK1-dependent phosphorylation of dJNK and Rel. However, I believe that my data may also uncover an additional physiological role for Pvr. I speculate that the infection-driven production of Pvf2 and Pvf3 engages Pvr receptors on hemocytes and thereby stimulates the Ras/dERK-responsive proliferation of hemocytes. Such an increase in hemocytes numbers would provide a timely measure for the phagocytic elimination of invading extracellular microbes at early stages of infection. In my research the precise mechanism for PVR pathway inhibition of IMD pathway signals remained elusive, however a viable model was proposed in a follow-up study as will be described below[358].

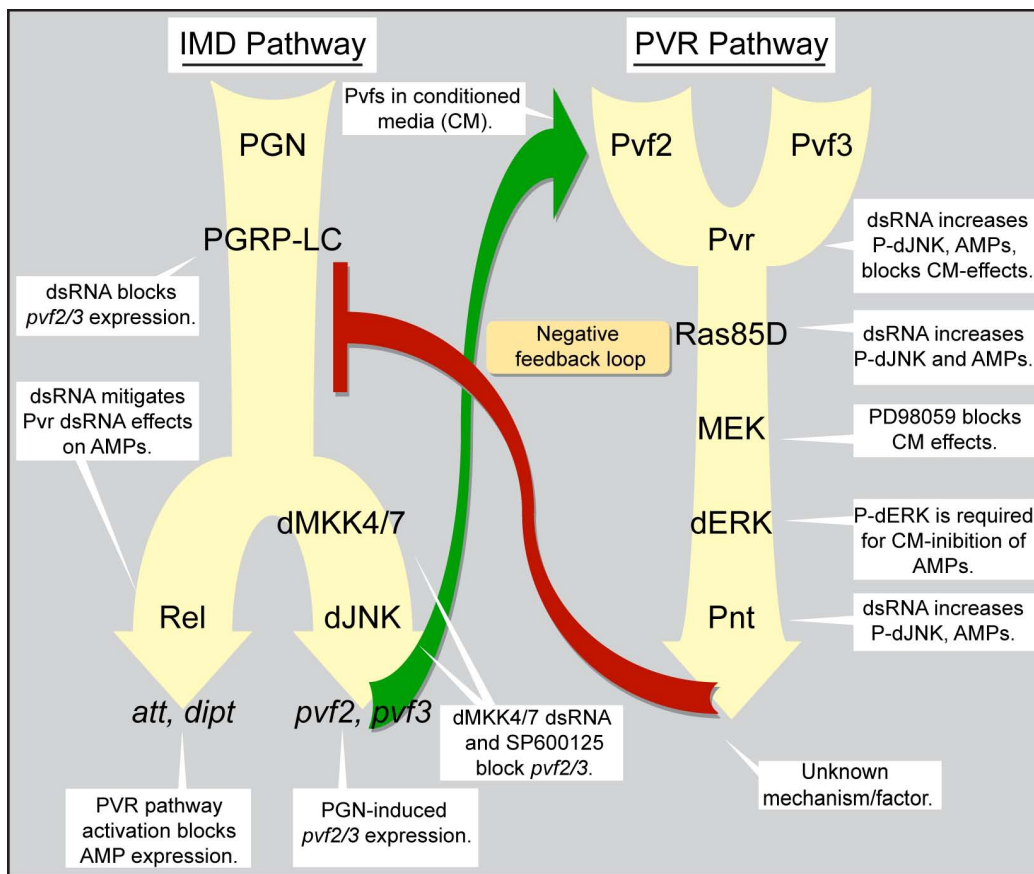


Figure 6.1. Summary model of how the PVR pathway negatively regulates the IMD pathway.

My data shows that PGN-induced IMD pathway activation drives the expression of AMPs *dipt* and *att* through the Rel signaling module, and *pvf2* and *pvf3* through the JNK signaling module. In turn, Pvf2 and Pvf3 activate the PVR pathway (green arrow) and establish a negative feedback loop that blocks Rel-dependent AMP production, and dJNK phosphorylation events, in the IMD pathway (red arrow). PVR pathway components Pvr, Ras85D, MEK, dERK, and Pnt are required for the negative regulation of IMD pathway signals.

A subsequent high-throughput RNAi screen for modifiers of PGN-induced AMP-reporter (*Metchnikowin*, fused to firefly luciferase) expression in S2 cells, essentially replicated my identification of Ras/dERK axis (8 of the 29 hits) as a modifier of IMD responses[358]. Notably, this screen failed to identify Pvr. Pirk is a recently identified negative regulator of the IMD pathway that binds to PGRP-LC and blocks receptor complex signaling[169, 170, 359]. To determine if Pirk was responsible for Pvr-mediated inhibition of IMD pathway signals, the authors activated the Pvr/Ras/dERK signals through the overexpression of Pvf2 or constitutively active Ras85D^{V12} in S2 cells[358]. Expression of Pvf2 and Ras85D^{V12} in S2 cells, or Ras85D^{V12} in flies significantly increased *pirk* expression in the absence of infection[358]. In epistasis experiments, overexpression of Ras85D^{V12} in the fatbodies of adult flies failed to suppress infection-induced *dipt* expression in *pirk* mutant flies. These data indicate that *pirk* acts downstream of Ras to suppress IMD pathway activities. Interestingly, I also identified Pirk as a significant suppressor of PGN-induced dJNK activity (z-score=7.2, $p < 1 \times 10^{-10}$). Further experimentation is required to determine if the PVR pathway directly induces *pirk* expression through the transcription factor Pnt.

I find it intriguing that proliferative signals inhibit activation of immune pathways. It may be that both processes require major metabolic commitments and that hemocytes preferentially reserve resources for proliferation. An alternative and non-exclusive hypothesis reflects the primary role of *Drosophila* hemocytes in immunity. Hemocytes are the major phagocytic cell type in *Drosophila* and are ideally suited for the engulfment of extracellular microbes. Plasmacyte-depleted adult flies are highly susceptible to microbial infections

despite normal systemic production of AMPs[360]. Therefore, I believe that Pvr-mediated inhibition of the IMD pathway in hemocytes is unlikely to impact global AMP responses. I consider it possible that induction of immune responses drives Pvr-mediated proliferation of hemocytes to facilitate rapid neutralization of extracellular microbes through phagocytosis (Figure 6.2). In this situation, it is advantageous for proliferative signals to suppress JNK activation, as hyper or prolonged activation of JNK in *Drosophila* often results in cell death[361, 362].

Preliminary data in our lab suggest that links between Pvr and immune signaling may be evolutionarily conserved, as Anja Schindler detected suppression of NF- κ B activity through the PDGF receptor superfamily member c-Kit in human cell culture assays[363]. Additionally, a study of the MCF7 human breast cancer cell line suggests that TNF-activation of JNK promotes the expression of VEGF through AP-1 transcription sites found in the VEGFR promoter region[364]. Furthermore, treatment of MCF-7 cells with the JNK inhibitor SP600125 abrogated TNF-induced VEGF expression, indicating a direct role of JNK signals in the production of VEGF[364]. However, PVR pathway antagonism of IMD pathway signals in *Drosophila* has yet to be experimentally modeled in the mammalian VEGFR/PDGFR and TNF pathways.

6.5. Intestinal immunity.

To determine the relevance of the screen findings in an immune relevant *in vivo* system, I shifted my research to the *Drosophila* posterior midgut model. The metazoan gut is under constant bombardment from environmental pressures that damage exposed epithelial cells and corrupt intestinal tissue integrity. The

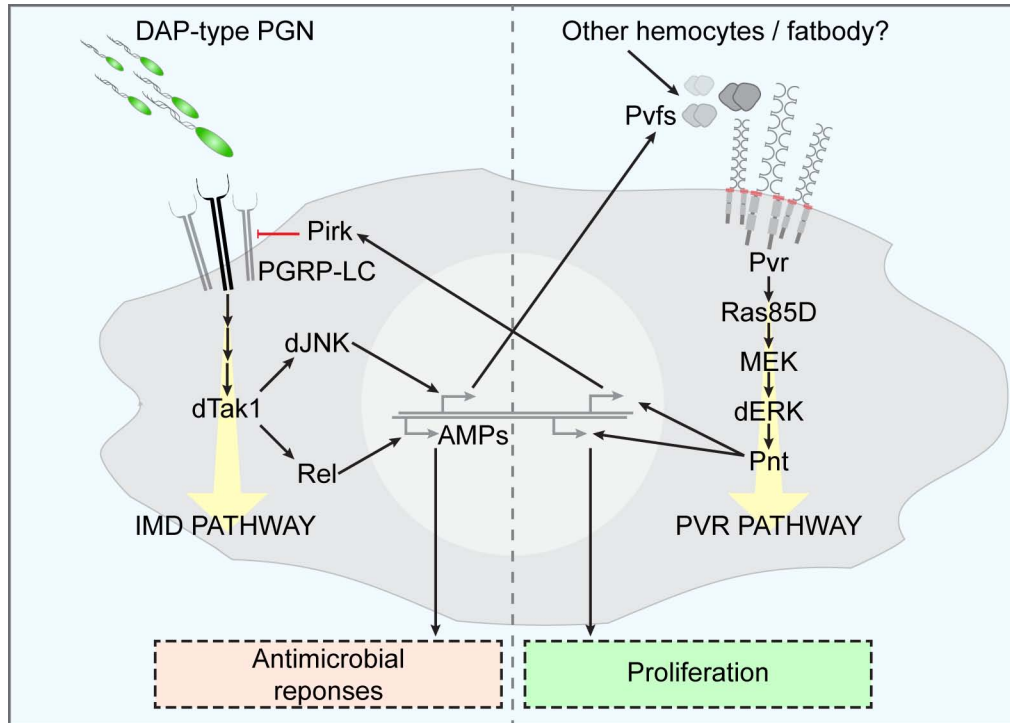


Figure 6.2. Pvr controls of cell-mediated immunity.

Activation of the IMD pathway in hemocytes engages antimicrobial responses, and simultaneously produces Pvf2 and Pvf3 that engage the PVR pathway. PVR pathway activation drives hemocyte activation and proliferation, and establishes a negative feedback loop on the IMD pathway to restrict AMP production. In this manner, PGN recognition by hemocytes drives an initial antimicrobial response through the IMD pathway, followed by a secondary proliferative response mediated by the PVR pathway.

human intestinal tract alone is home to over 10 trillion bacteria[212], which equals approximately 10 fold more bacterial cells than human somatic and germ cells combined. As a result, the intestinal microbiome may contain greater than 100 times more unique genetic sequences than are present in the entire human genome[212]. This highlights the remarkably complex relationship between metazoans and their intestinal environment, and the requirement for sophisticated intercellular communication networks that coordinate homeostatic responses to protect organ function from enteropathogenic challenges.

6.5.1. *Drosophila* intestinal homeostasis.

Studies of the *Drosophila* midgut model revealed that ISC homeostasis is maintained through an elaborate balance of multiple pathways that respond to extrinsic insults and intrinsic requirements for the orderly development of mature epithelial cell types[18, 19, 232, 239, 248, 251]. ISCs proliferate and differentiate rapidly in response to stress-signals. However in the absence of these signals, intrinsic cues guide low level ISC division to ensure a stable population of progenitor cells[232]. Previous studies highlighted the overlapping contributions of Jak/Stat, EGFR, InR, Hippo/Wts, and JNK pathways to meet intestinal tissue requirements[18, 19, 240, 248, 249]. The Jak/Stat pathway is a major regulator of intestinal homeostasis in response to injury or stress with additional contributions to stem cell differentiation under unstressed conditions[18, 365]. The EGFR pathway amalgamates paracrine stress responsive signals with autocrine signals to regulate ISC growth and proliferation[248, 250, 251, 253]. The InR pathway is a general regulator of homeostatic proliferative controls in posterior midgut ISCs and responds to nutritional requirements and epithelial damage[213, 240, 366-

368]. Along with the strong non-cell-autonomous requirement for the Wts/Hippo pathway in the generation of stress-signals, there is also evidence that Wts/Hippo plays a role in the regulation of ISC-autonomous homeostatic signals[246, 247, 249, 252, 369]. Finally, oxidative stress activates the dJNK pathway to guide the production of mitogenic signals that drive the rapid proliferation and differentiation of the underlying ISCs[16, 19, 340, 370].

6.5.2. PVR pathway guidance of intestinal homeostasis.

In this study, I uncovered a novel requirement for the Pvr/Ras signal transduction pathway in the regulation of ISC homeostatic controls in the posterior midgut. I showed that loss of the Pvr receptor in ISCs completely blocks the ISC/EB/EC developmental program. Instead, mutant cells fail to proliferate and retain their identity as DI positive ISCs. As the simultaneous deletion of *pvf2* and *pvf3* exclusively from ISCs in an otherwise heterozygous background phenocopies the *pvr* mutant phenotype, I conclude that Pvf2 and Pvf3 are ISC-autonomous regulators of ISC proliferation. Furthermore, these observations indicate that autocrine Pvf/Pvr signals guide ISC homeostasis. This hypothesis is entirely consistent with the observed ISC expression patterns for Pvr and Pvf2, where both ligand and receptor are restricted to ISCs. My findings also highlight a noteworthy distinction between Pvr and previously described intrinsic regulators, as extrinsic stress cues are epistatic to Pvr in relation to proliferation. This is in contrast to the findings of EGFR mutants that display proliferative defects under unstressed conditions and upon enteropathogenic infection[251, 253]. Thus, my studies suggest that Pvr is an ISC-autonomous homeostatic regulator (Figure 6.3).

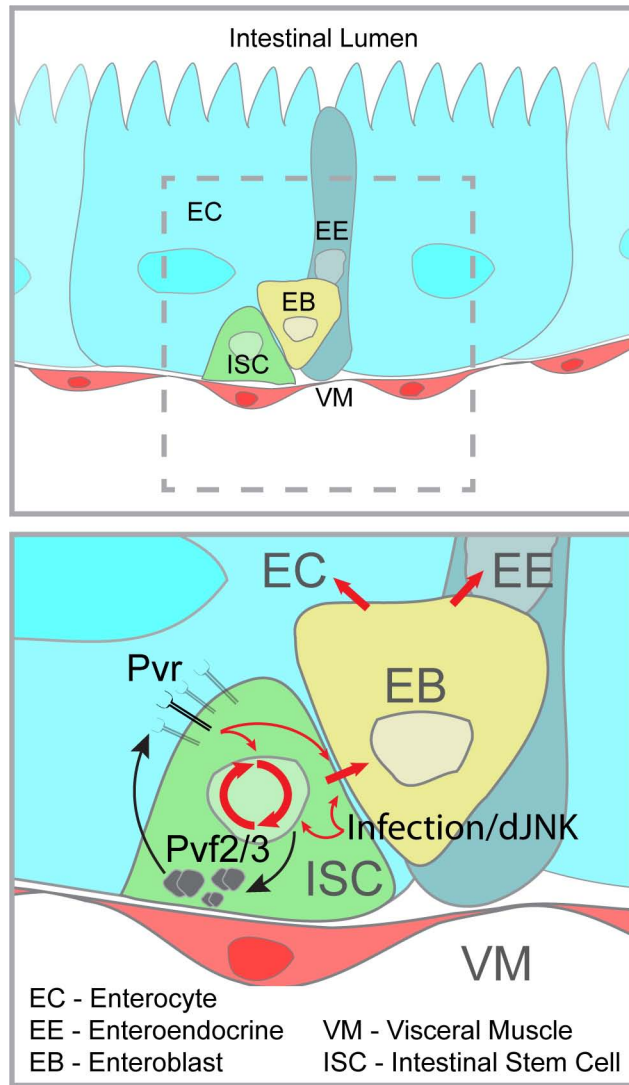


Figure 6.3. Model of Pvf/Pvr regulation of ISC homeostasis.

ISC intrinsic Pvr signals are engaged by autocrine Pvf2/3 expression to maintain homeostatic proliferation and differentiation in the *Drosophila* posterior midgut. Extrinsic stress signals overwhelm Pvr controls of ISC homeostasis and independently promote compensatory proliferation and differentiation in response to enteropathogenic infection. Pvr signals are required for the steady state turnover and fate determination of ISCs under unstressed conditions.

6.5.2.1. Public vs. private autocrine Pvr signals.

My studies of *pvf2-3* mutant MARCM clones in the *Drosophila* posterior midgut suggest that ISC-autonomous production of Pvf2 and Pvf3 engage the PVR pathway. While autocrine production of Pvf2 and Pvf3 is implicated in the regulation of cell size in *Drosophila* tissue culture, there are no other *in vivo* example of autocrine Pvf/Pvr signaling[279]. In this study, I generated *pvf2-3* mutant ISCs in an otherwise heterozygous background, and found that loss of Pvf2 and Pvf3 resulted in the persistence of small DI-positive ISCs defective in differentiation and proliferation. Interestingly, I frequently observed *pvf2-3* mutant ISCs in close proximity to heterozygous *pvf2-3* ISCs, however proximity alone to these Pvf2 and Pvf3 producing cells failed to rescue the mutant phenotype.

These observations bring into question whether the PVR pathway responds to public or private Pvf messages in ISCs. Private autocrine loops are established through intracellular growth factor/receptor interactions that transduce mitogenic signals and thereby bypass factor secretion[371]. If ISCs respond to public signals I would predict that overexpression of Pvfs in peripheral ECs or EBs should restore the *pvf2-3* mutant clone to a wildtype phenotype. Alternatively, if Pvr signals exclusively through private Pvf signals then only Pvf expression in *pvf2-3* mutant ISCs will overcome the mutant phenotype. Autocrine stimulation of RTK signaling pathways is not unique to *Drosophila* Pvr, in fact autocrine production of VEGF has wide reaching implications in mammalian biology from vascular homeostasis, to stem cell survival, to cancer cell biology[371-373]. Notably, private VEGF signals are implicated in hematopoietic stem cell survival in mice[371].

6.5.2.2. Relationship between Pvr and EGFR.

EGFR is a RTK that engages downstream signaling components that overlap with Pvr, including the Ras/dERK signaling axis[270, 301]. In fact, EGFR and Pvr have overlapping and partially redundant signaling functions in border cell migration in *Drosophila* embryos, as ectopically expressed EGFR-ligand (*vein*) rescues border cell migration defects in *pvf* mutant embryos[270]. I find it intriguing that Pvr and EGFR pathways have independent roles in regulating ISC homeostasis given that Pvr and EGFR signals intersect at so many levels. Like *pvr*⁵³⁶³ mutant clones, *egfr* mutant clones in the posterior midgut demonstrate decreased proliferation relative to wildtype clones[245, 251]. However, *egfr* mutant clones contain a variety of intestinal cell types, indicating that EGFR signals are not exclusively required for ISC differentiation[245].

Pe-induced compensatory ISC proliferation requires Jak/Stat-induced EGFR-ligand expression and EGFR pathway activation[251]. In contrast, I found that *Pe*-infection drives significant expansion of *pvr*⁵³⁶³ and *pvf2-3* mutant clones, equivalent to the wildtype controls. Together these data suggest that Pvr and EGFR activities are physiologically distinct. Whereas Pvr/Ras activity is required for the steady-state proliferation/differentiation of ISCs, EGFR/Ras signals control infection induced compensatory proliferation. Infection-induced EGFR/Ras/dERK activity in ISCs might explain why PVR pathway signals are dispensable for extrinsic proliferative cues. However, it is also possible that Pvr and EGFR engage unique arrangements of downstream signaling modules to control ISC proliferation and differentiation. Further investigations are required to fully

establish the effector molecules that guide intestinal homeostasis downstream of Pvr.

6.5.3. Implication of Pvr signals for intestinal aging.

Age-associated decline in stem cell activity is implicated in the development of several disease conditions such as progressive organ failure and cancer. As intrinsic signals are responsible for the maintenance of ISC pools over the lifetime of the animal, the loss or disruption of these pathways significantly affects age-related disease progression[370]. In aged *Drosophila* posterior midguts, ISCs hyperproliferate and the resultant pool of daughter cells fails to differentiate causing dysplasia and gradual degeneration of the intestinal epithelium[19]. In agreement with a connection between aging and deregulated ISC homeostasis, genetic manipulation of factors that suppress ISC proliferation are associated with reduced age-related intestinal dysplasia and prolonged longevity[19, 303, 304, 370]. I showed that Pvf/Pvr hyperactivity in ISCs drives intestinal dysplasia and previous studies found that production of Pvf2 by ISCs engages the PVR pathway to activate p38 and contributes to age-related changes in the *Drosophila* posterior midgut[303, 304]. These observations support my model of Pvr as an intrinsic regulator of ISC homeostasis.

6.6. Pvr/PDGFR controls of intestinal development.

The *Drosophila* Pvr protein shares significant sequence and structural similarity with the human VEGF- and PDGF-families of RTKs[268]. In mammals, the VEGF- and PDGF-receptors function in multiple cellular processes that include growth, proliferation, migration and differentiation[268]. For example,

studies of mice mutant in PDGF-A and PDGFR- α showed a spectrum of development defects in organogenesis[268]. Of particular relevance to my studies is the finding that PDGF-A and PDGFR- α mutant mice display severe defects in gastrointestinal tract architecture predominantly in the upper small intestine[374]. During organogenesis the paracrine expression of PDGF-A by epithelial cells engages PDGFR- α in underlying mesenchymal cells to cause cellular proliferation[374]. A breakdown of epithelial-mesenchymal PDGF-signals results in disrupted intestinal morphogenesis and epithelial differentiation defects[268]. It is currently unclear if the differentiation defects are secondary to the morphogenetic requirements for PDGF or if they reflect direct contributions of PDGFR positive mesenchymal cells to epithelial differentiation[268]. Although I found that autocrine signals guide Pvr activity, I also found that loss of Pvr results in profound defects in the differentiation program of the intestinal epithelium. Therefore, further studies of the morphogenetic requirements for Pvr signals in ISC differentiation within the *Drosophila* posterior midgut model may illuminate specific requirements for PDGF- and VEGF-pathway signals in epithelial cell development in mammals.

6.7. Pvr model of cellular proliferation.

In addition to developmental roles, deregulation of VEGF- and PDGF-receptor signals contributes significantly to the generation and progression of numerous cancer types[268]. One important hallmark of cancer is growth factor independence[375]. In this regard, PDGF has long been recognized as an important autocrine growth factor in the stimulation of neoplastic transformation[268]. PDGF/PDGFR proliferative signals promote tumorigenesis

in preneoplastic or genetically unstable cells that accumulate genetic changes and become malignant[268]. For example, nearly all glioblastomas express a multitude of PDGFs and PDGFRs that establish an autocrine PDGF/PDGFR signal loop[376-378]. More recently, autocrine VEGF/VGFR signals have been directly implicated in cancer progression through the increased renewal of cancer stem cells[372, 379]. Given the similarities between Pvr and the established roles of autocrine feedback loop activation of VEGF- and PDGF-families in cancer progression, I feel that further studies in the genetic regulation of Pvr signals in posterior midgut ISCs provides a fruitful model to study how these pathways promote disease.

6.8. Concluding remarks and future perspectives.

In this research project I performed the first whole genome screen for modifiers of dJNK phosphorylation. These studies uncovered the Pvf/PVR pathway as a novel negative feedback regulator of the *Drosophila* IMD pathway. I then transferred these initial findings to the established *in vivo* immune model provided by the *Drosophila* posterior midgut. Through these studies, I discovered that cell-autonomous Pvf/Pvr signals control ISC homeostasis in the posterior midgut under nonstressed conditions.

In my research I discovered two instances where Pvr activity controls adult *Drosophila* innate immune responses, *in vivo*. First, I showed that dsRNA-mediated depletion of *pvr in vivo*, with two independent non-overlapping Pvr-IR fly lines, results in elevated basal and infection induced AMP levels. Secondly, I found that inhibition of the PVR pathway in ISCs with *esg^{ts}>PvrDN*, increased

survival to oral infection with *Pe*. However, it remains unclear if these two findings are physiologically related. I speculate that improved survival of *esg.^{ts}>PvrDN* flies to *Pe* oral infection is a consequence of higher AMP levels in the gut. These findings are supported by an *in vivo* RNAi screen that serendipitously identified Pvr as a regulator of survival to oral infections with the gram-negative bacteria *Serratia marcescens*[210]. Secondary analysis of screen results showed that tissue specific depletion of *pvr* specifically in the gut or the hemocyte population resulted in enhanced survival to infection[210]. These data support my findings that Pvr is a global regulator of *Drosophila* innate responses, however they fail to address the molecular mechanism of PVR pathway signals.

In addition to central roles in innate immunity, I identified Pvf/Pvr autocrine signals as a critical regulator of *Drosophila* ISC homeostasis. On the molecular level, I have shown that a dominant negative Ras partially rescues Pvr-induced intestinal dysplasia, however additional downstream effectors remain unresolved. For this purpose, the MARCM clones offer an ideal setting to explore the downstream effector molecules in the PVR pathway. Examination of the roles of the MAPKs dERK and p38b would be a natural place to start, as both kinases are known downstream components in the PVR pathway and have established roles in the regulation of intestinal homeostasis[250, 304]. Further epistasis experiments in the *pvr* and *pvf2/3* mutant clones help to clarify the mechanism through which PVR pathway controls of ISC proliferation and differentiation. These finding may also elucidate Pvr regulation of intestinal immune responses.

In conclusion, in this study I uncovered complex molecular interaction networks between conserved signaling pathways that coordinately regulate *Drosophila* innate immune responses. Specifically, I discovered numerous novel regulators of dJNK phosphorylation in the *Drosophila* IMD pathway, including the PVR pathway. I showed that PVR pathway signals control intestinal homeostasis, and *Drosophila* humoral and gut-associated innate immune responses. I feel the findings in this study have illuminated many aspects of Pvr biology with significance that extends well beyond *Drosophila* innate immunity and intestinal homeostasis.

CHAPTER 7

Literature Cited

1. Hoffmann, J.A., Kafatos, F.C., Janeway, C.A., and Ezekowitz, R.A. (1999). Phylogenetic perspectives in innate immunity. *Science* 284, 1313-1318.
2. Janeway, C.A., Jr., and Medzhitov, R. (2002). Innate immune recognition. *Annu Rev Immunol* 20, 197-216.
3. Alder, M.N., Rogozin, I.B., Iyer, L.M., Glazko, G.V., Cooper, M.D., and Pancer, Z. (2005). Diversity and function of adaptive immune receptors in a jawless vertebrate. *Science* 310, 1970-1973.
4. Rajewsky, K. (1996). Clonal selection and learning in the antibody system. *Nature* 381, 751-758.
5. Rocha, B., and von Boehmer, H. (1991). Peripheral selection of the T cell repertoire. *Science* 251, 1225-1228.
6. Akira, S., Uematsu, S., and Takeuchi, O. (2006). Pathogen recognition and innate immunity. *Cell* 124, 783-801.
7. Medzhitov, R., and Janeway, C.A., Jr. (1997). Innate immunity: impact on the adaptive immune response. *Curr Opin Immunol* 9, 4-9.
8. Hoffmann, J.A. (2003). The immune response of *Drosophila*. *Nature* 426, 33-38.
9. Lemaitre, B., Nicolas, E., Michaut, L., Reichhart, J.M., and Hoffmann, J.A. (1996). The dorsoventral regulatory gene cassette *spatzle/Toll/cactus* controls the potent antifungal response in *Drosophila* adults. *Cell* 86, 973-983.
10. Medzhitov, R., Preston-Hurlburt, P., and Janeway, C.A., Jr. (1997). A human homologue of the *Drosophila* Toll protein signals activation of adaptive immunity. *Nature* 388, 394-397.

11. Poltorak, A., He, X., Smirnova, I., Liu, M.Y., Van Huffel, C., Du, X., Birdwell, D., Alejos, E., Silva, M., Galanos, C., Freudenberg, M., Ricciardi-Castagnoli, P., Layton, B., and Beutler, B. (1998). Defective LPS signaling in C3H/HeJ and C57BL/10ScCr mice: mutations in Tlr4 gene. *Science* 282, 2085-2088.
12. Lemaitre, B., and Hoffmann, J. (2007). The host defense of *Drosophila melanogaster*. *Annu Rev Immunol* 25, 697-743.
13. Behr, M., Riedel, D., and Schuh, R. (2003). The claudin-like megatrachea is essential in septate junctions for the epithelial barrier function in *Drosophila*. *Dev Cell* 5, 611-620.
14. Boman, H.G., Nilsson, I., and Rasmuson, B. (1972). Inducible antibacterial defence system in *Drosophila*. *Nature* 237, 232-235.
15. Vodovar, N., Vinals, M., Liehl, P., Basset, A., Degrouard, J., Spellman, P., Boccard, F., and Lemaitre, B. (2005). *Drosophila* host defense after oral infection by an entomopathogenic *Pseudomonas* species. *Proc Natl Acad Sci U S A* 102, 11414-11419.
16. Buchon, N., Broderick, N.A., Chakrabarti, S., and Lemaitre, B. (2009). Invasive and indigenous microbiota impact intestinal stem cell activity through multiple pathways in *Drosophila*. *Genes Dev* 23, 2333-2344.
17. Ohlstein, B., and Spradling, A. (2006). The adult *Drosophila* posterior midgut is maintained by pluripotent stem cells. *Nature* 439, 470-474.
18. Jiang, H., Patel, P.H., Kohlmaier, A., Grenley, M.O., McEwen, D.G., and Edgar, B.A. (2009). Cytokine/Jak/Stat signaling mediates regeneration and homeostasis in the *Drosophila* midgut. *Cell* 137, 1343-1355.

19. Biteau, B., Hochmuth, C.E., and Jasper, H. (2008). JNK activity in somatic stem cells causes loss of tissue homeostasis in the aging *Drosophila* gut. *Cell Stem Cell* 3, 442-455.
20. Tzou, P., Ohresser, S., Ferrandon, D., Capovilla, M., Reichhart, J.M., Lemaitre, B., Hoffmann, J.A., and Imler, J.L. (2000). Tissue-specific inducible expression of antimicrobial peptide genes in *Drosophila* surface epithelia. *Immunity* 13, 737-748.
21. Ferrandon, D., Jung, A.C., Criqui, M., Lemaitre, B., Uttenweiler-Joseph, S., Michaut, L., Reichhart, J., and Hoffmann, J.A. (1998). A drosomycin-GFP reporter transgene reveals a local immune response in *Drosophila* that is not dependent on the Toll pathway. *EMBO J* 17, 1217-1227.
22. Ha, E.M., Oh, C.T., Bae, Y.S., and Lee, W.J. (2005). A direct role for dual oxidase in *Drosophila* gut immunity. *Science* 310, 847-850.
23. Ryu, J.H., Ha, E.M., Oh, C.T., Seol, J.H., Brey, P.T., Jin, I., Lee, D.G., Kim, J., Lee, D., and Lee, W.J. (2006). An essential complementary role of NF-kappaB pathway to microbicidal oxidants in *Drosophila* gut immunity. *EMBO J* 25, 3693-3701.
24. Williams, M.J. (2007). *Drosophila* hemopoiesis and cellular immunity. *J Immunol* 178, 4711-4716.
25. Lebestky, T., Chang, T., Hartenstein, V., and Banerjee, U. (2000). Specification of *Drosophila* hematopoietic lineage by conserved transcription factors. *Science* 288, 146-149.
26. Tepass, U., Fessler, L.I., Aziz, A., and Hartenstein, V. (1994). Embryonic origin of hemocytes and their relationship to cell death in *Drosophila*. *Development* 120, 1829-1837.

27. Franc, N.C., Dimarcq, J.L., Lagueux, M., Hoffmann, J., and Ezekowitz, R.A. (1996). Croquemort, a novel *Drosophila* hemocyte/macrophage receptor that recognizes apoptotic cells. *Immunity* 4, 431-443.
28. Franc, N.C., Heitzler, P., Ezekowitz, R.A., and White, K. (1999). Requirement for croquemort in phagocytosis of apoptotic cells in *Drosophila*. *Science* 284, 1991-1994.
29. Lanot, R., Zachary, D., Holder, F., and Meister, M. (2001). Postembryonic hematopoiesis in *Drosophila*. *Dev Biol* 230, 243-257.
30. Crozatier, M., and Meister, M. (2007). *Drosophila* haematopoiesis. *Cell Microbiol* 9, 1117-1126.
31. Meister, M., and Lagueux, M. (2003). *Drosophila* blood cells. *Cell Microbiol* 5, 573-580.
32. Meister, M. (2004). Blood cells of *Drosophila*: cell lineages and role in host defence. *Curr Opin Immunol* 16, 10-15.
33. Rizki, T.M., and Rizki, R.M. (1992). Lamellocyte differentiation in *Drosophila* larvae parasitized by *Leptopilina*. *Dev Comp Immunol* 16, 103-110.
34. Holz, A., Bossinger, B., Strasser, T., Janning, W., and Klapper, R. (2003). The two origins of hemocytes in *Drosophila*. *Development* 130, 4955-4962.
35. Elrod-Erickson, M., Mishra, S., and Schneider, D. (2000). Interactions between the cellular and humoral immune responses in *Drosophila*. *Current biology* : CB 10, 781-784.
36. Dougherty, W.G., Lindbo, J.A., Smith, H.A., Parks, T.D., Swaney, S., and Proebsting, W.M. (1994). RNA-mediated virus resistance in transgenic

- plants: exploitation of a cellular pathway possibly involved in RNA degradation. *Mol Plant Microbe Interact* 7, 544-552.
37. Hannon, G.J. (2002). RNA interference. *Nature* 418, 244-251.
 38. Galiana-Arnoux, D., Dostert, C., Schneemann, A., Hoffmann, J.A., and Imler, J.L. (2006). Essential function in vivo for Dicer-2 in host defense against RNA viruses in drosophila. *Nat Immunol* 7, 590-597.
 39. van Rij, R.P., Saleh, M.C., Berry, B., Foo, C., Houk, A., Antoniewski, C., and Andino, R. (2006). The RNA silencing endonuclease Argonaute 2 mediates specific antiviral immunity in *Drosophila melanogaster*. *Genes Dev* 20, 2985-2995.
 40. Fire, A., Xu, S., Montgomery, M.K., Kostas, S.A., Driver, S.E., and Mello, C.C. (1998). Potent and specific genetic interference by double-stranded RNA in *Caenorhabditis elegans*. *Nature* 391, 806-811.
 41. Lemaitre, B., Kromer-Metzger, E., Michaut, L., Nicolas, E., Meister, M., Georgel, P., Reichhart, J.M., and Hoffmann, J.A. (1995). A recessive mutation, immune deficiency (*imd*), defines two distinct control pathways in the *Drosophila* host defense. *Proc Natl Acad Sci U S A* 92, 9465-9469.
 42. De Gregorio, E., Spellman, P.T., Tzou, P., Rubin, G.M., and Lemaitre, B. (2002). The Toll and Imd pathways are the major regulators of the immune response in *Drosophila*. *EMBO J* 21, 2568-2579.
 43. Adams, M.D., Celniker, S.E., Holt, R.A., Evans, C.A., Gocayne, J.D., Amanatides, P.G., Scherer, S.E., Li, P.W., Hoskins, R.A., Galle, R.F., George, R.A., Lewis, S.E., Richards, S., Ashburner, M., Henderson, S.N., Sutton, G.G., Wortman, J.R., Yandell, M.D., Zhang, Q., Chen, L.X., Brandon, R.C., Rogers, Y.H., Blazej, R.G., Champe, M., Pfeiffer, B.D., Wan,

K.H., Doyle, C., Baxter, E.G., Helt, G., Nelson, C.R., Gabor, G.L., Abril, J.F., Agbayani, A., An, H.J., Andrews-Pfannkoch, C., Baldwin, D., Ballew, R.M., Basu, A., Baxendale, J., Bayraktaroglu, L., Beasley, E.M., Beeson, K.Y., Benos, P.V., Berman, B.P., Bhandari, D., Bolshakov, S., Borkova, D., Botchan, M.R., Bouck, J., Brokstein, P., Brottier, P., Burtis, K.C., Busam, D.A., Butler, H., Cadieu, E., Center, A., Chandra, I., Cherry, J.M., Cawley, S., Dahlke, C., Davenport, L.B., Davies, P., de Pablos, B., Delcher, A., Deng, Z., Mays, A.D., Dew, I., Dietz, S.M., Dodson, K., Doup, L.E., Downes, M., Dugan-Rocha, S., Dunkov, B.C., Dunn, P., Durbin, K.J., Evangelista, C.C., Ferraz, C., Ferriera, S., Fleischmann, W., Fosler, C., Gabrielian, A.E., Garg, N.S., Gelbart, W.M., Glasser, K., Glodek, A., Gong, F., Gorrell, J.H., Gu, Z., Guan, P., Harris, M., Harris, N.L., Harvey, D., Heiman, T.J., Hernandez, J.R., Houck, J., Hostin, D., Houston, K.A., Howland, T.J., Wei, M.H., Ibegwam, C., Jalali, M., Kalush, F., Karpen, G.H., Ke, Z., Kennison, J.A., Ketchum, K.A., Kimmel, B.E., Kodira, C.D., Kraft, C., Kravitz, S., Kulp, D., Lai, Z., Lasko, P., Lei, Y., Levitsky, A.A., Li, J., Li, Z., Liang, Y., Lin, X., Liu, X., Mattei, B., McIntosh, T.C., McLeod, M.P., McPherson, D., Merkulov, G., Milshina, N.V., Mobarry, C., Morris, J., Moshrefi, A., Mount, S.M., Moy, M., Murphy, B., Murphy, L., Muzny, D.M., Nelson, D.L., Nelson, D.R., Nelson, K.A., Nixon, K., Nusskern, D.R., Pacleb, J.M., Palazzolo, M., Pittman, G.S., Pan, S., Pollard, J., Puri, V., Reese, M.G., Reinert, K., Remington, K., Saunders, R.D., Scheeler, F., Shen, H., Shue, B.C., Sidenkiamos, I., Simpson, M., Skupski, M.P., Smith, T., Spier, E., Spradling, A.C., Stapleton, M., Strong, R., Sun, E., Svirskas, R., Tector, C., Turner, R., Venter, E., Wang, A.H., Wang, X., Wang, Z.Y., Wassarman, D.A.,

- Weinstock, G.M., Weissenbach, J., Williams, S.M., Woodage T, Worley, K.C., Wu, D., Yang, S., Yao, Q.A., Ye, J., Yeh, R.F., Zaveri, J.S., Zhan, M., Zhang, G., Zhao, Q., Zheng, L., Zheng, X.H., Zhong, F.N., Zhong, W., Zhou, X., Zhu, S., Zhu, X., Smith, H.O., Gibbs, R.A., Myers, E.W., Rubin, G.M., and Venter, J.C. (2000). The genome sequence of *Drosophila melanogaster*. *Science* 287, 2185-2195.
44. Lehrer, R.I., and Ganz, T. (1999). Antimicrobial peptides in mammalian and insect host defence. *Curr Opin Immunol* 11, 23-27.
 45. Yang, L., Weiss, T.M., Lehrer, R.I., and Huang, H.W. (2000). Crystallization of antimicrobial pores in membranes: magainin and protegrin. *Biophys J* 79, 2002-2009.
 46. Zasloff, M. (2002). Antimicrobial peptides of multicellular organisms. *Nature* 415, 389-395.
 47. Ramet, M. (2012). The fruit fly *Drosophila melanogaster* unfolds the secrets of innate immunity. *Acta Paediatr* 101, 900-905.
 48. Reiter, L.T., Potocki, L., Chien, S., Gribskov, M., and Bier, E. (2001). A systematic analysis of human disease-associated gene sequences in *Drosophila melanogaster*. *Genome Res* 11, 1114-1125.
 49. Fortini, M.E., Skupski, M.P., Boguski, M.S., and Hariharan, I.K. (2000). A survey of human disease gene counterparts in the *Drosophila* genome. *J Cell Biol* 150, F23-30.
 50. Anderson, K.V., Jurgens, G., and Nusslein-Volhard, C. (1985). Establishment of dorsal-ventral polarity in the *Drosophila* embryo: genetic studies on the role of the Toll gene product. *Cell* 42, 779-789.

51. Hashimoto, C., Hudson, K.L., and Anderson, K.V. (1988). The Toll gene of *Drosophila*, required for dorsal-ventral embryonic polarity, appears to encode a transmembrane protein. *Cell* *52*, 269-279.
52. Gay, N.J., and Keith, F.J. (1991). *Drosophila* Toll and IL-1 receptor. *Nature* *351*, 355-356.
53. Valanne, S., Wang, J.H., and Ramet, M. (2011). The *Drosophila* Toll signaling pathway. *J Immunol* *186*, 649-656.
54. Rosetto, M., Engstrom, Y., Baldari, C.T., Telford, J.L., and Hultmark, D. (1995). Signals from the IL-1 receptor homolog, Toll, can activate an immune response in a *Drosophila* hemocyte cell line. *Biochem Biophys Res Commun* *209*, 111-116.
55. Hu, X., Yagi, Y., Tanji, T., Zhou, S., and Ip, Y.T. (2004). Multimerization and interaction of Toll and Spatzle in *Drosophila*. *Proc Natl Acad Sci U S A* *101*, 9369-9374.
56. Elbashir, S.M., Harborth, J., Lendeckel, W., Yalcin, A., Weber, K., and Tuschl, T. (2001). Duplexes of 21-nucleotide RNAs mediate RNA interference in cultured mammalian cells. *Nature* *411*, 494-498.
57. LeMosy, E.K., Tan, Y.Q., and Hashimoto, C. (2001). Activation of a protease cascade involved in patterning the *Drosophila* embryo. *Proc Natl Acad Sci U S A* *98*, 5055-5060.
58. Dissing, M., Giordano, H., and DeLotto, R. (2001). Autoproteolysis and feedback in a protease cascade directing *Drosophila* dorsal-ventral cell fate. *EMBO J* *20*, 2387-2393.

59. Tauszig-Delamasure, S., Bilak, H., Capovilla, M., Hoffmann, J.A., and Imler, J.L. (2002). *Drosophila* MyD88 is required for the response to fungal and Gram-positive bacterial infections. *Nat Immunol* 3, 91-97.
60. Horng, T., and Medzhitov, R. (2001). *Drosophila* MyD88 is an adapter in the Toll signaling pathway. *Proc Natl Acad Sci U S A* 98, 12654-12658.
61. Sun, H., Bristow, B.N., Qu, G., and Wasserman, S.A. (2002). A heterotrimeric death domain complex in Toll signaling. *Proc Natl Acad Sci U S A* 99, 12871-12876.
62. Xiao, T., Towb, P., Wasserman, S.A., and Sprang, S.R. (1999). Three-dimensional structure of a complex between the death domains of Pelle and Tube. *Cell* 99, 545-555.
63. Manfrulli, P., Reichhart, J.M., Steward, R., Hoffmann, J.A., and Lemaitre, B. (1999). A mosaic analysis in *Drosophila* fat body cells of the control of antimicrobial peptide genes by the Rel proteins Dorsal and DIF. *EMBO J* 18, 3380-3391.
64. Meng, X., Khanuja, B.S., and Ip, Y.T. (1999). Toll receptor-mediated *Drosophila* immune response requires Dif, an NF-kappaB factor. *Genes Dev* 13, 792-797.
65. Nicolas, E., Reichhart, J.M., Hoffmann, J.A., and Lemaitre, B. (1998). In vivo regulation of the IkappaB homologue cactus during the immune response of *Drosophila*. *J Biol Chem* 273, 10463-10469.
66. Weber, A.N., Tauszig-Delamasure, S., Hoffmann, J.A., Lelievre, E., Gascan, H., Ray, K.P., Morse, M.A., Imler, J.L., and Gay, N.J. (2003). Binding of the *Drosophila* cytokine Spatzle to Toll is direct and establishes signaling. *Nat Immunol* 4, 794-800.

67. Rutschmann, S., Jung, A.C., Zhou, R., Silverman, N., Hoffmann, J.A., and Ferrandon, D. (2000). Role of *Drosophila* IKK gamma in a toll-independent antibacterial immune response. *Nat Immunol* 1, 342-347.
68. Tauszig, S., Jouanguy, E., Hoffmann, J.A., and Imler, J.L. (2000). Toll-related receptors and the control of antimicrobial peptide expression in *Drosophila*. *Proc Natl Acad Sci U S A* 97, 10520-10525.
69. Lemaitre, B., Meister, M., Govind, S., Georgel, P., Steward, R., Reichhart, J.M., and Hoffmann, J.A. (1995). Functional analysis and regulation of nuclear import of dorsal during the immune response in *Drosophila*. *EMBO J* 14, 536-545.
70. Akira, S., Takeda, K., and Kaisho, T. (2001). Toll-like receptors: critical proteins linking innate and acquired immunity. *Nat Immunol* 2, 675-680.
71. Armant, M.A., and Fenton, M.J. (2002). Toll-like receptors: a family of pattern-recognition receptors in mammals. *Genome Biol* 3, REVIEWS3011.
72. Lee, C.C., Avalos, A.M., and Ploegh, H.L. (2012). Accessory molecules for Toll-like receptors and their function. *Nat Rev Immunol* 12, 168-179.
73. Kawai, T., and Akira, S. (2010). The role of pattern-recognition receptors in innate immunity: update on Toll-like receptors. *Nat Immunol* 11, 373-384.
74. Towb, P., Sun, H., and Wasserman, S.A. (2009). Tube Is an IRAK-4 homolog in a Toll pathway adapted for development and immunity. *J Innate Immun* 1, 309-321.
75. Lin, S.C., Lo, Y.C., and Wu, H. (2010). Helical assembly in the MyD88-IRAK4-IRAK2 complex in TLR/IL-1R signalling. *Nature* 465, 885-890.
76. Cao, Z., Henzel, W.J., and Gao, X. (1996). IRAK: a kinase associated with the interleukin-1 receptor. *Science* 271, 1128-1131.

77. Muzio, M., Ni, J., Feng, P., and Dixit, V.M. (1997). IRAK (Pelle) family member IRAK-2 and MyD88 as proximal mediators of IL-1 signaling. *Science* 278, 1612-1615.
78. Muzio, M., Natoli, G., Saccani, S., Levrero, M., and Mantovani, A. (1998). The human toll signaling pathway: divergence of nuclear factor kappaB and JNK/SAPK activation upstream of tumor necrosis factor receptor-associated factor 6 (TRAF6). *J Exp Med* 187, 2097-2101.
79. Honda, K., Yanai, H., Negishi, H., Asagiri, M., Sato, M., Mizutani, T., Shimada, N., Ohba, Y., Takaoka, A., Yoshida, N., and Taniguchi, T. (2005). IRF-7 is the master regulator of type-I interferon-dependent immune responses. *Nature* 434, 772-777.
80. Honda, K., Yanai, H., Mizutani, T., Negishi, H., Shimada, N., Suzuki, N., Ohba, Y., Takaoka, A., Yeh, W.C., and Taniguchi, T. (2004). Role of a transductional-transcriptional processor complex involving MyD88 and IRF-7 in Toll-like receptor signaling. *Proc Natl Acad Sci U S A* 101, 15416-15421.
81. Iwasaki, A., and Medzhitov, R. (2004). Toll-like receptor control of the adaptive immune responses. *Nat Immunol* 5, 987-995.
82. Visintin, A., Mazzoni, A., Spitzer, J.H., Wyllie, D.H., Dower, S.K., and Segal, D.M. (2001). Regulation of Toll-like receptors in human monocytes and dendritic cells. *J Immunol* 166, 249-255.
83. Hoshino, K., Takeuchi, O., Kawai, T., Sanjo, H., Ogawa, T., Takeda, Y., Takeda, K., and Akira, S. (1999). Cutting edge: Toll-like receptor 4 (TLR4)-deficient mice are hyporesponsive to lipopolysaccharide: evidence for TLR4 as the Lps gene product. *J Immunol* 162, 3749-3752.

84. Banchereau, J., and Steinman, R.M. (1998). Dendritic cells and the control of immunity. *Nature* 392, 245-252.
85. Leulier, F., Vidal, S., Saigo, K., Ueda, R., and Lemaitre, B. (2002). Inducible expression of double-stranded RNA reveals a role for dFADD in the regulation of the antibacterial response in *Drosophila* adults. *Curr Biol* 12, 996-1000.
86. Gottar, M., Gobert, V., Michel, T., Belvin, M., Duyk, G., Hoffmann, J.A., Ferrandon, D., and Royet, J. (2002). The *Drosophila* immune response against Gram-negative bacteria is mediated by a peptidoglycan recognition protein. *Nature* 416, 640-644.
87. Aggarwal, B.B., Kohr, W.J., Hass, P.E., Moffat, B., Spencer, S.A., Henzel, W.J., Bringman, T.S., Nedwin, G.E., Goeddel, D.V., and Harkins, R.N. (1985). Human tumor necrosis factor. Production, purification, and characterization. *J Biol Chem* 260, 2345-2354.
88. Pasparakis, M., Alexopoulou, L., Episkopou, V., and Kollias, G. (1996). Immune and inflammatory responses in TNF alpha-deficient mice: a critical requirement for TNF alpha in the formation of primary B cell follicles, follicular dendritic cell networks and germinal centers, and in the maturation of the humoral immune response. *J Exp Med* 184, 1397-1411.
89. Aggarwal, B.B. (2003). Signalling pathways of the TNF superfamily: a double-edged sword. *Nat Rev Immunol* 3, 745-756.
90. Carswell, E.A., Old, L.J., Kassel, R.L., Green, S., Fiore, N., and Williamson, B. (1975). An endotoxin-induced serum factor that causes necrosis of tumors. *Proc Natl Acad Sci U S A* 72, 3666-3670.

91. Pennica, D., Nedwin, G.E., Hayflick, J.S., Seeburg, P.H., Derynck, R., Palladino, M.A., Kohr, W.J., Aggarwal, B.B., and Goeddel, D.V. (1984). Human tumour necrosis factor: precursor structure, expression and homology to lymphotoxin. *Nature* 312, 724-729.
92. Eck, M.J., and Sprang, S.R. (1989). The structure of tumor necrosis factor- α at 2.6 Å resolution. Implications for receptor binding. *J Biol Chem* 264, 17595-17605.
93. Peschon, J.J., Slack, J.L., Reddy, P., Stocking, K.L., Sunnarborg, S.W., Lee, D.C., Russell, W.E., Castner, B.J., Johnson, R.S., Fitzner, J.N., Boyce, R.W., Nelson, N., Kozlosky, C.J., Wolfson, M.F., Rauch, C.T., Cerretti, D.P., Paxton, R.J., March, C.J., and Black, R.A. (1998). An essential role for ectodomain shedding in mammalian development. *Science* 282, 1281-1284.
94. Tartaglia, L.A., Ayres, T.M., Wong, G.H., and Goeddel, D.V. (1993). A novel domain within the 55 kd TNF receptor signals cell death. *Cell* 74, 845-853.
95. Jiang, Y., Woronicz, J.D., Liu, W., and Goeddel, D.V. (1999). Prevention of constitutive TNF receptor 1 signaling by silencer of death domains. *Science* 283, 543-546.
96. Chan, F.K., Chun, H.J., Zheng, L., Siegel, R.M., Bui, K.L., and Lenardo, M.J. (2000). A domain in TNF receptors that mediates ligand-independent receptor assembly and signaling. *Science* 288, 2351-2354.
97. Micheau, O., and Tschopp, J. (2003). Induction of TNF receptor I-mediated apoptosis via two sequential signaling complexes. *Cell* 114, 181-190.

98. Hsu, H., Shu, H.B., Pan, M.G., and Goeddel, D.V. (1996). TRADD-TRAF2 and TRADD-FADD interactions define two distinct TNF receptor 1 signal transduction pathways. *Cell* 84, 299-308.
99. Hsu, H., Huang, J., Shu, H.B., Baichwal, V., and Goeddel, D.V. (1996). TNF-dependent recruitment of the protein kinase RIP to the TNF receptor-1 signaling complex. *Immunity* 4, 387-396.
100. Rothe, M., Pan, M.G., Henzel, W.J., Ayres, T.M., and Goeddel, D.V. (1995). The TNFR2-TRAF signaling complex contains two novel proteins related to baculoviral inhibitor of apoptosis proteins. *Cell* 83, 1243-1252.
101. Varfolomeev, E., Goncharov, T., Fedorova, A.V., Dynek, J.N., Zobel, K., Deshayes, K., Fairbrother, W.J., and Vucic, D. (2008). c-IAP1 and c-IAP2 are critical mediators of tumor necrosis factor alpha (TNFalpha)-induced NF-kappaB activation. *J Biol Chem* 283, 24295-24299.
102. Lee, T.H., Shank, J., Cusson, N., and Kelliher, M.A. (2004). The kinase activity of Rip1 is not required for tumor necrosis factor-alpha-induced IkkappaB kinase or p38 MAP kinase activation or for the ubiquitination of Rip1 by Traf2. *J Biol Chem* 279, 33185-33191.
103. Kanayama, A., Seth, R.B., Sun, L., Ea, C.K., Hong, M., Shaito, A., Chiu, Y.H., Deng, L., and Chen, Z.J. (2004). TAB2 and TAB3 activate the NF-kappaB pathway through binding to polyubiquitin chains. *Mol Cell* 15, 535-548.
104. Ninomiya-Tsuji, J., Kishimoto, K., Hiyama, A., Inoue, J., Cao, Z., and Matsumoto, K. (1999). The kinase TAK1 can activate the NIK-I kappaB as well as the MAP kinase cascade in the IL-1 signalling pathway. *Nature* 398, 252-256.

105. DiDonato, J.A., Hayakawa, M., Rothwarf, D.M., Zandi, E., and Karin, M. (1997). A cytokine-responsive I κ B kinase that activates the transcription factor NF- κ B. *Nature* 388, 548-554.
106. Beg, A.A., Ruben, S.M., Scheinman, R.I., Haskill, S., Rosen, C.A., and Baldwin, A.S., Jr. (1992). I κ B interacts with the nuclear localization sequences of the subunits of NF- κ B: a mechanism for cytoplasmic retention. *Genes Dev* 6, 1899-1913.
107. Moriguchi, T., Toyoshima, F., Masuyama, N., Hanafusa, H., Gotoh, Y., and Nishida, E. (1997). A novel SAPK/JNK kinase, MKK7, stimulated by TNF α and cellular stresses. *EMBO J* 16, 7045-7053.
108. Westwick, J.K., Weitzel, C., Minden, A., Karin, M., and Brenner, D.A. (1994). Tumor necrosis factor α stimulates AP-1 activity through prolonged activation of the c-Jun kinase. *J Biol Chem* 269, 26396-26401.
109. Brenner, D.A., O'Hara, M., Angel, P., Chojkier, M., and Karin, M. (1989). Prolonged activation of jun and collagenase genes by tumour necrosis factor- α . *Nature* 337, 661-663.
110. Kischkel, F.C., Hellbardt, S., Behrmann, I., Germer, M., Pawlita, M., Krammer, P.H., and Peter, M.E. (1995). Cytotoxicity-dependent APO-1 (Fas/CD95)-associated proteins form a death-inducing signaling complex (DISC) with the receptor. *EMBO J* 14, 5579-5588.
111. Hsu, H., Xiong, J., and Goeddel, D.V. (1995). The TNF receptor 1-associated protein TRADD signals cell death and NF- κ B activation. *Cell* 81, 495-504.
112. Karin, M., and Lin, A. (2002). NF- κ B at the crossroads of life and death. *Nat Immunol* 3, 221-227.

113. Wang, C.Y., Mayo, M.W., Korneluk, R.G., Goeddel, D.V., and Baldwin, A.S., Jr. (1998). NF-kappaB antiapoptosis: induction of TRAF1 and TRAF2 and c-IAP1 and c-IAP2 to suppress caspase-8 activation. *Science* 281, 1680-1683.
114. Vallabhapurapu, S., and Karin, M. (2009). Regulation and function of NF-kappaB transcription factors in the immune system. *Annu Rev Immunol* 27, 693-733.
115. Digel, W., Stefanic, M., Schoniger, W., Buck, C., Raghavachar, A., Frickhofen, N., Heimpel, H., and Porzsolt, F. (1989). Tumor necrosis factor induces proliferation of neoplastic B cells from chronic lymphocytic leukemia. *Blood* 73, 1242-1246.
116. Elbaz, O., and Mahmoud, L.A. (1994). Tumor necrosis factor and human acute leukemia. *Leuk Lymphoma* 12, 191-195.
117. Kassiotis, G., and Kollias, G. (2001). Uncoupling the proinflammatory from the immunosuppressive properties of tumor necrosis factor (TNF) at the p55 TNF receptor level: implications for pathogenesis and therapy of autoimmune demyelination. *J Exp Med* 193, 427-434.
118. Hotamisligil, G.S., Budavari, A., Murray, D., and Spiegelman, B.M. (1994). Reduced tyrosine kinase activity of the insulin receptor in obesity-diabetes. Central role of tumor necrosis factor-alpha. *J Clin Invest* 94, 1543-1549.
119. Uysal, K.T., Wiesbrock, S.M., and Hotamisligil, G.S. (1998). Functional analysis of tumor necrosis factor (TNF) receptors in TNF-alpha-mediated insulin resistance in genetic obesity. *Endocrinology* 139, 4832-4838.
120. Tracey, K.J., Fong, Y., Hesse, D.G., Manogue, K.R., Lee, A.T., Kuo, G.C., Lowry, S.F., and Cerami, A. (1987). Anti-cachectin/TNF monoclonal

- antibodies prevent septic shock during lethal bacteraemia. *Nature* 330, 662-664.
121. Georgel, P., Naitza, S., Kappler, C., Ferrandon, D., Zachary, D., Swimmer, C., Kopczynski, C., Duyk, G., Reichhart, J.M., and Hoffmann, J.A. (2001). *Drosophila* immune deficiency (IMD) is a death domain protein that activates antibacterial defense and can promote apoptosis. *Dev Cell* 1, 503-514.
122. Dziarski, R. (2004). Peptidoglycan recognition proteins (PGRPs). *Mol Immunol* 40, 877-886.
123. Choe, K.M., Werner, T., Stoven, S., Hultmark, D., and Anderson, K.V. (2002). Requirement for a peptidoglycan recognition protein (PGRP) in Relish activation and antibacterial immune responses in *Drosophila*. *Science* 296, 359-362.
124. Kaneko, T., Goldman, W.E., Mellroth, P., Steiner, H., Fukase, K., Kusumoto, S., Harley, W., Fox, A., Golenbock, D., and Silverman, N. (2004). Monomeric and polymeric gram-negative peptidoglycan but not purified LPS stimulate the *Drosophila* IMD pathway. *Immunity* 20, 637-649.
125. Leulier, F., Parquet, C., Pili-Floury, S., Ryu, J.H., Caroff, M., Lee, W.J., Mengin-Lecreulx, D., and Lemaitre, B. (2003). The *Drosophila* immune system detects bacteria through specific peptidoglycan recognition. *Nat Immunol* 4, 478-484.
126. Ramet, M., Manfrulli, P., Pearson, A., Mathey-Prevot, B., and Ezekowitz, R.A. (2002). Functional genomic analysis of phagocytosis and identification of a *Drosophila* receptor for *E. coli*. *Nature* 416, 644-648.

127. Takehana, A., Yano, T., Mita, S., Kotani, A., Oshima, Y., and Kurata, S. (2004). Peptidoglycan recognition protein (PGRP)-LE and PGRP-LC act synergistically in *Drosophila* immunity. *EMBO J* 23, 4690-4700.
128. Neyen, C., Poidevin, M., Roussel, A., and Lemaitre, B. (2012). Tissue- and Ligand-Specific Sensing of Gram-Negative Infection in *Drosophila* by PGRP-LC Isoforms and PGRP-LE. *J Immunol* 189, 1886-1897.
129. Choe, K.M., Lee, H., and Anderson, K.V. (2005). *Drosophila* peptidoglycan recognition protein LC (PGRP-LC) acts as a signal-transducing innate immune receptor. *Proc Natl Acad Sci U S A* 102, 1122-1126.
130. Hu, S., and Yang, X. (2000). dFADD, a novel death domain-containing adapter protein for the *Drosophila* caspase DREDD. *J Biol Chem* 275, 30761-30764.
131. Naitza, S., Rosse, C., Kappler, C., Georgel, P., Belvin, M., Gubb, D., Camonis, J., Hoffmann, J.A., and Reichhart, J.M. (2002). The *Drosophila* immune defense against gram-negative infection requires the death protein dFADD. *Immunity* 17, 575-581.
132. Guntermann, S., and Foley, E. (2011). The protein Dredd is an essential component of the c-Jun N-terminal kinase pathway in the *Drosophila* immune response. *J Biol Chem* 286, 30284-30294.
133. Meinander, A., Runchel, C., Tenev, T., Chen, L., Kim, C.H., Ribeiro, P.S., Broemer, M., Leulier, F., Zvelebil, M., Silverman, N., and Meier, P. (2012). Ubiquitylation of the initiator caspase DREDD is required for innate immune signalling. *EMBO J* 31, 2770-2783.
134. Paquette, N., Broemer, M., Aggarwal, K., Chen, L., Husson, M., Erturk-Hasdemir, D., Reichhart, J.M., Meier, P., and Silverman, N. (2010).

- Caspase-mediated cleavage, IAP binding, and ubiquitination: linking three mechanisms crucial for *Drosophila* NF-kappaB signaling. *Mol Cell* 37, 172-182.
135. Leulier, F., Rodriguez, A., Khush, R.S., Abrams, J.M., and Lemaitre, B. (2000). The *Drosophila* caspase Dredd is required to resist gram-negative bacterial infection. *EMBO Rep* 1, 353-358.
 136. Stoven, S., Silverman, N., Junell, A., Hedengren-Olcott, M., Erturk, D., Engstrom, Y., Maniatis, T., and Hultmark, D. (2003). Caspase-mediated processing of the *Drosophila* NF-kappaB factor Relish. *Proc Natl Acad Sci U S A* 100, 5991-5996.
 137. Foley, E., and O'Farrell, P.H. (2004). Functional Dissection of an Innate Immune Response by a Genome-Wide RNAi Screen. *PLoS Biol* 2, E203.
 138. Dushay, M.S., Asling, B., and Hultmark, D. (1996). Origins of immunity: Relish, a compound Rel-like gene in the antibacterial defense of *Drosophila*. *Proc Natl Acad Sci U S A* 93, 10343-10347.
 139. Hedengren, M., Asling, B., Dushay, M.S., Ando, I., Ekengren, S., Wihlborg, M., and Hultmark, D. (1999). Relish, a central factor in the control of humoral but not cellular immunity in *Drosophila*. *Mol Cell* 4, 827-837.
 140. Erturk-Hasdemir, D., Broemer, M., Leulier, F., Lane, W.S., Paquette, N., Hwang, D., Kim, C.H., Stoven, S., Meier, P., and Silverman, N. (2009). Two roles for the *Drosophila* IKK complex in the activation of Relish and the induction of antimicrobial peptide genes. *Proc Natl Acad Sci U S A*.
 141. Silverman, N., Zhou, R., Stoven, S., Pandey, N., Hultmark, D., and Maniatis, T. (2000). A *Drosophila* IkappaB kinase complex required for Relish cleavage and antibacterial immunity. *Genes Dev* 14, 2461-2471.

142. Stoven, S., Ando, I., Kadalayil, L., Engstrom, Y., and Hultmark, D. (2000). Activation of the *Drosophila* NF-kappaB factor Relish by rapid endoproteolytic cleavage. *EMBO Rep* 1, 347-352.
143. Lu, Y., Wu, L.P., and Anderson, K.V. (2001). The antibacterial arm of the *Drosophila* innate immune response requires an IkappaB kinase. *Genes Dev* 15, 104-110.
144. Wu, L.P., and Anderson, K.V. (1998). Regulated nuclear import of Rel proteins in the *Drosophila* immune response. *Nature* 392, 93-97.
145. Riesgo-Escovar, J.R., Jenni, M., Fritz, A., and Hafen, E. (1996). The *Drosophila* Jun-N-terminal kinase is required for cell morphogenesis but not for DJun-dependent cell fate specification in the eye. *Genes Dev* 10, 2759-2768.
146. Sluss, H.K., Han, Z., Barrett, T., Goberdhan, D.C., Wilson, C., Davis, R.J., and Ip, Y.T. (1996). A JNK signal transduction pathway that mediates morphogenesis and an immune response in *Drosophila*. *Genes Dev* 10, 2745-2758.
147. Stronach, B.E., and Perrimon, N. (1999). Stress signaling in *Drosophila*. *Oncogene* 18, 6172-6182.
148. Kim, E.K., and Choi, E.J. (2010). Pathological roles of MAPK signaling pathways in human diseases. *Biochim Biophys Acta* 1802, 396-405.
149. Hibi, M., Lin, A., Smeal, T., Minden, A., and Karin, M. (1993). Identification of an oncoprotein- and UV-responsive protein kinase that binds and potentiates the c-Jun activation domain. *Genes Dev* 7, 2135-2148.
150. Davis, R.J. (2000). Signal transduction by the JNK group of MAP kinases. *Cell* 103, 239-252.

151. Gupta, S., Barrett, T., Whitmarsh, A.J., Cavanagh, J., Sluss, H.K., Derijard, B., and Davis, R.J. (1996). Selective interaction of JNK protein kinase isoforms with transcription factors. *EMBO J* 15, 2760-2770.
152. Wagner, E.F., and Nebreda, A.R. (2009). Signal integration by JNK and p38 MAPK pathways in cancer development. *Nat Rev Cancer* 9, 537-549.
153. Weston, C.R., and Davis, R.J. (2007). The JNK signal transduction pathway. *Curr Opin Cell Biol* 19, 142-149.
154. Jürgens, G., Wieschaus, E., Nüsslein-Volhard, C., and Kluding, H. (1984). Mutations affecting the pattern of the larval cuticle in *Drosophila melanogaster*. *Dev Genes Evol* 193, 283-295.
155. Nüsslein-Volhard, C., Wieschaus, E., and Kluding, H. (1984). Mutations affecting the pattern of the larval cuticle in *Drosophila melanogaster*. *Dev Genes Evol* 193, 267-282.
156. Wieschaus, E., Nüsslein-Volhard, C., and Jürgens, G. (1984). Mutations affecting the pattern of the larval cuticle in *Drosophila melanogaster*. *Dev Genes Evol* 193, 296-307.
157. Kuan, C.Y., Yang, D.D., Samanta Roy, D.R., Davis, R.J., Rakic, P., and Flavell, R.A. (1999). The Jnk1 and Jnk2 protein kinases are required for regional specific apoptosis during early brain development. *Neuron* 22, 667-676.
158. Boutros, M., Agaisse, H., and Perrimon, N. (2002). Sequential Activation of Signaling Pathways during Innate Immune Responses in *Drosophila*. *Dev Cell* 3, 711-722.
159. Park, J.M., Brady, H., Ruocco, M.G., Sun, H., Williams, D., Lee, S.J., Kato, T., Jr., Richards, N., Chan, K., Mercurio, F., Karin, M., and Wasserman,

- S.A. (2004). Targeting of TAK1 by the NF-kappa B protein Relish regulates the JNK-mediated immune response in *Drosophila*. *Genes Dev* 18, 584-594.
160. Kockel, L., Homsy, J.G., and Bohmann, D. (2001). *Drosophila* AP-1: lessons from an invertebrate. *Oncogene* 20, 2347-2364.
161. Martin-Blanco, E. (1998). Regulatory control of signal transduction during morphogenesis in *Drosophila*. *Int J Dev Biol* 42, 363-368.
162. Martin-Blanco, E., Gampel, A., Ring, J., Virdee, K., Kirov, N., Tolkovsky, A.M., and Martinez-Arias, A. (1998). puckered encodes a phosphatase that mediates a feedback loop regulating JNK activity during dorsal closure in *Drosophila*. *Genes Dev* 12, 557-570.
163. Kallio, J., Leinonen, A., Ulvila, J., Valanne, S., Ezekowitz, R.A., and Ramet, M. (2005). Functional analysis of immune response genes in *Drosophila* identifies JNK pathway as a regulator of antimicrobial peptide gene expression in S2 cells. *Microbes Infect* 7, 811-819.
164. Delaney, J.R., Stoven, S., Uvell, H., Anderson, K.V., Engstrom, Y., and Mlodzik, M. (2006). Cooperative control of *Drosophila* immune responses by the JNK and NF-kappaB signaling pathways. *EMBO J* 25, 3068-3077.
165. Kim, T., Yoon, J., Cho, H., Lee, W.B., Kim, J., Song, Y.H., Kim, S.N., Yoon, J.H., Kim-Ha, J., and Kim, Y.J. (2005). Downregulation of lipopolysaccharide response in *Drosophila* by negative crosstalk between the AP1 and NF-kappaB signaling modules. *Nat Immunol* 6, 211-218.
166. Miethke, T., Wahl, C., Heeg, K., Echtenacher, B., Krammer, P.H., and Wagner, H. (1992). T cell-mediated lethal shock triggered in mice by the

- superantigen staphylococcal enterotoxin B: critical role of tumor necrosis factor. *J Exp Med* 175, 91-98.
167. Zerofsky, M., Harel, E., Silverman, N., and Tatar, M. (2005). Aging of the innate immune response in *Drosophila melanogaster*. *Aging Cell* 4, 103-108.
168. Paredes, J.C., Welchman, D.P., Poidevin, M., and Lemaitre, B. (2011). Negative regulation by amidase PGRPs shapes the *Drosophila* antibacterial response and protects the fly from innocuous infection. *Immunity* 35, 770-779.
169. Aggarwal, K., Rus, F., Vriesema-Magnuson, C., Erturk-Hasdemir, D., Paquette, N., and Silverman, N. (2008). Rudra interrupts receptor signaling complexes to negatively regulate the IMD pathway. *PLoS Path* 4, e1000120.
170. Lhocine, N., Ribeiro, P.S., Buchon, N., Wepf, A., Wilson, R., Tenev, T., Lemaitre, B., Gstaiger, M., Meier, P., and Leulier, F. (2008). PIMS modulates immune tolerance by negatively regulating *Drosophila* innate immune signaling. *Cell Host Microbe* 4, 147-158.
171. Guntermann, S., Primrose, D.A., and Foley, E. (2009). Dnr1-dependent regulation of the *Drosophila* immune deficiency signaling pathway. *Dev Comp Immunol* 33, 127-134.
172. Tsuda, M., Langmann, C., Harden, N., and Aigaki, T. (2005). The RING-finger scaffold protein Plenty of SH3s targets TAK1 to control immunity signalling in *Drosophila*. *EMBO reports* 6, 1082-1087.
173. Kim, L.K., Choi, U.Y., Cho, H.S., Lee, J.S., Lee, W.B., Kim, J., Jeong, K., Shim, J., Kim-Ha, J., and Kim, Y.J. (2007). Down-regulation of NF-kappaB

- target genes by the AP-1 and STAT complex during the innate immune response in *Drosophila*. *PLoS Biol* 5, e238.
174. Napoli, C., Lemieux, C., and Jorgensen, R. (1990). Introduction of a Chimeric Chalcone Synthase Gene into *Petunia* Results in Reversible Co-Suppression of Homologous Genes in trans. *Plant Cell* 2, 279-289.
 175. Hammond, S.M., Bernstein, E., Beach, D., and Hannon, G.J. (2000). An RNA-directed nuclease mediates post-transcriptional gene silencing in *Drosophila* cells. *Nature* 404, 293-296.
 176. Bernstein, E., Caudy, A.A., Hammond, S.M., and Hannon, G.J. (2001). Role for a bidentate ribonuclease in the initiation step of RNA interference. *Nature* 409, 363-366.
 177. Liu, Q., Rand, T.A., Kalidas, S., Du, F., Kim, H.E., Smith, D.P., and Wang, X. (2003). R2D2, a bridge between the initiation and effector steps of the *Drosophila* RNAi pathway. *Science* 301, 1921-1925.
 178. Marques, J.T., Kim, K., Wu, P.H., Alleyne, T.M., Jafari, N., and Carthew, R.W. (2010). Loqs and R2D2 act sequentially in the siRNA pathway in *Drosophila*. *Nat Struct Mol Biol* 17, 24-30.
 179. Ma, J.B., Ye, K., and Patel, D.J. (2004). Structural basis for overhang-specific small interfering RNA recognition by the PAZ domain. *Nature* 429, 318-322.
 180. Tomari, Y., Matranga, C., Haley, B., Martinez, N., and Zamore, P.D. (2004). A protein sensor for siRNA asymmetry. *Science* 306, 1377-1380.
 181. Matranga, C., Tomari, Y., Shin, C., Bartel, D.P., and Zamore, P.D. (2005). Passenger-strand cleavage facilitates assembly of siRNA into Ago2-containing RNAi enzyme complexes. *Cell* 123, 607-620.

182. Harborth, J., Elbashir, S.M., Bechert, K., Tuschl, T., and Weber, K. (2001). Identification of essential genes in cultured mammalian cells using small interfering RNAs. *J Cell Sci* 114, 4557-4565.
183. Kennerdell, J.R., and Carthew, R.W. (1998). Use of dsRNA-mediated genetic interference to demonstrate that frizzled and frizzled 2 act in the wingless pathway. *Cell* 95, 1017-1026.
184. Saleh, M.C., van Rij, R.P., Hekele, A., Gillis, A., Foley, E., O'Farrell, P.H., and Andino, R. (2006). The endocytic pathway mediates cell entry of dsRNA to induce RNAi silencing. *Nat Cell Bio* 8, 793-802.
185. Ulvila, J., Parikka, M., Kleino, A., Sormunen, R., Ezekowitz, R.A., Kocks, C., and Ramet, M. (2006). Double-stranded RNA is internalized by scavenger receptor-mediated endocytosis in *Drosophila* S2 cells. *J Biol Chem* 281, 14370-14375.
186. Clemens, J.C., Worby, C.A., Simonson-Leff, N., Muda, M., Maehama, T., Hemmings, B.A., and Dixon, J.E. (2000). Use of double-stranded RNA interference in *Drosophila* cell lines to dissect signal transduction pathways. *Proc Natl Acad Sci U S A* 97, 6499-6503.
187. Yoneyama, M., Kikuchi, M., Natsukawa, T., Shinobu, N., Imaizumi, T., Miyagishi, M., Taira, K., Akira, S., and Fujita, T. (2004). The RNA helicase RIG-I has an essential function in double-stranded RNA-induced innate antiviral responses. *Nat Immunol* 5, 730-737.
188. Meylan, E., Curran, J., Hofmann, K., Moradpour, D., Binder, M., Bartenschlager, R., and Tschopp, J. (2005). Cardif is an adaptor protein in the RIG-I antiviral pathway and is targeted by hepatitis C virus. *Nature* 437, 1167-1172.

189. Geiss, G., Jin, G., Guo, J., Bumgarner, R., Katze, M.G., and Sen, G.C. (2001). A comprehensive view of regulation of gene expression by double-stranded RNA-mediated cell signaling. *J Biol Chem* 276, 30178-30182.
190. Alexopoulou, L., Holt, A.C., Medzhitov, R., and Flavell, R.A. (2001). Recognition of double-stranded RNA and activation of NF-kappaB by Toll-like receptor 3. *Nature* 413, 732-738.
191. Kulkarni, M.M., Booker, M., Silver, S.J., Friedman, A., Hong, P., Perrimon, N., and Mathey-Prevot, B. (2006). Evidence of off-target effects associated with long dsRNAs in *Drosophila melanogaster* cell-based assays. *Nat Methods* 3, 833-838.
192. Jackson, A.L., Bartz, S.R., Schelter, J., Kobayashi, S.V., Burchard, J., Mao, M., Li, B., Cavet, G., and Linsley, P.S. (2003). Expression profiling reveals off-target gene regulation by RNAi. *Nat Biotechnol* 21, 635-637.
193. Mittal, V. (2004). Improving the efficiency of RNA interference in mammals. *Nat Rev Genet* 5, 355-365.
194. Kumar, R., Conklin, D.S., and Mittal, V. (2003). High-throughput selection of effective RNAi probes for gene silencing. *Genome Res* 13, 2333-2340.
195. Boutros, M., Kiger, A.A., Armknecht, S., Kerr, K., Hild, M., Koch, B., Haas, S.A., Paro, R., and Perrimon, N. (2004). Genome-wide RNAi analysis of growth and viability in *Drosophila* cells. *Science* 303, 832-835.
196. Lum, L., Yao, S., Mozer, B., Rovescalli, A., Von Kessler, D., Nirenberg, M., and Beachy, P.A. (2003). Identification of Hedgehog pathway components by RNAi in *Drosophila* cultured cells. *Science* 299, 2039-2045.
197. Ivanov, A.I., Rovescalli, A.C., Pozzi, P., Yoo, S., Mozer, B., Li, H.P., Yu, S.H., Higashida, H., Guo, V., Spencer, M., and Nirenberg, M. (2004).

- Genes required for *Drosophila* nervous system development identified by RNA interference. *Proc Natl Acad Sci U S A* *101*, 16216-16221.
198. Goshima, G., Wollman, R., Goodwin, S.S., Zhang, N., Scholey, J.M., Vale, R.D., and Stuurman, N. (2007). Genes required for mitotic spindle assembly in *Drosophila* S2 cells. *Science* *316*, 417-421.
199. Moffat, J., Grueneberg, D.A., Yang, X., Kim, S.Y., Kloepfer, A.M., Hinkle, G., Piqani, B., Eisenhaure, T.M., Luo, B., Grenier, J.K., Carpenter, A.E., Foo, S.Y., Stewart, S.A., Stockwell, B.R., Hacohen, N., Hahn, W.C., Lander, E.S., Sabatini, D.M., and Root, D.E. (2006). A lentiviral RNAi library for human and mouse genes applied to an arrayed viral high-content screen. *Cell* *124*, 1283-1298.
200. Silva, J.M., Li, M.Z., Chang, K., Ge, W., Golding, M.C., Rickles, R.J., Siolas, D., Hu, G., Paddison, P.J., Schlabach, M.R., Sheth, N., Bradshaw, J., Burchard, J., Kulkarni, A., Cavet, G., Sachidanandam, R., McCombie, W.R., Cleary, M.A., Elledge, S.J., and Hannon, G.J. (2005). Second-generation shRNA libraries covering the mouse and human genomes. *Nat Genet* *37*, 1281-1288.
201. Paddison, P.J., Silva, J.M., Conklin, D.S., Schlabach, M., Li, M., Aruleba, S., Balija, V., O'Shaughnessy, A., Gnoj, L., Scobie, K., Chang, K., Westbrook, T., Cleary, M., Sachidanandam, R., McCombie, W.R., Elledge, S.J., and Hannon, G.J. (2004). A resource for large-scale RNA-interference-based screens in mammals. *Nature* *428*, 427-431.
202. DasGupta, R., Kaykas, A., Moon, R.T., and Perrimon, N. (2005). Functional genomic analysis of the Wnt-wingless signaling pathway. *Science* *308*, 826-833.

203. Mohr, S., Bakal, C., and Perrimon, N. (2010). Genomic screening with RNAi: results and challenges. *Annu Rev Biochem* 79, 37-64.
204. Gesellchen, V., Kuttenukeuler, D., Steckel, M., Pelte, N., and Boutros, M. (2005). An RNA interference screen identifies Inhibitor of Apoptosis Protein 2 as a regulator of innate immune signalling in *Drosophila*. *EMBO Rep* 6, 979-984.
205. Kleino, A., Valanne, S., Ulvila, J., Kallio, J., Myllymaki, H., Enwald, H., Stoven, S., Poidevin, M., Ueda, R., Hultmark, D., Lemaitre, B., and Ramet, M. (2005). Inhibitor of apoptosis 2 and TAK1-binding protein are components of the *Drosophila* Imd pathway. *EMBO J* 24, 3423-3434.
206. Bond, D., Primrose, D.A., and Foley, E. (2008). Quantitative evaluation of signaling events in *Drosophila* s2 cells. *Biol Proced Online* 10, 20-28.
207. Valanne, S., Kallio, J., Kleino, A., and Ramet, M. (2012). Large-scale RNAi screens add both clarity and complexity to *Drosophila* NF-kappaB signaling. *Dev Comp Immunol* 37, 9-18.
208. Neely, G.G., Kuba, K., Cammarato, A., Isobe, K., Amann, S., Zhang, L., Murata, M., Elmen, L., Gupta, V., Arora, S., Sarangi, R., Dan, D., Fujisawa, S., Usami, T., Xia, C.P., Keene, A.C., Alayari, N.N., Yamakawa, H., Elling, U., Berger, C., Novatchkova, M., Koggruber, R., Fukuda, K., Nishina, H., Isobe, M., Pospisilik, J.A., Imai, Y., Pfeufer, A., Hicks, A.A., Pramstaller, P.P., Subramaniam, S., Kimura, A., Ocorr, K., Bodmer, R., and Penninger, J.M. (2010). A global in vivo *Drosophila* RNAi screen identifies NOT3 as a conserved regulator of heart function. *Cell* 141, 142-153.

209. Lesch, C., Jo, J., Wu, Y., Fish, G.S., and Galko, M.J. (2010). A targeted UAS-RNAi screen in *Drosophila* larvae identifies wound closure genes regulating distinct cellular processes. *Genetics* 186, 943-957.
210. Cronin, S.J., Nehme, N.T., Limmer, S., Liegeois, S., Pospisilik, J.A., Schramek, D., Leibbrandt, A., Simoes Rde, M., Gruber, S., Puc, U., Ebersberger, I., Zoranovic, T., Neely, G.G., von Haeseler, A., Ferrandon, D., and Penninger, J.M. (2009). Genome-wide RNAi screen identifies genes involved in intestinal pathogenic bacterial infection. *Science* 325, 340-343.
211. Arendt, D., Technau, U., and Wittbrodt, J. (2001). Evolution of the bilaterian larval foregut. *Nature* 409, 81-85.
212. Backhed, F., Ley, R.E., Sonnenburg, J.L., Peterson, D.A., and Gordon, J.I. (2005). Host-bacterial mutualism in the human intestine. *Science* 307, 1915-1920.
213. Shin, S.C., Kim, S.H., You, H., Kim, B., Kim, A.C., Lee, K.A., Yoon, J.H., Ryu, J.H., and Lee, W.J. (2011). *Drosophila* microbiome modulates host developmental and metabolic homeostasis via insulin signaling. *Science* 334, 670-674.
214. Backhed, F., Ding, H., Wang, T., Hooper, L.V., Koh, G.Y., Nagy, A., Semenkovich, C.F., and Gordon, J.I. (2004). The gut microbiota as an environmental factor that regulates fat storage. *Proc Natl Acad Sci U S A* 101, 15718-15723.
215. Round, J.L., and Mazmanian, S.K. (2009). The gut microbiota shapes intestinal immune responses during health and disease. *Nat Rev Immunol* 9, 313-323.

216. Blikslager, A.T., Moeser, A.J., Gookin, J.L., Jones, S.L., and Odle, J. (2007). Restoration of barrier function in injured intestinal mucosa. *Physiol Rev* 87, 545-564.
217. van der Flier, L.G., and Clevers, H. (2009). Stem cells, self-renewal, and differentiation in the intestinal epithelium. *Annu Rev Physiol* 71, 241-260.
218. Mowat, A.M. (2003). Anatomical basis of tolerance and immunity to intestinal antigens. *Nat Rev Immunol* 3, 331-341.
219. Rakoff-Nahoum, S., Paglino, J., Eslami-Varzaneh, F., Edberg, S., and Medzhitov, R. (2004). Recognition of commensal microflora by toll-like receptors is required for intestinal homeostasis. *Cell* 118, 229-241.
220. Niess, J.H., Brand, S., Gu, X., Landsman, L., Jung, S., McCormick, B.A., Vyas, J.M., Boes, M., Ploegh, H.L., Fox, J.G., Littman, D.R., and Reinecker, H.C. (2005). CX3CR1-mediated dendritic cell access to the intestinal lumen and bacterial clearance. *Science* 307, 254-258.
221. Wen, L., Ley, R.E., Volchkov, P.Y., Stranges, P.B., Avanesyan, L., Stonebraker, A.C., Hu, C., Wong, F.S., Szot, G.L., Bluestone, J.A., Gordon, J.I., and Chervonsky, A.V. (2008). Innate immunity and intestinal microbiota in the development of Type 1 diabetes. *Nature* 455, 1109-1113.
222. Garrett, W.S., Gordon, J.I., and Glimcher, L.H. (2010). Homeostasis and inflammation in the intestine. *Cell* 140, 859-870.
223. Cario, E., Rosenberg, I.M., Brandwein, S.L., Beck, P.L., Reinecker, H.C., and Podolsky, D.K. (2000). Lipopolysaccharide activates distinct signaling pathways in intestinal epithelial cell lines expressing Toll-like receptors. *J Immunol* 164, 966-972.

224. Hisamatsu, T., Suzuki, M., Reinecker, H.C., Nadeau, W.J., McCormick, B.A., and Podolsky, D.K. (2003). CARD15/NOD2 functions as an antibacterial factor in human intestinal epithelial cells. *Gastroenterology* 124, 993-1000.
225. Neish, A.S., Gewirtz, A.T., Zeng, H., Young, A.N., Hobert, M.E., Karmali, V., Rao, A.S., and Madara, J.L. (2000). Prokaryotic regulation of epithelial responses by inhibition of I κ B-alpha ubiquitination. *Science* 289, 1560-1563.
226. Zaph, C., Troy, A.E., Taylor, B.C., Berman-Booty, L.D., Guild, K.J., Du, Y., Yost, E.A., Gruber, A.D., May, M.J., Greten, F.R., Eckmann, L., Karin, M., and Artis, D. (2007). Epithelial-cell-intrinsic IKK-beta expression regulates intestinal immune homeostasis. *Nature* 446, 552-556.
227. Nenci, A., Becker, C., Wullaert, A., Gareus, R., van Loo, G., Danese, S., Huth, M., Nikolaev, A., Neufert, C., Madison, B., Gumucio, D., Neurath, M.F., and Pasparakis, M. (2007). Epithelial NEMO links innate immunity to chronic intestinal inflammation. *Nature* 446, 557-561.
228. Ryu, J.H., Kim, S.H., Lee, H.Y., Bai, J.Y., Nam, Y.D., Bae, J.W., Lee, D.G., Shin, S.C., Ha, E.M., and Lee, W.J. (2008). Innate immune homeostasis by the homeobox gene *caudal* and commensal-gut mutualism in *Drosophila*. *Science* 319, 777-782.
229. Bosco-Drayon, V., Poidevin, M., Boneca, I.G., Narbonne-Reveau, K., Royet, J., and Charroux, B. (2012). Peptidoglycan Sensing by the Receptor PGRP-LE in the *Drosophila* Gut Induces Immune Responses to Infectious Bacteria and Tolerance to Microbiota. *Cell Host Microbe* 12, 153-165.

230. Bischoff, V., Vignal, C., Duvic, B., Boneca, I.G., Hoffmann, J.A., and Royet, J. (2006). Downregulation of the *Drosophila* immune response by peptidoglycan-recognition proteins SC1 and SC2. *PLoS Path* 2, e14.
231. Micchelli, C.A., and Perrimon, N. (2006). Evidence that stem cells reside in the adult *Drosophila* midgut epithelium. *Nature* 439, 475-479.
232. Biteau, B., Hochmuth, C.E., and Jasper, H. (2011). Maintaining tissue homeostasis: dynamic control of somatic stem cell activity. *Cell Stem Cell* 9, 402-411.
233. Apidianakis, Y., and Rahme, L.G. (2011). *Drosophila melanogaster* as a model for human intestinal infection and pathology. *Dis Model Mech* 4, 21-30.
234. Jiang, H., and Edgar, B.A. (2011). Intestinal stem cells in the adult *Drosophila* midgut. *Exp Cell Res* 317, 2780-2788.
235. Shanbhag, S., and Tripathi, S. (2009). Epithelial ultrastructure and cellular mechanisms of acid and base transport in the *Drosophila* midgut. *J Exp Biol* 212, 1731-1744.
236. Terra, W.R. (2001). The origin and functions of the insect peritrophic membrane and peritrophic gel. *Arch Insect Biochem Physiol* 47, 47-61.
237. Kuraishi, T., Binggeli, O., Opota, O., Buchon, N., and Lemaitre, B. (2011). Genetic evidence for a protective role of the peritrophic matrix against intestinal bacterial infection in *Drosophila melanogaster*. *Proc Natl Acad Sci U S A* 108, 15966-15971.
238. Ohlstein, B., and Spradling, A. (2007). Multipotent *Drosophila* intestinal stem cells specify daughter cell fates by differential notch signaling. *Science* 315, 988-992.

239. Lin, G., Xu, N., and Xi, R. (2008). Paracrine Wingless signalling controls self-renewal of *Drosophila* intestinal stem cells. *Nature* *455*, 1119-1123.
240. Amcheslavsky, A., Jiang, J., and Ip, Y.T. (2009). Tissue damage-induced intestinal stem cell division in *Drosophila*. *Cell Stem Cell* *4*, 49-61.
241. Reya, T., Morrison, S.J., Clarke, M.F., and Weissman, I.L. (2001). Stem cells, cancer, and cancer stem cells. *Nature* *414*, 105-111.
242. Morrison, S.J., and Spradling, A.C. (2008). Stem cells and niches: mechanisms that promote stem cell maintenance throughout life. *Cell* *132*, 598-611.
243. Liu, W., Singh, S.R., and Hou, S.X. (2010). JAK-STAT is restrained by Notch to control cell proliferation of the *Drosophila* intestinal stem cells. *J Cell Biochem* *109*, 992-999.
244. Takashima, S., Adams, K.L., Ortiz, P.A., Ying, C.T., Moridzadeh, R., Younossi-Hartenstein, A., and Hartenstein, V. (2011). Development of the *Drosophila* entero-endocrine lineage and its specification by the Notch signaling pathway. *Dev Biol* *353*, 161-172.
245. Xu, N., Wang, S.Q., Tan, D., Gao, Y., Lin, G., and Xi, R. (2011). EGFR, Wingless and JAK/STAT signaling cooperatively maintain *Drosophila* intestinal stem cells. *Dev Biol* *354*, 31-43.
246. Staley, B.K., and Irvine, K.D. (2010). Warts and Yorkie mediate intestinal regeneration by influencing stem cell proliferation. *Current biology : CB* *20*, 1580-1587.
247. Ren, F., Wang, B., Yue, T., Yun, E.Y., Ip, Y.T., and Jiang, J. (2010). Hippo signaling regulates *Drosophila* intestine stem cell proliferation through multiple pathways. *Proc Natl Acad Sci U S A* *107*, 21064-21069.

248. Jiang, H., and Edgar, B.A. (2009). EGFR signaling regulates the proliferation of *Drosophila* adult midgut progenitors. *Development* 136, 483-493.
249. Karpowicz, P., Perez, J., and Perrimon, N. (2010). The Hippo tumor suppressor pathway regulates intestinal stem cell regeneration. *Development* 137, 4135-4145.
250. Biteau, B., and Jasper, H. (2011). EGF signaling regulates the proliferation of intestinal stem cells in *Drosophila*. *Development* 138, 1045-1055.
251. Jiang, H., Grenley, M.O., Bravo, M.J., Blumhagen, R.Z., and Edgar, B.A. (2011). EGFR/Ras/MAPK signaling mediates adult midgut epithelial homeostasis and regeneration in *Drosophila*. *Cell Stem Cell* 8, 84-95.
252. Shaw, R.L., Kohlmaier, A., Polesello, C., Veelken, C., Edgar, B.A., and Tapon, N. (2010). The Hippo pathway regulates intestinal stem cell proliferation during *Drosophila* adult midgut regeneration. *Development* 137, 4147-4158.
253. Buchon, N., Broderick, N.A., Kuraishi, T., and Lemaitre, B. (2010). *Drosophila* EGFR pathway coordinates stem cell proliferation and gut remodeling following infection. *BMC Biol* 8, 152.
254. Chatterjee, M., and Ip, Y.T. (2009). Pathogenic stimulation of intestinal stem cell response in *Drosophila*. *J Cell Physiol* 220, 664-671.
255. Liehl, P., Blight, M., Vodovar, N., Bocard, F., and Lemaitre, B. (2006). Prevalence of local immune response against oral infection in a *Drosophila/Pseudomonas* infection model. *PLoS Path* 2, e56.

256. Buchon, N., Broderick, N.A., Poidevin, M., Pradervand, S., and Lemaitre, B. (2009). *Drosophila* intestinal response to bacterial infection: activation of host defense and stem cell proliferation. *Cell Host Microbe* 5, 200-211.
257. Jiang, H., and Edgar, B.A. (2012). Intestinal stem cell function in *Drosophila* and mice. *Curr Opin Genet Dev* 22, 354-360.
258. Wang, P., and Hou, S.X. (2010). Regulation of intestinal stem cells in mammals and *Drosophila*. *J Cell Physiol* 222, 33-37.
259. Barker, N., van Es, J.H., Kuipers, J., Kujala, P., van den Born, M., Cozijnsen, M., Haegebarth, A., Korving, J., Begthel, H., Peters, P.J., and Clevers, H. (2007). Identification of stem cells in small intestine and colon by marker gene *Lgr5*. *Nature* 449, 1003-1007.
260. Tian, H., Biehs, B., Warming, S., Leong, K.G., Rangell, L., Klein, O.D., and de Sauvage, F.J. (2011). A reserve stem cell population in small intestine renders *Lgr5*-positive cells dispensable. *Nature* 478, 255-259.
261. Barker, N., Ridgway, R.A., van Es, J.H., van de Wetering, M., Begthel, H., van den Born, M., Danenberg, E., Clarke, A.R., Sansom, O.J., and Clevers, H. (2009). Crypt stem cells as the cells-of-origin of intestinal cancer. *Nature* 457, 608-611.
262. Youssef, K.K., Van Keymeulen, A., Lapouge, G., Beck, B., Michaux, C., Achouri, Y., Sotiropoulou, P.A., and Blanpain, C. (2010). Identification of the cell lineage at the origin of basal cell carcinoma. *Nat Cell Bio* 12, 299-305.
263. Sancho, R., Nateri, A.S., de Vinuesa, A.G., Aguilera, C., Nye, E., Spencer-Dene, B., and Behrens, A. (2009). JNK signalling modulates intestinal homeostasis and tumourigenesis in mice. *EMBO J* 28, 1843-1854.

264. Fre, S., Huyghe, M., Mourikis, P., Robine, S., Louvard, D., and Artavanis-Tsakonas, S. (2005). Notch signals control the fate of immature progenitor cells in the intestine. *Nature* *435*, 964-968.
265. Fevr, T., Robine, S., Louvard, D., and Huelsken, J. (2007). Wnt/beta-catenin is essential for intestinal homeostasis and maintenance of intestinal stem cells. *Mol Cell Biol* *27*, 7551-7559.
266. Ireland, H., Kemp, R., Houghton, C., Howard, L., Clarke, A.R., Sansom, O.J., and Winton, D.J. (2004). Inducible Cre-mediated control of gene expression in the murine gastrointestinal tract: effect of loss of beta-catenin. *Gastroenterology* *126*, 1236-1246.
267. Korinek, V., Barker, N., Moerer, P., van Donselaar, E., Huls, G., Peters, P.J., and Clevers, H. (1998). Depletion of epithelial stem-cell compartments in the small intestine of mice lacking Tcf-4. *Nat Genet* *19*, 379-383.
268. Andrae, J., Gallini, R., and Betsholtz, C. (2008). Role of platelet-derived growth factors in physiology and medicine. *Genes Dev* *22*, 1276-1312.
269. Heino, T.I., Karpanen, T., Wahlstrom, G., Pulkkinen, M., Eriksson, U., Alitalo, K., and Roos, C. (2001). The Drosophila VEGF receptor homolog is expressed in hemocytes. *Mech Dev* *109*, 69-77.
270. Duchek, P., Somogyi, K., Jekely, G., Beccari, S., and Rorth, P. (2001). Guidance of cell migration by the Drosophila PDGF/VEGF receptor. *Cell* *107*, 17-26.
271. Cho, N.K., Keyes, L., Johnson, E., Heller, J., Ryner, L., Karim, F., and Krasnow, M.A. (2002). Developmental control of blood cell migration by the Drosophila VEGF pathway. *Cell* *108*, 865-876.

272. Hoch, R.V., and Soriano, P. (2003). Roles of PDGF in animal development. *Development* 130, 4769-4784.
273. Fulga, T.A., and Rorth, P. (2002). Invasive cell migration is initiated by guided growth of long cellular extensions. *Nat Cell Bio* 4, 715-719.
274. Munier, A.I., Doucet, D., Perrodou, E., Zachary, D., Meister, M., Hoffmann, J.A., Janeway, C.A., Jr., and Lagueux, M. (2002). PVF2, a PDGF/VEGF-like growth factor, induces hemocyte proliferation in *Drosophila* larvae. *EMBO Rep* 3, 1195-1200.
275. Macias, A., Romero, N.M., Martin, F., Suarez, L., Rosa, A.L., and Morata, G. (2004). PVF1/PVR signaling and apoptosis promotes the rotation and dorsal closure of the *Drosophila* male terminalia. *Int J Dev Biol* 48, 1087-1094.
276. Ishimaru, S., Ueda, R., Hinohara, Y., Ohtani, M., and Hanafusa, H. (2004). PVR plays a critical role via JNK activation in thorax closure during *Drosophila* metamorphosis. *EMBO J* 23, 3984-3994.
277. Bruckner, K., Kockel, L., Duchek, P., Luque, C.M., Rorth, P., and Perrimon, N. (2004). The PDGF/VEGF receptor controls blood cell survival in *Drosophila*. *Dev Cell* 7, 73-84.
278. Wu, Y., Brock, A.R., Wang, Y., Fujitani, K., Ueda, R., and Galko, M.J. (2009). A blood-borne PDGF/VEGF-like ligand initiates wound-induced epidermal cell migration in *Drosophila* larvae. *Current biology : CB* 19, 1473-1477.
279. Sims, D., Duchek, P., and Baum, B. (2009). PDGF/VEGF signaling controls cell size in *Drosophila*. *Genome Biol* 10, R20.

280. Bond, D., and Foley, E. (2009). A quantitative RNAi screen for JNK modifiers identifies Pvr as a novel regulator of *Drosophila* immune signaling. *PLoS Path* 5, e1000655.
281. Koch, S., Tugues, S., Li, X., Gualandi, L., and Claesson-Welsh, L. (2011). Signal transduction by vascular endothelial growth factor receptors. *The Biochemical journal* 437, 169-183.
282. Duchek, P., and Rorth, P. (2001). Guidance of cell migration by EGF receptor signaling during *Drosophila* oogenesis. *Science* 291, 131-133.
283. Harris, K.E., Schnittke, N., and Beckendorf, S.K. (2007). Two ligands signal through the *Drosophila* PDGF/VEGF receptor to ensure proper salivary gland positioning. *Mech Dev* 124, 441-448.
284. Sears, H.C., Kennedy, C.J., and Garrity, P.A. (2003). Macrophage-mediated corpse engulfment is required for normal *Drosophila* CNS morphogenesis. *Development* 130, 3557-3565.
285. Zettervall, C.J., Anderl, I., Williams, M.J., Palmer, R., Kurucz, E., Ando, I., and Hultmark, D. (2004). A directed screen for genes involved in *Drosophila* blood cell activation. *Proc Natl Acad Sci U S A* 101, 14192-14197.
286. Ullrich, A., and Schlessinger, J. (1990). Signal transduction by receptors with tyrosine kinase activity. *Cell* 61, 203-212.
287. Leppanen, V.M., Prota, A.E., Jeltsch, M., Anisimov, A., Kalkkinen, N., Strandin, T., Lankinen, H., Goldman, A., Ballmer-Hofer, K., and Alitalo, K. (2010). Structural determinants of growth factor binding and specificity by VEGF receptor 2. *Proc Natl Acad Sci U S A* 107, 2425-2430.

288. Wiesmann, C., Fuh, G., Christinger, H.W., Eigenbrot, C., Wells, J.A., and de Vos, A.M. (1997). Crystal structure at 1.7 Å resolution of VEGF in complex with domain 2 of the Flt-1 receptor. *Cell* *91*, 695-704.
289. Lemmon, M.A., and Schlessinger, J. (2010). Cell signaling by receptor tyrosine kinases. *Cell* *141*, 1117-1134.
290. Christinger, H.W., Fuh, G., de Vos, A.M., and Wiesmann, C. (2004). The crystal structure of placental growth factor in complex with domain 2 of vascular endothelial growth factor receptor-1. *J Biol Chem* *279*, 10382-10388.
291. Fuh, G., Li, B., Crowley, C., Cunningham, B., and Wells, J.A. (1998). Requirements for binding and signaling of the kinase domain receptor for vascular endothelial growth factor. *J Biol Chem* *273*, 11197-11204.
292. Hanks, S.K., Quinn, A.M., and Hunter, T. (1988). The protein kinase family: conserved features and deduced phylogeny of the catalytic domains. *Science* *241*, 42-52.
293. Honegger, A.M., Dull, T.J., Felder, S., Van Obberghen, E., Bellot, F., Szapary, D., Schmidt, A., Ullrich, A., and Schlessinger, J. (1987). Point mutation at the ATP binding site of EGF receptor abolishes protein-tyrosine kinase activity and alters cellular routing. *Cell* *51*, 199-209.
294. Kazlauskas, A., and Cooper, J.A. (1989). Autophosphorylation of the PDGF receptor in the kinase insert region regulates interactions with cell proteins. *Cell* *58*, 1121-1133.
295. Chen, W.S., Lazar, C.S., Poenie, M., Tsien, R.Y., Gill, G.N., and Rosenfeld, M.G. (1987). Requirement for intrinsic protein tyrosine kinase in the immediate and late actions of the EGF receptor. *Nature* *328*, 820-823.

296. Molloy, C.J., Bottaro, D.P., Fleming, T.P., Marshall, M.S., Gibbs, J.B., and Aaronson, S.A. (1989). PDGF induction of tyrosine phosphorylation of GTPase activating protein. *Nature* 342, 711-714.
297. Koch, C.A., Anderson, D., Moran, M.F., Ellis, C., and Pawson, T. (1991). SH2 and SH3 domains: elements that control interactions of cytoplasmic signaling proteins. *Science* 252, 668-674.
298. Lee, T., Hacohen, N., Krasnow, M., and Montell, D.J. (1996). Regulated Breathless receptor tyrosine kinase activity required to pattern cell migration and branching in the *Drosophila* tracheal system. *Genes Dev* 10, 2912-2921.
299. Wennstrom, S., Siegbahn, A., Yokote, K., Arvidsson, A.K., Heldin, C.H., Mori, S., and Claesson-Welsh, L. (1994). Membrane ruffling and chemotaxis transduced by the PDGF beta-receptor require the binding site for phosphatidylinositol 3' kinase. *Oncogene* 9, 651-660.
300. Kundra, V., Escobedo, J.A., Kazlauskas, A., Kim, H.K., Rhee, S.G., Williams, L.T., and Zetter, B.R. (1994). Regulation of chemotaxis by the platelet-derived growth factor receptor-beta. *Nature* 367, 474-476.
301. Friedman, A., and Perrimon, N. (2006). A functional RNAi screen for regulators of receptor tyrosine kinase and ERK signalling. *Nature* 444, 230-234.
302. Bjorklund, M., Taipale, M., Varjosalo, M., Saharinen, J., Lahdenpera, J., and Taipale, J. (2006). Identification of pathways regulating cell size and cell-cycle progression by RNAi. *Nature* 439, 1009-1013.

303. Choi, N.H., Kim, J.G., Yang, D.J., Kim, Y.S., and Yoo, M.A. (2008). Age-related changes in *Drosophila* midgut are associated with PVF2, a PDGF/VEGF-like growth factor. *Aging Cell* 7, 318-334.
304. Park, J.S., Kim, Y.S., and Yoo, M.A. (2009). The role of p38b MAPK in age-related modulation of intestinal stem cell proliferation and differentiation in *Drosophila*. *Aging (Milano)* 1, 637-651.
305. Zeng, X., Chauhan, C., and Hou, S.X. (2010). Characterization of midgut stem cell- and enteroblast-specific Gal4 lines in *Drosophila*. *Genesis* 48, 607-611.
306. Furriols, M., and Bray, S. (2001). A model Notch response element detects Suppressor of Hairless-dependent molecular switch. *Current biology : CB* 11, 60-64.
307. Weber, U., Paricio, N., and Mlodzik, M. (2000). Jun mediates Frizzled-induced R3/R4 cell fate distinction and planar polarity determination in the *Drosophila* eye. *Development* 127, 3619-3629.
308. Lee, T., Feig, L., and Montell, D.J. (1996). Two distinct roles for Ras in a developmentally regulated cell migration. *Development* 122, 409-418.
309. Parks, A.L., Cook, K.R., Belvin, M., Dompe, N.A., Fawcett, R., Huppert, K., Tan, L.R., Winter, C.G., Bogart, K.P., Deal, J.E., Deal-Herr, M.E., Grant, D., Marcinko, M., Miyazaki, W.Y., Robertson, S., Shaw, K.J., Tabios, M., Vysotskaia, V., Zhao, L., Andrade, R.S., Edgar, K.A., Howie, E., Killpack, K., Milash, B., Norton, A., Thao, D., Whittaker, K., Winner, M.A., Friedman, L., Margolis, J., Singer, M.A., Koczyński, C., Curtis, D., Kaufman, T.C., Plowman, G.D., Duyk, G., and Francis-Lang, H.L. (2004). Systematic

- generation of high-resolution deletion coverage of the *Drosophila melanogaster* genome. *Nat Genet* 36, 288-292.
310. Lee, T., and Luo, L. (2001). Mosaic analysis with a repressible cell marker (MARCM) for *Drosophila* neural development. *Trends Neurosci* 24, 251-254.
311. Schindelin, J., Arganda-Carreras, I., Frise, E., Kaynig, V., Longair, M., Pietzsch, T., Preibisch, S., Rueden, C., Saalfeld, S., Schmid, B., Tinevez, J.Y., White, D.J., Hartenstein, V., Eliceiri, K., Tomancak, P., and Cardona, A. (2012). Fiji: an open-source platform for biological-image analysis. *Nat Methods* 9, 676-682.
312. Silverman, N., Zhou, R., Erlich, R.L., Hunter, M., Bernstein, E., Schneider, D., and Maniatis, T. (2003). Immune activation of NF-kappaB and JNK requires *Drosophila* TAK1. *J Biol Chem* 278, 48928-48934.
313. Schneider, I. (1972). Cell lines derived from late embryonic stages of *Drosophila melanogaster*. *J Embryol Exp Morphol* 27, 353-365.
314. Yanagawa, S., Lee, J.S., and Ishimoto, A. (1998). Identification and characterization of a novel line of *Drosophila* Schneider S2 cells that respond to wingless signaling. *J Biol Chem* 273, 32353-32359.
315. Cherbas, L., Willingham, A., Zhang, D., Yang, L., Zou, Y., Eads, B.D., Carlson, J.W., Landolin, J.M., Kapranov, P., Dumais, J., Samsonova, A., Choi, J.H., Roberts, J., Davis, C.A., Tang, H., van Baren, M.J., Ghosh, S., Dobin, A., Bell, K., Lin, W., Langton, L., Duff, M.O., Tenney, A.E., Zaleski, C., Brent, M.R., Hoskins, R.A., Kaufman, T.C., Andrews, J., Graveley, B.R., Perrimon, N., Celniker, S.E., Gingeras, T.R., and Cherbas, P. (2011). The

- transcriptional diversity of 25 *Drosophila* cell lines. *Genome Res* 21, 301-314.
316. Hay, B.A., Wassarman, D.A., and Rubin, G.M. (1995). *Drosophila* homologs of baculovirus inhibitor of apoptosis proteins function to block cell death. *Cell* 83, 1253-1262.
317. Liu, H., Su, Y.C., Becker, E., Treisman, J., and Skolnik, E.Y. (1999). A *Drosophila* TNF-receptor-associated factor (TRAF) binds the *ste20* kinase *Misshapen* and activates Jun kinase. *Current biology : CB* 9, 101-104.
318. Rutschmann, S., Jung, A.C., Zhou, R., Silverman, N., Hoffmann, J.A., and Ferrandon, D. (2000). Role of *Drosophila* IKK gamma in a toll-independent antibacterial immune response. *Nature immunology* 1, 342-347.
319. Su, Y.C., Treisman, J.E., and Skolnik, E.Y. (1998). The *Drosophila* *Ste20*-related kinase *misshapen* is required for embryonic dorsal closure and acts through a JNK MAPK module on an evolutionarily conserved signaling pathway. *Genes Dev* 12, 2371-2380.
320. Igaki, T., Kanda, H., Yamamoto-Goto, Y., Kanuka, H., Kuranaga, E., Aigaki, T., and Miura, M. (2002). *Eiger*, a TNF superfamily ligand that triggers the *Drosophila* JNK pathway. *EMBO J* 21, 3009-3018.
321. Rodriguez, A., Oliver, H., Zou, H., Chen, P., Wang, X., and Abrams, J.M. (1999). *Dark* is a *Drosophila* homologue of *Apaf-1/CED-4* and functions in an evolutionarily conserved death pathway. *Nat Cell Bio* 1, 272-279.
322. Glise, B., Bourbon, H., and Noselli, S. (1995). *hemipterous* encodes a novel *Drosophila* MAP kinase kinase, required for epithelial cell sheet movement. *Cell* 83, 451-461.

323. Vidal, S., Khush, R.S., Leulier, F., Tzou, P., Nakamura, M., and Lemaitre, B. (2001). Mutations in the *Drosophila* dTAK1 gene reveal a conserved function for MAPKKKs in the control of rel/NF-kappaB-dependent innate immune responses. *Genes Dev* 15, 1900-1912.
324. Colussi, P.A., Quinn, L.M., Huang, D.C., Coombe, M., Read, S.H., Richardson, H., and Kumar, S. (2000). Debcl, a proapoptotic Bcl-2 homologue, is a component of the *Drosophila melanogaster* cell death machinery. *J Cell Biol* 148, 703-714.
325. Dumanis, J., Quinn, L., Richardson, H., and Kumar, S. (2001). STRICA, a novel *Drosophila melanogaster* caspase with an unusual serine/threonine-rich prodomain, interacts with DIAP1 and DIAP2. *Cell Death Differ* 8, 387-394.
326. White, K., Grether, M.E., Abrams, J.M., Young, L., Farrell, K., and Steller, H. (1994). Genetic control of programmed cell death in *Drosophila*. *Science* 264, 677-683.
327. Kanda, H., Igaki, T., Kanuka, H., Yagi, T., and Miura, M. (2002). Wengen, a member of the *Drosophila* tumor necrosis factor receptor superfamily, is required for Eiger signaling. *J Biol Chem* 277, 28372-28375.
328. Fraser, A.G., and Evan, G.I. (1997). Identification of a *Drosophila melanogaster* ICE/CED-3-related protease, drICE. *EMBO J* 16, 2805-2813.
329. Dorstyn, L., Read, S.H., Quinn, L.M., Richardson, H., and Kumar, S. (1999). DECAY, a novel *Drosophila* caspase related to mammalian caspase-3 and caspase-7. *J Biol Chem* 274, 30778-30783.

330. Harvey, N.L., Daish, T., Mills, K., Dorstyn, L., Quinn, L.M., Read, S.H., Richardson, H., and Kumar, S. (2001). Characterization of the *Drosophila* caspase, DAMM. *J Biol Chem* 276, 25342-25350.
331. Song, Z., McCall, K., and Steller, H. (1997). DCP-1, a *Drosophila* cell death protease essential for development. *Science* 275, 536-540.
332. Zhou, R., Silverman, N., Hong, M., Liao, D.S., Chung, Y., Chen, Z.J., and Maniatis, T. (2005). The role of ubiquitination in *Drosophila* innate immunity. *J Biol Chem* 280, 34048-34055.
333. Chen, H.W., Marinissen, M.J., Oh, S.W., Chen, X., Melnick, M., Perrimon, N., Gutkind, J.S., and Hou, S.X. (2002). CKA, a novel multidomain protein, regulates the JUN N-terminal kinase signal transduction pathway in *Drosophila*. *Mol Cell Biol* 22, 1792-1803.
334. Brunner, D., Ducker, K., Oellers, N., Hafen, E., Scholz, H., and Klambt, C. (1994). The ETS domain protein pointed-P2 is a target of MAP kinase in the sevenless signal transduction pathway. *Nature* 370, 386-389.
335. Tsuda, L., Inoue, Y.H., Yoo, M.A., Mizuno, M., Hata, M., Lim, Y.M., Adachi-Yamada, T., Ryo, H., Masamune, Y., and Nishida, Y. (1993). A protein kinase similar to MAP kinase activator acts downstream of the raf kinase in *Drosophila*. *Cell* 72, 407-414.
336. Gaengel, K., and Mlodzik, M. (2003). Egfr signaling regulates ommatidial rotation and cell motility in the *Drosophila* eye via MAPK/Pnt signaling and the Ras effector Canoe/AF6. *Development* 130, 5413-5423.
337. Casali, A., and Batlle, E. (2009). Intestinal stem cells in mammals and *Drosophila*. *Cell Stem Cell* 4, 124-127.

338. Brand, A.H., and Perrimon, N. (1993). Targeted gene expression as a means of altering cell fates and generating dominant phenotypes. *Development* *118*, 401-415.
339. McGuire, S.E., Le, P.T., Osborn, A.J., Matsumoto, K., and Davis, R.L. (2003). Spatiotemporal rescue of memory dysfunction in *Drosophila*. *Science* *302*, 1765-1768.
340. Apidianakis, Y., Pitsouli, C., Perrimon, N., and Rahme, L. (2009). Synergy between bacterial infection and genetic predisposition in intestinal dysplasia. *Proc Natl Acad Sci U S A* *106*, 20883-20888.
341. Bardin, A.J., Perdigoto, C.N., Southall, T.D., Brand, A.H., and Schweisguth, F. (2010). Transcriptional control of stem cell maintenance in the *Drosophila* intestine. *Development* *137*, 705-714.
342. Adachi-Yamada, T., Nakamura, M., Irie, K., Tomoyasu, Y., Sano, Y., Mori, E., Goto, S., Ueno, N., Nishida, Y., and Matsumoto, K. (1999). p38 mitogen-activated protein kinase can be involved in transforming growth factor beta superfamily signal transduction in *Drosophila* wing morphogenesis. *Mol Cell Biol* *19*, 2322-2329.
343. Towbin, H., Staehelin, T., and Gordon, J. (1979). Electrophoretic transfer of proteins from polyacrylamide gels to nitrocellulose sheets: procedure and some applications. *Proc Natl Acad Sci U S A* *76*, 4350-4354.
344. Egorina, E.M., Sovershaev, M.A., and Osterud, B. (2006). In-cell Western assay: a new approach to visualize tissue factor in human monocytes. *J Thromb Haemost* *4*, 614-620.
345. Boutros, M., and Ahringer, J. (2008). The art and design of genetic screens: RNA interference. *Nat Rev Genet* *9*, 554-566.

346. Chu, W.M., Ostertag, D., Li, Z.W., Chang, L., Chen, Y., Hu, Y., Williams, B., Perrault, J., and Karin, M. (1999). JNK2 and IKKbeta are required for activating the innate response to viral infection. *Immunity* 11, 721-731.
347. Lee, S.Y., Reichlin, A., Santana, A., Sokol, K.A., Nussenzweig, M.C., and Choi, Y. (1997). TRAF2 is essential for JNK but not NF-kappaB activation and regulates lymphocyte proliferation and survival. *Immunity* 7, 703-713.
348. Dhanasekaran, D.N., and Reddy, E.P. (2008). JNK signaling in apoptosis. *Oncogene* 27, 6245-6251.
349. Huang, C., Jacobson, K., and Schaller, M.D. (2004). MAP kinases and cell migration. *J Cell Sci* 117, 4619-4628.
350. Varfolomeev, E.E., and Ashkenazi, A. (2004). Tumor necrosis factor: an apoptosis JuNKie? *Cell* 116, 491-497.
351. Ma, Y., Creanga, A., Lum, L., and Beachy, P.A. (2006). Prevalence of off-target effects in Drosophila RNA interference screens. *Nature* 443, 359-363.
352. Booker, M., Samsonova, A.A., Kwon, Y., Flockhart, I., Mohr, S.E., and Perrimon, N. (2011). False negative rates in Drosophila cell-based RNAi screens: a case study. *BMC Genomics* 12, 50.
353. Perkins, K.K., Admon, A., Patel, N., and Tjian, R. (1990). The Drosophila Fos-related AP-1 protein is a developmentally regulated transcription factor. *Genes Dev* 4, 822-834.
354. Perrimon, N., Lanjuin, A., Arnold, C., and Noll, E. (1996). Zygotic lethal mutations with maternal effect phenotypes in Drosophila melanogaster. II. Loci on the second and third chromosomes identified by P-element-induced mutations. *Genetics* 144, 1681-1692.

355. Bakal, C., Linding, R., Llense, F., Heffern, E., Martin-Blanco, E., Pawson, T., and Perrimon, N. (2008). Phosphorylation networks regulating JNK activity in diverse genetic backgrounds. *Science* 322, 453-456.
356. McDonald, J.A., Pinheiro, E.M., and Montell, D.J. (2003). PVF1, a PDGF/VEGF homolog, is sufficient to guide border cells and interacts genetically with Taiman. *Development* 130, 3469-3478.
357. Bianco, A., Poukkula, M., Cliffe, A., Mathieu, J., Luque, C.M., Fulga, T.A., and Rorth, P. (2007). Two distinct modes of guidance signalling during collective migration of border cells. *Nature* 448, 362-365.
358. Ragab, A., Buechling, T., Gesellchen, V., Spirohn, K., Boettcher, A.L., and Boutros, M. (2011). Drosophila Ras/MAPK signalling regulates innate immune responses in immune and intestinal stem cells. *EMBO J* 30, 1123-1136.
359. Kleino, A., Myllymaki, H., Kallio, J., Vanha-aho, L.M., Oksanen, K., Ulvila, J., Hultmark, D., Valanne, S., and Ramet, M. (2008). Pirk is a negative regulator of the Drosophila Imd pathway. *J Immunol* 180, 5413-5422.
360. Charroux, B., and Royet, J. (2009). Elimination of plasmacytes by targeted apoptosis reveals their role in multiple aspects of the Drosophila immune response. *Proc Natl Acad Sci U S A* 106, 9797-9802.
361. Adachi-Yamada, T., Fujimura-Kamada, K., Nishida, Y., and Matsumoto, K. (1999). Distortion of proximodistal information causes JNK-dependent apoptosis in Drosophila wing. *Nature* 400, 166-169.
362. Geuking, P., Narasimamurthy, R., and Basler, K. (2005). A genetic screen targeting the tumor necrosis factor/Eiger signaling pathway: identification of

- Drosophila* TAB2 as a functionally conserved component. *Genetics* 171, 1683-1694.
363. Schindler, A., and Foley, E. (2010). A functional RNAi screen identifies hexokinase 1 as a modifier of type II apoptosis. *Cell Signal* 22, 1330-1340.
364. Yin, Y., Wang, S., Sun, Y., Matt, Y., Colburn, N.H., Shu, Y., and Han, X. (2009). JNK/AP-1 pathway is involved in tumor necrosis factor-alpha induced expression of vascular endothelial growth factor in MCF7 cells. *Biomedicine & pharmacotherapy = Biomedecine & pharmacotherapie* 63, 429-435.
365. Beebe, K., Lee, W.C., and Micchelli, C.A. (2010). JAK/STAT signaling coordinates stem cell proliferation and multilineage differentiation in the *Drosophila* intestinal stem cell lineage. *Dev Biol* 338, 28-37.
366. McLeod, C.J., Wang, L., Wong, C., and Jones, D.L. (2010). Stem cell dynamics in response to nutrient availability. *Current biology : CB* 20, 2100-2105.
367. O'Brien, L.E., Soliman, S.S., Li, X., and Bilder, D. (2011). Altered modes of stem cell division drive adaptive intestinal growth. *Cell* 147, 603-614.
368. Choi, N.H., Lucchetta, E., and Ohlstein, B. (2011). Nonautonomous regulation of *Drosophila* midgut stem cell proliferation by the insulin-signaling pathway. *Proc Natl Acad Sci U S A* 108, 18702-18707.
369. Poernbacher, I., Baumgartner, R., Marada, S.K., Edwards, K., and Stocker, H. (2012). *Drosophila* pez acts in hippo signaling to restrict intestinal stem cell proliferation. *Current biology : CB* 22, 389-396.

370. Biteau, B., Karpac, J., Supoyo, S., Degennaro, M., Lehmann, R., and Jasper, H. (2010). Lifespan extension by preserving proliferative homeostasis in *Drosophila*. *PLoS Genet* 6, e1001159.
371. Gerber, H.P., Malik, A.K., Solar, G.P., Sherman, D., Liang, X.H., Meng, G., Hong, K., Marsters, J.C., and Ferrara, N. (2002). VEGF regulates haematopoietic stem cell survival by an internal autocrine loop mechanism. *Nature* 417, 954-958.
372. Lichtenberger, B.M., Tan, P.K., Niederleithner, H., Ferrara, N., Petzelbauer, P., and Sibilio, M. (2010). Autocrine VEGF signaling synergizes with EGFR in tumor cells to promote epithelial cancer development. *Cell* 140, 268-279.
373. Lee, S., Chen, T.T., Barber, C.L., Jordan, M.C., Murdock, J., Desai, S., Ferrara, N., Nagy, A., Roos, K.P., and Iruela-Arispe, M.L. (2007). Autocrine VEGF signaling is required for vascular homeostasis. *Cell* 130, 691-703.
374. Karlsson, L., Lindahl, P., Heath, J.K., and Betsholtz, C. (2000). Abnormal gastrointestinal development in PDGF-A and PDGFR-(alpha) deficient mice implicates a novel mesenchymal structure with putative instructive properties in villus morphogenesis. *Development* 127, 3457-3466.
375. Hanahan, D., and Weinberg, R.A. (2000). The hallmarks of cancer. *Cell* 100, 57-70.
376. Hermansson, M., Nister, M., Betsholtz, C., Heldin, C.H., Westermark, B., and Funai, K. (1988). Endothelial cell hyperplasia in human glioblastoma: coexpression of mRNA for platelet-derived growth factor (PDGF) B chain and PDGF receptor suggests autocrine growth stimulation. *Proc Natl Acad Sci U S A* 85, 7748-7752.

377. Hermanson, M., Funa, K., Hartman, M., Claesson-Welsh, L., Heldin, C.H., Westermark, B., and Nister, M. (1992). Platelet-derived growth factor and its receptors in human glioma tissue: expression of messenger RNA and protein suggests the presence of autocrine and paracrine loops. *Cancer Res* 52, 3213-3219.
378. Hermanson, M., Funa, K., Koopmann, J., Maintz, D., Waha, A., Westermark, B., Heldin, C.H., Wiestler, O.D., Louis, D.N., von Deimling, A., and Nister, M. (1996). Association of loss of heterozygosity on chromosome 17p with high platelet-derived growth factor alpha receptor expression in human malignant gliomas. *Cancer Res* 56, 164-171.
379. Beck, B., Driessens, G., Goossens, S., Youssef, K.K., Kuchnio, A., Caauwe, A., Sotiropoulou, P.A., Loges, S., Lapouge, G., Candi, A., Mascre, G., Drogat, B., Dekoninck, S., Haigh, J.J., Carmeliet, P., and Blanpain, C. (2011). A vascular niche and a VEGF-Nrp1 loop regulate the initiation and stemness of skin tumours. *Nature* 478, 399-403.

CHAPTER 8

Appendices

Table A1. Suppressors of 15 min PGN-induced P-JNK.

z-score analysis of dsRNA-mediated depletion of suppressors of 15 min PGN-induced dJNK phosphorylation. In-cell Western z-scores were calculated from P-JNK:f-actin values from S2 cells incubated with 15,683 dsRNAs and treated with PGN for 15 or 60 min. dsRNAs that modified 15 min PGN-induced P-JNK:f-actin z-scores above 1.96 (95% CI) are ordered from highest to lowest z-score. The fold change in dJNK phosphorylation relative to the plate median is shown alongside the z-score values for both 15 and 60 min time points. Each dsRNA is identified by its symbol and Celera Genome (CG) number or by its Heidelberg Drosophila Consortium identification number (HCDID). (15 - 15 min PGN exposure, 60 - 60min PGN exposure, z - z-score, Δ P - fold change in dJNK phosphorylation)

Symbol	FBGN	CG	HCDID	Function	15 z	15 Δ P	60 z	60 Δ P
key	41205	16910		Immune signaling	9.06	2.85	9.23	3.43
HDC03194			3194	Unknown	7.72	1.77	-0.33	0.92
Cka	44323	7392		Immune signaling	7.70	2.51	7.20	2.11
CG11526	35437	11526		Unknown	7.35	2.26	4.67	1.50
HDC12197			12197	Unknown	7.11	1.99	-1.10	1.00
ird5	24222	4201		Immune signaling	6.23	1.76	7.74	2.18
CG11799	36134	11799		DNA binding	5.89	1.58	1.56	0.84
porin	4363	6647		Other	5.88	1.41	5.50	1.28
HDC06860			6860	Unknown	5.85	1.76	-0.53	1.01
bun	10460	5461		DNA binding	5.75	1.54	2.05	1.20
CG15732	30385	15732		Other	5.72	1.74	-0.74	0.98
drpr	27594	2086		Signaling	5.56	1.60		1.23
HLHm3	2609	8346		DNA binding	5.37	2.00	2.54	0.92
RpII140	3276	3180		DNA binding	5.37	1.88	2.74	1.41
pnt	3118	17077		DNA binding	5.32	1.17	-1.34	0.70
CG14314	38581	14314		Unknown	5.24	1.50	1.76	1.34
cnk	21818	6556		Signaling	5.20	2.04	3.63	1.31
Taf1	10355	17603		DNA binding	5.08	1.65	0.38	1.04
ken	11236	5575		DNA binding	5.07	1.35	3.57	1.19
HDC02525			2525	Unknown	5.04	1.61	0.61	1.13
CG12264	32393	12264		Metabolism	5.02	1.65	-0.49	0.98
Pvr	32006	8222		Signaling	5.01	1.99	1.77	0.99
HDC02579			2579	Unknown	5.01	1.51	-0.59	1.01
CG3403	33094	3403		Unknown	5.00	2.44	0.24	1.37
UBL3	26076	9038		Other	4.96	1.72	6.13	1.29
CG10936	34253	10936		Unknown	4.92	1.30	0.57	1.15
Act5C	42	4027		Cytoskeleton	4.90	1.37	4.28	1.42

Table A1. Continued.

Symbol	FBGN	CG	HDCID	Function	15 z	15 ΔP	60 z	60 ΔP
RpP1	3274	4918		Translation	4.80	0.77	1.75	1.15
CG11848	39282	11848		Unknown	4.78	1.77	-0.66	1.01
CG15321	30150	15321		Unknown	4.76	1.41	0.71	1.04
HDC09403			9403	Unknown	4.73	1.60	1.68	1.18
gw	51992	31992		RNA binding	4.71	1.40	0.70	1.00
HDC12021			12021	Unknown	4.69	1.50	0.91	1.09
CG8828	33740	8828		Unknown	4.69	1.23	1.46	1.11
Elongin-C	23211	9291		RNA Binding	4.69	1.45	0.59	1.11
CG32681	52681	32681		Unknown	4.66	1.46	0.25	0.96
pims	34647	15678		Unknown	4.63	1.82	7.28	2.40
dm	472	10798		DNA binding	4.62	1.36	1.06	1.05
HDC08340			8340	Unknown	4.61	1.33	-0.04	1.00
CG8954	19890	8954		RNA binding	4.59	1.80	2.12	1.25
CG9864	34490	9864		Other	4.57	1.85	-0.08	1.13
CG13083	32789	13083		Unknown	4.57	1.35	-0.89	0.98
Mst35Ba	13300	4479		DNA binding	4.57	1.25	1.52	1.04
CG10158	31871	10158		Unknown	4.57	1.34	3.88	1.42
RplI215	3277	1554		DNA binding	4.52	1.91	1.65	1.29
dec-1	427	2175		Other	4.47	1.57	-0.90	1.00
Src42A	4603	7873		Signaling	4.31	1.35	2.30	1.25
HDC05820			5820	Unknown	4.24	1.46	-1.12	0.99
HDC10149			10149	Unknown	4.24	1.29	2.05	1.14
HDC00113			113	Unknown	4.24	1.39	-0.18	1.00
HDC02195			2195	Unknown	4.23	1.66	1.40	1.24
Acox57D-d	34629	9709		Metabolism	4.23	1.40	1.57	0.98
kto	1324	8491		RNA Binding	4.23	1.28	2.05	1.19
Pxd	4577	3477		Other	4.23	2.20	0.64	1.51
Rpb10	39218	13628		DNA binding	4.23	1.42	-0.82	0.99
HDC06790			6790	Unknown	4.20	1.70	-0.92	0.95
RhoGAP18 B	30986	7481		Signaling	4.20	1.42	3.12	1.29
CG4729	36623	4729		Metabolism	4.19	1.34	4.63	1.35
CG12263	34346	12263		Metabolism	4.17	1.60	1.96	1.29
CG17494	40011	12002		Unknown	4.16	1.47	2.38	1.27
Pez	31799	9493		Signaling	4.12	1.57	1.54	1.11
CG15674	34642	15674		Unknown	4.07	1.61	0.75	1.18
CG4320	29840	4320		Signaling	4.07	1.30	3.48	1.21

Table A1. Continued.

Symbol	FBGN	CG	HDCID	Function	15 z	15 ΔP	60 z	60 ΔP
MED19	36761	5546		DNA binding	4.06	1.55	2.40	1.22
CG12663	29961	12663		Unknown	4.06	1.59	-1.23	1.01
CG18172	35261	2086		Signaling	4.03	1.35	2.58	1.17
dome	43903	14226		Signaling	3.99	1.27	1.64	1.16
Ca-alpha1T	29846	15899		Other	3.96	1.28	-1.47	0.79
CG3176	29524	3176		Unknown	3.94	1.67	-1.04	0.98
igl	13467	18285		Unknown	3.93	1.33	1.43	1.14
Rac2	14011	8556		Signaling	3.93	1.27	1.48	1.02
CG13363	25639	13363		Other	3.92	1.14	4.00	1.22
mthl7	35847	7476		Signaling	3.89	1.26	0.28	0.94
l(3)mbt	2441	5954		DNA binding	3.88	1.68	0.03	1.28
CG8446	34089	8446		Other	3.86	1.53	0.84	0.97
Rpl18	3275	1163		DNA binding	3.86	1.44	1.16	1.16
RfC40	15287	14999		DNA binding	3.83	1.34	0.67	1.10
HDC05815			5815	Unknown	3.81	1.52	-1.31	0.96
HDC11835			11835	Unknown	3.81	1.26	0.06	0.94
RpP2	2593	4087		Translation	3.80	1.62	1.38	1.05
CG32000	52000	32000		Metabolism	3.76	1.23	3.14	1.29
CG32690	52690	32690		Unknown	3.75	1.29	-1.10	0.98
CG3891	35993	3891		DNA binding	3.70	1.52	2.55	1.35
CG17233	36958	17233		Unknown	3.70	1.33	-0.19	0.96
CG5360	34873	5360		Unknown	3.67	1.14	1.26	1.14
CG31047	51047	31047		Unknown	3.66	1.49	0.84	1.02
HDC17826			17826	Unknown	3.65	1.33	1.41	0.96
CG6280	33866	6280		Unknown	3.65	1.30	0.27	1.06
Trf2	26758	18009		DNA binding	3.64	1.29	2.18	1.20
CG10189	32793	10189		Unknown	3.63	1.43	-0.85	1.00
HDC10185			10185	Unknown	3.63	1.25	1.40	1.07
CG4119	28474	4119		RNA binding	3.62	1.43	2.24	1.23
CG14782	25381	14782		Cytoskeleton	3.61	1.44	-0.03	1.02
CG11132	34537	11132		DNA binding	3.61	1.74	1.91	1.38
HDC17828			17828	Unknown	3.60	1.40	1.19	0.95
Taf6	10417	32211		DNA binding	3.59	1.53	1.61	1.22
cnc	338	17894		DNA binding	3.58	1.47	2.70	1.34
CG11984	37655	11984		Other	3.57	1.40	2.69	1.13
Doa	53553	31049		Signaling	3.57	1.53	1.65	1.12

Table A1. Continued.

Symbol	FBGN	CG	HDCID	Function	15 z	15 ΔP	60 z	60 ΔP
HDC04702			4702	Unknown	3.56	1.37	0.66	1.14
Bx	242	6500		DNA binding	3.56	1.37	2.96	1.28
HDC13104			13104	Unknown	3.51	1.28	0.22	0.99
CG5757	34299	5757		Metabolism	3.51	1.47	0.50	1.04
Rpb11	32634	6840		DNA binding	3.49	1.32	1.28	1.17
CG7215	38571	32920		Unknown	3.49	1.28	1.00	1.05
CG9663	31516	9663		Other	3.48	1.38	0.36	0.90
HDC00888			888	Unknown	3.48	1.42	1.43	1.19
CG8771	33766	8771		Unknown	3.48	1.08	2.99	1.08
Iz	2576	1689		DNA binding	3.47	1.24	0.54	0.94
Dref	15664	5838		DNA binding	3.47	1.22	0.72	1.02
HDC19487			19487	Unknown	3.46	1.26	1.61	0.95
CG31739	51739	31739		RNA binding	3.46	1.61	-0.08	1.11
CG10225	39110	10225		Other	3.45	1.43	1.83	1.21
HDC00403			403	Unknown	3.45	1.31	-1.56	0.83
HDC00897			897	Unknown	3.45	1.49	-0.14	1.05
Ras85D	3205	9375		Signaling	3.44	1.42	0.72	1.03
HDC08321			8321	Unknown	3.44	1.17	0.25	0.96
Tom40	16041	12157		Other	3.42	1.62	1.32	1.16
Eip74EF	567	32180		DNA binding	3.42	1.32	2.51	1.19
CG15121	34456	15121		Unknown	3.42	1.39	-0.76	0.97
B52	4587	10851		RNA binding	3.42	1.27	2.63	1.29
CG12341	33550	12341		Unknown	3.41	1.08	0.04	0.81
CG14313	38579	14313		Unknown	3.41	1.50	4.46	1.72
mys	4657	1560		Cytoskeleton	3.40	1.39	1.59	0.97
CG6735	36472	6735		Cytoskeleton	3.40	1.71	2.16	1.26
MED10	36581	5057		DNA binding	3.39	1.52	0.72	1.10
HDC09508			9508	Unknown	3.38	1.30	0.65	1.00
maf-S	34534	9954		DNA binding	3.38	1.43	2.03	1.10
CG12923	33461	12923		Unknown	3.36	1.26	0.14	0.94
CG9304	34674	9304		Unknown	3.36	1.40	4.28	1.22
HDC08330			8330	Unknown	3.35	1.20	-0.16	0.92
srp	3507	3992		DNA binding	3.35	1.15		0.65
CG8517	34472	8517		Metabolism	3.33	1.60	0.62	1.12
HDC14726			14726	Unknown	3.33	1.39	-0.19	0.90
HDC09514			9514	Unknown	3.33	1.54	-0.74	0.98

Table A1. Continued.

Symbol	FBGN	CG	HDCID	Function	15 z	15 ΔP	60 z	60 ΔP
CG15119	34430	15119		Unknown	3.32	1.46	-1.27	0.84
zf30C	22720	3998		DNA binding	3.31	1.44	-0.22	0.82
Hrb98DE	1215	9983		RNA binding	3.31	1.60	0.98	1.08
CG8057	33383	8057		Signaling	3.31	1.53	1.84	1.10
HDC02034			2034	Unknown	3.30	1.30	1.24	1.12
CG15324	29966	15324		Other	3.28	1.50	-1.28	0.97
Act57B	44	10067		Cytoskeleton	3.28	1.20	4.28	1.13
HDC14831			14831	Unknown	3.27	1.17	1.35	1.05
Taf12	11290	17358		DNA binding	3.27	1.63	-0.24	1.07
CG1910	22349	1910		Unknown	3.26	1.30	1.62	1.09
thr	3701	5785		Unknown	3.25	1.42	-0.89	0.97
CG9394	34588	9394		Unknown	3.24	1.42	1.66	1.11
Tektin-C	35638	10541		Cytoskeletal	3.24	1.78	0.53	1.12
HDC03047			3047	Unknown	3.24	1.46	-0.61	1.01
CG7808	39713	7808		Translation	3.23	1.45	0.33	1.10
CG12050	32915	12050		Unknown	3.22	1.16	3.17	1.00
Rpt3	28686	16916		Proteolysis	3.20	1.41	-1.13	0.93
sec23	37357	1250		Signaling	3.19	1.51	-0.29	1.10
HDC10130			10130	Unknown	3.19	1.30	1.92	1.21
scaf6	52168	32168		RNA binding	3.19	1.13	3.41	1.09
CG32817	52817	32817		Unknown	3.18	1.28	-0.57	1.04
if	1250	9623		Signaling	3.18	1.42	0.59	1.08
CG3476	31881	3476		Metabolism	3.18	1.92	0.90	1.52
CG4631	32590	4631		Unknown	3.17	1.22	-0.14	1.07
CG14160	36066	14160		Unknown	3.16	1.15	1.55	1.13
CG16865	28919	16865		Unknown	3.15	1.17	1.22	1.15
CG11245	30388	11245		Unknown	3.15	1.14	2.01	0.93
spz	3495	6134		Signaling	3.15	1.20	1.12	1.14
CG13609	39170	13609		Unknown	3.14	1.25	-0.56	0.83
CG30217	50217	30217		Unknown	3.13	1.19	1.20	1.01
CG13802	35330	13802		Unknown	3.13	1.19	1.61	1.06
CG7177	37098	7177		Signaling	3.12	1.45	2.33	1.35
HDC09397			9397	Unknown	3.12	1.36	1.38	1.03
HDC11912			11912	Unknown	3.12	1.45	-1.49	0.95
HDC00497			497	Unknown	3.12	1.33	1.09	1.15
CG11321	31857	11321		Unknown	3.12	1.32	1.48	1.10

Table A1. Continued.

Symbol	FBGN	CG	HDCID	Function	15 z	15 ΔP	60 z	60 ΔP
CG1244	35357	1244		Unknown	3.10	1.48	2.40	1.27
CG13675	35845	13675		Unknown	3.09	1.33	0.55	1.02
fidipidine	25519	7773		Other	3.09	1.64	-0.38	1.03
CG3731	38271	3731		Proteolysis	3.08	1.06	1.00	1.01
CG5746	39186	5746		Unknown	3.08	1.23	0.06	1.12
Pvf2	31888	13780		Signaling	3.06	1.50	-0.96	1.03
kay	1297	15509		DNA binding	3.06	1.27	3.56	1.48
CG9895	34810	9895		DNA binding	3.06	1.38	-0.84	0.92
CG18545	37812	18545		Unknown	3.05	1.13	2.74	1.13
CG14722	37943	14722		Unknown	3.04	1.10	1.71	1.09
HDC17852			17852	Unknown	3.04	1.33	1.35	0.96
Appl	108	7727		Unknown	3.01	1.50	1.72	1.27
CG11227	31139	11227		Unknown	3.01	1.26	0.85	1.09
CG12681	29730	12681		Unknown	3.01	1.47	-0.62	1.03
rtet	28468	5760		Other	3.00	1.42	0.57	1.03
CG9523	31812	9523		Unknown	3.00	1.30	2.69	1.22
CG2083	35376	2083		Unknown	2.99	1.32	0.22	0.84
RpL1	3279	5502		Translation	2.99	1.31	1.98	0.99
CG8260	30684	8260		Unknown	2.98	1.17	0.12	0.94
CG2652	25838	2652		Unknown	2.96	1.40	-1.90	0.91
mRpL-CI-B8	34893	5479		Translation	2.96	1.25	3.05	1.18
HDC17815			17815	Unknown	2.95	1.34	0.33	0.97
HDC14028			14028	Unknown	2.95	1.15	1.23	1.00
CG13845	38971	13845		Unknown	2.95	1.08	0.22	1.04
Hem	11771	5837		Signaling	2.95	1.45	-0.02	0.94
CG4896	31319	4896		RNA binding	2.94	1.62	2.69	1.27
CG31394	51394	31394		Unknown	2.94	1.32	0.58	1.16
HDC19488			19488	Unknown	2.94	1.25	1.49	0.95
CG33296	53296	33296		Unknown	2.94	1.28	1.47	1.21
CG32104	52104	32104		Unknown	2.94	1.36	-0.21	0.96
CG1553	33224	1553		Unknown	2.94	1.31	-0.74	1.05
CG15488	32440	15488		Unknown	2.94	1.25	1.89	1.05
HDC14817			14817	Unknown	2.93	1.19	2.81	1.15
Act42A	43	12051		Cytoskeleton	2.92	1.08	4.13	1.00
CG30034	50034	30034		Unknown	2.92	1.36	0.21	1.00
SCAR	41781	4636		Cytoskeleton	2.90	1.19	1.50	1.09

Table A1. Continued.

Symbol	FBGN	CG	HDCID	Function	15 z	15 ΔP	60 z	60 ΔP
PQBP-1	51369	31369		Unknown	2.89	1.13	0.35	0.94
CG18166	29526	18166		Unknown	2.88	1.26	-0.58	1.02
HDC09406			9406	Unknown	2.88	1.30	0.22	0.92
CG9122	35187	9122		Metabolism	2.87	1.52	0.64	1.02
dap	10316	1772		Signaling	2.87	1.45	0.55	1.04
CG3777	24989	3777		Unknown	2.87	1.24	0.63	1.09
HDC07441			7441	Unknown	2.87	1.36	-1.35	0.98
Arp53D	11743	5409		Cytoskeleton	2.87	1.13	1.57	0.94
CG4612	35016	4612		RNA binding	2.87	1.09	1.32	1.01
Arc92	38760	12254		DNA binding	2.85	1.02		0.55
Obp58d	34770	13519		Other	2.85	1.09	0.95	1.04
HDC15864			15864	Unknown	2.85	1.12	0.90	0.93
HDC12184			12184	Unknown	2.84	1.29	1.07	0.99
DI	463	3619		Signaling	2.84	1.06	3.40	1.22
HDC13103			13103	Unknown	2.83	1.30	0.29	0.98
HDC08318			8318	Unknown	2.83	1.19	-0.35	0.91
CG12255	36618	12255		Unknown	2.83	1.08	1.05	0.99
I(2)k01209	22029	4798		Metabolism	2.82	1.06	2.44	1.10
HDC07043			7043	Unknown	2.82	1.13	0.54	1.00
CG13041	36605	13041		Unknown	2.81	1.25	-1.28	0.98
dsf	15381	9019		DNA binding	2.81	1.40	-0.69	0.92
CG16817	37728	16817		Unknown	2.80	1.14	1.93	1.24
CG6369	39260	6369		RNA binding	2.80	1.46	1.54	1.23
RluA-2	32256	6187		Metabolism	2.79	1.34	1.82	1.13
ear	26441	4913		DNA binding	2.78	1.25	0.99	1.07
HDC07585			7585	Unknown	2.78	1.19	0.57	1.06
so	3460	11121		DNA binding	2.78	1.34	1.15	1.12
CG8509	30696	8509		Signaling	2.78	1.60	1.76	1.18
HDC06322			6322	Unknown	2.78	1.23	2.10	1.14
CG15006	35510	15006		Unknown	2.77	1.13	0.84	1.03
HDC17406			17406	Unknown	2.77	1.10	0.48	1.01
TfIIE&bgr;	15829	1276		DNA binding	2.76	1.27	2.90	1.35
mRpL21	36853	9730		Translation	2.75	1.27	1.23	1.00
HDC14730			14730	Unknown	2.74	1.38	-1.37	0.92
CkII&agr;-i1	15025	6215		Unknown	2.74	1.55	0.67	1.15
CG5800	30855	5800		RNA binding	2.73	1.20	0.06	1.04

Table A1. Continued.

Symbol	FBGN	CG	HDCID	Function	15 z	15 ΔP	60 z	60 ΔP
CG9862	34646	9862		RNA binding	2.72	1.51	-0.04	1.05
eIF-2&bgr;	4926	4153		Translation	2.72	1.56	1.18	1.20
CG11843	39630	11843		Proteolysis	2.72	1.39	0.78	1.04
AlstR	28961	2872		signaling	2.71	1.54	-3.14	0.78
pAbp	3031	5119		RNA binding	2.71	1.21	4.48	1.39
Pomp	32884	9324		Proteolysis	2.71	1.58	5.65	1.95
CG15185	37449	15185		Unknown	2.71	1.13	1.51	1.04
Mov34	2787	3416		Proteolysis	2.71	1.23	1.92	1.12
CG18446	33458	18446		Unknown	2.71	1.23	-0.11	0.97
HDC19486			19486	Unknown	2.70	1.08	1.30	0.94
CG10320	34645	10320		Other	2.70	1.14	0.33	1.07
CG12175	30502	12175		DNA binding	2.70	1.23	1.07	0.93
PRL-1	24734	4993		Signaling	2.70	1.18	0.47	1.01
CG11260	39912	11260		Unknown	2.70	1.40	-0.55	1.00
CG8885	31656	8885		Metabolism	2.70	1.50	-0.09	1.07
HDC17312			17312	Unknown	2.70	1.14	1.30	1.06
CG7366	35855	7366		Unknown	2.69	1.26	-0.01	0.91
CG33346	53346	33346		Unknown	2.69	1.38	1.00	1.05
Hexo2	41629	1787		Metabolism	2.69	1.34	2.39	1.19
CG3838	32130	3838		Unknown	2.68	1.37	-3.08	0.75
HDC10201			10201	Unknown	2.68	1.19	0.56	1.00
HDC13864			13864	Unknown	2.68	1.19	-0.05	0.99
HDC15843			15843	Unknown	2.68	1.09	1.03	0.94
scaf6	53522	6615		RNA binding	2.68	1.03	1.94	1.03
CG12744	33459	12744		Unknown	2.67	1.20	0.86	0.96
HDC19511			19511	Unknown	2.67	1.36	0.01	1.00
HDC14841			14841	Unknown	2.67	1.13	0.39	0.98
CG15326	29965	15326		Unknown	2.66	1.49	-1.17	0.99
mud	2873	12047		Unknown	2.65	1.16	0.96	1.25
Lasp	63485	3849		Cytoskeleton	2.65	1.21	0.40	1.11
bw	241	17632		Other	2.64	1.36	-0.32	1.00
HDC08316			8316	Unknown	2.63	1.19	-0.69	0.91
CG12582	37215	12582		Metabolism	2.62	1.25	0.59	1.02
CG13358	26874	13358		Unknown	2.62	1.21	0.01	0.98
CG30196	50196	30196		Unknown	2.61	1.09	1.31	1.07
CG10990	30520	10990		Unknown	2.60	1.25	0.60	1.21

Table A1. Continued.

Symbol	FBGN	CG	HDCID	Function	15 z	15 ΔP	60 z	60 ΔP
CG32058	52058	32058		Unknown	2.60	1.09	1.49	1.13
HDC07692			7692	Unknown	2.59	1.30	-0.81	1.03
Mes2	37207	11100		Unknown	2.59	1.35	1.68	1.10
CG13047	36594	13047		Unknown	2.59	1.08	2.01	1.14
HDC13099			13099	Unknown	2.59	1.33	0.06	0.91
CG15909	33090	15909		Unknown	2.59	1.36	-0.96	0.94
Arp66B	11744	7558		Cytoskeleton	2.58	1.13	3.28	1.12
CG12091	35228	12091		Signaling	2.58	1.37	0.03	0.99
rut	3301	9533		Signaling	2.58	1.35	-0.61	1.02
CG6674	36063	6674		Unknown	2.58	1.15	1.18	1.14
tun	50084	30084		Unknown	2.58	1.50	1.48	0.93
peb	3053	12212		DNA binding	2.57	1.41	0.90	1.17
CG31712	51712	31712		Unknown	2.56	1.18	0.13	0.97
CG32054	52054	32054		Other	2.56	1.17	0.57	1.09
HDC14728			14728	Unknown	2.56	1.29	0.03	0.96
CG10630	35608	10630		Unknown	2.56	1.30	0.80	1.13
CG2556	30396	2556		Unknown	2.55	1.18	0.63	1.01
Prosβ2	23174	3329		Proteolysis	2.55	1.77	1.08	1.52
Os-E	10403	11422		Signaling	2.55	1.14	0.73	0.97
Sra-1	38320	4931		Signaling	2.54	1.09	1.90	1.07
HDC19504			19504	Unknown	2.54	1.29	0.58	0.96
Cap-H2	37831	14685		Other	2.54	1.16	1.34	1.00
CG9293	32516	9293		DNA binding	2.52	1.15	0.51	0.82
CG8223	37624	8223		Unknown	2.52	1.04	1.62	1.02
Tbp-1	28684	10370		proteolysis	2.51	1.51	0.17	1.05
Mdr50	10241	8523		Other	2.51	1.58	0.15	1.23
CG9973	35378	9973		Unknown	2.50	1.13	1.30	1.10
Ets97D	4510	6338		DNA binding	2.50	1.43	0.15	1.12
CG8042	27554	8042		Unknown	2.50	1.22	-0.96	0.96
CG8066	38243	8066		Unknown	2.50	1.23	1.30	1.15
CG15894	29864	15894		Unknown	2.50	1.17	1.07	1.03
rl	3256	12559		Signaling	2.50	1.34	0.13	1.07
Pros25	10405	5266		Proteolysis	2.49	1.53	1.58	1.31
HDC17817			17817	Unknown	2.49	1.32	0.19	0.94
CG32755	52755	32755		Unknown	2.49	1.14	-0.35	0.88
UbcD6	4436	2013		Other	2.48	1.24	1.08	1.10

Table A1. Continued.

Symbol	FBGN	CG	HDCID	Function	15 z	15 ΔP	60 z	60 ΔP
CG6685	36062	6685		Unknown	2.48	1.17	0.85	1.12
CG31607	51607	31607		Unknown	2.48	1.01	0.88	1.00
msi	11666	5099		RNA binding	2.48	1.48	1.90	1.36
CG33203	53203	33203		Unknown	2.47	1.36	1.69	1.09
zormin	52311	33484		Unknown	2.47	1.26	2.36	1.18
HDC12190			12190	Unknown	2.47	1.26	0.35	0.97
CG1973	39692	1973		Signaling	2.46	1.00	1.46	0.92
NHP2	29148	5258		RNA binding	2.46	1.14	1.97	1.09
HDC06940			6940	Unknown	2.46	1.16	0.37	0.99
can	11569	6577		DNA binding	2.46	1.06	0.63	1.02
CG33187	53187	33187		Unknown	2.46	1.06	1.22	1.18
CG14194	30996	14194		Unknown	2.46	1.10	0.71	0.94
CG32946	52946	32946		Unknown	2.45	1.13	0.49	0.97
beat-Vb	38092	31298		Unknown	2.45	1.16	0.84	0.99
HDC17821			17821	Unknown	2.45	1.35	-0.49	0.97
Taf10b	26324	3069		DNA binding	2.45	1.10	1.52	1.07
HDC06591			6591	Unknown	2.44	1.20	0.52	1.03
CG12920	33481	12920		Unknown	2.44	1.34	-0.85	0.96
HDC06795			6795	Unknown	2.44	1.44	-0.91	0.98
smg	16070	5263		RNA binding	2.43	1.16	2.15	1.06
CG12119	30102	12119		Unknown	2.43	1.27	0.46	1.03
fne	40222	4396		RNA binding	2.43	1.28	0.71	1.13
HDC00033			33	Unknown	2.42	1.31	-2.48	0.76
slpr	30018	2272		Signaling	2.42	1.40	-0.09	0.97
HDC14799			14799	Unknown	2.42	1.33	-0.51	0.92
HDC14842			14842	Unknown	2.41	1.09	0.07	0.94
CG10752	36325	10752		Unknown	2.41	1.07	2.20	1.06
CG7763	40503	7763		Unknown	2.41	1.31	-1.23	0.94
Taf8	22724	7128		DNA binding	2.40	1.28	1.16	1.11
CG8501	33724	8501		Unknown	2.40	1.13	0.51	1.03
Rpn6	28689	10149		Proteolysis	2.40	1.10	5.02	1.44
Hsc70-1	1216	8937		Other	2.40	1.29	0.97	0.91
ss	3513	6993		DNA binding	2.40	1.28	3.91	1.25
HDC16223			16223	Unknown	2.39	1.38	0.06	0.97
HDC11436			11436	Unknown	2.39	1.15	0.58	1.00
HDC13111			13111	Unknown	2.39	1.26	-0.31	0.96

Table A1. Continued.

Symbol	FBGN	CG	HDCID	Function	15 z	15 ΔP	60 z	60 ΔP
CG13338	33867	13338		Unknown	2.39	1.25	0.12	1.09
HDC06912			6912	Unknown	2.39	1.30	-1.56	0.93
CG4367	38783	4367		Unknown	2.39	1.11	-0.17	0.98
TER94	24923	2331		Other	2.38	1.21	1.63	1.10
CG11575	39879	11575		Unknown	2.38	1.20	0.87	1.03
mus201	2887	32956		DNA binding	2.38	1.02	1.23	1.08
Pp2A-29B	5776	33297		Signaling	2.38	1.29	-0.22	0.96
CG18266	31724	18266		Unknown	2.38	1.12	0.71	1.04
ksr	15402	2899		Signaling	2.38	1.11	2.01	1.05
CG12069	39796	12069		Signaling	2.37	1.53	0.12	1.31
CG11486	35397	11486		Unknown	2.37	1.48	0.35	1.17
CG32368	52368	32368		Unknown	2.36	1.20	-0.07	1.00
CG9603	40529	9603		Metabolism	2.36	1.10	-0.17	0.94
CG3528	31430	3528		Unknown	2.36	1.22	1.46	1.23
snRNP70K	16978	8749		RNA binding	2.36	1.44	-0.54	1.09
Cip4	35533	15015		Signaling	2.36	1.23	1.65	1.34
HDC19521			19521	Unknown	2.36	1.42	0.30	1.09
CG4615	29935	4615		Unknown	2.36	1.11	0.57	1.12
CG12773	24365	12773		Other	2.35	1.22	1.33	1.19
CG13530	34777	13530		Unknown	2.35	1.11	1.76	1.14
CG13932	35259	13932		Unknown	2.35	1.06	0.24	0.92
CG14801	24988	14801		Metabolism	2.35	0.86	0.41	0.86
HDC20230			20230	Unknown	2.35	1.35	0.01	1.03
CG17540	40024	7371		RNA binding	2.34	1.25	1.82	1.24
v(2)k05816	42627	3524		Metabolism	2.34	1.38	0.02	0.96
CG17265	31488	17265		Unknown	2.34	1.14	-2.31	0.65
CG30264	50264	30264		Unknown	2.34	1.08	1.76	1.07
P5cr	15781	6009		Metabolism	2.33	1.31	1.02	1.08
CG6006	63649	6006		Other	2.33	1.11	2.79	1.32
Chd1	16132	3733		DNA binding	2.33	1.17	0.23	1.07
Trap19	40020	11023		DNA binding	2.33	1.13	2.56	1.29
CG12237	31048	12237		Unknown	2.33	1.52	-0.70	0.99
Gr59f	41234	33150		Signaling	2.32	0.99	1.74	1.07
mthl6	35789	16992		Signaling	2.32	1.23	-0.01	1.06
CG9650	29939	9650		DNA binding	2.32	1.16	1.75	0.90
CG9346	34572	9346		RNA binding	2.32	1.45	0.08	1.16

Table A1. Continued.

Symbol	FBGN	CG	HDCID	Function	15 z	15 ΔP	60 z	60 ΔP
CG7678	38613	7678		Other	2.32	1.28	0.04	1.13
Dot	15663	2788		Metabolism	2.32	1.28	1.25	1.04
CG6023	30912	6023		Unknown	2.32	1.06	1.22	1.04
CG1746	39830	1746		Metabolism	2.31	1.14	0.77	0.97
HDC07586			7586	Unknown	2.31	1.14	1.08	1.04
CG31044	51044	31044		Unknown	2.31	1.30	0.67	0.99
CG8710	33265	8710		Unknown	2.31	1.11	0.54	0.96
CG14998	35500	14998		Unknown	2.31	1.15	2.27	1.17
HDC19522			19522	Unknown	2.30	1.43	0.25	1.05
CG13198	33640	13198		Unknown	2.30	1.33	-0.23	0.98
CG7876	31000	7876		Other	2.30	1.25	-0.81	1.00
Su(Tpl)	14037	32217		DNA binding	2.29	1.13	2.74	1.29
CG13564	34973	13564		Unknown	2.29	1.11	0.61	1.00
Arc70	39923	1793		DNA binding	2.29	1.49	2.59	1.46
HDC16885			16885	Unknown	2.29	1.04	1.50	0.97
CG14520	39618	14520		Unknown	2.28	1.25	1.13	1.03
CG9350	34576	9350		Unknown	2.28	1.29	0.48	1.08
Rpt4	28685	3455		Proteolysis	2.28	1.58	2.28	1.62
Adar	26086	12598		RNA binding	2.28	1.30	-0.12	0.96
HDC09478			9478	Unknown	2.28	1.10	1.75	1.09
CG8290	26573	8290		DNA binding	2.27	1.04	1.19	0.96
CG1906	39672	1906		Signaling	2.26	1.22	0.48	1.04
HDC19473			19473	Unknown	2.26	1.22	0.96	0.99
HDC07589			7589	Unknown	2.26	1.09	1.29	1.00
insv	31434	3227		Unknown	2.26	1.14	2.29	1.20
CG7349	30975	7349		Metabolism	2.26	1.12	-0.40	0.93
CG9757	3060	9757		Unknown	2.25	1.20	0.45	1.16
Trap37	37359	1245		DNA binding	2.25	1.33	0.76	1.12
eIF2B-ε	23512	3806		DNA binding	2.24	1.25	-0.42	0.99
HDC14720			14720	Unknown	2.24	1.28	-0.49	0.91
Mlp84B	14863	1019		Unknown	2.24	1.18	1.09	1.08
Nap1	15268	5330		DNA binding	2.24	1.32	-0.70	0.96
HDC02627			2627	Unknown	2.24	1.18	-0.37	0.93
lig	20279	8715		Unknown	2.23	0.99	1.34	1.02
Egfr	3731	10079		Signaling	2.23	1.15	1.67	1.32
wibg	34918	30176		Unknown	2.23	1.05	0.44	0.98

Table A1. Continued.

Symbol	FBGN	CG	HDCID	Function	15 z	15 ΔP	60 z	60 ΔP
mRNA-capping-enzyme	30556	1810		RNA binding	2.23	1.22	4.60	1.51
CG14683	37822	14683		Unknown	2.23	1.14	1.39	1.05
Gp150	13272	5820		Signaling	2.23	1.23	0.23	1.01
CG12842	33131	12842		Unknown	2.23	1.12	0.79	1.01
CG18397	32723	18397		Unknown	2.22	1.14	0.19	0.95
dnk	22338	5452		Metabolism	2.22	1.13	2.34	1.14
CG1458	62442	1458		Unknown	2.22	1.32	0.85	1.01
HDC12145			12145	Unknown	2.22	1.16	1.33	1.05
ik2	28633	2615		Signaling	2.22	1.18	2.99	1.20
CG15263	28853	15263		Unknown	2.22	1.08	1.74	1.07
CG14972	35450	14972		Unknown	2.22	1.21	0.66	1.08
HDC13135			13135	Unknown	2.21	1.30	-0.29	0.94
CG8877	33688	8877		RNA binding	2.21	1.29	0.15	0.96
CG7181	37097	7181		Metabolism	2.21	1.12	1.31	1.05
CG10419	36850	10419		Unknown	2.21	1.10	1.61	1.08
CG14853	38246	14853		Unknown	2.20	1.18	0.74	0.96
CG13283	32613	13283		Unknown	2.19	1.14	1.27	1.14
CG12584	37257	12584		Unknown	2.19	1.30	0.44	1.11
CG32673	52673	32673		Signaling	2.19	1.24	-1.04	1.00
CG32148	47338	32148		Unknown	2.19	1.09	1.03	1.08
Os9	14000	10658		Unknown	2.19	1.14	0.81	1.03
CG3934	37783	3934		Unknown	2.19	1.16	-0.21	1.03
CG13288	35648	13288		Unknown	2.18	1.11	0.77	0.98
CG2082	27608	2082		Unknown	2.18	1.31	0.13	0.88
CG14909	38458	14909		Metabolism	2.18	1.23	-0.73	0.99
CG32053	52053	32053		Unknown	2.18	1.09	0.65	1.05
CG5375	32221	5375		Unknown	2.18	1.16	1.66	1.02
CG5454	38667	5454		RNA binding	2.18	1.12	1.22	1.14
Scg&agr;	32013	7851		Cytoskeleton	2.18	1.77	5.58	2.34
Hsc70-4	1219	4264		Other	2.18	1.29	0.85	0.95
HDC17108			17108	Unknown	2.17	1.01	1.28	1.01
CG15403	31504	15403		Unknown	2.17	1.06	1.09	1.02
csul	15925	3730		Signaling	2.17	0.99	1.56	0.96
CG11971	22347	11971		Unknown	2.17	1.06	1.81	1.13
CG3708	40345	3708		DNA binding	2.17	1.14	0.26	0.98

Table A1. Continued.

Symbol	FBGN	CG	HDCID	Function	15 z	15 ΔP	60 z	60 ΔP
CG18748	42105	18748		Unknown	2.17	1.32	0.69	1.10
e(y)1	617	6474		DNA binding	2.17	1.16	3.33	1.14
Os-C	10401	3250		Unknown	2.17	1.04	0.77	0.95
CG3713	40343	3713		Unknown	2.16	1.06	-0.01	0.96
Gr59e	41233	33151		Unknown	2.16	1.05	1.25	1.03
CG31238	51238	31238		Unknown	2.16	1.00	1.19	1.01
puc	4210	7850		Immune signaling	2.16	1.74	5.23	2.31
HDC05276			5276	Unknown	2.15	1.17	0.26	1.04
CG32638	52638	32638		Unknown	2.15	1.09	1.50	1.00
CG5048	36437	5048		Unknown	2.15	1.30	0.68	1.11
Her	30899	5927		DNA binding	2.15	1.02	0.27	0.96
HDC18862			18862	Unknown	2.15	1.11	1.17	1.02
HDC03592			3592	Unknown	2.14	1.17	0.92	1.02
Cyp9c1	15040	3616		Metabolism	2.14	1.00	1.75	1.08
CG12493	35571	12493		Unknown	2.13	1.28	-0.15	1.06
CG33339	53339	33339		Unknown	2.13	1.12	0.54	0.95
HDC16673			16673	Unknown	2.13	1.43	-1.33	0.89
HDC13081			13081	Unknown	2.12	1.35	-0.82	0.96
CG32102	52102	32102		Unknown	2.12	1.02	1.42	1.00
Tsp29Fb	32075	9496		Unknown	2.12	1.27	0.11	0.98
CG32365	52365	32365		Unknown	2.12	1.26	-0.44	0.96
CG15627	31634	15627		Signaling	2.12	1.12	0.75	1.10
Alas	20764	3017		Metabolism	2.11	1.22	1.32	0.94
CG32428	52428	32428		Unknown	2.11	1.05	1.70	1.02
CG9098	31762	9098		Signaling	2.11	1.26	0.04	0.87
CG6121	26080	6121		DNA binding	2.10	1.22	2.57	1.26
HDC05924			5924	Unknown	2.10	1.30	0.34	1.10
CG33309	53309	33309		Unknown	2.10	1.21	0.53	0.99
CG30495	50495	30495		Metabolism	2.10	1.34	-0.92	0.91
HDC04697			4697	Unknown	2.10	1.08	1.54	1.09
CG7498	40833	7498		Unknown	2.10	1.29	0.51	1.06
bonsai	26261	4207		DNA binding	2.10	1.07	-0.29	0.98
HDC15882			15882	Unknown	2.09	1.04	0.82	0.92
CG14305	38630	14305		Signaling	2.09	1.11	1.15	1.10
CG4461	35982	4461		Unknown	2.09	1.18	1.30	1.15
CG32745	52745	32745		DNA binding	2.09	1.26	-0.90	1.01

Table A1. Continued.

Symbol	FBGN	CG	HDCID	Function	15 z	15 ΔP	60 z	60 ΔP
zip	5634	15792		Cytoskeletal	2.09	1.30	1.13	1.17
CG18586	35642	18586		Metabolism	2.09	1.32	-1.11	1.13
HDC17872			17872	Unknown	2.09	1.30	0.27	0.99
CG9561	31203	16788		RNA binding	2.08	1.26	0.78	1.01
CG30270	61435	30270		Unknown	2.08	1.07	0.97	1.05
CG31427	51427	31427		Proteolysis	2.08	1.30	0.73	1.00
AGO1	26611	6671		Other	2.08	1.32	0.13	1.02
HDC06022			6022	Unknown	2.08	1.06	1.35	1.08
HDC08262			8262	Unknown	2.08	1.31	-1.04	1.01
slmo	29161	9131		Unknown	2.07	1.20	2.45	1.31
CG13474	36439	13474		Unknown	2.07	1.20	-0.22	1.00
janB	1281	7931		Unknown	2.07	1.45	-0.50	0.95
CG1287	37506	1287		Unknown	2.07	1.20	0.97	1.11
mit(1)15	4643	9900		Other	2.07	1.34	-1.57	0.98
CG33260	53260	33260		Unknown	2.07	1.25	0.12	1.05
Sr-CII	20377	8856		Other	2.07	1.35	1.60	1.13
CG5742	34304	5742		Unknown	2.07	1.12	0.63	1.10
alien	13746	9556		Proteolysis	2.07	1.20	1.27	0.94
CG5107	39342	5107		Unknown	2.06	1.17	-1.18	0.89
CG17855	32124	17855		Unknown	2.06	1.16	0.33	1.07
CG14635	29535	14635		Unknown	2.06	1.10	0.46	0.98
CG15256	28880	15256		Unknown	2.06	1.23	1.30	1.04
CG8550	33742	8550		Other	2.06	1.14	1.63	1.08
Pros26	2284	4097		Proteolysis	2.06	1.28	1.74	1.19
HDC07058			7058	Unknown	2.06	1.14	-0.29	1.00
CG14545	40602	14545		Unknown	2.06	1.09	0.52	0.91
CG9086	30809	9086		Other	2.06	1.55	0.48	1.12
CG17666	36311	17666		Unknown	2.06	1.04	1.11	1.00
msta	53548	32800		Unknown	2.06	1.37	-1.07	1.01
CG13167	33706	13167		Metabolism	2.05	1.27	-1.47	0.78
CG31787	51787	31787		Unknown	2.05	1.06	0.37	1.07
Rpn1	28695	7762		Proteolysis	2.05	1.31	1.09	1.20
HDC14836			14836	Unknown	2.05	1.05	0.13	0.95
org-1	21767	11202		DNA binding	2.05	1.16	0.21	0.88
l(3)82Fd	13576	32464		Unknown	2.05	1.18	0.57	1.00
tim	14396	3234		Other	2.05	1.10	1.18	0.93

Table A1. Continued.

Symbol	FBGN	CG	HDCID	Function	15 z	15 ΔP	60 z	60 ΔP
CG31423	51423	31423		Unknown	2.05	1.15	0.77	1.09
CG12581	37213	12581		Unknown	2.05	1.26	0.77	1.05
CG9822	34623	9822		Unknown	2.05	1.25	0.55	1.08
CG3065	34946	3065		DNA binding	2.04	1.19	1.92	1.22
CG6479	36710	6479		Unknown	2.04	1.02	1.18	0.98
CG13800	35338	13800		Unknown	2.04	1.03	1.76	1.03
ine	11603	15444		Other	2.04	1.24	0.00	0.95
Taf4	10280	5444		DNA binding	2.04	1.42	2.36	1.17
CG9641	31483	9641		Unknown	2.04	1.12	1.03	1.07
CG8310	40377	8310		Other	2.04	1.49	1.94	1.08
Pros26.4	15282	5289		Proteolysis	2.03	1.34	1.01	1.32
Cyp6d5	38194	3050		Metabolism	2.03	1.00	1.68	0.98
CG6124	39484	6124		Unknown	2.03	1.07	1.17	1.02
Gr22e	45497	31936		Unknown	2.03	1.07	0.65	1.12
CG31638	51638	31638		Unknown	2.03	1.09	1.24	1.09
CG33182	53182	33182		Unknown	2.03	1.00	1.49	1.02
zfh2	4607	1449		DNA binding	2.02	1.31	0.38	1.08
Ikb1	38167	9374		Signaling	2.02	1.32	0.41	1.00
HDC07059			7059	Unknown	2.02	1.18	-0.58	0.99
CG2249	40773	2249		Metabolism	2.02	1.16	-0.65	0.92
CG14113	40814	14113		Unknown	2.01	1.04	1.44	1.05
CG30265	50265	30265		Other	2.01	1.09	1.94	1.12
CG14223	31053	14223		Unknown	2.01	1.10	-0.06	1.04
CG31128	51128	31128		Unknown	2.01	1.02	1.07	0.95
CG32016	52016	32016		Unknown	2.01	1.37	-0.87	0.99
CG2079	29944	2079		Signaling	2.01	1.33	-1.06	0.78
CG17612	31597	17612		DNA binding	2.01	1.28	-0.33	0.89
CG14384	38097	14384		Unknown	2.00	1.16	-0.12	0.93
HDC09412			9412	Unknown	2.00	1.22	0.04	0.92
dpr12	33044	14469		Unknown	2.00	1.12	2.02	1.06
Med24	40339	3034		Unknown	2.00	1.04	1.69	1.04
CG11872	37806	11872		Unknown	2.00	1.13	0.28	1.01
HDC04700			4700	Unknown	2.00	1.54	-0.76	1.01
CG4629	31299	4629		Signaling	2.00	1.04	-0.17	1.03
RplI33	26373	7885		DNA binding	2.00	1.29	1.68	1.26
CG7236	31730	7236		Signaling	1.99	1.25	1.95	1.22

Table A1. Continued.

Symbol	FBGN	CG	HDCID	Function	15 z	15 ΔP	60 z	60 ΔP
CG4945	34137	4945		Signaling	1.99	0.93	-0.11	1.08
CG7071	38949	7071		Unknown	1.99	1.03	1.18	1.00
HDC00770			770	Unknown	1.99	1.08	-0.27	0.92
CG5783	32670	5783		Unknown	1.99	1.12	0.83	0.97
CG32937	52937	32937		Unknown	1.99	1.12	1.37	1.12
HDC02900			2900	Unknown	1.99	1.32	-1.06	1.04
CG32297	52297	32297		RNA binding	1.99	1.35	-0.21	1.08
HDC12189			12189	Unknown	1.98	1.17	0.69	0.98
Acyp2	38363	18505		Unknown	1.98	1.10	0.73	0.98
CG5604	32208	5604		Other	1.98	1.24	1.54	1.28
east	10110	4399		Unknown	1.98	1.25	1.25	1.27
Fur1	4509	10772		Proteolysis	1.97	1.23	0.46	1.17
CG11110	34535	11110		Proteolysis	1.97	1.25	1.66	1.14
CG31213	51213	31213		Other	1.97	1.02	0.59	1.02
CG11050	31836	11050		Unknown	1.97	1.26	0.81	1.07
CG32553	52553	32553		Unknown	1.97	1.03	-0.11	0.95
CG14633	29537	14633		Unknown	1.97	1.19	-0.17	0.99
hay	1179	8019		DNA binding	1.97	1.40	-0.65	0.98
skl	36786	13701		Signaling	1.97	1.05	0.38	0.93
CG8120	37675	8120		DNA binding	1.97	1.34	2.12	1.08
CG31082	51082	31082		Unknown	1.96	1.05	0.85	1.03
HDC20240			20240	Unknown	1.96	1.30	1.74	1.04
CG16941	38464	16941		RNA binding	1.96	1.16	0.89	1.15
CG5694	32197	5694		Unknown	1.96	1.06	0.84	1.08
Trap170	35145	12031		DNA binding	1.96	1.43	1.35	1.24

Table A2. Suppressors of 60 min PGN-induced P-dJNK.

z-score analysis of dsRNA-mediated depletion of suppressors of 60 min PGN-induced dJNK phosphorylation. In-cell Western z-scores were calculated from P-JNK:f-actin values from S2 cells incubated with 15,683 dsRNAs and treated with PGN for 15 or 60 min. dsRNAs that modified 60 min PGN-induced P-JNK:f-actin z-scores above 1.96 (95% CI) are ordered from highest to lowest z-score. The fold change in dJNK phosphorylation relative to the plate median is shown alongside the z-score values for both 15 and 60 min time points. Each dsRNA is identified by its symbol, Celera Genome (CG) number, Heidelberg Drosophila Consortium identification number (HCDID) and general function. (15min - 15 min PGN exposure, 60min - 60min PGN exposure, Δ P-JNK - fold change in dJNK phosphorylation)

Symbol	FBGN	CG	HCDID	Function	60min z-score	60min Δ P-JNK	15min z-score	15min Δ P-JNK
key	41205	16910		Immune Signaling	9.23	3.43	9.06	2.85
ird5	24222	4201		Immune Signaling	7.74	2.18	6.23	1.76
pims	34647	15678		Immune Signaling	7.28	2.40	4.63	1.82
Cka	44323	7392		Signaling	7.20	2.11	7.70	2.51
UBL3	26076	9038		Other	6.13	1.29	4.96	1.72
Pomp	32884	9324		Proteolysis	5.65	1.95	2.71	1.58
Scg α	32013	7851		Cytoskeletal	5.58	2.34	2.18	1.77
porin	4363	6647		Other	5.50	1.28	5.88	1.41
CG14852	38242	14852		Unknown	5.36	1.46	-0.47	1.06
puc	4210	7850		Immune Signaling	5.23	2.31	2.16	1.74
Rpn6	28689	10149		Proteolysis	5.02	1.44	2.40	1.10
CG11526	35437	11526		Unknown	4.67	1.50	7.35	2.26
CG4729	36623	4729		Metabolism	4.63	1.35	4.19	1.34
mRNA-capping-enzyme	30556	1810		RNA binding	4.60	1.51	2.23	1.22
Spt6	28982	12225		RNA binding	4.58	1.60	1.72	1.39
dup	996	8171		DNA binding	4.54	1.16	0.64	0.93
pAbp	3031	5119		RNA binding	4.48	1.39	2.71	1.21
CG14313	38579	14313		Unknown	4.46	1.72	3.41	1.50
Act57B	44	10067		Cytoskeletal	4.28	1.13	3.28	1.20
CG9304	34674	9304		Unknown	4.28	1.22	3.36	1.40
Act5C	42	4027		Cytoskeletal	4.28	1.42	4.90	1.37
CG31386	51386	31386		Unknown	4.18	1.42	1.30	1.04
Act42A	43	12051		Cytoskeletal	4.13	1.00	2.92	1.08
Suv4-20	25639	13363		Other	4.00	1.22	3.92	1.14
ss	3513	6993		DNA binding	3.91	1.25	2.40	1.28
CG10158	31871	10158		Unknown	3.88	1.42	4.57	1.34
CG11294	30058	11294		DNA binding	3.75	1.22	0.75	1.05

Table A2. Continued.

Symbol	FBGN	CG	HDCID	Function	60min z-score	60min Δ P-JNK	15min z-score	15min Δ P-JNK
CG9769	37270	9769		Translation	3.72	1.19	0.94	1.01
CG5819	34717	5819		Unknown	3.69	1.64	0.23	1.00
cnk	21818	6556		Signaling	3.63	1.31	5.20	2.04
SNF4A γ	25803	17299		Signaling	3.62	1.68	1.66	1.37
ken	11236	5575		DNA binding	3.57	1.19	5.07	1.35
kay	1297	15509		DNA binding	3.56	1.48	3.06	1.27
HDC081 61			8161	Unknown	3.54	1.19	1.12	1.03
raptor	29840	4320		Signaling	3.48	1.21	4.07	1.30
not	13717	4166		Other	3.42	1.45	1.72	1.26
scaf6	52168	32168		RNA binding	3.41	1.09	3.19	1.13
DI	463	3619		Signaling	3.40	1.22	2.84	1.06
CG6028	38924	6028		Metabolism	3.39	1.66	0.00	1.07
e(y)1	617	6474		DNA binding	3.33	1.14	2.17	1.16
CG9297	38181	9297		Unknown	3.32	1.04	1.83	1.20
Arp66B	11744	7558		Cytoskeletal	3.28	1.12	2.58	1.13
RpS23	33912	8415		Translation	3.27	1.00	0.34	0.89
RpS3A	17545	2168		Translation	3.26	1.16	1.19	1.08
dve	20307	5799		DNA binding	3.25	1.67	1.45	1.09
HmgD	4362	17950		DNA binding	3.25	1.44	1.13	1.15
SNF1A	23169	3051		Signaling	3.24	1.42	0.45	0.99
CG6012	32615	6012		Metabolism	3.24	1.56	-0.30	1.02
Ef2b	559	2238		Translation	3.24	1.29	-0.53	1.01
Rpn12	28693	4157		Proteolysis	3.19	1.43	1.20	1.29
gce	30627	6211		Unknown	3.17	1.32	0.16	1.15
CG12050	32915	12050		Unknown	3.17	1.00	3.22	1.16
CG6013	38675	6013		Unknown	3.17	1.66	-0.06	1.14
CG32000	52000	32000		Other	3.14	1.29	3.76	1.23
Pros β 3	26380	11981		Proteolysis	3.12	1.29	1.88	1.24
RhoGAP 18B	30986	7481		Signaling	3.12	1.29	4.20	1.42
mRpL- Cl-B8	34893	5479		Translation	3.05	1.18	2.96	1.25
CG5114	36460	5114		Unknown	3.04	1.38	1.09	1.02
CG5728	39182	5728		RNA binding	3.02	1.72	0.87	1.09
lilli	41111	8817		Other	3.01	1.28	1.23	1.07
CG8771	33766	8771		Unknown	2.99	1.08	3.48	1.08
ik2	28633	2615		Signaling	2.99	1.20	2.22	1.18
Bx	242	6500		DNA binding	2.96	1.28	3.56	1.37
Jon99Ci	3358	31039		Proteolysis	2.95	1.39	1.57	1.13

Table A2. Continued.

Symbol	FBGN	CG	HDCID	Function	60min z-score	60min Δ P-JNK	15min z-score	15min Δ P-JNK
CG31406	51406	31406		Unknown	2.92	1.12	0.81	1.06
Rel	14018	11992		Immune Signaling	2.91	1.57	0.01	1.03
dpr9	38282	33485		Unknown	2.90	1.21	0.69	1.01
TfIIIE β	15829	1276		DNA binding	2.90	1.35	2.76	1.27
CG9886	31428	9886		Metabolism	2.88	1.10	-0.80	0.88
rept	40075	9750		DNA binding	2.88	1.15	1.79	1.11
AnnX	84	9579		Other	2.88	1.12	0.84	1.05
CG8243	33349	8243		Signaling	2.88	1.03	0.11	0.96
CG32628	52628	32628		Unknown	2.87	1.22	1.41	1.18
CycT	25455	6292		Signaling	2.87	1.30	0.73	1.07
CG5909	39495	5909		Proteolysis	2.86	1.50	1.36	1.27
RpS12	14027	11271		Translation	2.86	1.05	-0.28	0.81
CG8436	37670	8436		Unknown	2.85	1.25	1.00	1.00
HDC148 17			14817	Unknown	2.81	1.15	2.93	1.19
HDC195 89			19589	Unknown	2.81	0.98		0.96
CG32073	52073	32073		Unknown	2.80	1.15	1.56	1.01
CG8793	36894	8793		Unknown	2.80	1.27	1.24	1.13
CG6006	63649	6006		Other	2.79	1.32	2.33	1.11
CG11436	29713	11436		Unknown	2.77	1.09	1.77	1.13
CanB2	15614	11217		Signaling	2.77	1.40	-0.35	1.04
RpL18	35753	8615		Translation	2.75	1.23	1.56	1.19
RpII140	3276	3180		DNA binding	2.74	1.41	5.37	1.88
Su(Tpl)	14037	32217		DNA binding	2.74	1.29	2.29	1.13
CG18545	37812	18545		Unknown	2.74	1.13	3.05	1.13
CG16791	38881	16791		Unknown	2.71	1.63	-0.49	1.03
cnc	338	17894		DNA binding	2.70	1.34	3.58	1.47
CG9523	31812	9523		Unknown	2.69	1.22	3.00	1.30
CG11984	37655	11984		Other	2.69	1.13	3.57	1.40
Camta	33417	8809		DNA binding	2.69	0.83	1.95	0.98
CG4896	31319	4896		RNA binding	2.69	1.27	2.94	1.62
CG33330	53330	33330		Unknown	2.67	1.24	-0.78	1.06
CG5823	38515	5823		Proteolysis	2.67	1.43	1.00	0.95
CG12992	30846	12992		Unknown	2.67	1.50	-0.16	1.11
UbcD10	26316	5788		Proteolysis	2.67	1.41	-0.02	0.94
Syx1A	13343	31136		Other	2.66	1.33	-0.41	0.94
AnnIX	83	5730		Signaling	2.65	1.49	-0.01	1.01
CG11811	36099	11811		Metabolism	2.65	1.23	0.20	1.01

Table A2. Continued.

Symbol	FBN	CG	HDCID	Function	60min z-score	60min ΔP-JNK	15min z-score	15min ΔP-JNK
caup	15919	10605		DNA binding	2.64	1.10	1.21	0.86
B52	4587	10851		RNA binding	2.63	1.29	3.42	1.27
Fs(2)Ket	986	2637		Other	2.62	1.19	1.75	1.14
nec	2930	1857		Signaling	2.61	1.47	-0.13	1.09
MED26	39923	1793		DNA binding	2.59	1.46	2.29	1.49
LBR	34657	17952		Unknown	2.59	1.24	1.70	1.14
CG13647	39256	13647		Unknown	2.58	1.17	1.26	0.99
HDC14013			14013	Unknown	2.58	1.08	1.00	1.01
drpr	35261	2086		Signaling	2.58	1.17	4.03	1.35
Tip60	26080	6121		DNA binding	2.57	1.26	2.10	1.22
MED21	40020	11023		DNA binding	2.56	1.29	2.33	1.13
CG3891	35993	3891		DNA binding	2.55	1.35	3.70	1.52
HLHm3	2609	8346		DNA binding	2.54	0.92	5.37	2.00
CG9572	31089	9572		Unknown	2.52	1.13	0.40	0.90
Eip74EF	567	32180		DNA binding	2.51	1.19	3.42	1.32
norpA	4625	3620		Metabolism	2.51	1.24	0.11	0.89
CG8636	29629	8636		RNA binding	2.51	1.33	-0.71	0.91
RpS18	10411	8900		Translation	2.51	0.97	1.06	0.95
CG5822	31674	31919		Unknown	2.49	1.41	0.50	0.98
aur	147	3068		Signaling	2.49	1.24	1.78	1.10
sprt	50023	30023		Unknown	2.46	1.11		1.05
Cyp4d2	11576	3466		Metabolism	2.45	1.49	0.99	1.09
slmo	29161	9131		Unknown	2.45	1.31	2.07	1.20
drk	4638	6033		Signaling	2.44	1.49	1.57	1.43
l(2)k01209	22029	4798		Metabolism	2.44	1.10	2.82	1.06
CG9360	30332	9360		Metabolism	2.43	1.31	-0.04	1.00
Ppox	20018	5796		Metabolism	2.41	1.38	0.94	1.13
MED19	36761	5546		DNA binding	2.40	1.22	4.06	1.55
CG1244	35357	1244		Unknown	2.40	1.27	3.10	1.48
α-Cat	10215	17947		Cytoskeletal	2.39	1.34	1.55	1.23
CG30352	50352	30352		Unknown	2.39	1.11	1.00	1.04
Hexo2	41629	1787		Metabolism	2.39	1.19	2.69	1.34
CG17494	40011	12002		Other	2.38	1.27	4.16	1.47
CG2616	37512	2616		Other	2.38	1.06	0.47	0.92
HDC07791			7791	Unknown	2.37	1.13	0.89	1.10
CG18363	36808	18363		Other	2.37	1.27	0.62	1.12
CG17745	32386	17745		Unknown	2.37	1.08	0.13	0.91

Table A2. Continued.

Symbol	FBGN	CG	HDCID	Function	60min z-score	60min Δ P-JNK	15min z-score	15min Δ P-JNK
CG7231	31968	7231		Unknown	2.37	1.01	1.36	1.05
CG31524	51524	31524		Metabolism	2.36	1.43	-0.78	1.03
Taf4	10280	5444		DNA binding	2.36	1.17	2.04	1.42
HDC024 60			2460	Unknown	2.36	1.06	1.24	1.04
zormin	52311	33484		Cytoskeletal	2.36	1.18	2.47	1.26
CG7069	38952	7069		Metabolism	2.35	1.08	1.57	1.04
dnk	22338	5452		Metabolism	2.34	1.14	2.22	1.13
CG8105	30661	8105		Metabolism	2.34	1.12	0.29	0.99
CG6095	39401	6095		Unknown	2.33	1.21	0.52	1.00
CG7177	37098	7177		Signaling	2.33	1.35	3.12	1.45
HDC161 88			16188	Unknown	2.32	1.06	0.25	0.93
HDC063 46			6346	Unknown	2.32	1.08	-0.16	0.85
HDC029 79			2979	Unknown	2.32	1.13	-0.91	0.86
Src42A	4603	7873		Signaling	2.30	1.25	4.31	1.35
insv	31434	3227		Unknown	2.29	1.20	2.26	1.14
CG9522	30587	9522		Metabolism	2.29	1.20	1.25	1.10
CG5861	15338	5861		Unknown	2.29	1.36	0.16	1.02
CG10481	32827	10481		Signaling	2.29	1.11	0.23	1.01
CG32564	52564	32564		Unknown	2.29	1.14	1.21	1.03
CG12169	35143	12169		Signaling	2.29	1.26	1.84	1.22
CG31666	51666	31666		Unknown	2.28	1.35	-1.29	1.05
Rpt4	28685	3455		Proteolysis	2.28	1.62	2.28	1.58
HDC094 75			9475	Unknown	2.27	1.10	0.25	0.95
dco	2413	2048		Signaling	2.27	1.24	0.39	0.95
CG14998	35500	14998		Unknown	2.27	1.17	2.31	1.15
AP- 2sigma	43012	6056		Other	2.26	1.39	-1.70	0.97
CG10440	34636	10440		Other	2.26	1.17	1.32	1.05
CG32354	52354	32354		Unknown	2.24	1.47	-0.63	1.03
Osi13	37422	15595		Unknown	2.24	1.04	1.14	1.00
CG11505	35424	11505		RNA binding	2.24	1.12	1.86	1.21
CG4119	28474	4119		RNA binding	2.24	1.23	3.62	1.43
CG3960	29876	3960		Cytoskeletal	2.23	1.43	0.75	1.10
l(1)G002 2	30681	8231		Other	2.23	1.07	0.45	1.05
RpS5	2590	8922		Translation	2.23	0.98	1.13	1.02
CG3940	37788	3940		Metabolism	2.23	1.26	0.73	0.98
CG32033	52033	32033		Unknown	2.23	1.19	0.58	0.96

Table A2. Continued.

Symbol	FBGN	CG	HDCID	Function	60min z-score	60min Δ P-JNK	15min z-score	15min Δ P-JNK
CG30085	50085	30085		Unknown	2.23	1.08	0.77	0.86
CG5888	28523	5888		Unknown	2.22	1.50	-0.93	0.95
CG33251	53251	33251		Unknown	2.21	1.12	0.79	1.00
CG32373	52373	32373		Unknown	2.21	1.47	-1.46	0.98
CG10752	36325	10752		Unknown	2.20	1.06	2.41	1.07
Trf2	26758	18009		DNA binding	2.18	1.20	3.64	1.29
CG12972	37076	12972		DNA binding	2.17	1.15	1.21	1.07
CSN6	28837	6932		Unknown	2.16	1.05	1.17	1.06
CG5948	39386	5948		Metabolism	2.16	1.46	-0.15	0.96
CG6735	36472	6735		Cytoskeletal	2.16	1.26	3.40	1.71
CG5326	38983	5326		Metabolism	2.15	1.41	-0.44	0.99
smg	16070	5263		RNA binding	2.15	1.06	2.43	1.16
HDC19535			19535	Unknown	2.15	1.05	0.75	0.99
CG31030	51030	31030		Metabolism	2.15	1.14	0.34	0.98
CG11790	39265	11790		Other	2.15	1.13	1.10	1.06
Ccp84Ag	4777	2342		Other	2.14	1.15	-0.19	1.03
CG2901	29679	2901		Signaling	2.14	1.03	1.74	0.99
SeiR	37847	6584		Other	2.14	1.11	1.61	1.06
CG9576	31091	9576		Unknown	2.13	0.95	-0.81	0.78
HP1e	37675	8120		DNA binding	2.12	1.08	1.97	1.34
Smg5	19890	8954		RNA binding	2.12	1.25	4.59	1.80
CG5284	36566	5284		Other	2.12	1.08	1.21	0.96
CG5804	35926	5804		Other	2.12	1.14	1.17	1.02
CG4404	30432	4404		Unknown	2.12	1.08	0.86	1.00
pita	34878	3941		DNA binding	2.12	1.34	0.55	0.93
CG13749	33353	13749		Unknown	2.11	1.07	0.89	1.08
TfIIFa	10282	10281		DNA binding	2.11	1.21	0.47	0.93
Ef1 α 48D	556	8280		Translation	2.11	1.23	-0.20	0.99
tun	34046	8253		Unknown	2.11	0.99	1.01	0.92
CG5946	36211	5946		Metabolism	2.11	1.31	0.95	1.07
CG11666	40648	11666		Unknown	2.11	1.08	1.57	1.04
HDC03637			3637	Unknown	2.10	1.06	0.21	0.88
CG3597	31417	3597		Metabolism	2.10	1.22	-0.07	0.89
TepIII	41181	7068		Unknown	2.10	1.08	0.45	0.96
Trip1	15834	8882		Translation	2.10	1.03	0.99	1.07
CG31525	51525	31525		Unknown	2.10	1.10	1.43	1.03
HDC06322			6322	Unknown	2.10	1.14	2.78	1.23

Table A2. Continued.

Symbol	FBN	CG	HDCID	Function	60min z-score	60min Δ P-JNK	15min z-score	15min Δ P-JNK
Syx8	36643	4109		Other	2.10	1.08	1.53	1.02
CG15211	30234	15211		Unknown	2.09	1.13	1.07	0.96
CG14638	37223	14638		Unknown	2.09	1.04	0.89	1.06
CG9727	37445	9727		DNA binding	2.09	1.05	0.39	0.94
Orc4	23181	2917		Other	2.09	1.07	1.01	0.91
Asph	34075	8421		Unknown	2.09	1.24	-1.50	0.83
HDC19532			19532	Unknown	2.08	1.02	0.79	1.06
CG12000	37314	12000		Proteolysis	2.08	1.15	1.11	1.10
CG11727	30299	11727		Signaling	2.08	1.06	0.50	1.06
CG3590	38467	3590		Metabolism	2.08	1.03	0.76	0.94
CG9598	36424	9598		Unknown	2.07	0.93	1.69	1.09
dj	19828	1980		Unknown	2.07	1.14	-1.11	0.96
CG6016	33844	6016		Metabolism	2.07	1.43	0.00	1.14
eca	53104	33104		Other	2.07	0.97	0.63	1.05
HDC10149			10149	Unknown	2.05	1.14	4.24	1.29
CG6194	38325	6194		Proteolysis	2.05	1.33	0.33	1.08
kto	1324	8491		DNA binding	2.05	1.19	4.23	1.28
bun	10460	5461		DNA binding	2.05	1.20	5.75	1.54
CG17737	35423	17737		Translation	2.05	1.10	0.51	0.99
put	3169	7904		Signaling	2.04	1.12	0.23	0.87
CG5116	39339	5116		Unknown	2.04	1.21	1.20	1.04
Sry- δ	3512	17958		DNA binding	2.04	1.16	1.45	1.12
CG18358	30782	18358		Unknown	2.04	1.17	0.49	1.01
maf-S	34534	9954		DNA binding	2.03	1.10	3.38	1.43
CG8740	27585	8740		Unknown	2.03	1.10	0.40	1.00
CG31738	51738	31738		Cytoskeletal	2.03	1.04	1.37	1.02
sgg	3371	2621		Signaling	2.03	1.12	0.43	0.96
CG3622	34778	3622		Proteolysis	2.03	1.28	1.26	1.16
HDC01229			1229	Unknown	2.02	1.12	-0.11	0.92
CG8603	33923	8603		Unknown	2.02	1.18	0.65	1.05
orb	4882	10868		RNA binding	2.02	1.12	0.64	0.85
CG2614	32873	2614		Unknown	2.02	1.05	1.03	1.00
dpr12	33044	14469		Unknown	2.02	1.06	2.00	1.12
HDC03347			3347	Unknown	2.02	1.13	0.18	0.95
hdc	10113	15532		Unknown	2.02	1.35	0.60	1.08
Optix	25360	18455		DNA binding	2.01	1.15	1.76	1.14

Table A2. Continued.

Symbol	FBGN	CG	HDCID	Function	60min z-score	60min Δ P-JNK	15min z-score	15min Δ P-JNK
HDC062 57			6257	Unknown	2.01	1.07	0.58	0.93
CG13047	36594	13047		Unknown	2.01	1.14	2.59	1.08
ksr	15402	2899		Signaling	2.01	1.05	2.38	1.11
CG11245	30388	11245		Unknown	2.01	0.93	3.15	1.14
HDC036 21			3621	Unknown	2.00	1.04	0.41	0.96
CG6769	30878	6769		Unknown	2.00	1.12	0.45	1.09
CG14741	37989	14741		Metabolism	2.00	1.22	1.77	1.12
dia	11202	1768		Cytoskeletal	2.00	1.09	1.54	1.01
CG3474	28871	3474		Other	1.99	1.05	1.46	1.03
yCop	28968	1528		Other	1.99	1.16	-0.55	0.78
HDC161 20			16120	Unknown	1.99	1.03	0.95	1.00
CG2191	39873	2191		Other	1.99	1.12	-0.03	0.89
CG17570	32948	17570		Unknown	1.99	1.08	0.54	0.95
Cyp28d1	31689	10833		Metabolism	1.99	1.03	0.99	0.90
cas	4878	2102		DNA binding	1.99	1.13	1.37	1.00
Rpl1	3279	5502		Translation	1.98	0.99	2.99	1.31
CG3259	38221	3259		Unknown	1.98	0.99	1.83	1.21
CG10795	34626	10795		Unknown	1.98	1.30	0.35	1.06
Pka-R1	275	3263		Signaling	1.98	1.18	1.36	1.06
NHP2	29148	5258		RNA binding	1.97	1.09	2.46	1.14
HDC170 98			17098	Unknown	1.97	1.01	1.76	1.02
Parg	23216	2864		Metabolism	1.97	1.09	0.97	1.04
Nmdar1	10399	2902		Signaling	1.97	1.01	0.65	0.96
CG15778	29788	15778		Unknown	1.97	1.05	0.87	0.97
MED17	38578	7957		DNA binding	1.97	1.19	1.43	1.26
CG3077	31457	3077		Unknown	1.96	1.36	0.58	1.19
debcl	29131	33134		Signaling	1.96	1.37	-0.28	1.09
CG12112	30048	12112		Unknown	1.96	1.02	0.90	0.99

Table A3. Enhancers of 15min PGN-induced P-JNK.

In-cell Western z-scores were calculated from P-JNK:f-actin values from S2 cells incubated with 15,683 dsRNAs and treated with PGN for 15min. dsRNAs that modified P-JNK:f-actin z-scores below 1.96 (95% CI) are ordered from smallest to highest z-score. The fold change in dJNK phosphorylation relative to the plate median is shown alongside the z-score values. Each dsRNA is identified by its symbol and Celera Genome (CG) number or by its Heidelberg Drosophila Consortium identification number (HCDID).

Symbol	FBGN	CG	HCDID	Function	z-score	Δ P-JNK
Tak1	26323	18492		Immune signaling	-5.70	0.33
CG7185	35872	7185		RNA binding	-5.22	0.40
HDC18088			18088	Unknown	-4.96	0.63
raw	3209	12437		Signaling	-4.72	0.77
PGRP-LC	35976	4432		Immune signaling	-4.66	0.21
ush	3963	2762		DNA binding	-4.53	0.61
dFadd	38928	12297		Immune signaling	-4.47	0.52
PNUTS	31291	31657		Signaling	-4.38	0.69
Tab2	34431	7417		Immune signaling	-4.28	0.62
CG15881	36909	15881		Unknown	-4.02	0.47
imd	13983	5576		Immune signaling	-3.75	0.60
CG14564	37131	14564		Unknown	-3.75	0.87
CG6393	34685	6393		Unknown	-3.73	0.47
RpL31	25286	1821		Translation	-3.57	0.62
HDC00271			271	Unknown	-3.53	0.70
CG14187	36938	14187		Unknown	-3.52	0.74
PNUTS	31291	4124		Signaling	-3.50	0.42
Dredd	20381	7486		Immune signaling	-3.49	0.25
msl-2	5616	3241		DNA binding	-3.47	0.78
CG7274	30965	7274		DNA binding	-3.44	0.59
Hrb27C	4838	10377		RNA binding	-3.42	0.57
Sin3A	22764	8815		DNA binding	-3.42	0.50
ImpL3	1258	10160		Metabolism	-3.41	0.60
crc	370	8669		DNA binding	-3.37	0.77
CG32105	52105	32105		DNA binding	-3.32	0.43
TfIIA-S	13347	5163		DNA binding	-3.32	0.40
RpL11	13325	7726		Translation	-3.31	0.69
CG11006	27534	11006		Unknown	-3.24	0.73
Rm62	3261	10279		RNA binding	-3.24	0.40
CG11200	34500	11200		Metabolism	-3.23	0.62
Sox21b	42630	32139		DNA binding	-3.20	0.74

Table A3. Continued.

Symbol	FBGN	CG	HDCID	Function	z-score	ΔP-JNK
CG5060	38780	5060		Unknown	-3.19	0.79
CG18375	34606	18375		Unknown	-3.17	0.58
msn	10909	16973		Immune signaling	-3.15	0.70
bsk	229	5680		Immune signaling	-3.15	0.58
HDC01143			1143	Unknown	-3.14	0.88
RpL37A	28696	5827		Translation	-3.14	0.62
Pros54	15283	7619		Proteolysis	-3.13	0.68
scrt	4880	1130		DNA binding	-3.12	0.53
CG15742	30462	15742		Unknown	-3.07	0.72
CG31353	51353	31353		Unknown	-3.06	0.84
hep	10303	4353		Immune signaling	-3.04	0.46
eIF-3p40	22023	9124		RNA binding	-2.98	0.71
foi	24236	6817		Other	-2.93	0.72
crol	20309	14938		DNA binding	-2.93	0.86
CG7065	30091	7065		Unknown	-2.90	0.61
CG13044	36599	13044		Unknown	-2.89	0.80
Prat2	41194	10078		Metabolism	-2.87	0.97
CG15630	31627	15630		Other	-2.87	0.62
CG10375	39116	10375		Other	-2.86	0.74
CG15864	40528	15864		Metabolism	-2.85	0.73
spen	16977	18497		RNA binding	-2.85	0.75
z	4050	7803		DNA binding	-2.84	0.71
shn	3396	7734		DNA binding	-2.81	0.57
CG3563	38259	3563		Unknown	-2.78	0.87
bel	171	9748		RNA binding	-2.78	0.64
lap2	15247	8293		Immune signaling	-2.76	0.30
CG1874	33425	1874		Unknown	-2.75	0.86
Duox	31464	3131		Other	-2.73	0.74
CG10576	35630	10576		Unknown	-2.72	0.94
HDC10534			10534	Unknown	-2.70	0.76
HDC16589			16589	Unknown	-2.68	0.73
Treh	3748	9364		Metabolism	-2.67	0.94
Sh	3380	12348		Other	-2.67	0.49
CG13779	40954	13779		Unknown	-2.66	0.83
CG10600	32717	10600		Unknown	-2.65	0.78
CG12361	35292	12361		DNA binding	-2.62	0.57
CG17041	33822	17041		Unknown	-2.62	0.99
tai	41092	13109		Signaling	-2.61	0.89

Table A3. Continued.

Symbol	FBGN	CG	HDCID	Function	z-score	ΔP-JNK
CG14351	31349	14351		Unknown	-2.60	0.47
CG31545	51545	31545		Unknown	-2.59	0.81
Ptp69D	14007	10975		Signaling	-2.59	0.95
CG14258	39482	14258		Unknown	-2.57	0.96
CG16742	34529	16742		Unknown	-2.55	0.92
HDC08833			8833	Unknown	-2.55	0.78
Mkk4	24326	9738		Immune signaling	-2.53	0.62
CG15737	30353	15737		DNA binding	-2.52	0.79
CG15884	39481	15884		Unknown	-2.52	0.97
CG14126	36223	14126		Unknown	-2.50	0.93
Lcp65Ac	20642	6956		Unknown	-2.49	0.89
CG10359	35452	10359		Unknown	-2.49	0.73
CG9948	35721	9948		Unknown	-2.47	0.89
Ance	12037	8827		Metabolism	-2.46	0.82
ato	10433	7508		DNA binding	-2.43	0.82
CG17896	23537	17896		Metabolism	-2.43	0.83
bhr	35773	8580		Unknown	-2.42	0.65
HDC17686			17686	Unknown	-2.41	0.93
Rca1	17551	10800		Other	-2.41	0.85
CG7716	35800	7716		Cytoskeletal	-2.40	0.88
CG8851	31546	8851		Cytoskeletal	-2.39	0.72
CG2063	33400	2063		Unknown	-2.38	0.69
CG6091	36180	6091		Proteolysis	-2.38	0.67
Mef2	11656	1429		DNA binding	-2.38	0.62
HDC02074			2074	Unknown	-2.38	0.94
CG7518	38108	7518		Unknown	-2.38	0.70
Mkp3	36844	14080		Signaling	-2.38	0.78
lectin-46Cb	40092	1652		Unknown	-2.37	0.86
CG15599	30667	15599		Unknown	-2.36	0.90
MED30	35149	17183		DNA binding	-2.36	0.63
CG17298	38879	17298		Unknown	-2.36	0.97
CG14891	38445	14891		Unknown	-2.35	1.06
CG8949	30812	8949		Unknown	-2.35	0.83
up	4169	7107		Cytoskeletal	-2.35	0.65
RpL23	10078	3661		Translation	-2.34	0.70
Neos	24542	8614		Unknown	-2.34	0.73
CG14657	37282	14657		Unknown	-2.34	0.74
CG10396	33020	10396		Metabolism	-2.33	0.75

Table A3. Continued.

Symbol	FBGN	CG	HDCID	Function	z-score	ΔP-JNK
Ccp84Ab	4782	1252		Unknown	-2.32	0.87
HDC08157			8157	Unknown	-2.31	0.81
Vm32E	14076	16874		Unknown	-2.31	0.94
CG3817	38275	3817		Unknown	-2.31	0.79
plexA	25741	11081		Signaling	-2.30	0.67
CG33292	53292	33292		Unknown	-2.30	0.87
Khc-73	19968	8183		Cytoskeletal	-2.30	0.74
CG2042	32944	2042		Unknown	-2.30	0.91
CG14435	29911	14435		Unknown	-2.29	0.62
CG2291	33279	2291		Unknown	-2.29	0.78
CG1259	35513	1259		Unknown	-2.29	0.81
CG15057	30908	15057		Unknown	-2.29	0.86
CG10495	32750	10495		Metabolism	-2.28	0.60
mib2	32742	17492		Signaling	-2.28	0.79
Rbp1	10252	17136		RNA binding	-2.27	0.72
CG10793	29656	10793		Other	-2.26	0.82
CG3689	35987	3689		RNA binding	-2.26	0.74
Rbp9	10263	3151		RNA binding	-2.25	0.83
Cyp4e1	15034	2062		Metabolism	-2.25	0.83
HDC07335			7335	Unknown	-2.25	0.89
CG15816	30866	15816		Unknown	-2.25	0.94
misl-1	5617	10385		DNA binding	-2.24	0.74
CG7028	27587	7028		Unknown	-2.24	0.86
g	1087	10986		Other	-2.22	0.76
CG33465	53465	33465		Unknown	-2.22	0.81
CG32499	52499	32499		Metabolism	-2.20	0.67
lama	16031	10645		Other	-2.20	0.92
l(1)G0060	29797	3125		Unknown	-2.19	0.63
CG33324	53324	33324		Unknown	-2.19	0.81
CG16903	40394	16903		DNA binding	-2.19	0.77
grp	11598	17161		Signaling	-2.19	0.75
cnn	13765	4832		Other	-2.18	1.01
w	3996	2759		Metabolism	-2.18	0.90
CG3875	34740	3875		RNA binding	-2.18	0.89
HDC18629			18629	Unknown	-2.16	0.80
Sug	36191	7334		DNA binding	-2.16	0.81
GckIII	38477	5169		Signaling	-2.16	0.78
Pep	4401	6143		RNA binding	-2.16	0.94

Table A3. Continued.

Symbol	FBGN	CG	HDCID	Function	z-score	ΔP-JNK
CG5366	27568	5366		DNA binding	-2.16	0.84
CG14968	35431	14968		Unknown	-2.15	0.97
FucTA	36485	6869		Metabolism	-2.15	0.89
CG12928	33432	12928		Unknown	-2.14	0.87
CG11284	30056	11284		Metabolism	-2.14	0.69
CG6694	35900	6694		Unknown	-2.14	0.87
CG6169	36534	6169		RNA binding	-2.14	0.60
CG32570	52570	32570		Unknown	-2.13	1.03
HDC08154			8154	Unknown	-2.13	0.87
HDC18630			18630	Unknown	-2.13	0.79
HDC15592			15592	Unknown	-2.13	0.88
Tango10	30330	1841		Other	-2.12	0.82
CG32132	52132	32132		Unknown	-2.12	0.87
CG12976	37053	12976		Unknown	-2.12	0.95
xl6	28554	10203		RNA binding	-2.12	0.89
CG18157	30563	18157		Unknown	-2.11	1.04
CG13625	39210	13625		Unknown	-2.10	0.74
CG12997	30831	12997		Unknown	-2.10	1.02
CG2812	34931	2812		Unknown	-2.10	0.87
dro2	52279	32279		Other	-2.09	0.97
CG31537	51537	31537		Unknown	-2.09	0.93
RpL28	35422	12740		Translation	-2.09	0.64
CG5877	30625	5877		Unknown	-2.09	0.98
CG2767	37537	2767		Metabolism	-2.08	0.92
CG12377	37168	12377		Unknown	-2.08	0.99
ng3	10295	10788		Unknown	-2.08	0.81
CG15646	30665	15646		Unknown	-2.08	0.96
CG8489	38225	8489		Unknown	-2.07	0.91
CG33125	53125	33125		Unknown	-2.07	1.12
Pop2	36239	5684		RNA binding	-2.07	0.76
HDC10097			10097	Unknown	-2.07	0.84
CG4982	36598	4982		Unknown	-2.06	0.90
CG12384	33624	12384		Unknown	-2.06	0.94
CG14073	36814	14073		Unknown	-2.05	0.98
CG5172	30830	5172		Unknown	-2.05	0.84
CG7023	39025	7023		Proteolysis	-2.04	0.91
spag	15544	13570		Unknown	-2.04	0.98
I(2)NC136	33029	8426		DNA binding	-2.04	0.64

Table A3. Continued.

Symbol	FBGN	CG	HDCID	Function	z-score	ΔP-JNK
CG6153	32445	6153		Unknown	-2.04	0.71
CG13465	40809	13465		Unknown	-2.04	0.97
CG14619	31187	14619		Proteolysis	-2.03	0.87
HDC13887			13887	Unknown	-2.03	0.84
Scgbeta	38042	5657		Cytoskeletal	-2.03	0.98
mip120	33846	6061		DNA binding	-2.03	0.74
CG5792	32455	5792		Unknown	-2.03	0.97
UbcD2	15320	6720		Other	-2.03	0.83
HDC02356			2356	Unknown	-2.02	0.85
CG7914	30995	7914		Unknown	-2.02	0.92
CG4577	31306	4577		Unknown	-2.02	1.02
CG1839	30555	1839		Unknown	-2.02	0.77
HDC16059			16059	Unknown	-2.02	0.96
Hel25E	14189	7269		RNA binding	-2.01	0.76
kal-1	39155	6173		Other	-2.00	0.72
CG14939	32378	14939		Unknown	-2.00	1.00
CG10513	39311	10513		Unknown	-1.99	0.87
CG5506	36766	5506		Unknown	-1.99	0.94
RpL9	15756	6141		Translation	-1.99	0.59
drosha	26722	8730		RNA binding	-1.99	0.71
CG3173	34964	3173		Unknown	-1.99	0.78
CG13643	40601	13643		Other	-1.99	0.82
CG30458	50458	30458		Unknown	-1.99	0.93
capt	28388	5061		Cytoskeletal	-1.98	0.72
CG12590	37294	12590		Unknown	-1.98	1.00
MenI-2	29153	30097		Metabolism	-1.98	0.81
CG9632	38377	9632		Unknown	-1.98	0.82
pxb	53207	33207		Unknown	-1.98	0.85
CG11899	14427	11899		Metabolism	-1.98	0.77
CG9392	36895	9392		Unknown	-1.98	0.88
CG32467	52467	32467		Unknown	-1.98	0.96
CG4090	38492	4090		Other	-1.97	0.87
CG14365	38177	14365		Unknown	-1.97	0.83
CG15383	31394	15383		Unknown	-1.97	0.94
Ssdp	11481	7187		DNA binding	-1.96	0.86
CG17841	28480	17841		Unknown	-1.96	0.83

Table A4. Enhancers of f-actin levels in S2 cells.

Analysis of dsRNA-mediated depletion of regulators f-actin levels at 15 min and 60 min PGN-exposures. Fold change from the plate median values were calculated from S2 cells incubated with 15,852 dsRNAs and treated with PGN for 15 or 60 min by In-cell Western. dsRNAs that decreased f-actin levels in the bottom 1% for both 15 and 60 min time points are arranged from lowest to highest 15 min fold changes. dsRNAs that significantly altered the fold change in dJNK phosphorylation relative to the plate median is were excluded from the analysis. Each dsRNA is identified by its symbol and Celera Genome (CG) number or by its Heidelberg Drosophila Consortium identification number (HCDID). dsRNAs that specifically target actin are shown in bold.

Symbol	CG	HDC ID	15min	60min
CHES-1-like	12690		0.317	0.413
CG32133	32133		0.408	0.275
CG12071	12071		0.457	0.296
CG11265	11265		0.493	0.317
Act88F	5178		0.569	0.514
		819	0.582	0.763
Act79B	7478		0.598	0.654
CG6700	6700		0.614	0.584
CG7633	33253		0.616	0.713
kek5	12199		0.629	0.409
Pp1-87B	5650		0.638	0.705
CG1379	1379		0.662	0.682
Med21	6884		0.663	0.672
Act5C	4027		0.665	0.714
Act87E	18290		0.668	0.676
srp	3992		0.671	0.588
CG32742	32742		0.678	0.606
chic	9553		0.686	0.660
CG1973	1973		0.691	0.758
		7599	0.695	0.789
porin	6647		0.700	0.774
vvl	10037		0.707	0.546
CanA1	1455		0.707	0.771
sob	3242		0.710	0.711
Arc92	12254		0.716	0.460
DI	3619		0.724	0.781
Alg10	32076		0.725	0.715
CG2893	14168		0.725	0.763
scaf6	32168		0.726	0.774
Gug	6964		0.726	0.754
		7625	0.727	0.681
CG9426	9426		0.733	0.617
CG3394	3394		0.736	0.787
rin	9412		0.741	0.613
CG12912	12912		0.743	0.668
Act42A	12051		0.743	0.612

Table A4. Continued

Symbol	CG	HDC ID	15min	60min
Mob1	11711		0.744	0.501
	31754		0.748	0.788
CG2901	2901		0.749	0.781
Cyp6d5	3050		0.751	0.766
GATAe	10278		0.754	0.742
		15001	0.757	0.780
Grip84	3917		0.758	0.732
		19589	0.765	0.770

Table A5. dsRNA effects on f-actin and P-JNK in S2 cells.

Analysis of dsRNA-mediated depletion of regulators f-actin and P-dJNK levels at 15 min and 60 min PGN-exposures. Fold change from the plate median values were calculated from S2 cells incubated with 15,852 dsRNAs and treated with PGN for 15 or 60 min by In-cell Western. dsRNAs that decreased f-actin levels in the bottom 1% for both 15 and 60 min time points are arranged from lowest to highest 15 min fold changes. dsRNAs that significantly altered the fold change in dJNK phosphorylation relative to the plate median were included in the analysis. Each dsRNA is identified by its symbol and Celera Genome (CG) number or by its Heidelberg Drosophila Consortium identification number (HCDID).

Symbol	CG	15min	60min
CG32778	32778	0.028	0.069
th	12284	0.045	0.031
bib	4722	0.186	0.213
Hr4	16902	0.202	0.284
CG6191	6191	0.215	0.315
CG14366	14366	0.220	0.383
CG3638	3638	0.222	0.309
Clk	7391	0.236	0.193
CG11700	11700	0.265	0.110
Hey	11194	0.275	0.135
pros	17228	0.292	0.558
CG32296	32296	0.334	0.140
CG12852	12852	0.341	0.595
wts	12072	0.343	0.097
CG18656	33277	0.360	0.526
sr	7847	0.407	0.295
CG3323	3323	0.409	0.673
RpS27A	5271	0.417	0.342
Tim9b	33066	0.426	0.616
Ubi-p63E	11624	0.428	0.121
dmrt99B	15504	0.463	0.623
ena	15112	0.478	0.614
dl	6667	0.485	0.490
CG31158	31158	0.496	0.467
fzy	4274	0.514	0.400
CG18599	18599	0.563	0.595
ind	11551	0.569	0.275
CG15365	15365	0.575	0.581
Atx2	5166	0.598	0.435
CG31705	31705	0.612	0.665
CG4136	4136	0.623	0.474
Toll-6	7250	0.629	0.589
RpL40	2960	0.630	0.583
CG18282	32744	0.631	0.718
CG7368	7368	0.646	0.692
CG9469	33352	0.672	0.436

Table A5. Continued.

Symbol	CG	15min	60min
CG32479	32479	0.678	0.722
M(3)62F	3195	0.705	0.757
Qm	17521	0.707	0.759
CG30497	30497	0.725	0.729
CG7830	7830	0.728	0.655
ara	10571	0.754	0.700
abd-A	10325	0.756	0.426
amd	10501	0.758	0.665

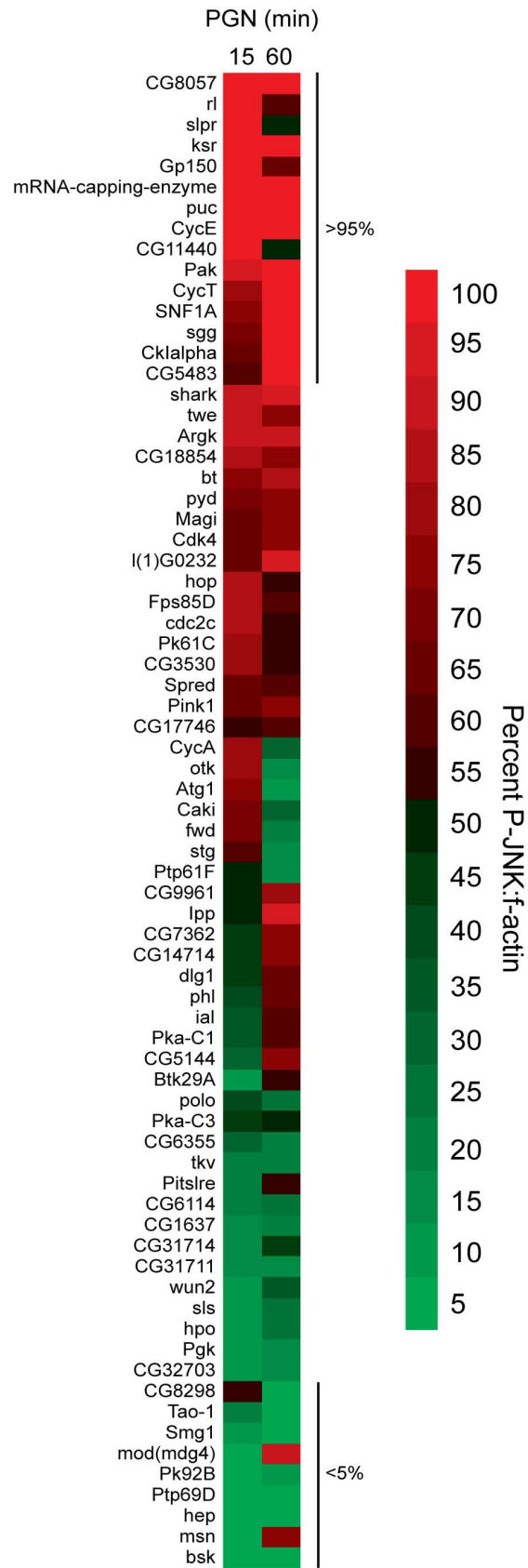


Figure A1. P-JNK screen comparative analysis.

Comparative analysis of 15min and 60min PGN-induced P-JNK:f-actin screen results relative to Bakal C. et. al. 2008[355]. 15min and 60min P-JNK:f-actin z-scores were ordered from highest to lowest and organized according to confidence intervals. Genes identified as modifiers of dJNK activity in Bakal C. et. al. 2008 were cross referenced with the PGN-induced percent P-JNK:f-actin at 15min and 60min. Genes indicated in more red demonstrated a stronger suppressive phenotype on PGN-induced JNK phosphorylation, while gene indicated in more green demonstrated a stronger enhancing phenotype on PGN-induced dJNK phosphorylation. Vertical lines indicate genes that suppress JNK phosphorylation in the top 95th percentile and genes that enhance JNK phosphorylation in the bottom 5th percentile[355].